Photobiomodulation in Animal Models of Ageing and Alzheimer's Disease

DUGGETT, NATALIE,AMY

Photobiomodulation in Animal Models of Ageing and Alzheimer's Disease

Natalie Amy Duggett

B.Sc. (Hons) (Dunelm)

A thesis submitted to the University of Durham in accordance with the requirements for the degree of Doctor of Philosophy

School of Biological and Biomedical Sciences

University of Durham

2013

Supervisor: Dr. Paul Chazot

Abstract

Photobiomodulation refers to low-intensity light therapy, utilising wavelengths in the near-infrared region of the electromagnetic spectrum to elicit biological effects.

The principle aim of this investigation was to explore signalling pathways initiated by IR1072, with particular focus on heat shock proteins (HSPs), a family of proteins known to target cellular aggregates which are involved in the maintenance of cellular homeostasis. This was further examined by exploring the role of age and sex in the magnitude of biological effects induced. Another aim of this study was to explore the cytoprotective potential of IR1072 in conjunction with Alzheimer's disease-related insults.

The results of this study show chronic IR1072 exposure altered the expression of a number of HSPs in both CD-1 and TASTPM mice; including HSP105, HSP70, HSP27, and αB crystallin. The magnitude of effect differed with age and sex of CD-1 and TASTPM mice respectively; these differences coincided with altered endogenous activity of electron transport chain components. Acute exposure of CAD neuronal cultures provided significant neuroprotection against oxidative-stress and β-amyloid insults.

Further characterisation of the CD-1 and TASTPM strains during ageing was established. CD-1 mice demonstrated reduced TARP γ2 with age, which may underlie learning deficits that become apparent during ageing. Chronic IR1072 exposure significantly increased TARP γ2 in 7 and 13 month old CD-1 mice, perhaps explaining improved working-memory reported following IR1072 exposure. Acute treatments of CD-1 mice altered Complex I and II activity in mitochondria.

Chronic IR1072 exposure *Caenorhabditis elegans* was shown to consistently extend lifespan. This model system aided in establishing pathways essential for biological effects of IR1072, demonstrating the importance of HSF1 driven pathways, in particular those requiring HSP70. In conclusion, this research revealed mechanisms initiated by photobiomodulation at IR1072 that act to re-establish homeostasis, profoundly reduce amyloid load, prevent cell stress and cell death.

Acknowledgements

I have been fortunate to work with a number of excellent lab members, particularly Mwape Katebe, Rushdie Abuhamdah, Dilwar Hussain, Simon Cork, Solmaz Boroumand and Boo Virk. I would like to thank Dr Piers Hemsley who has provided endless, invaluable advice – despite being a plant scientist!

I will be eternally indebted to my supervisor, Dr Paul Chazot, for all of his guidance, patience, encouragement and support during my project.

Huge thanks also go to the LSSU staff, particularly Claire Robinson and Heather Crawford, for all of their help and assistance.

Special thanks go to a number of members of the Physics department for all of their help and patience, Dr Helen Cramman for all her assistance with LabView™, and Prof. Damien Hampshire and Dr Chris Saunter for equipment and advice with setting up of the thermocouple.

Thanks also go to Christine Richardson in the Electron Microscopy suite of Durham University for her help in staining and imaging the β-amyloid peptide.

I would also like to acknowledge the support of Simon and my parents during my project, without them none of this would have been possible.

Declaration

I confirm that no part of the material presented has previously been submitted for a degree in this or any other university. If material has been generated through joint work, my independent contribution has been clearly indicated. In all other cases, material from the work of others has been clearly indicated, acknowledged and quotations and paragraphs indicated.

Table of Contents

List of Figures

Chapter 1

Chapter 2

Chapter 3

Chapter 4

Chapter 5

Chapter 6

Chapter 7

Appendix II

List of Tables

Chapter 1

Chapter 3

Chapter 4

Chapter 5

Chapter 6

Chapter 7

Abbreviations

aa	Amino acid
AD	Alzheimer's disease
ADP	Adenosine 5’ diphosphate
AIF	Apoptosis inducing factor
AMP	Adenosine 5’ monophosphate
AMPA	α-amino-3-hydroxy-5-methyl-4-isoxazolepropionic acid
ANT	Adenine nucleotide translocator
AP1	Activator protein 1
APAF-1	Apoptotic protease activating factor 1
APOE	Apolipoprotein E
APP	Amyloid precursor protein
APPsw	Swedish APP mutation
ASK1	Apoptosis signal regulating-kinase 1
AT8	Hyperphosphorylated tau Ser202/Thr205
ATP	Adenosine 5’ triphosphate
Aβ	β-amyloid
$A\beta_{(1-40)}$	40 amino acid isoform of β-amyloid
$A\beta_{(1-42)}$	42 amino acid isoform of β-amyloid
BAG-1	BCL2 associated athanogene
BAK	Bcl-2 antagonist/killer
BAX	Bcl-2 associated X protein
Bcl-2	B-cell lymphoma 2
$BCL\text{-}X_L$	B-cell lymphoma-extra large
BDNF	Brain derived neurotrophic factor
BID	BH3 interacting domain death agonist
BSA	Bovine serum albumin
CA	Cornu ammonis

CAD	Cath.a differentiated
cAMP	Cyclic adenosine monophosphate
Caspase	Cysteine aspartic specific protease
Cb	Cerebellum
CBF	Cerebral blood flow
Cdk-5	Cyclin-dependent kinase-5
CFU	Colony forming units
CHIP	Carboxy terminus of HSP70-binding protein
CK2	Casein kinase II
CNS	Central nervous system
Complex I	NADH-ubiquinone reductase
Complex II	Succinate-ubiquinone reductase
Complex III	Ubiquinone-cytochrome *c* reductase
Complex IV	Cytochrome *c* oxidase
Complex V	ATP synthase
CPu	Caudate putamen
CREB	cAMP response element binding protein
CSF	Cerebral spinal fluid
Ctx	Cerebral cortex
Cu	Copper
CY	Cyclophilin
Cyt *c*	Cytochrome *c*
DAB	3,3-Diaminobenzidine
DAPI	4',6-diamidino-2-phenylindole
DAXX	Death domain associated protein
DG	Dentate gyrus
dH_2O	Distilled water
DIABLO	*Drosophila melanogaster* homologue

DMEM	Dulbecco’s modified eagle medium
DMSO	Dimethyl sulphoxide
DNA	Deoxyribonucleic acid
DTT	Dithiothreitol
e^-	Electron
EDTA	Ethylenediaminetetraacetic acid
EGTA	Ethyleneglycotetraacetic acid
E_h	Redox potential
ELISA	Enzyme-linked immunosorbant assay
EM	Electromagnetic
E_m	Plasma membrane potential
ER	Endoplasmic reticulum
ERAD	Endoplasmic reticulum associated degradation
ERK	Extracellular signal regulated kinase
ETC	Electron transport chain
FAD	Flavine adenine dinucleotide
FADD	Fas-associated death domain
$FADH_2$	Reduced flavine adenine dinucleotide
FAS	Apoptosis antigen-1
FASL	Fas ligand
FCS	Foetal calf serum
FOXO	Forkhead family box O
GABA	γ-aminobutyric acid
GFAP	Glial fibrillary acidic protein
GFP	Green fluorescent protein
GluA1	Glutamate receptor 1
GluA2	Glutamate receptor 2
GRP	Glucose regulated protein

GSK-3β	Glycogen synthase kinase-3β
H^+	Hydrogen ion
H_2O_2	Hydrogen peroxide
Hb	Haemoglobin
HbO_2	Oxyhaemoglobin
HRP	Horse radish peroxidase
HSC	Heat shock cognate
HSE	Heat shock element
HSF	Heat shock factor
HSP	Heat shock protein
HSPA4L	heat shock 70 kDa protein 4-like
IDE	Insulin degrading enzyme
IMM	Inner mitochondrial membrane
iNOS	Inducible NO-synthase
IR	Infrared
IR1072	Infrared wavelength 1072 nm
JAK	Janus kinase
jBID	BID cleavage product
JC-1	5,5’,6,6’-tetrachloro-1,1’,3,3’ tetraethylbenzimidazolylcarbocyanine iodide
JNK	c-Jun N-terminal kinase
LAMP	Lysosomal associated membrane protein
LASER	Light amplification by the stimulated emission of radiation
LB	Luria-Bertani broth
LDH	Lactate dehydrogenase
LEDs	Light emitting diodes
LILT	Low-intensity light therapy
LLLT	Low level light therapy

LTD	Long term depression
LTP	Long term potentiation
MAP	Microtubule associated protein
MAPK	Mitogen activated protein kinase
MAPKAPK2	Mitogen-activated protein kinase-activated protein kinase 2
Mg	Magnesium
MPP^+	1-methyl-4-phenylpyridinium
MPTP	Mitochondrial permeability transition pore
MtHSP	Mitochondria heat shock protein
MTT	3-(4,5-dimethylthiazol-2-yl)-2,5-diphenyltetrazolium bromide
N/D	Not determined
NAD	Nicotinamide adenine dinucleotide
NADH	Reduced nicotinamide adenine dinucleotide
NES	Nuclear exclusion signal
NFT	Neurofibrillary tangle
NFκB	Nuclear factor kappa B
NGM	Nematode growth medium
NIR	Near infrared
NLS	Nuclear localisation signal
$NO^{\cdot}$	Nitric oxide
NOS	Nitric oxide synthase
NS	Non-significant
OD	Optical density
PAGE	Polyacrylamide gel electrophoresis
PBS	Phosphate buffered saline
PHF	Paired helical filament
PI3K	Phosphoinositide 3-Kinase
PS1	Presenilin 1

PSD	Postsynaptic density
P-tau (S519)	Phosphorylated tau Ser 199/202
Q	Ubiquinone
RCI	Respiratory control index
Redox	Reduction-oxidation
RNA	Ribonucleic acid
RNAi	RNA interference
ROS	Reactive oxygen species
SAPK	Stress activated protein kinase
SDHC	Succinate dehydrogenase complex II
SDS	Sodium dodecyl sulphate
SEM	Standard error of the mean
sHSP	Small heat shock protein
SMAC	Second mitochondrial-derived activator of caspases
SNAP25	Synaptsomal-associated protein 25
SP	Senile plaque
STAT3	Signal transducer and activator of transcription-3
TARP	Transmembrane AMPA regulatory protein
tBID	Truncated BID
TBS	Tris buffered saline
TEMED	Tetramethylethylenediamine
TF	Transcription factor
TGF-β1	Transforming growth factor-β1
TLR	Toll like receptor
TNFR	Tumour necrosis factor receptors
TRAILR1	TNF-related apoptosis inducing ligand receptor 1
TRiC	T-Complex protein 1 ring complex
UV	Ultraviolet

Zn	Zinc
αB Crys	αB Crystallin
$\Delta\psi_m$	Mitochondrial membrane potential

Chapter 1: Literature Review and Aims

1.1 Photobiomodulation and Infrared Light

1.1.1 Electromagnetic Spectrum and Infrared Light

The electromagnetic spectrum, EM, is composed of different categories of light, as shown in figure 1.1. These 'categories' of light differ due to the unique properties of the individual photons which make up each wavelength within these groupings of light. The photons at a specific wavelength possess different properties, both magnetic and electrical, to photons which comprise other wavelengths (Enwemeka, 2004, Hamblin and Demidova, 2006). Wavelengths in the infrared category are longer than wavelengths of visible light and are thus not visible to the human eye.

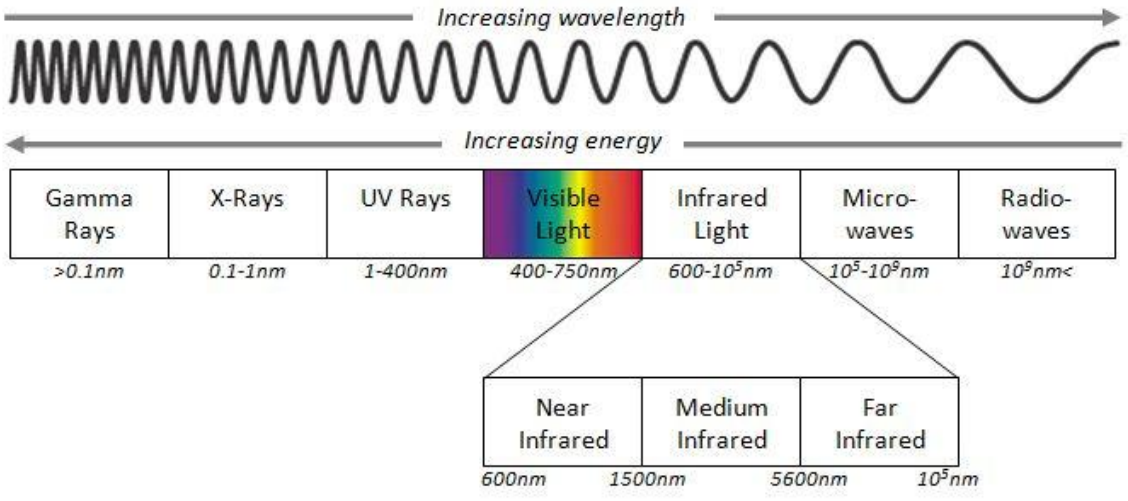

Figure 1.1. Electromagnetic Spectrum of Light, demonstrating the subcategories that infrared light is split into.

Infrared radiation accounts for 40% of the solar radiation that reaches the earth's surface (Frank *et al.*, 2004). Near Infrared (NIR) light, typically defined as 600-1500 nm, has been shown to have a wide range of biological actions and therapeutic benefits. A great deal of research has been undertaken to establish the optimal parameters; whether that be wavelength, fluence, dosage or light source, for optimal biological effect (Laser or LEDs; Hamblin and Demidova, 2006, Tsai *et al.*, 2001).

There are advantages and disadvantages for the use of both lasers and LEDs (Light Emitting Diodes) in the clinical application of NIR to biological tissues. LASERs (Light Amplification by the Stimulated Emission of Radiation) have advantages over LEDs as they are able to specifically emit monochromatic light and typically have an easily tuneable wavelength; whereas LEDs have a typical bandwidth of approximately 25 nm. Lasers have other limitations; they emit a large amount of heat, potentially causing tissue damage, they usually have a small beam width making the treatment of large areas of tissue difficult, as well as a risk of blinding to the user if correct safety measures are not taken (Desmet *et al.*, 2006, Karu, 1999, Whelan *et al.*, 2001, Wong-Riley *et al.*, 2005).

LEDs offer an efficient alternative to lasers; they are easily able to be configured to emit a range of wavelengths, particularly important as some data show combined wavelengths are required for optimal beneficial effects (Whelan *et al.*, 2001). They are also more affordable, portable and are able to be arranged in a variety of array conformations for the treatment of large or complex areas; they produce very little heat and have been reported to penetrate to a depth of approximately 23 cm in human tissue, depending on the use of an appropriate wavelength (Desmet *et al.*, 2006, Whelan *et al.*, 2001, Wong-Riley *et al.*, 2005).

1.1.2 Photobiomodulation

Photobiomodulation is the use of a low energy light source to elicit biological effects. It is also commonly referred to as Low-Level Light Therapy, LLLT, or Low-Intensity Light Therapy, LILT. Following the development of the laser by Theodore Maiman in 1960, a mechanism was available to study the effects of monochromatic, or coherent light, on biological tissues (Enwemeka, 2004).

Work with NIR began in Budapest, Hungary, in 1967 with Endre Mester. Using a laser emitting infrared light, Mester undertook experiments to investigate the effects of the laser on tumour cells in mice. Mester implanted cancer cells underneath the skin of the mice, to determine whether laser stimulation would cause the proliferation or eradication of the cells. Surprisingly, Mester found that following irradiation with his ruby laser, the cells did not form tumours, nor did the irradiation kill the cancer cells. Mester did discover that the incisions made to introduce the cancer cells, healed more quickly in irradiated animals. Also, the dorsal hair removed prior to the incisions grew back at a significantly faster rate in irradiated mice (Enwemeka, 2004, Hamblin and Demidova, 2006).

LLLT is frequently termed as having a ‘biphasic dose response’, whereby levels above or below the optimum exposure conditions result in diminished biological effects, suggesting the magnitude of effect is determined by the fluence, energy density over a given area, of the light therapy. LLLT appears to follow the Arndt-Schulz law, if insufficient energy is applied no effect will be observed, and if too much energy is supplied, ‘bio-inhibition’ occurs (Hamblin and Demidova, 2006, Huang *et al.*, 2009).

An important factor to consider is the potential depth of tissue infiltration by NIR before proposing therapeutic use. Depth of tissue penetration is proportional to absorption and scattering coefficients, which are intrinsically linked to the structure and function of tissues. As LLLT passes through tissue, some will be absorbed by chromophores, this is dependent on wavelength and on the density of chromophores, for example blood-rich tissues absorb more infrared light at certain wavelengths due to high haemoglobin level and some NIR is lost through scattering due to organelles in the cell. Investigation of photon-scattering in a number of tissues from the rat, found that mitochondria content was proportional to the degree of scattering during NIR exposure (Beauvoit *et al.*, 1995). The fact that defined action spectra can be constructed for specific cellular responses confirms light absorption by specific molecular chromophores (Huang *et al.*, 2009).

Spectroscopic data investigating propagation of NIR through human tissue is under investigation. NIR, ranging from 630-800 nm, has been shown to have high tissue penetrability; investigations using muscle in the forearm and calf have shown NIR can travel up to 23 cm through the skin into the muscle tissue. The magnitude of infiltration differs depending on tissue type, wavelength and fluence; a great deal of investigation is still required in this area in order to exploit the full biological effect of LLLT (Beauvoit *et al.*, 1994, Whelan *et al.*, 2001).

In order for LLLT to have biological action in neurodegenerative disorders, it must be able to infiltrate the head. It has been hypothesised that NIR follows an arc of transmission through the human head; with the theory that the light will pass through the scalp, bone, dura and tissues and return to the point of

transmission. Young, 2000, investigated the elliptical transmission of NIR (776.5, 819, 871 and 909 nm) through the human head of patients undergoing elective neurosurgery procedures. Metal probes were fitted to the skulls of patients in two conditions, shown in figure 1.2. The transmission of NIR was investigated at 'baseline' levels, shown on the left, and the manner of layer removal is shown on the right. The experimenters found that the detectable optical density of the light returning to the detector was greatly reduced when the bone was removed (14-fold reduction), and much smaller, but significant, reductions in detected intensity were observed following the removal of the CSF (cerebral spinal fluid) and dura. The experimenters therefore concluded that the skull is able to act as an optical channel, providing a preferential path for NIR to enter the head. These data provide evidence to support the previously held concept that bone is seen as 'translucent' to NIR, with CSF and CBF (cerebral blood flow) acting as useful NIR propagators. Such data suggest that photobiomodulation in these tissues is conceivable and that photons are able to travel sufficiently to penetrate the brain (Okada *et al.*, 1997, Owen-Reece *et al.*, 1996, Young *et al.*, 2000).

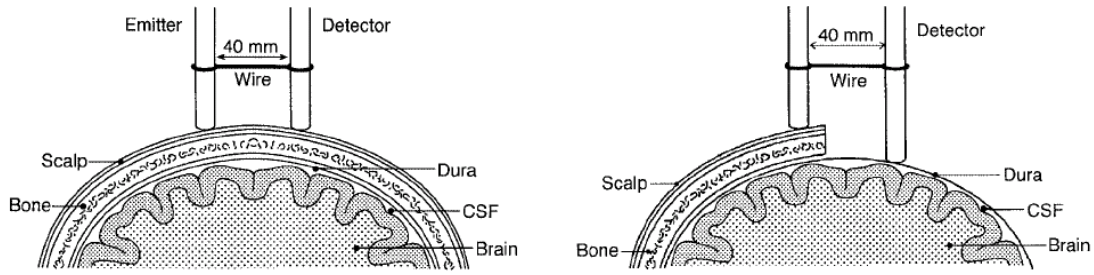

Figure 1.2. NIR emitter and detector settings, indicating how transmission of infrared light was measured through the heads of patients undergoing elective neurosurgery procedures (From Young *et al.*, 2000).

1.1.3 Photoacceptors

In order for any wavelength of LLLT to have a therapeutic effect, photons of that wavelength must be absorbed by a photoacceptor or a molecular chromophore. Chromophores typically occur in one of two forms; metal complexes or conjugated pi electron systems, with examples including haemoglobin, cytochrome *c* oxidase and porphyrins (Gao and Xing, 2009, Hamblin and Demidova, 2006, Huang *et al.*, 2009, Karu, 1999). A second important factor to consider is the diffraction and absorption properties of the tissue which is being irradiated and the overall wavelength in the infrared range. Haemoglobin, the primary photoacceptor in biological tissue; and melanin, have high absorption at wavelengths lower than 600 nm and water absorbs strongly at wavelengths longer than 1300 nm. This resulted in the coinage of the term ‘optical window’ (figure 1.3.), which ranges from approximately 650 – 1200 nm, wavelengths that have low absorption by haemoglobin and melanin and therefore higher tissue propagation. The NIR absorption properties of biological tissues vary considerably depending on the constituents; water, fat, collagen etc., with high water containing tissues typically having an NIR absorption spectra similar to the absorption profile of water (Hamblin and Demidova, 2006, Huang *et al.*, 2009, Karu, 1999, Tsai *et al.*, 2001). Temperature, ion concentration and ion content can also affect intrinsic absorption spectra, but under homeostasis they vary to a typically vary to a very small degree (Tsai *et al.*, 2001). Photoacceptor molecules are believed to act through either directly absorbing the energy of photons, becoming electrically excited and then directly partaking in chemical reactions, or by the transference of energy of the absorbed photon to another molecule, which is then able to induce chemical reactions and ultimately a

biological effect (Karu, 1999). Absorption is likely to occur via internal conversion, the first excited singlet state of the chromophore undergoes a transition to a lower electronic state and this energy is then given off as vibration, causing localised heating and altered biochemical activity (Hamblin and Demidova, 2006, Karu *et al.*, 1995, Karu *et al.*, 1994).

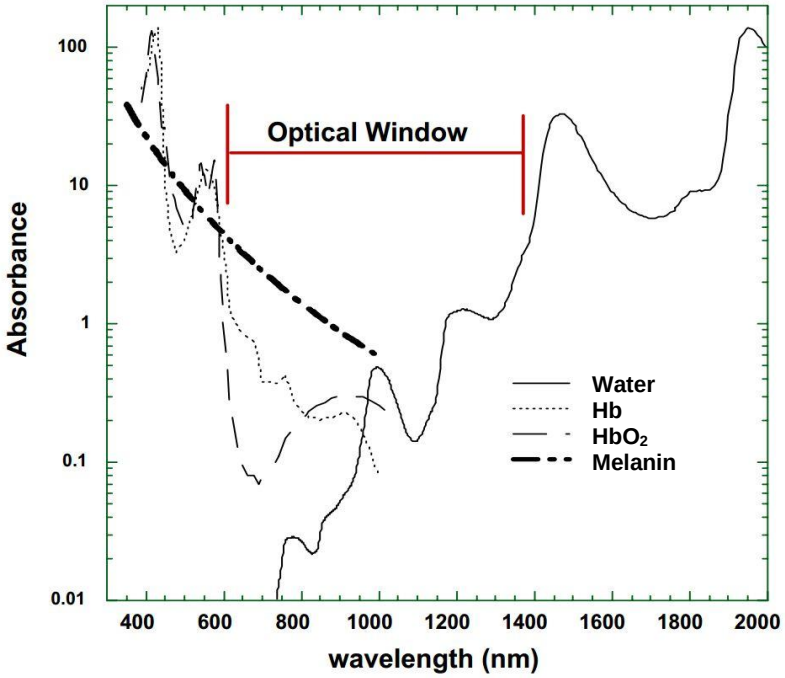

Figure 1.3. Optical Window of Near Infrared Light (Hamblin and Demidova, 2006)

Abbreviations: Hb, Haemoglobin, HbO_2, Oxyhaemoglobin.

1.1.4 Molecular Mechanism of Action - Electron Transport Chain (ETC)

Mitochondria are an important intracellular organelle; they are integral to the cell and the maintenance of cell homeostasis; through involvement in signal transduction, energy production, apoptosis, amino acid, lipid, nucleotide and steroid metabolism. Therefore the manipulation of a single factor within the

mitochondrion can have a dramatic effect on a significant number of cellular processes (Chinnery and Schon, 2003, Nicholls and Budd, 2000).

Mitochondria are composed of an outer membrane which is separated from the matrix by an inner mitochondrial membrane (IMM), which is made up of very small folds called cristae, which increase membrane surface area, with an intermembrane space in between the inner and outer membranes (Scheffler, 2001). Each complex of the electron transport chain is made up of multiple subunits, located at the cristae of the IMM. Each chain comprises of five enzymatic-membrane bound subunits, Complexes I-V, see figure 1.4., through which electrons pass to generate ATP with the help of soluble electron carriers; ubiquinone (Co-enzyme Q) which shuttles electrons from Complex I to Complex II and III, and Cytochrome *c* which transports electrons between Complex III and IV. These carriers are also assisted by iron sulphur proteins (Chinnery and Schon, 2003, Nicholls and Budd, 2000, Ow *et al.*, 2008).

The principle function of mitochondria in actively respiring eukaryotic cells is aerobic catabolism (metabolic reactions that cause the release of energy). This process utilises three stages, the first is glycolysis, which broadly speaking converts glucose into pyruvate. At the second stage, pyruvate dehydrogenase transports the pyruvate into the mitochondrial matrix. Here, one carbon molecule is removed from pyruvate by oxidative decarboxylation, creating acetyl CoA. Acetyl CoA then enters the Kreb's cycle, where it becomes fully oxidised, generating carbon dioxide, water and NADH (reduced nicotinamide adenine dinucleotide). NADH then enters stage three, oxidative phosphorylation (Chinnery and Schon, 2003, Nicholls and Budd, 2000, Scheffler, 2001).

NADH oxidation to NAD (nicotinamide adenine dinucleotide) transfers electrons to Complex I, which is the largest of the ETC components with over 40 subunits. Complex II gains electrons through oxidation of $FADH_2$ (reduced flavin adenine dinucleotide) to FAD (flavin adenine dinucleotide), which are then transferred to ubiquinone. Ubiquinone then carries the electrons to Complex III and Complex III donates the electrons to Cytochrome *c*. These electrons are then moved to cytochrome *c* oxidase, Complex IV, where they are donated to oxygen, generating H_2O, see figure 1.4 (Chinnery and Schon, 2003, Nicholls and Budd, 2000, Scheffler, 2001).

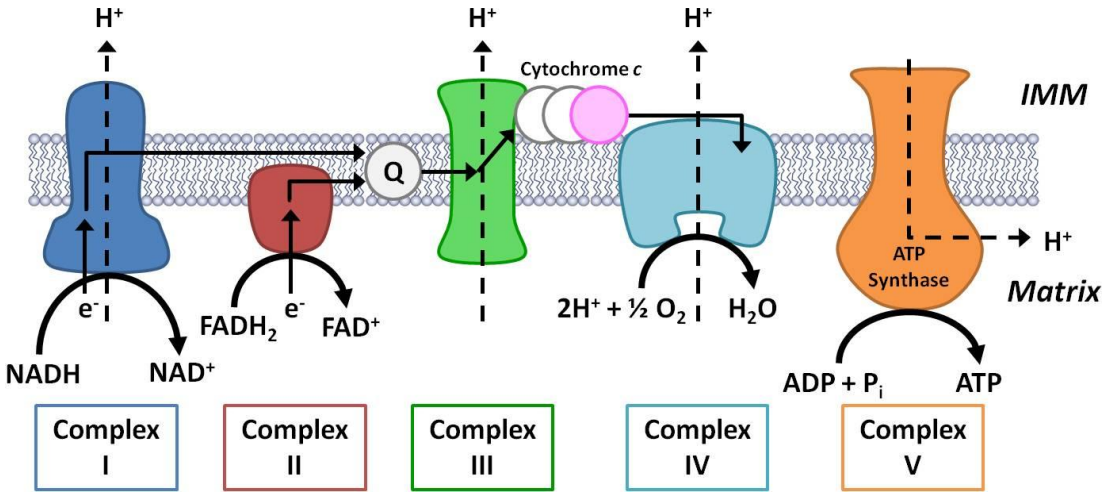

Figure 1.4. The Electron Transport Chain. Complex I (NADH-ubiquinone reductase), Complex II (succinate-ubiquinone reductase), Complex III (ubiquinone-cytochrome *c* reductase), Complex IV (cytochrome *c* oxidase) and Complex V (ATP synthase).

Abbreviations: ADP, adenosine diphosphate; ATP, adenosine triphosphate; e^-, electron; H^+, hydrogen ion, FAD, flavin adenine dinucleotide; NAD, nicotinamide adenine dinucleotide; Pi, Inorganic phosphate; Q, ubiquinone; IMM, inner mitochondrial membrane.

The transfer of electrons through the ETC yields a highly exergonic reaction which enables protons to be pumped out of the matrix, via Complexes I, III and IV, and this generates a mitochondrial membrane potential, $\Delta\psi_m$, which is heavily negative to the cytosol, at approximately 150-180 mV (Duchen, 2004, Nicholls and Budd, 2000). The generation of this proton motive force drives ADP phosphorylation, as protons passively move through the proton pore in Complex V (ATP Synthase) into the matrix (Nicholls and Budd, 2000, Ow *et al.*, 2008). ATP is the energy source for essentially all metabolically active processes in the cell; it is exchanged for ADP by the ANT, adenine nucleotide translocator, and released from the mitochondria into the cytosol (Chinnery and Schon, 2003, Duchen, 2004).

It has been previously reported that mitochondria are sensitive to NIR wavelengths, with up to 50% of NIR absorbed by mitochondrial chromophores, including cytochrome *c* oxidase (Beauvoit *et al.*, 1995, Beauvoit *et al.*, 1994). Absorption of light by cytochrome *c* oxidase has been reported to increase mitochondrial membrane potential, ATP production and reactive oxygen species (ROS) production, all of which can result in induction of signalling pathways and increased energy availability (Reviewed - Gao and Xing, 2009). It has been reported that LLLT increased ATP production and oxygen consumption in mitochondria isolated from the rat, with reports specifically stating that LLLT increased the activity of respiratory chain components, Complex II and cytochrome *c* oxidase and altered proton motive force following LLLT (Passarella *et al.*, 1984, Silveira *et al.*, 2007).

1.1.5 Cytochrome *c* Oxidase – NIR Photoacceptor?

Mitochondrial respiratory chain components are believed to be required for the absorption of red to NIR light. Absorption of NIR, results in changes in the oxidation state of metals within cytochrome *c* oxidase, increasing electron transfer and subsequently increased ROS (reactive oxygen species) production, ATP and/or cAMP (cyclic adenosine monophosphate) levels resulting in the initiation of signalling cascades which are able to promote cell proliferation and cytoprotection. However, cytochrome *c* oxidase is only able to act as the primary photoacceptor for NIR when it is of mixed valence and not when the metals it contains (two copper sites, two haem moieties, and a magnesium and a zinc site, shown in figure 1.5) are fully reduced or fully oxidised (Gao and Xing, 2009, Karu, 1999, Karu *et al.*, 2004, Karu *et al.*, 2005). Action spectra of mitochondria have been determined for specific biochemical reactions. These show which wavelengths of light are absorbed most effectively for a variety of cellular processes, demonstrating absorption of light by a photoacceptor, and which wavelengths are potentially able to modulate processes including DNA and RNA synthesis rates and cell adhesion (Huang *et al.*, 2009, Karu and Kolyakov, 2005, Karu *et al.*, 2005).

Absorption spectra of cytochrome *c* oxidase, in a variety of oxidation states, were found to be analogous to that of a generalised spectrum created by Tiina Karu for a variety of biological materials, including HeLa cells (Karu *et al.*, 2005). It was then discovered that the transfer of electrons between metals complexed within the cytochrome *c* oxidase, altering the oxidation state of these metals, was responsible for different peaks in the action spectra, metals are shown in figure 1.5. However, the upper limit of the wavelengths examined was

860 nm, therefore critical information regarding the role of cytochrome *c* oxidase in the absorption of infrared light at 1072 nm is unavailable and it is difficult to draw conclusions regarding absorption of IR1072, the wavelength used in this investigation (Hamblin and Demidova, 2006, Huang *et al.*, 2009, Karu *et al.*, 2004, Karu *et al.*, 2005). During respiration, the pair of Cu_A residues of cytochrome *c* oxidase accept electrons from the cytochrome *c* molecule, where internal electron transfer between Cu_A and haem a (Oxidised Cu_A accepts at 825 nm, reduced Cu_A accepts at 620 nm), and the haem a_3-Cu_B centre (Oxidised Cu_B accepts at 680 nm, reduced Cu_B accepts at 760 nm) utilises a minimum of seven redox intermediates to reduce molecular oxygen (Gao and Xing, 2009, Karu, 1999, Karu *et al.*, 2005).

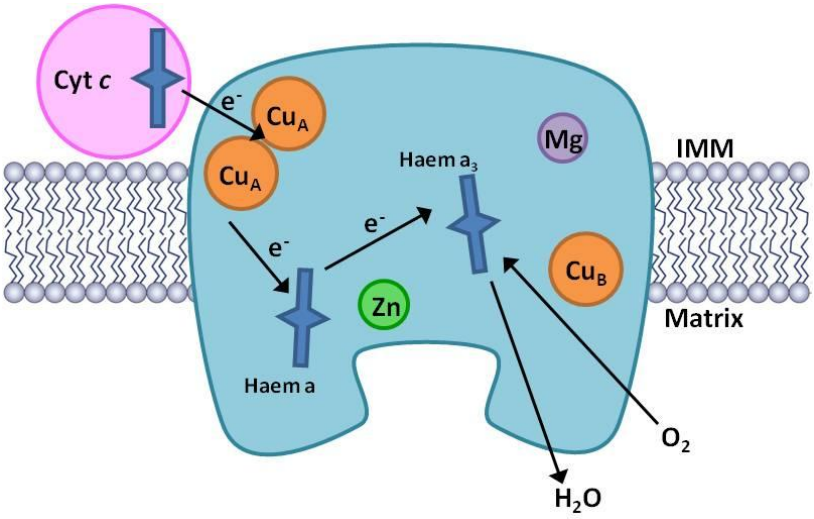

Figure 1.5. Structure of Cytochrome *c* oxidase, denoting how electrons are transferred between metal residues and donated to molecular oxygen to generate water. Adapted from (Karu, 1999). Abbreviations; Cyt *c*, Cytochrome *c*; Cu, copper; e^-, Electron; IMM, inner mitochondrial membrane; Mg, magnesium; Zn, zinc.

It has been postulated that the electron transfer between haem a and haem a_3-$Cu_{B,}$ normally the rate limiting step of respiration, is sped up during LLLT and this makes more electrons available to reduce molecular oxygen (Karu *et al.*, 2005). This may occur through structural changes in cytochrome *c* oxidase following NIR absorbance (Karu *et al.*, 2004)

Uncoupled mitochondria do not show sensitivity to LLLT, nor does purified cytochrome *c* oxidase, suggesting an intact electron transport chain is required for absorption of NIR. Indeed, beneficial effects of NIR can be attenuated by the use of the potent cytochrome *c* oxidase inhibitor, potassium cyanide (Karu *et al.*, 2005). Frank *et al*. (2004), reported that IR (700 - 4000 nm) was able to induce cytochrome *c* release from the mitochondria; however IR exposure was found not to disrupt the mitochondrial membrane and release did not result in activation of caspases or caspase-independent cell proteins which normally drive cell death following cytochrome *c* release (detailed in section 1.3.2). The recorded partial release of cytochrome *c* oxidase, without deleterious effects, suggests IR is capable of mobilising loosely-bound cytochrome *c* that is sensitive to electrostatic changes. Release of cytochrome *c* oxidase may occur due to transient opening of mitochondria permeability transition pore (MPTP) due to calcium release (detailed in 1.1.6). This release triggers upregulation of pro-apoptotic proteins, including BAX (BCL2 associated athanogene), in the short term, but was shown to be swiftly followed by the increased expression of anti-apoptotic proteins Bcl-2 (B-Cell Lymphoma 2) and BCL-X_L (B Cell Lymphoma-Extra Large) over a longer time period. High levels of these anti-apoptotic proteins are able to temporarily reduce $\Delta\Psi m$, leading to a more reduced state of the cell and potentially leaving the cell more sensitive to further

irradiation (detailed in 1.1.6). As the ΔΨm returns to normal, anti-apoptotic proteins were shown to accumulate, resulting in a cell more resistant to stress. This release of cytochrome *c* has been shown to occur in a number of cell types, including human dermal and lung fibroblasts (Frank *et al.*, 2004).

1.1.6 Secondary Effects – Cell Signalling

The magnitude of the secondary biological effects are dependent upon the redox state of the tissue that is being irradiated, cells with a more reduced state are more sensitive to irradiation as reduced forms of cytochrome *c* oxidase promote electron transport. This increase in activity has a potential downside, with a higher rate of electron flow, the likelihood of superoxide anion production increases. This would in turn result in increased hydrogen peroxide levels and other free radicals, an increase in pH and cause the release of calcium, amongst other processes. However, in relatively small concentrations, the combination of these molecules are capable of modulating the redox state of the cell and potentially perpetuating any biological effects via this apparent mitochondrial-nuclear retrograde signalling (Butow and Avadhani, 2004, Gao and Xing, 2009, Hamblin and Demidova, 2006, Karu, 1999, Karu, 2008, Karu *et al.*, 2005). Signalling is believed to be a two part reaction; with primary redox changes increasing electron transfer which is followed by secondary ‘dark’ biochemical reactions inducing cell signalling (Karu *et al.*, 2004).

Several signal transduction pathways have been implicated in the therapeutic effects of LLLT; including ERK (extracellular signal-regulated protein kinase), MAPK (mitogen associated protein kinase), PI3K (phosphoinositide 3 kinase)

and even ATP-related signalling pathways (For a review of these data see Gao and Xing, 2009). Examples of mitochondrial retrograde signalling pathways initiated following LLLT are shown in figure 1.6.

ATP has recently received attention as a signalling molecule, in addition to acting as an energy source. Even small changes in ATP can significantly alter cellular metabolism. The discovery of specific receptors for ATP, P_2 family of receptors, and receptors for its final breakdown product, adenosine, P_1 receptor family, enabled further understanding of intercellular communication. Binding of ATP to P_{2X} receptors forms a channel for Na^+ and Ca^{2+} to enter the cell and binding to P_{2Y} receptors triggers intracellular cascades, releasing internal calcium stores. Altered calcium and ROS levels within the mitochondria would also have impact on mitochondrial membrane potential, thus mitochondrial activity, mitochondrial proliferation, and ultimately ATP production via a mitochondrial-nuclear retrograde signalling mechanism, see figure 1.6 (Karu, 2010a, Karu, 2008, 2010b, Khakh and Burnstock, 2009).

Mitochondria also play an important role in calcium storage and release; the organelles are able to accumulate Ca^{2+}, which can be important for protecting the cell when cytosolic levels rise to critical concentrations. Alterations in Ca^{2+} concentrations have also been reported following LLLT; increased levels of intracellular Ca^{2+} have been reported in hepatocytes and mast cells with intramitochondrial levels reported to be three to eight times greater following NIR (Reviewed - Butow and Avadhani, 2004, Karu, 2008, Scheffler, 2001). Sustained increased levels of Ca^{2+} in the mitochondria has been shown to have both a direct impact on the Krebs cycle (stage effected depends on the cellular location of the free calcium; Wan *et al.*, 1989), $\Delta\psi_m$, and thus indirectly on the

pool of available ATP/ADP. Ca^{2+} is believed to be the principal effector of the mitochondrial-retrograde signalling mechanisms, see figure 1.6. Disruption of ΔΨm causes the release of Ca2+ cytosolically, increasing the intracellular concentration and therefore increase activities NF-κB (nuclear factor κB), a number of kinases, amongst other signalling pathways for the cell ultimately leading to activation of nuclear genes (Butow and Avadhani, 2004, Karu, 2008, Nicholls and Budd, 2000).

Increased intramitochondrial Ca^{2+} can trigger the opening of the MPTP, directly or indirectly as a result of altered ΔΨm. This can cause the release of calcium and protons into the cytosol which lead to membrane depolarisation. In a transient 'spike' opening manner this is beneficial to the cell and the principal mechanism through which NIR initiates its response. The involvement of MPTP in LLLT may explain why previous reports have shown cytochrome *c* release following NIR without deleterious effects (Frank *et al.*, 2004, Nicholls and Budd, 2000).

Production of ROS has also been a reported secondary signalling molecule following LLLT. ROS at high levels can be detrimental, but its production is a normal by-product of respiration. It is estimated that between 2-5% of electrons that pass through the ETC actually leak from brain mitochondria and result in the production of ROS, including hydrogen peroxide and superoxide anions (Hurtado *et al.*, 2003). A shift in cellular redox state towards oxidation following LLLT results in increased ROS production (Hamblin and Demidova, 2006, Huang *et al.*, 2009). ROS has the capability to modulate a range of cellular processes, including protein synthesis and nucleic acid production. ROS has been shown to have influence over a range of transcription factors; including

NF-κB (nuclear factor κB), AP-1 (activator protein-1), Ref-1 (redox factor-1), CREB (cAMP response element binding protein) and p53 (Reviewed - Hamblin and Demidova, 2006, Huang *et al.*, 2009). ROS can also activate TNFα and vice versa, the initiation of such factors is thought to be responsible for a number of the secondary effects observed following LLLT (Brookes *et al.*, 2002).

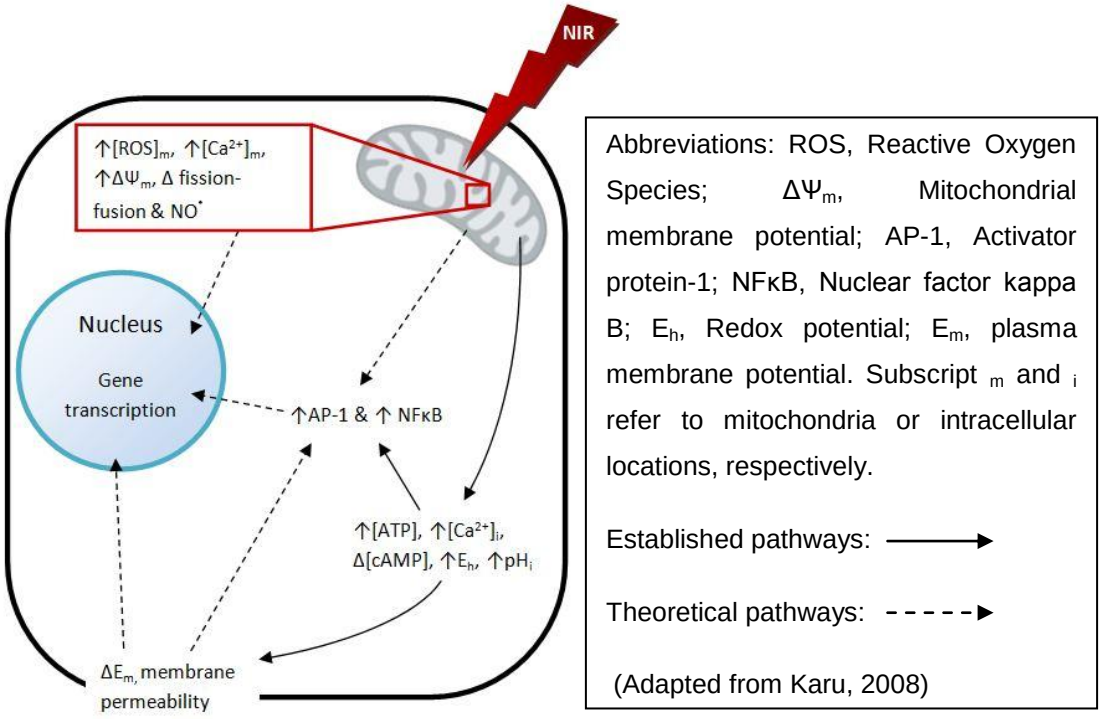

Figure 1.6. Putative mitochondrial retrograde signalling pathways believed to be initiated following LLLT.

$NO^{\cdot}$ and N_3 are widely reported physiologic modulators of cytochrome *c* oxidase activity and thus important regulators of intra-mitochondrial signalling. $NO^{\cdot}$ is able to competitively bind cytochrome *c* oxidase, dislodging oxygen and to a degree inhibiting respiration in stressed cells. $NO^{\cdot}$ is also able to prevent increasing levels of free radicals, including hydrogen peroxide, by inhibiting

respiration. Cytochrome *c* oxidase shares responsibility for ATP production with other oxidative phosphorylation machinery, and rarely has more than 20% control over respiratory activity (Reviewed - Brookes *et al.*, 2002, Karu, 2008, Karu *et al.*, 2004). Notably, NIR at 670 nm was able to reverse the inhibition of cytochrome *c* oxidase of nitric oxide occupying the oxygen binding site (Trimmer *et al.*, 2009, Zhang *et al.*, 2009). Binding of $NO^{\cdot}$ to cytochrome *c* oxidase has been shown to induce ROS production in the mitochondria and initiate signalling pathways; it is thought that increased $NO^{\cdot}$ levels may also be able to initiate signalling through altering the $\Delta\psi_m$ (Butow and Avadhani, 2004, Karu, 2008). A proposed overall mechanism of action is shown in figure 1.7.

1.1.7 Experimental Findings

Photobiomodulation or LLLT, has also been reported to have beneficial effects in reducing the oxidative stress associated with diabetes in an animal model of the disease (Henshel *et al.*, 2009, Tsai *et al.*, 2001), restorative action towards axonal transport deficits seen in Parkinson's disease through increasing ATP (adenosine triphosphate) levels and mitochondrial velocity (Trimmer *et al.*, 2009), as well as accelerating wound healing and tissue regeneration (Desmet *et al.*, 2006, Medrado *et al.*, 2008, Whelan *et al.*, 2001). LLLT has also been reported to protect against retinal toxicity (Desmet *et al.*, 2006, Eells *et al.*, 2003) and protect against apoptosis of visual cortical neurons (Liang *et al.*, 2006). Of a large range of wavelengths that have been tested *in vitro* and *in vivo,* the most beneficial and effective wavelengths parallel the absorption spectra of cytochrome *c* oxidase, which peaks at 670 and 830 nm and

beneficial effects are observed at doses ranging from 1-6 J/cm^2 (Hamblin and Demidova, 2006). LLLT has been found to modulate the expression of a range of genes which control critical cellular functions, including DNA (deoxyribonucleic acid) repair proteins, molecular chaperones, trafficking and degradation driving proteins, antioxidant enzymes and proteins that drive cell growth and maintenance (Desmet *et al.*, 2006).

Neurite outgrowth, neuronal maturation and protection against oxidative stress have all been demonstrated to occur in PC12 cells following NIR exposure at 670 nm (Giuliani *et al.*, 2009). In an *in* vitro model of Alzheimer's disease, NIR at 670 nm has also been found to reduce the quantity of β-amyloid aggregates in HeLa neuroblastoma cells, clearance which occurred at the expense of a great deal of cellular ATP although the direct mechanism remains unclear. This study also found the NIR at 670 nm was able to facilitate in the uptake of drugs into the HeLa cell line. The study also reported increased levels of ATP in the absence of β-amyloid. These data provide an interesting new therapeutic angle of functional interplay, as well a mechanism to explore potential synergistic effects of NIR and drugs for the treatment of neurological disorders (Sommer *et al.*, 2012).

Medrado (2008) investigated the effects of LLLT on connective tissue remodelling during the healing of subcutaneous wounds in the rat. The research found that laser irradiation at 670 nm improved the differentiation and deposition of collagen fibres, resulting in more efficient re-establishment of the appropriate tensile strength and fibre organisation in healed tissue, when compared to control treated wounds (Medrado *et al.*, 2008).

Whelan, 2001, reported significant therapeutic effects of NIR on wound healing. Using LLLT with combined wavelengths (670, 728 and 880 nm), skin-based wound healing rates increased by 50% and skeletal muscle-based wounds increased by 40% in human subjects, with up to 200% increases in cell growth reported in mouse fibroblasts, rat osteoblasts, rat skeletal muscle cells, and human epithelial cells that were exposed to the combined wavelengths. These data suggest that there is a great deal of potential to optimise the parameters of LLLT to promote wound healing in a number of tissues. Alterations in electron transport chain activity have been reported by Silveira *et al.* (2007) following NIR. The researchers were investigating the effect of NIR for 10 days on the rate of wound healing in rats. They found that LLLT resulted in wound healing occurring faster than in control treated animals, and irradiation at 904 nm, dose per session of 3 J/cm^2, not only increased the activity of cytochrome *c* oxidase (Complex IV), but for the first time increased Complex II (Succinate-Ubiquinone Reductase) activity were also reported. No change in the levels of soluble succinate dehydrogenase was reported, confirming tight coupling of the mitochondria membrane following irradiation, further supporting the consensus of mitochondrial involvement in photobiomodulation (Silveira *et al.*, 2007). Additionally, increased ATP production, mitochondrial membrane potential and proton gradient were all reported following irradiation of isolated liver mitochondria from Wistar rats exposed to 633 nm. The authors propose that absorption of NIR by the mitochondria increases the proton motive force, and this drives an increased level of ATP production (Passarella *et al.*, 1984).

Investigations of NIR at 830 nm have also reported increased ATP production in the rat brain. Through holes made in the skull, an area of the cerebral cortex

was irradiated whilst the animals were anaesthetised. It was found that a 15 minute irradiation period was sufficient to significantly increase the concentration of ATP determined to be in the tissue, with no significant alteration in ADP (adenosine diphosphate) levels. Interestingly, 15 minute irradiation at 652 nm had no effect on ATP or ADP levels (Mochizuki-Oda *et al.*, 2002), emphasising the importance of wavelength choice.

A single exposure of 40 seconds at 810 nm was able to restore the sporadic axonal transport in Parkinson's disease cybrid neurites to that of control levels. LLLT was also found to restore mitochondrial mobility, something reported as essential for neuronal survival (Trimmer *et al.*, 2009). Due to their high metabolic rate, neurons require a large, continuous supply of ATP which is sourced through the electron transport chain within the mitochondria. However, mitochondria are not static and are transported around the cell to where they are required via microtubule-based anterograde transport, but this process itself is dependent on ATP. The compromise of this transport mechanism may underlie the progressive loss of neurons associated with neurodegenerative disorders, such as Alzheimer's disease and Parkinson's disease, as without normal mitochondrial fission, fusion and movement; neurons are unable to survive (De Vos *et al.*, 2008, Mattson and Liu, 2003).

Investigations have also noted that the more protective wavelengths parallel the action spectra of more oxidised cytochrome *c* oxidase which had been previously reported (Karu, 1999). Photobiomodulation at 670 nm using LEDs has also been shown to directly protect neurons against exposure to toxins; moreover, particular wavelengths were more effective than others (Wong-Riley *et al.*, 2005). Investigations with NIR and visual cortical neurons also found a

protective effect. Pre-treatment of the visual cortical neurons with LEDs emitting 670 nm reduced apoptosis by up to 50% when the neurons were exposed to potassium cyanide, demonstrating potassium cyanide and NIR compete for cytochrome *c* oxidase. Liang *et al*. (2006) proposed the mechanism of this protection was via prevention of caspase-driven apoptosis; utilising reduced ROS (reactive oxygen species) levels and down-regulation of pro-apoptotic proteins, together with upregulation of anti-apoptotic proteins (Liang *et al.*, 2006). Further work using 670 nm by Eells *et al.,* (2003), found that three brief exposures (144 seconds in total) was able to dissipate the toxicity of methanol-derived formate, a toxin detrimental to mitochondria, which induces damage to the retina. Mitochondrial dysfunction/damage is believed to be a significant factor in ocular disease/injury; these data suggest LLLT may be of therapeutic benefit in such conditions (Eells *et al.*, 2003). Microarray analysis has shown 670 nm exposure can directly induce upregulation of a number of genes which are expressed in pathways involved in mitochondrial energy production (Eells *et al.*, 2004, Giuliani *et al.*, 2009).

LLLT has also been shown to protect human fibroblasts from UVB (Ultraviolet-B) toxicity; this effect was accompanied by alterations in mitochondrial membrane potential, partial cytochrome *c* release, and increased expression of HSP27, an established inhibitor of apoptosome formation (detailed in section 1.3.2.; Frank *et al.*, 2004).

The majority of these studies report an increase in mitochondrial membrane potential; some report an increase of up to 30% (Reviewed -Karu, 2008), accompanied by heightened ATP and ROS production, Complex II and Cytochrome *c* oxidase (Complex IV) activity (Desmet *et al.*, 2006, Gao and

Xing, 2009, Silveira *et al.*, 2007, Tsai *et al.*, 2001, Wong-Riley *et al.*, 2005), and some even report increased mitochondrial velocity (Trimmer *et al.*, 2009) following NIR exposure. The magnitude of the effect of NIR on mitochondria depends on the wavelength used and how this wavelength correlates to the action spectra of cytochrome *c* oxidase, for example LLLT at 725 nm which does not correlate to a peak in the action spectra, has actually been shown to result in decreased ATP production, further signifying the importance of wavelength selection to elicit therapeutic benefit (Gordon and Surrey, 1960).

1.1.8 Applications and Therapeutic Effects of IR1072

The strong absorption of NIR at long wavelengths by water generally limits the infiltration of light into deep tissue. NIR at 1072 nm represents a peak in the transmission of the infrared spectrum through the water molecule, therefore NIR at 1072 nm requires less energy and less intensity to safely enter biological matter, without causing thermal stress, than wavelengths 1300 nm and beyond (Bradford *et al.*, 2005, Burroughs, 2010, Tsai *et al.*, 2001).

A recent clinical trial conducted by Dougal & Kelly, found that a single five minute exposure to IR1072 significantly reduced the healing time of *herpes labialis* flair-ups by four days for patients, when compared to treatment with acyclovir five times daily. The clinicians do not propose a mechanism of action for this improved recovery time but do also state that the NIR did not appear to attenuate the virulence of the *herpes labialis;* it is therefore possible that the LLLT may be affecting the integrity of the cell membrane. The more resistant the cell membrane, the greater difficulty the virus will have in infecting cells and

in doing so an enhanced local immune response could be mounted (Dougal and Kelly, 2001).

Experiments conducted by our group (Bradford *et al.*, 2005), demonstrated protective action of IR1072 on lymphocytes isolated from human whole blood that were subsequently exposed to UVA (Ultraviolet-A). This study showed that exposure of lymphocytes to IR1072 provided a rapid and long-lasting protective effect, possibly elicited through iNOS (inducible Nitric Oxide Synthase) upregulation, a rapidly produced, easily diffusible signalling molecule which does not require the presence of calcium for activity. The study also reported that upregulation of iNOS levels occurred in a wavelength-dependent manner; with IR1072 the only wavelength demonstrating a significantly increased level of expression (660, 880, 950 and 1267 nm were all also tested). This is particularly important as iNOS is believed to play a role in the prevention of apoptosis via prevention of the activation of or by inhibiting caspase-3-like proteases (Bradford *et al.*, 2005). Our group has also demonstrated that six minute exposures to IR1072 for 10 consecutive days had no detrimental effect on anxiety or exploratory behaviour in CD-1 mice (4 months and 12 months of age) in a 3D radial maze test; a strain which develops premature learning deficits (Ennaceur *et al.*, 2008, Michalikova *et al.*, 2008). The working memory of middle-aged (12 month) CD-1 mice was actually found to significantly improve following IR1072 exposure. Furthermore, the middle-aged IR treated mice showed the most beneficial effect in the ‘acquisition phase’ of the behavioural experiment, with more consideration taken over decision making, resulting in a cognitive performance similar to that observed in young (4 month) CD-1 mice (Michalikova *et al.*, 2008). The use of IR1072 as a treatment for Alzheimer’s

disease was investigated with recruitment of patients initiated in December 2010 (double-blind, placebo-controlled clinical trial). The results of these trials will enable statistically valid conclusions to be drawn, sanctioning the use of IR1072 in a clinical neurological setting.

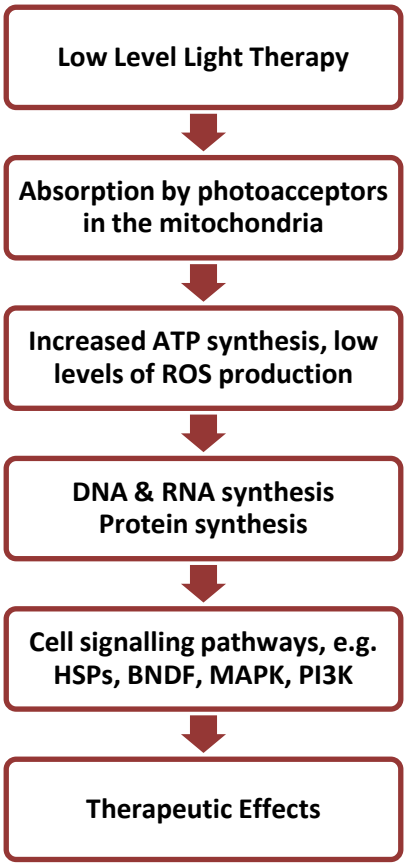

Figure 1.7. Proposed overall mechanism of action. Abbreviations: ATP, adenosine 5' triphosphate; BDNF, brain-derived neurotrophic factor; DNA, deoxyribonucleic acid; HSP, heat shock protein; MAPK, mitogen-associated protein kinase; PI3K, phosphoinositide 3-kinase; RNA, ribonucleic acid; ROS, reactive oxygen species.

1.1.9 Experimental Limitations - Questions relating to the use of LLLT clinically

A range of wavelengths are currently in use clinically; longer wavelengths (up to 1300 nm) have deeper tissue infiltration distances and shorter wavelengths (typically around 600 nm) are used for more superficial tissue treatments. It has been reported that a combination of wavelengths may have an additive effect which could prove useful in treating complex disorders. However, there remains a great deal of work to do to define the optimal parameters for NIR in particular conditions (Hamblin and Demidova, 2006). LLLT is currently applied to a diverse range of clinical situations; including wound healing and treatment of *herpes labialis*, using a varied assortment of wavelengths and parameters, light sources, and treatment protocols. However, despite mechanistic questions, a significant limitation to the progression of LLLT into conventional medical practice is the lack of adequately controlled clinical trials. The reported biphasic dose-response that is commonly observed with NIR treatment of biological tissue also raises the question of dosage. The fluence of NIR and the total energy conveyed differ greatly between studies, as do the reported effects of pulsed or continuous wave light. Work to further understand the best boundaries for using NIR as a clinical treatment need to be investigated.

1.2 Alzheimer's disease

Alzheimer's disease is the leading cause of dementia in the world, it is a progressive dementia characterised by the deposition of β-amyloid (Aβ), found in large extracellular structures known as senile plaques (SPs), which are

thought to induce toxicity through affecting the stability of the cell membrane and therefore reducing synaptic transmission (Kamenetz *et al.*, 2003) and impairing synaptic plasticity (Shankar *et al.*, 2008). Aβ also acts intracellularly as small oligomers, which are believed to be the more toxic Aβ structure. Oligomers of Aβ are thought to dissociate from large SPs, move into the cell and, as their structure has exposed hydrophobic moieties, and sequester proteins essential for cell homeostasis. Senile plaques are thought to act as pools of 'available' Aβ with oligomers able to dissociate and cause neuronal death at locations away from their originating SP. SPs have also been shown to be a magnet for free metals and aggregates, exacerbating their toxicity to neurons within their vicinity.

Aβ was first purified in 1984 by Glenner & Wong, who identified the substance as a 4.2 kDa peptide, composed of 40 or 42 amino acids but it wasn't until 1987, when Kang *et al.* cloned the amyloid precursor protein, that Aβ was established as a cleavage product of a larger protein, although this was previously hypothesised to be the case (Glenner and Wong, 1984, Kang *et al.*, 1987). The exact physiological function of APP remains unclear, although roles have been established in synaptic pruning, neuronal plasticity and synaptic physiology/processing (Abramov *et al.*, 2009, Kamenetz *et al.*, 2003, O'Brien and Wong, 2011). Over expression appears to have a positive effect on cell growth and health. Deletion of APP doesn't induce a severe phenotype, but mice 'fail to thrive' (O'Brien and Wong, 2011, Zheng *et al.*, 1995). APP is a ubiquitously expressed single transmembrane domain protein, APP can be cleaved following the α-secretase pathway, which does not generate Aβ, or via the β-secretase pathway which does generate Aβ (Reviewed - Hardy, 1997). In

order to produce Aβ, APP is sequentially cleaved by β-secretase and γ-secretase, depending on where APP is cleaved determines the length of fragment created. Cleavage by γ-secretase can produce a number of Aβ variants, including $Aβ_{37}$, $Aβ_{38}$, $Aβ_{40}$, $Aβ_{42}$ and $Aβ_{43}$, with $Aβ_{40}$ and $Aβ_{42}$ the most common (subscript number denoting the amino acid length; Reviewed - Benilova *et al.*, 2012, Hardy, 1997, O'Brien and Wong, 2011). γ-secretase is crucial for the sequential intramembranous cleavage of a number of transmembrane proteins, and itself is comprised of presenilin 1, presenilin 2, nicastrin and two transmembrane proteins (Bergmans and De Strooper, 2010).

The pathology of sporadic AD is very similar to that of autosomal dominant AD and there have been a number of mutations identified in the APP gene which act to alter the β- or γ-secretase cleavage site and mutations in Presenilin genes which alter the amino acids in their transmembrane domains. There are other genetic mutations that attribute risk to the development of late onset AD, including the presence of the APOE (apolipoprotein) ε4 allele (other non-risk associated variants of APOE are ε2 and ε3) which is believed to be present in up to 70% of sporadic AD in aged individuals, with Apoε4 reducing Aβ clearance and increasing Aβ deposition (Avramopoulos, 2009, Huang and Mucke, 2012, O'Brien and Wong, 2011).

In the disease state, production of the aggregation prone $Aβ_{42}$ is increased (it accounts for approximately 5% of Aβ generated in the physiological state) and its levels can be elevated through mutations in the aforementioned genes, while reduced clearance can arise from lessened expression of factors responsible for its removal, such as HSPs and IDE (insulin degrading enzyme; Gandy, 2005) and reduced clearance across the blood brain barrier. Aβ oligomers can

cause aberrant neuronal network communication, synaptic dysfunction and alter related signalling pathways, leading to impaired LTP (long term potentiation). The presence of Aβ leads to altered neuronal activity and can cause excitotoxicity, via impairing interneurons, stimulating glutamate receptors and causing release of neurotoxic intermediates from adjacent glial cells (Benilova *et al.*, 2012, Gandy, 2005, Haass and Selkoe, 2007, Hardy, 1997, Huang and Mucke, 2012, LaFerla, 2010, O'Brien and Wong, 2011). As well as accumulating cellular proteins and free metals as mentioned previously (Kamenetz *et al.*, 2003, Shankar *et al.*, 2008), the formation of fibrillar amyloid senile plaques causes distortion and displacement of neuronal processes. Deposition of Aβ can also occur vascularly, resulting in impairment of nutrient supply and waste product removal. This in turn can cause infarcts, activate microglia and exacerbate existing excitotoxicity. An overview of these mechanisms is shown in figure 1.8 (Huang and Mucke, 2012).

Another key characteristic is the presence of NFTs, which are primarily intracellular structures, composed of hyperphosphorylated tau. Phosphorylation of tau results in its dissociation from the microtubule cytoskeleton, ultimately destabilising the neuron and these tangles then commandeer fundamental proteins and intracellular Aβ (Benilova *et al.*, 2012, Fandrich *et al.*, 2011, Guo and Lee, 2011, Haass and Selkoe, 2007, LaFerla, 2010). Tau is a microtubule associated protein which a significant role in the outgrowth of neuronal processes, stabilisation of microtubule and their dynamics. Tau is abundantly expressed in the CNS, principally in axons and is also required for membrane interactions and axonal transport of organelles to and from terminal boutons (Ittner and Gotz, 2011, Reddy, 2011). The loss of cytoskeletal associated tau

also results in the reduced transport of mitochondria, resulting in defective mitochondria function; increased ROS and decreased ATP production, and in itself exacerbating neuronal damage (Eckert *et al.*, 2011, Reddy, 2011, Schmitt *et al.*, 2012).

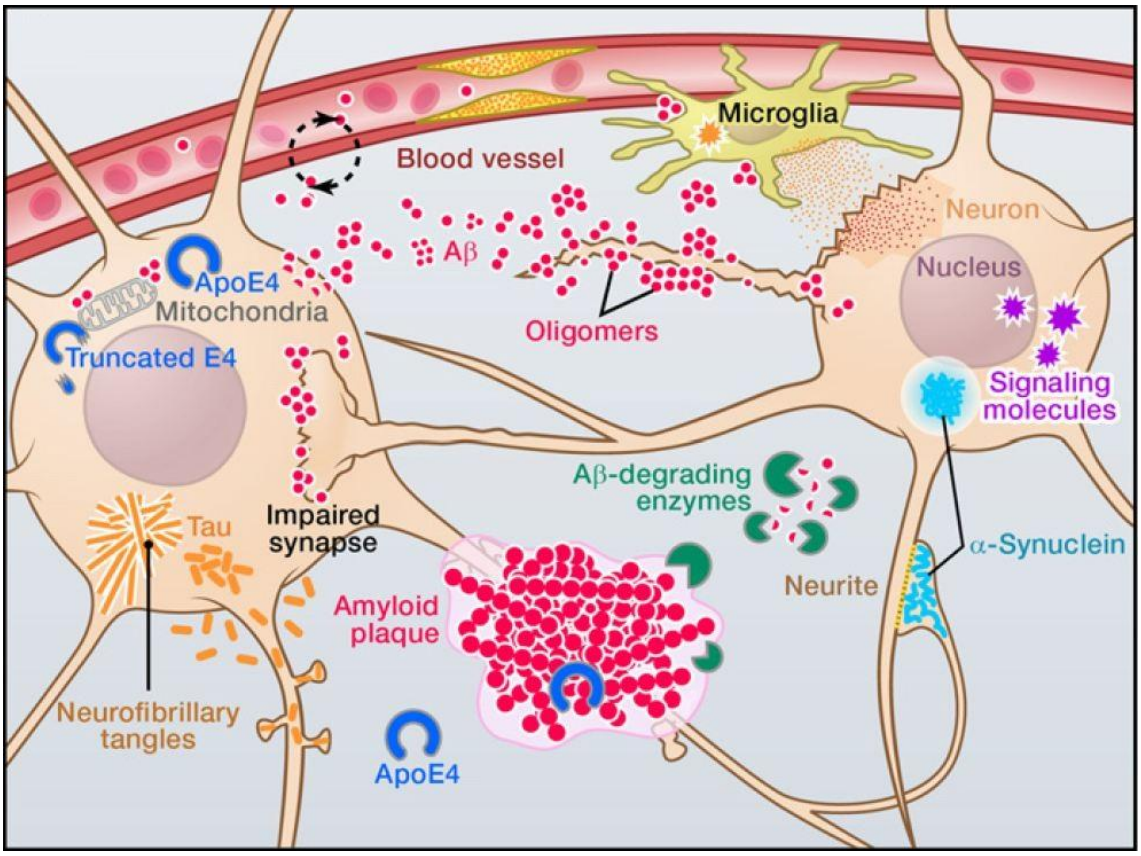

Figure 1.8. Complex basis of Alzheimer's disease. Accumulation and aggregation of Aβ, shown in pink, may result from reduced clearance, lower levels of degrading enzymes or increased Aβ production. Aβ plaques disrupt neuronal processes and Aβ oligomers impair synaptic function, both altering neuronal activity and triggering release of neurotoxic substances. Apoε4 increases Aβ deposition and reduces its removal; it also acts to impair mitochondrial activity and stability of the cytoskeleton. Tau becomes phosphorylated, mislocalised to dendrites and begins to form NFTs. P-Tau can be released extracellularly, affecting adjacent neurons (Figure obtained from Huang and Mucke, 2012).

The neuronal loss associated with Alzheimer's disease is not specific to one type of neurotransmitter; serotonergic, cholinergic, dopaminergic, noradrenergic and peptide neurotransmitter systems are all affected, but neuronal loss does appear to be anatomically determined (Hardy and Allsop, 1991, Pearson and Powell, 1989). The onset of memory impairment is one of the earliest symptoms of Alzheimer's disease, this is followed by language impairment and once the substantia nigra and striatum become damaged in the latter stages of disease, motor dysfunction (hypertonic-hyperkinetic syndrome) becomes apparent (Reviewed - Braak and Braak, 1991, 1995, Braak and Braak, 1997, Forstl and Kurz, 1999, Hardy and Allsop, 1991). Braak & Braak, 1991, defined six stages of Alzheimer's disease progression, each distinguishable by location of amyloid and NFT deposition and the severity of that deposition, a summary of which is shown in figure 1.9.

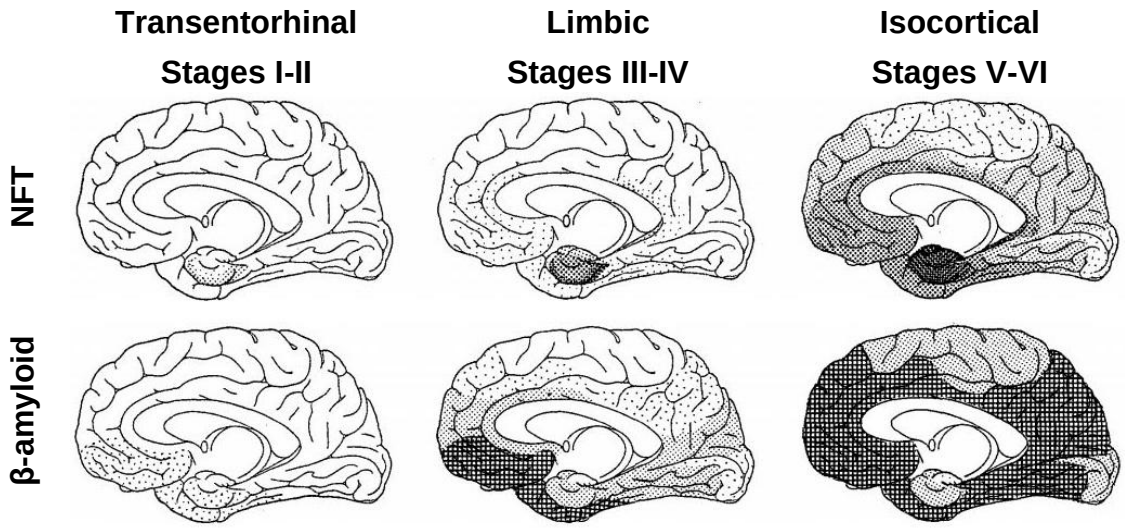

Figure 1.9 Distribution of amyloid and tau neurofibrillary tangles in Alzheimer's disease. Shading represents density/severity of deposition. (Figure modified from Braak and Braak, 1991).

The initial, clinically silent, transentorhinal stages I-II are characterised by development of intraneuronal lesions found in poorly myelinated areas of the neocortex and typically these changes do not contain amyloid deposits. Stages III-IV involve the limbic system, with the entorhinal, transentorhinal regions and the hippocampus affected. Amyloid deposition becomes apparent, starting in the CA1 (cornu ammonis) region and radiating throughout the hippocampus. The extent of damage that occurs at this stage results in the appearance of clinical symptoms, as the limbic region is crucial in the conversion of sensory information to memories. Stages V-VI are characterised by profound destruction of the all sections of the cerebral cortex by the presence of NFTs, SPs and amyloid, deposits also apparent in the striatum, hypothalamus and thalamic nuclei (Braak and Braak, 1991, 1995, 1997). Stages V-VI signify fully developed Alzheimer's disease, with patients demonstrating impaired motor skills and long term memory, as well as behavioural changes including aggression, apathy and loss of vocabulary (Reviewed - Forstl and Kurz, 1999, Hardy and Allsop, 1991).

Despite Alois Alzheimer first publishing the histological pathology of this dementia in 1907, a great deal remains unknown about the pathology of the disease (Balducci and Forloni, 2011, O'Brien and Wong, 2011).

1.3 Roles of Heat Shock Proteins in cell maintenance and disease

1.3.1 Overview of Heat Shock Proteins

There are more than 100 different proteins that comprise the chaperone protein family found in mammalian cells. Chaperones are a widely expressed and

highly conserved protein family, and have been reported to constitute approximately 5% of cellular proteins (Koren *et al.*, 2009, Soti and Csermely, 2003). The primary role of this family is to protect proteins against stress and aid in the correct folding of nascent proteins. It is only as a final resort do they function to direct proteins toward degradation mechanisms, see figure 1.10. Chaperones are crucial in the assembly and disassembly of multimeric complexes, regulation of vesicular transportation, as well as interaction with signalling and translocation of proteins across cellular membranes (Reviews - Koren *et al.*, 2009, Ohtsuka and Suzuki, 2000, Voisine *et al.*, 2010). Chaperones do not usually increase speed of folding, but by binding they extend the folding time and increase the yield of the final protein (Soti and Csermely, 2000).

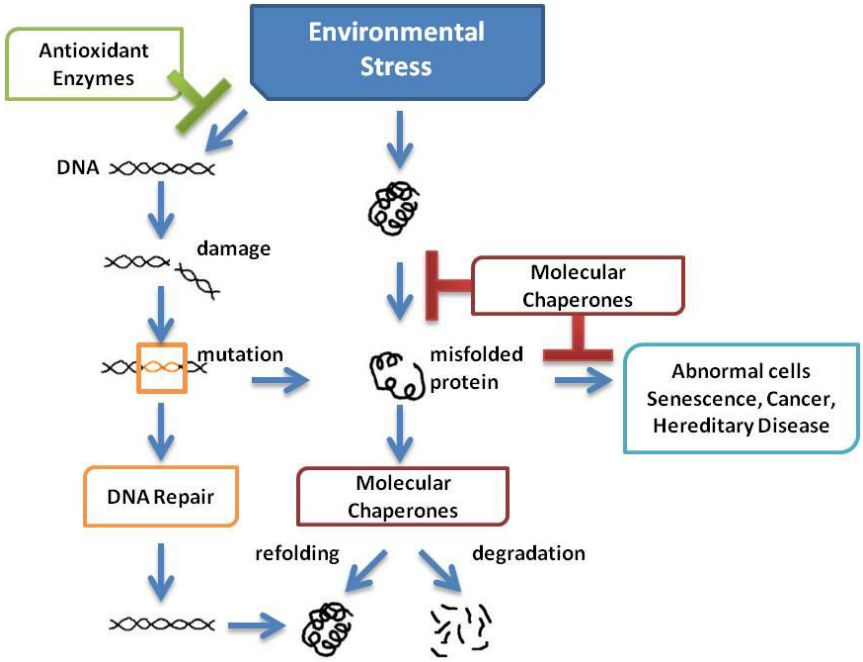

Figure 1.10. Basic Chaperone Roles (Based on Ohtsuka and Suzuki, 2000).

Ellis, *et al.*, 1991, defined heat shock proteins as *'a family of unrelated classes of protein that mediate the correct assembly of other polypeptides, but are not themselves components of the final structure'*. As more detail concerning chaperone function was discovered this definition was later extended by Hendrick & Hartl, 1993, who define a heat shock protein as '*a molecular chaperone protein that binds to and stabilises an otherwise unstable conformer of another protein – and by controlled binding and release of the substrate protein, facilitates its correct fate in vivo: be it folding, oligomerise assembly, transport to a particular subcellular compartment, or a controlled switching between active/inactive conformations'* (Ellis and van der Vies, 1991, Hendrick and Hartl, 1993).

Inducible transcription of heat shock protein genes is initiated through the translocation of HSFs, heat shock factors, into the nucleus where they bind HSEs, heat shock responsive elements, which then activate gene transcription (Samali *et al.*, 1999, Yenari *et al.*, 1999). Under normal cellular conditions, HSF1 activity is repressed by a HSP90 complex (containing HSP90, HSP40, HSP70, p23 and cyclophilin) by maintaining it in an inactive conformation (Reviewed - Turturici *et al.*, 2011) which can only be activated by a multifaceted process involving many modification steps. Under stress, these HSFs dissociate, trimerise and are then able to enter the nucleus to initiate transcription. During stress, HSPs act as a negative feedback mechanism to HSF1 activity, ensuring gene expression is tightly coupled to the cell environment, the more vacant chaperones there are available, the greater the number of HSP90 molecules binding to HSF1, thus preventing transcription of

more chaperones than required and vice versa, see figure 1.11 (Anckar and Sistonen, 2011, Calderwood *et al.*, 2009, Sherman and Goldberg, 2001).

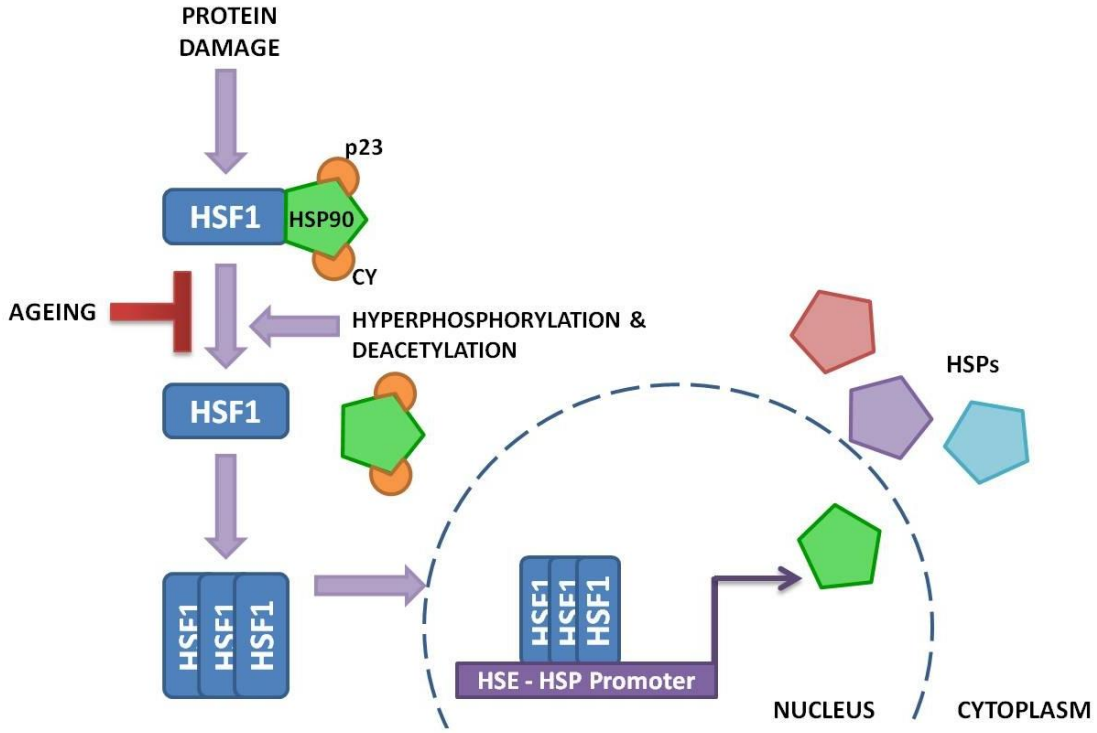

Figure 1. 11. Regulation of HSF1. Accumulation of damaged proteins results in the release of HSF1 from complexes which normally suppress its action. These consist of HSP90 and co-chaperones which include p23 and cyclophilins. HSF1 then trimerises and locates to the nucleus, where it binds HSEs, ultimately resulting in HSP expression. HSF1, Heat Shock Factor 1, HSE, Heat shock Elements, HSP, Heat shock protein, CY, cyclophilin. Based on figure from (Calderwood *et al.*, 2009).

It is beneficial for the cell to remove misfolded proteins quickly, as formation of aggregates can act as 'seeds' for more misfolded or unfolded proteins to begin to associate with. Nascent protein production can be impacted upon by the presence of aggregates and reduced control of protein production can result in cell death. Neurons are particularly vulnerable to the effects of aggregation as they are post-mitotic, and it is essential to remove aggregated proteins as they

cannot dilute their build-up through cell division (Chen and Brown, 2007, Sherman and Goldberg, 2001).

Chaperone molecules do not typically act alone; they commonly associate with another molecule or molecules, which may be another chaperone, such as HSP90 or HSP70, or they may associate with co-chaperones such as HSP40 or CHIP (Carboxy terminus of HSC70/HSP70-binding protein; Connell *et al.*, 2001, Macario and Conway de Macario, 2005, Soo *et al.*, 2008, Soti and Csermely, 2003).

The ability for cells to remove/handle cellular aggregates appears to become dampened with age. Interestingly, the level of HSF1 has not been found to alter with age; however it has been reported that the binding of HSF1 to HSEs is reduced in aged animals, although the mechanism of this reduction is not known (Calderwood *et al.*, 2009, Soti and Csermely, 2000). This results in the reduced induction of heat shock proteins and more aggregates forming following initial 'seeding' of misfolded proteins, congruently, protein degradation pathways have also been reported to become diminished. Impairment of both pathways ultimately leading to neurodegeneration. A particularly reduced response has been reported in aged individuals that are exposed to high oxidative stress, evident in degenerative disorders, in mammalian, *Drosophila melanogaster* and *Caenorhabditis elegans* systems (Reviewed - Sherman and Goldberg, 2001).

Current thinking suggests that the chaperone system primarily revolves around the ATPase activities of HSP70 and HSP90; which are thought to be the two major chaperone scaffolds. Other chaperones and co-chaperones work by

manipulating the ATPase activities of HSP70 and HSP90, enabling the refolding/folding of the bound protein or leading to its degradation (Koren *et al.*, 2009). A brief overview of HSP roles is shown in figure 1.10 and 1.12. HSPs have a well established role in the interference of apoptosis; by preventing JNK (c-Jun N-terminal kinase), AIF (Apoptosis Inducing Factor) and APAF-1 (Apoptosis protease activating factor-1) recruitment, also interfering with procaspase-9, procaspase-3 activation and Cytochrome *c* release amongst other roles (Reviewed - Olsson *et al.*, 2004, Yenari *et al.*, 2005).

The importance of heat shock proteins is emphasised via chaperonopathies, any pathological condition whereby a defective or absent chaperone is an aetiological factor. Depending on the number of clients which bind the chaperone the cost to the cell can be significant if the chaperone family is defective. Defective chaperones may still bind proteins but this can result in the formation of large precipitates and affect a complex number of cellular processes, the effects of which become more profound with the age of the organism (Macario and Conway de Macario, 2005, 2007).

1.3.2 Heat Shock Proteins and Cell death

The capacity of HSPs to prevent cell death relies on their ability to inhibit caspase activation and apoptosis, rather than being heavily influenced by their chaperone capabilities. Apoptosis occurs via two main pathways, intrinsic and extrinsic. The intrinsic and extrinsic pathways usually occur independently of each other, but the intrinsic pathway is also able to trigger the extrinsic pathway at the stage of mitochondria involvement. The intrinsic pathway is characterised

by permeabilisation of the outer mitochondria membrane. This causes the release of SMAC/DIABLO (second mitochondrial-derived activator of caspases and the *Drosophila melanogaster* homologue), AIF and Cytochrome *c*, this binds APAF-1 which recruits and activates procaspase-9 to form the apoptosome. Apoptosome formation in turn activates more procaspase-9 molecules and procaspase-3, beginning degradation of substrates (Beere, 2004, 2005, Benn and Woolf, 2004).

Caspases (cysteine aspartic specific proteases) are generally categorised by their mechanism of activation; there are initiator caspases, including caspases 2, 8 and 9, and executioner caspases, such as caspases 3, 6 and 7 (Beere, 2004, 2005). Initiator caspases dimerise with adaptor molecules to become catalytically active; these active initiator caspases are then able to cleave the executioner caspases and in turn activate them. Executioner caspases are able to cleave Initiator caspases, but the reason for this is debated; it may serve to stabilise their structure or result in their regulation (Beere, 2005, Thornberry, 1998).

The extrinsic pathway is initiated through the binding of specific ligands to 'death receptors' located on the cell membrane, with the major death receptor family being TNFR (Tumour necrosis factor receptors); members including apoptosis antigen-1 (FAS) and TNFR1, and main binding partners include TNF-related apoptosis-inducing ligand (TRAILR1) and FAS ligand (Benn and Woolf, 2004). The binding of FAS ligand to FAS in the neuron engages the FAS-associated death domain (FADD) and activates procaspase-8. Caspase-8 can then cleave BID (BH3 interacting domain death agonist) to tBID (truncated BID). As a pro-apoptotic member of the Bcl-2 (B-cell lymphoma 2) family, tBID

oligomerises BAX (Bcl-2 associated X protein) and BAK (Bcl-2 antagonist/killer) to form pores in the outer mitochondria membrane, thus causing cytochrome *c* release. Caspase-8 is then also able to activate executioner caspases including caspase-3. JNK (c-Jun N-terminal kinase) pathway is also activated by FAS, through the recruitment of DAXX (death domain associated protein) and ASK1 (apoptosis-signal regulating kinase 1). JNK then phosphorylates and inactivates the anti-apoptotic members of the Bcl-2 family, BCL2 and BCL-X_L (B-cell lymphoma-extra large), whilst converting BID to jBID (BID cleavage product). jBID is then able to recruit SMAC/DIABLO which further activates caspases and induces apoptosis (Beere, 2004, 2005, Benn and Woolf, 2004). HSP involvement is summarised in figure 1.12.

Several HSPs have been implicated in protection of the cell from apoptosis, including HSP27 and members of the HSP70 family. Pivotal roles of HSPs have been found in both the intrinsic and extrinsic pathways providing an essential mechanism to protect cells at times of severe cellular stress. HSP70 has been shown to inhibit the release of cytochrome *c* from the mitochondria, although whether this mechanism is direct or upstream of the mitochondria is debated, through directly effecting mitochondrial membrane integrity or through prevention of MPTP formation (Beere, 2004, 2005, Mosser *et al.*, 2000). HSP70 has also been shown to prevent TNFR induced release of Cytochrome *c* through inhibition of caspase-8 driven BID activation, as well as prevention of BAX translocation to the mitochondria membrane. In conjunction with interference of the intrinsic pathway, HSP70 is also capable of preventing the formation of a functional apoptosome via binding to APAF-1. This in turn, limits

activation of procaspase-9 (Beere, 2004, 2005, Benn and Woolf, 2004, Calabrese *et al.*, 2002).

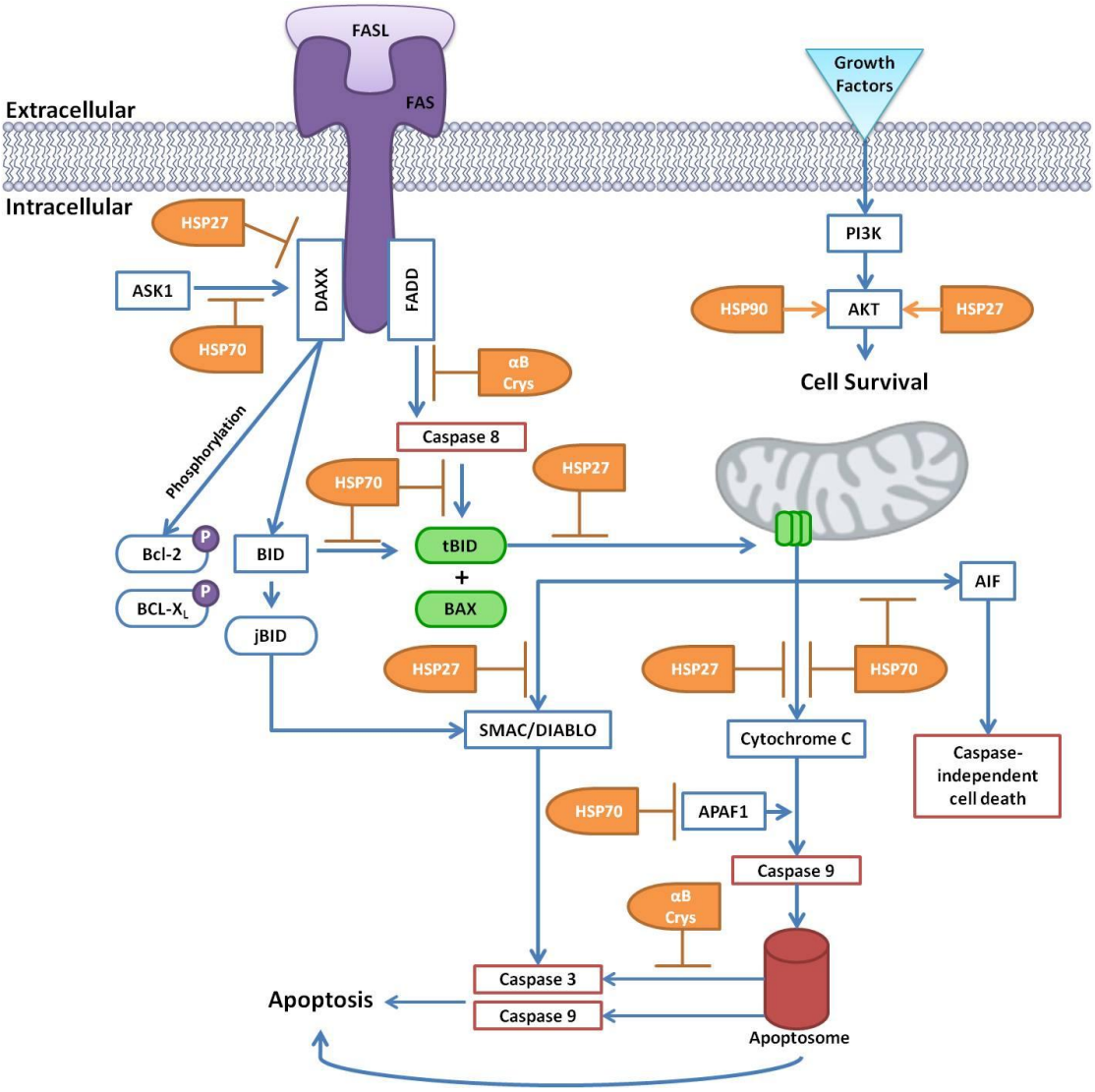

Figure 1.12. An Overview of HSP Involvement in the Prevention of Apoptosis. Abbreviations: αB Crys, αB Crystallin; AIF, apoptosis inducing factor; APAF-1, apoptotic protease activating factor 1; ASK1, apoptosis signal-regulating factor 1; BAX, Bcl-associated X protein; Bcl-2, B cell lymphoma 2; B cell lymphoma-extra large; BID, BH3 interacting domain death agonist; DAXX, death domain associated protein; FADD, FAS-associated death domain; FAS, apoptosis antigen-1; FASL, FAS ligand, HSP27, heat shock protein 27; HSP70, heat shock protein 70; P, phosphorylation; SMAC/DIABLO, second mitochondrial-derived activator of caspases and the *Drosophila melanogaster* homologue.

HSP70 and HSP27 have been specifically implicated in the regulation of the extrinsic pathway, via the inhibition of ASK1 by HSP70 and through HSP27 binding to DAXX, arresting JNK pathway progression. HSP27 has also been shown to prevent BID translocation to the outer mitochondria membrane preventing release of Cytochrome *c*, it has also been shown to sequester Cytochrome *c* once it has been released, preventing apoptosome formation. Indeed, αB Crystallin has also been implicated in promotion of cell survival through an ability to suppress the activities of caspase-3 and caspase-8 by preventing their complete processing (Beere, 2004, 2005, Benn and Woolf, 2004, Calabrese *et al.*, 2002, Stetler *et al.*, 2009).

HSPs have been implicated in the regulation of TRAIL, FAS and TNF driven apoptotic pathways, but the mechanisms are complex with several studies providing conflicting evidence as to whether the effect of HSP intervention is positive or negative regarding long term cell maintenance, for example; cells may be stopped from undergoing apoptosis through HSP intervention when in some instances this may be to the organism's detriment rather than advantage (Beere, 2005). An outline of major HSP roles in apoptosis are shown in figure 1.12.

1.3.3 Altered Expression of HSPs in Disease

Induction of the heat shock protein response has been frequently found to become impaired with age in a variety of tissues, including neurons. A decline in protein quality control occurs as cells lose the ability to activate the transcriptional pathways required for HSP synthesis, potentially due to reduced

DNA binding capabilities (Calderwood *et al.*, 2009, Soti and Csermely, 2003, Winklhofer *et al.*, 2008).

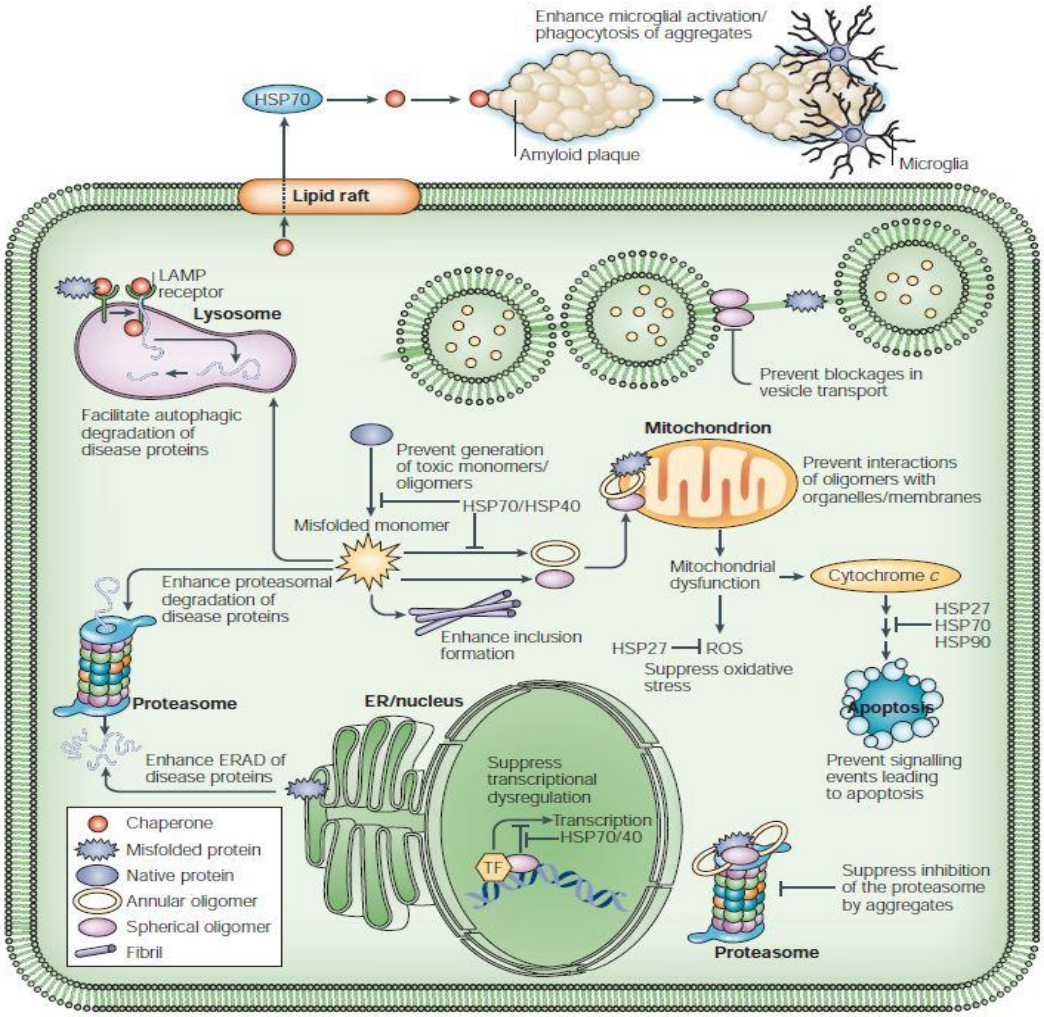

Figure 1.13. Established roles of chaperones in protein toxicity diseases. Abbreviations: ER, endoplasmic reticulum; ERAD, endoplasmic reticulum associated degradation; HSP, heat shock protein; LAMP, lysosomal associated membrane protein; ROS, reactive oxygen species; TF, transcription factor (Figure from Muchowski and Wacker, 2005).

HSF1, Heat shock factor 1, is the required transcription factor for heat shock protein induction when cells become stressed. HSF1 is constitutively expressed in most tissues, and can be found in both the nucleus and cytoplasm, but during

stress it becomes highly concentrated in the nucleus. High constitutive levels of HSF1 activity are tightly linked to increased longevity in both nematodes and flies (Calderwood *et al.*, 2009, Hsu *et al.*, 2003).

Altered HSP expression has been reported in Alzheimer's disease (AD); Yoo *et al.,* (2001) reported aberrant expression of multiple HSPs; including αB crystallin, HSP70, HSC70 and HSP60, in a range of regions of the human brain (Yoo *et al.*, 2001). Compared to control patients, Alzheimer's disease sufferers demonstrated increased HSP27 and αB crystallin levels in the cerebral cortex (Shinohara *et al.*, 1993) and higher HSP70 expression in the temporal cortex (Perez *et al.*, 1991).

Chaperones have been found to co-localise with the Aβ plaques and PHFs (paired helical filaments) of Alzheimer's disease, they have also been reported to induce conformational changes in and encourage the removal of Aβ via transport over the blood-brain-barrier or through phagocytosis (Wilhelmus *et al.*, 2007). A summary of the direct and indirect processes that have been attributed to chaperones in protein-based toxicity are summarised in figure 1.13.

1.3.4 HSP70

HSP70 family has two major members, HSC70 (heat shock cognate), a constitutively expressed form, and HSP70, an inducible form. HSC70 is the major chaperone expressed in healthy cells and HSP70 is the predominant inducible-heat shock protein. HSC70 and HSP70 share approximately 95% sequence homology and have similar biochemical functions (Welch, 1992).

HSP70 family proteins are found in most intracellular compartments, and also include an ER localised member, GRP78 (glucose regulated protein 78), and a mitochondrial localised member, MtHSP75 (mitochondrial heat shock protein 75), which are both also constitutively expressed (Turturici *et al.*, 2011). The HSP70 family is important for the correct folding of nascent proteins, promotion of ubiquitination/lysosome mediated autophagy, interaction with signal transduction proteins and translocation of proteins through the intracellular membrane. The HSP70 family are able to do this as they possess both an NES (nuclear export signal) and an NLS (nuclear localisation signal), so they are able to move between the nucleus and cytoplasm (Reviewed - Mayer and Bukau, 2005, Muchowski and Wacker, 2005, Saito *et al.*, 2007, Turturici *et al.*, 2011).

HSP70 binds exposed hydrophobic regions of misfolded/damaged proteins in an ATP-dependent manner. Binding of ATP to the ATP-domain at the N-terminal is required before the substrate binding domain at the C-terminal can be active (Mayer and Bukau, 2005, Yenari *et al.*, 1999). The precise mechanism of how HSP70 enables folding of a protein into its native state is unknown. There are two principle theories; ‘kinetic partitioning’ in which HSP70 plays a passive role in binding free substrates in order to reduce their concentration sufficiently to prevent aggregation and to allow correct folding to occur naturally, and ‘local unfolding’, in which HSP70 repeatedly binds and releases sections of the misfolded substrate, refolding small areas until the native confirmation can arise (Reviewed - Mayer and Bukau, 2005).

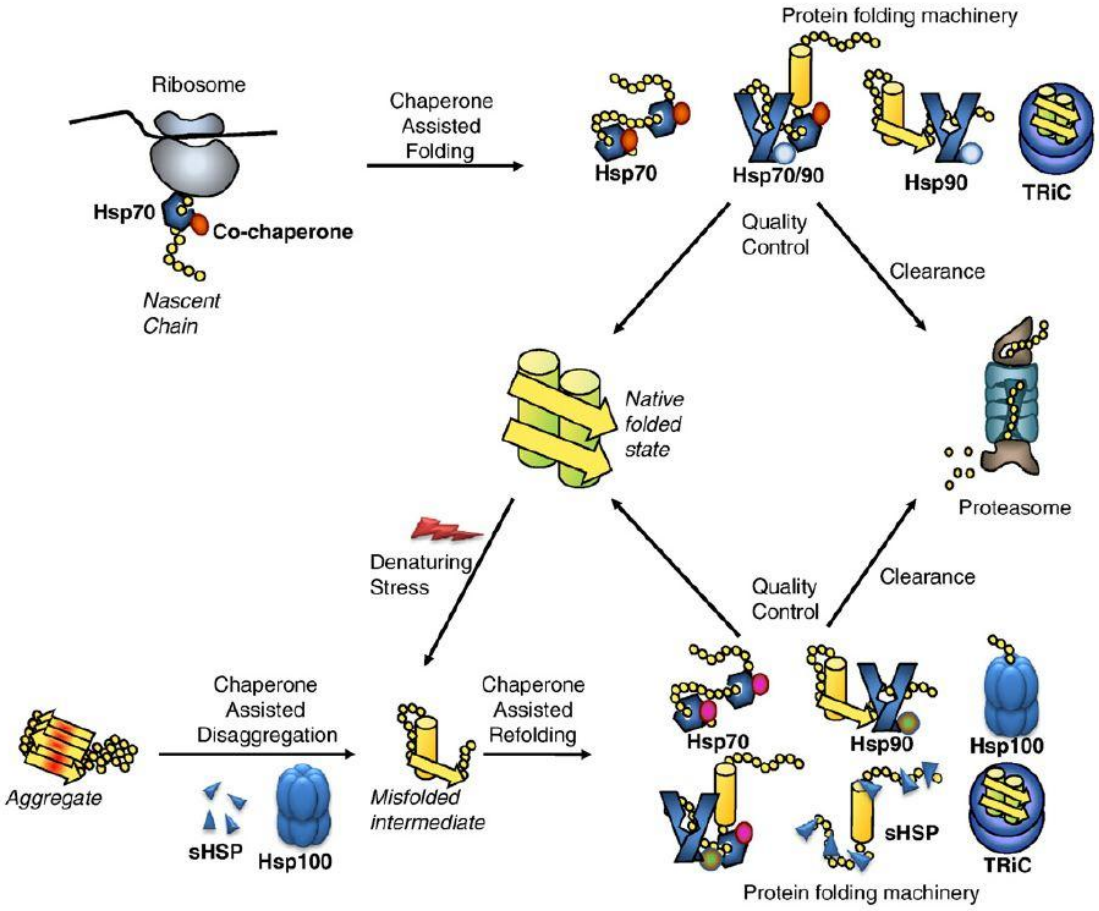

Figure 1.14. Overview of Chaperone Families and Their Roles – Core families HSP70, HSP90 and TRiC (T-Complex Protein 1 Ring Complex). Small HSPs and HSP100 (referred to as HSP105/110 in text). Cochaperones are shown as coloured circles, attached to the blue hexagon of HSP70 (Voisine *et al.*, 2010).

Chaperones and the ubiquitin-proteasome systems have been shown to work competitively and synergistically in directing proteins for degradation. Proteins that HSC70/HSP70 cannot refold can be sent for degradation, which occurs through the association with CHIP and BAG-1 (BCL2 Associated Athanogene 1). CHIP is an ubiquitin E3 ligase, which adds an ubiquitin molecule to the lysine residue(s) of the substrate, assuring the substrates degradation (Lanneau *et al.*, 2010). A number of HSP70 driven roles are shown in figure 1.14.

Overexpression of HSP70 has been found to protect against insults in both peripheral and hippocampal neurons, with the suggestion that expression of HSP70 in glia is able to be transferred to neurons, directly aiding in neuronal protection (Guzhova *et al.*, 2001, Yenari *et al.*, 1999, Yenari *et al.*, 2005). Indeed HSP70 has been shown to directly reduce the toxicity of intracellular Aβ in neurons (Magrane *et al.*, 2004). The ability for HSPs to not only act intracellularly, is supported by a wide range of reports that demonstrate that HSC70/HSP70 can be released from glial cells and internalised in its active form by other cell types, including neurons; taken into the cytoplasm and nucleus to support the probability of cell survival, presumably through chaperone capabilities and proteasome activation (Guzhova *et al.*, 2001, Magrane *et al.*, 2004). HSP70 can also act extracellularly, with roles including cytokine release, microglia activation and clearance of Aβ - potentially through microglial-driven phagocytosis (Evans *et al.*, 2006, Kakimura *et al.*, 2002), amongst other potential roles as HSP70 does not express a secretion sequence. The precise mechanism of release and uptake of HSP70 remains undetermined, although current thinking suggests release occurs via secretory vesicles, secretory lysosomal endosomes or even via calcium induced interaction with lipid rafts and uptake may occur via TLRs (Toll-Like Receptors). Notably, TLR2 and TLR4 on antigen presenting cells are believed to be involved, suggesting immune system interplay and CD40 is also thought to act as a receptor for HSP70 (Calderwood *et al.*, 2007, Mayer and Bukau, 2005, Muchowski and Wacker, 2005, Novoselova *et al.*, 2006, Turturici *et al.*, 2011). However, the neuroprotective capabilities of HSP70 have been reported to be limited by the levels of co-chaperone HSP40, as well as by the severity and

type of insult as mentioned previously (Turturici *et al.*, 2011). Although there is evidence for HSP70 to function in a beneficial manner in the absence of HSP40 (Oh *et al.*, 1999).

High expression of HSP70 has been found to occur in a range of pathological conditions, including neurodegenerative diseases, epilepsy and ischemia. HSP70 is predominately expressed in endothelial cells, but is also found in glia and in the majority of neuronal subtypes - neurons typically contain high levels of HSC70 and low levels of HSP70 (Sharp *et al.*, 1999, Yenari *et al.*, 1999). HSC70 levels differ between neuronal types; for example neurons of the hippocampus and entorhinal cortex have higher expression levels than expression levels in neurons of the substantia nigra, but neurons of other areas, such as the spinal cord, have constitutively much higher levels still. It has been hypothesised that neurons with high constitutive levels of HSC70, have a greater ability to buffer against the accumulation of misfolded proteins. Areas of the brain damaged in disorders characterised by misfolded proteins/aggregates are sequentially affected by their chaperone expression levels, explaining why the substantia nigra is often the first affected area, followed by the cortex and hippocampus (Chen and Brown, 2007).

Increased synthesis of HSP70, interaction of HSP70 with intracellular Aβ and prevention of Aβ accumulation have all been observed in models of AD and patient samples from Alzheimer's disease sufferers (Magrane *et al.*, 2004, Perez *et al.*, 1991). Indeed, Hoshino, *et al*., 2011, have also shown that high expression levels of HSP70 suppress the Alzheimer's disease phenotype and cognitive defects in APPsw (Swedish APP mutation) mice. The experimenters found high HSP70 levels had no effect on Aβ production, but reduced levels of

Aβ, plaque deposition and Aβ-associated neurotoxicity, potentially via extracellular/intracellular HSP70 stimulating microglia. Upregulation of IDE (Insulin Degrading Enzyme), an Aβ degrading enzyme, and TGF-β1 (Transforming Growth Factor β1) were both observed and are both expressed by microglia (Hoshino *et al.*, 2011). In conjunction with HSP90, HSP70 has been shown to interact with cytosolic Aβ, preventing early stages of aggregation and interaction of Aβ with cell survival proteins, resulting in neuroprotection (Koren *et al.*, 2009, Magrane *et al.*, 2004).

HSP70 has also been found to attenuate tau toxicity, of all six isoforms, by facilitating its degradation and by binding to tau and preventing aggregation. HSP70 has not been shown to be effective at decreasing fibrillar tau fibre formation, effective at reducing the ability of tau to oligomerise as it binds tau oligomers more readily, potentially due to greater exposure of hydrophobic binding regions. Tau and HSP70 levels demonstrate an inverse relationship to levels of tau aggregation (Dou *et al.*, 2003, Voss *et al.*, 2012) HSP70, independent of ATP binding, is then able to remove tau monomers from the ends of aggregates, as well as directly aid in the refolding of tau and in transferring tau to other chaperones for refolding (Patterson *et al.*, 2011, Voss *et al.*, 2012). HSP70 is also able to promote partitioning of tau to microtubules and its solubilisation, preventing insoluble tau from affecting fast axonal transport (Dou *et al.*, 2003, Voss *et al.*, 2012). It has been suggested that this ability of HSP70 also requires the presence of co-chaperone HSP40 (Sahara *et al.*, 2007).

Evans, *et al.,* (2006), found that HSP70/40 and HSP90 were both able to directly prevent polymerisation of Aβ monomers *in vitro* and the HSPs were able

to manipulate pre-formed Aβ oligomers and reduce their aggregation, also thought to be due to the exposed hydrophobic regions enabling HSP binding. High HSP70/40 and HSP90 levels had no significant effect on pre-formed fibrils; however this could be explained through a lack of exposed hydrophobic residues due to the compact nature of their structure. But the presence of co-chaperones are not essential for function, however they do increase the potency of the main chaperone (Evans *et al.*, 2006, Muchowski and Wacker, 2005).

1.3.5 HSP105

The HSP105/110 family of heat shock proteins are a group of mammalian proteins that have been shown to be related to the main HSP family, HSP70. However, there are significant differences between the two groups. HSP105 is sometimes referred to as HSP110; there is no consistent format used in the literature, thus in the remainder of this report the chaperone will be referred to as HSP105.

HSP105 has been shown to be the most strongly expressed member of the HSP105/110 family, and expression is significantly higher in the brain compared to other regions (Reviewed - Hylander *et al.*, 2000). However, expression levels vary across the brain, Hylander, *et al.*, 2000, showed that neurons are the predominate cell type expressing HSP105 throughout brain hemispheres, with the exception of the cerebellum where very little expression was detected, bar Purkinje fibres located in this area which showed strong expression (Hylander *et al.*, 2000).

The members of the HSP105/110 family are HSP105α and HSP105β, and the group also includes HSPA4L (heat shock 70 kDa protein 4-like, also called Apg1) and HSP94 (Apg2) but the latter proteins only share ~60% homology with the former HSP105α and β members (Hylander *et al.*, 2000).

The two principle members of the HSP105/110 family are HSP105α, a constitutively expressed form which is upregulated in response to a variety of stresses, and HSP105β, a protein specifically induced following mild heat stress (Ishihara *et al.*, 1999). HSP105α is 858 amino acids in length, whereas HSP105β is thought to be an alternatively spliced version at 814 amino acids (Yasuda *et al.*, 1995). HSP105α has been found to be predominately expressed in the cytoplasm, whereas HSP105β is expressed in the nucleus exclusively. This differential expression pattern has been attributed to the presence of a NLS in both isoforms, but the extra 44 amino acids in HSP105α encode a NES and mask the NLS (Saito *et al.*, 2007, 2009). The combination of this sequence and the strong interaction of HSP105α with microtubules cause the protein to be retained in the cytoplasm, suggesting the isoforms may have minor differences in function (Saito *et al.*, 2007).

HSP105 overexpression has been shown to confer cellular heat resistance and to prevent protein aggregation by keeping misfolded proteins in a folding-competent state, apparently to a greater magnitude than HSC70/HSP70 (Oh *et al.*, 1999). HSP105α, in particular, has been shown to protect against stress induced cell death through interaction with HSP70 to refold proteins (Yamagishi *et al.*, 2011). HSP105 has an ATP binding domain, like HSC70/HSP70, but ATP is not required to be bound for the chaperone to act in a ‘holding’ manner, but

the ATP domain is believed to be required for HSP105 to refold proteins although this has not yet been investigated in great depth (Oh *et al.*, 1999).

Perhaps unsurprisingly, considering their close evolutionary lineage, HSP105 (α and β) are able to exist in high molecular mass complexes with HSC70/HSP70 and HSP70 in mammalian cells, the dissociation of which is not dependent on binding ATP. This led to the suggestion that HSC70/HSP70 may have functional support from HSP105, such as regulation of HSC70/HSP70 by HSP105 or vice versa under both normal and stressed cellular conditions (Hatayama and Yasuda, 1998).

HSP105α in particular has been identified as a repressor of HSC70/HSP70 activity, and may act as a modulator of its chaperone capabilities. HSP105α has been reported to interfere with the chaperone function of HSC70/HSP70 through inhibiting the ATP-dependent refolding of substrates. HSP105α was not found to prevent the interaction of HSC70 with misfolded proteins but in the presence of HSC70, HSP105α is able to bind ATP and hydrolyse it to ADP, thus reducing the ATP concentration, reducing the ability for HSC70/HSP70 to bind substrates rapidly, with low affinity. The ADP-bound HSC70/HSP70 is able to bind substrates but this occurs more slowly, with a higher affinity for the substrate. In these conditions, HSC70/HSP70 becomes a ‘holding’ chaperone with the HSP105 family acting as nucleotide exchange factors (Particularly HSP105α; Reviewed - Yamagishi *et al.*, 2003, Yamagishi *et al.*, 2011). In the presence of ADP or ATP, HSP105 is still able to suppress protein aggregation and its ability to modulate HSC70/HSP70 activity can be removed by phosphorylation of HSP105α at Ser509 by protein kinase CK2 (Casein Kinase II; Yamagishi *et al.*, 2004, Yamagishi *et al.*, 2000). When a cell becomes

severely compromised and the HSP70 main family of chaperones are unable to function, the HSP105 family are able to efficiently suppress aggregation of proteins in ATP depleted conditions in order to protect the cell until normal function can be regained. In the absence of ATP, HSP105 can direct aggregates to CHIP (Yamagishi *et al.*, 2004) but ATP is required for HSP105 to function in conjunction with other chaperones (Yamagishi *et al.*, 2000).

Nuclear-located HSP105β has been shown to be capable of inducing HSP70 expression, but not of other HSPs, in mammalian cells whereas HSP105α is unable to influence HSP70 expression (Saito *et al.*, 2009). HSP105β was found to be able to do this by binding to STAT3 (Signal Transducer and Activator of Transcription-3) rather than via HSFs, which are the usual mechanism of HSP upregulation (Yamagishi *et al.*, 2009). STAT3 is monomeric until specific tyrosine phosphorylation by JAK (Janus Kinase), causing trimerisation and migration to the nucleus and activation of gene expression. STAT3 then binds the *hsp70* promoter at a position different to that which HSF1 binds. The mechanism through which increased HSP105β causes increase phosphorylation remains unknown. HSP105α is also thought to have an important anti-apoptotic role through preventing JNK activation in stressed cells (Hatayama *et al.*, 2001); illustrating the significant role HSP105α may play in neuronal protection. HSP105 has also been shown to reduce signalling to activate procaspase-3 (Meares *et al.*, 2008).

HSP105α and HSP105β also been shown to suppresses aggregate formation and cytotoxicity in poly-Q expressing cell lines, through the induction of HSP70 and under these circumstances, HSP105α was able to localise in the nucleus. This suggests that under certain critical circumstances, the NES of HSP105α is

able to be overcome and the NLS is dominant (Yamagishi *et al.*, 2010). Indeed, using *hsp105*$^{-/-}$ mice, tau hyperphosphorylation and accumulation of Aβ have been shown to be increased. This study also demonstrated that HSP70 and HSP105 have a critical role in maintaining tau in an unphosphorylated state, as hyperphosphorylation of tau leads to the loss of microtubule stability and the formation of NFTs (neurofibrillary tangles), as seen in Alzheimer's disease. The loss of HSP105, in conjunction with APP over-expression (in murine models), also appeared to have a dramatic impact on APP (amyloid precursor protein) processing, resulting in the formation of $A\beta_{(1-42)}$ peptide and Aβ deposition (Eroglu *et al.*, 2010).

These studies provide important understanding and models to further understand mechanisms involved in neurodegenerative disease but also give valuable insights into potential therapeutic targets.

The HSP105β protein is thought of only being induced upon heat-stress to 42^{o}C, as the preliminary work that identified this protein only found its expression occurs under the heating conditions and not following other stresses – ethanol, copper sulphate, sodium arsensite, puromycin or canavanine (Hatayama *et al.*, 1986). However, this work was only completed in HeLa cells and as the majority of work on HSP105 has been done by one laboratory, little else has been looked at, including the expression of HSP105 (α and β) in neurodegenerative disorders.

1.3.6 Small Heat Shock Proteins (sHSPs)

There are currently 10 known small heat shock proteins (sHSPs) in the human chaperone family, they are between 12-43 kDa in size, do not require ATP to stabilise and refold their substrates and they function by forming dynamic oligomers which can be heterogeneous in nature and up to 1 MDa in size. Under normal conditions in the cell, sHSPs are stored as large assemblies, upon the onset of stress; these assemblies are broken down into functional oligomers by protein kinases (Eyles and Gierasch, 2010, Koren *et al.*, 2009, Sun and MacRae, 2005, Wilhelmus *et al.*, 2006a). The dodecamer is the most common conformation of sHSPs in normal cellular conditions, in this dynamic configuration the sHSPs are unable to bind substrates, but act as a reserve of subunits should they be required (Eyles and Gierasch, 2010).

Much like larger molecular weight HSPs, sHSPs are able to act as ‘holdases’ or ‘holding’ chaperones, binding partially folded proteins, preventing the aggregation of the misfolded proteins until the HSP90/HSP70 machinery can refold the misfolded protein or target it for degradation (Eyles and Gierasch, 2010). The C- and N- terminal extensions of the sHSPs are essential to their function, enabling the formation of large sHSP oligomers and arbitrate the recognition of substrates (Jaya *et al.*, 2009).

The function of sHSPs is able to be altered by post-translational modifications, such as phosphorylation. These modifications are typically reversible and are a response to particular stress, such as cytokines or mitogens. The phosphorylation of sHSPs leads to an altered ability of monomers to oligomerise, smaller oligomers form following a greater degree of

phosphorylation. This modification of function allows a range of transcriptional pathways to adapt sHSP function (Arrigo *et al.*, 2007, Garrido *et al.*, 2012, Parcellier *et al.*, 2005). The phosphorylation of sHSPs also results in the formation of more specialised conformations, which are able to target specific substrates. The nature of this capability means sHSPs are able to target an ample range of proteins (Garrido *et al.*, 2012), indeed some have reported up to 300 different sHSP:substrate interactions (Eyles and Gierasch, 2010).

A variety of sHSPs have also been shown to directly interact with the proteasome, ubiquitin ligase complexes, cell redox (reduction/oxidation) potential and apoptotic proteins when required. sHSPs, including HSP27 and αB crystallin, also interact with the cytoskeleton – actin, microtubules and intermediate filaments (including desmin and GFAP (glial fibrillary acidic protein)). But some of these interactions require direct phosphorylation of the sHSP; P-HSP27 is needed for HSP27 to interact with actin (Reviewed - Ecroyd and Carver, 2009, Garrido *et al.*, 2012, Nicholl and Quinlan, 1994).

sHSPs are not only expressed in stress conditions, they are expressed in cells throughout development and during adulthood. Their cellular location differs in response to the environmental conditions (Sun and MacRae, 2005). HSP27 and αB crystallin are the two main sHSPs, their expression often associated with tissues which have high rates of oxidative metabolism, such as the brain, heart and skeletal muscle fibres (type I and IIa), although both proteins are not expressed at the same concentration. These sHSPs protect against ischemic and reperfusion damage due to blood flow occlusion, with αB crystallin predominately known as a major constituent of the eye lens, with αB crystallin

(and αA) important in preventing cataract formation (Arrigo *et al.*, 2007, Sun and MacRae, 2005).

In neurodegenerative disorders, including Alzheimer's and Parkinson's diseases, the upregulation of HSP27 and αB crystallin at damaged neurons and astrocytes has been observed and are frequently associated with amyloid deposits (Ecroyd and Carver, 2009, Sun and MacRae, 2005). Their role in Alzheimer's disease will be explored in sections dedicated to each sHSP, particular expression of sHSPs in AD is thought to be as a result of the cell recognising the formation of amyloid fibrils as a stress and responding appropriately.

1.3.7 HSP27 and Phosphorylated HSP27

HSP27 expression is induced following cellular stress, forming stable dimers which can also form oligomers of up to 32 subunits (~800 kDa), but these are typically unstable (Garrido, 2002). Dephosphorylation promotes oligomer formation, whereas phosphorylation promotes dimer formation, one particular kinase associated with HSP27 phosphorylation is MAPKAPK2 (mitogen-activated protein kinase-activated protein kinase 2). HSP27 is modified via phosphorylation at serine sites, and therefore differential oligomerisation, following exposure to a range of stressors, results in a very specific ability to control the function of HSP27 (Garrido, 2002, Read and Gorman, 2009, Stetler *et al.*, 2009).

HSP27 is able to act as a chaperone when it is present as large unphosphorylated oligomers, usually of 24 subunits. The chaperone capability is down-regulated upon phosphorylation, with this phosphorylation most commonly resulting in the formation of short rod-shaped tetramers. Phosphorylation was not initially thought to be as advantageous to the cell as it diminishes the chaperone capabilities of HSP27, but it has been suggested that phosphorylation of HSP27 acts as a mechanism to remove proteins that cannot be successfully refolded from the cell. P-HSP27 targets these proteins towards ubiquitination, acting as an E4 factor. Ubiquitination is an enzyme based, multistep process, interaction with E4 factors can cause the association of E3 ligases to substrates and act as functional bridging for ubiquitin moieties, stabilising the aggregates before their removal. This interaction increases the efficiency and speed of the transference of ubiquitin chains from the E3 ligase to the misfolded substrate. The rapid adaptability of large HSP27 oligomers, via phosphorylation and dephosphorylation, enables fast, dynamic responses to a variety of cellular stresses (Reviewed - Lanneau *et al.*, 2010, Rogalla *et al.*, 1999, Sahara *et al.*, 2007, Stetler *et al.*, 2009).

Through the chaperone function of HSP27 cell fate can be influenced to a degree, but HSP27 is also associated with cell survival through the stabilisation of the actin cytoskeleton and inhibition of apoptotic pathways. Known as a powerful anti-apoptotic protein, HSP27 at high levels is able to suppress caspase activation, Cytochrome *c* release (Samali *et al.*, 2001) and the translocation of other molecules required for apoptosis. But the direct site of HSP27 interaction in apoptosis initiation is debated, HSP27 is able to bind to cytochrome *c* after it is released from the mitochondria, preventing apoptosome

formation, it has also been shown to bind to DAXX preventing FAS driven cell death, see figure 1.12, but HSP27 is also thought to be able to act upstream of the mitochondria, interfering with caspase recruitment (Reviewed - Beere, 2005, Garrido, 2002, Read and Gorman, 2009, Stetler *et al.*, 2009).

Reduction of HSP27 expression has been associated with the onset of neuronal cell death and elevated levels of HSP27 have been frequently found in individuals with neurodegenerative disorders, such as Alzheimer's disease, widely hypothesised to be part of a chaperone driven protective response to enhance protein folding capacity of the affected neurons (Read and Gorman, 2009, Sherman and Goldberg, 2001, Shimura *et al.*, 2004).

Expression of HSP27 varies across different cell types, with constitutive expression level varying; it is highest in the spinal ganglia and brain stem with neurons expressing HSP27 at a relatively low level and prominent expression in glia cells (Reviewed - Stetler *et al.*, 2009). Despite differential expression of HSP27 across neuronal populations; neurons that express both proteins (HSP70 and HSP27) have a higher 'defence' capacity against misfolded proteins (Chen and Brown, 2007).

Expression of HSP27 has been reported to be increased by approximately 20% in the Alzheimer's disease brain (Bjorkdahl *et al.*, 2008); expression has been frequently associated with degenerating hippocampal neurons, hyperphosphorylated tau, senile plaques and NFTs, as well as proliferating and astrocytes (Bjorkdahl *et al.*, 2008, Wilhelmus *et al.*, 2006b).

HSP27 has also been shown to prevent the deformation and limited dynamics of mitochondria that arise when exposed to Aβ, both of which are commonly

linked to Alzheimer's pathology (King *et al.*, 2009). HSP27 can positively reinforce the activity of ATP-dependent chaperones, such as HSP70, through an ability to maintain mitochondrial membrane potential, ensuring ATP production through increasing and maintaining glutathione levels at times of cellular stress (Preville *et al.*, 1999).

HSP27 has been widely reported to bind to fibrillar amyloid plaques and to inhibit de novo fibrillisation (Koren *et al.*, 2009, Wilhelmus *et al.*, 2007), this is thought to be possible through HSP27 targeting the 'seeding' step of fibril formation, with less impact of HSP27 found on established fibrils (Kudva *et al.*, 1997). HSP27 is also associated with senile plaques and degenerating neurons in the brains of AD patients, particularly localised found in temporal, parietal and frontal lobes (Shinohara *et al.*, 1993). This has been directly reported in cerebrovascular cells; HSP27 was shown to bind Aβ, prevent its aggregation and accumulation at the cell surface, promoting cell survival (Wilhelmus *et al.*, 2006a). Despite limited neuronal endogenous expression levels, HSP27 expression by glia and transference to neurons has been proposed as a mechanism of how this protection is elicited (King *et al.*, 2009).

P-HSP27 has not been shown to bind 'normal' tau and preferentially binds to hyperphosphorylated tau (including PHFs), and targets it for dephosphorylation or removal in conjunction with HSP70 and CHIP by altering its confirmation, but the sHSP also appears to be able to remove hyperphosphorylated tau independently of the HSP70/CHIP ubiquitin pathway, although the mechanisms of this have not been established. It has been suggested to directly feed p-tau into the proteasome, suppressing cell death (Koren *et al.*, 2009, Shimura *et al.*, 2004), through acting as an E4 factor (Lanneau *et al.*, 2010). HSP27 and P-

HSP27 have both been shown to bind tau in Alzheimer's disease, but HSP27 is only able to target tau for removal if it itself is not phosphorylated, P-HSP27 has been shown to actually stabilise tau structures (Abisambra *et al.*, 2010, Bjorkdahl *et al.*, 2008). P-HSP27 has been found in the nucleus and cytoplasm of the cell, potentially its small size enabling shuttling between both locations. This enables P-HSP27 to target both, cytosolic and nuclear proteins for degradation (Lanneau *et al.*, 2010), cycling enables HSP27 to hand P-tau to P-HSP27 to degrade via ubiquitination, emphasising the importance of the dynamic cycling of HSP27 and P-HSP27 (Abisambra *et al.*, 2010).

1.3.8 αB Crystallin

A range of studies have shown that αB crystallin interacts predominately in the early stages of protein folding, with amorphous, intermediately folded aggregates, resulting in the formation of a large, stable complex that is less likely to aggregate with other nascent proteins (Ecroyd and Carver, 2009). Despite lacking the ability to refold aggregates, during times of cellular stress when cellular levels of ATP are low this can be advantageous. The lack of ability to refold aggregates can be advantageous at times of cell stress, when ATP levels are low sHSPs can incapacitate misfolded aggregates thus limiting further cell stress through the build up of aggregates until cellular conditions become more favourable and ATP levels increase. At this point, the aggregates can be refolded through the action of HSP70. It has been suggested that HSP70 and αB crystallin act synergistically *in vivo* (Ecroyd and Carver, 2009, Haslbeck *et al.*, 2005).

Examination of αB crystallin expression in the Alzheimer's disease brain has shown that some areas show up to 30% higher expression than in control patients (Bjorkdahl *et al.*, 2008). Increased expression was identified in several areas including in the hippocampal gyrus, temporal cortex, cingulated cortex and superior frontal cortex, with particular expression noted in microglia that were associated with NFTs and SPs (senile plaques), suggesting expression associated with Aβ deposition (Mao *et al.*, 2001, Renkawek *et al.*, 1994, Yoo *et al.*, 2001). Strong αB crystallin expression has been noted in neurons in areas strongly associated with damage in Alzheimer's disease, levels increasing proportionally to neuronal loss, with the highest concentration found in layers III and V of the cerebral cortex (Mao *et al.*, 2001, Renkawek *et al.*, 1994), Accumulation was also noted in astrocytes, microglia and degenerated neurons (Wilhelmus *et al.*, 2006b). It has been suggested that αB crystallin is involved in the latter stages of disease progression, levels consistently correlate with the formation of intracellular NFTs which ultimately lead to neuronal death, and the formation of extracellular NFTs (Mao *et al.*, 2001).

αB Crystallin has been reported to prevent formation of mature $A\beta_{(1-40)}$ fibrils *in vitro*, however, presence of αB crystallin also increased the toxic effect of $A\beta_{(1-40)}$ through encouraging the formation of smaller aggregates and the formation of β-pleated sheet rich structures in which αB crystallin is complexed with $A\beta_{(1-40)}$ (Stege *et al.*, 1999, Yoo *et al.*, 2001), verified by Thioflavin T assays and Far-UV circular dichroism (Liang, 2000) and believed to be the more toxic Aβ structure. The formation of these types of structures has been reported to occur due to Aβ interfering with the normally dynamic structure of αB crystallin oligomers. The αB crystallin oligomers are made of monomers that rapidly

associate and dissociate with the larger structure, the presence of Aβ prevent monomers re-associating, so the forming Aβ structure becomes coated in αB crystallin monomers (Liang, 2000). Oxidation of Met35, found on side chains of $A\beta_{(1-40)}$, limits the ability of Aβ to structurally form fibrils and acts to promote oligomer formation, which is thought to be the principle reason for the increased toxicity of Aβ in the presence of αB crystallin (Narayanan *et al.*, 2006). Met35 oxidation induces increased neurotoxicity; this facilitates the propagation of free radical production among adjacent residues (Kanski *et al.*, 2002). Narayanan, *et al*., 2006, also found that fibril formation in the presence of αB crystallin was restricted due to the sHSP competing for $A\beta_{(1-40)}$ monomer interactions. Shammas, *et al*., 2011, further investigated this suggestion through looking at the effect of αB crystallin on pre-formed fibrils *in vitro*. αB crystallin was shown to tightly bind $A\beta_{(1-42)}$ and whilst bound, impede fibril elongation. High concentrations of αB crystallin were not found to impede $A\beta_{(1-42)}$ fibril formation de novo (Narayanan *et al.*, 2006, Shammas *et al.*, 2011), pre-incubation of neurons with αB crystallin, was also found to increase the toxicity of Aβ upon exposure (Stege *et al.*, 1999).

Wilhelmus, *et al.*, (2006), have also shown αB crystallin to promote protofibril formation, but in cerebrovascular cells this structure was not toxic and indeed protected cells from the toxicity of Aβ through limiting the availability of Aβ at the cell surface. These data suggest the mechanism and regulation of Aβ toxicity may vary between cell types (Wilhelmus *et al.*, 2006a).

Others have suggested that the prevention of fibril formation through interaction of αB crystallin with Aβ, is able to directly reduce the toxicity of Aβ on the cell (Dehle *et al.*, 2010). However, the work by Dehle, *et al.*, 2010, did not

investigate oligomer formation and utilised MTT (3-(4,5-dimethylthiazol-2-yl)-2,5-diphenyltetrazolium bromide), a marker of mitochondrial dehydrogenase activity and a commonly used dye, for assessment of neuronal viability. Aβ has been shown to directly reduce this dye, providing false positive absorbances when the dye intensity is measured. MTT is a widely used dye, but there are now significant questions regarding its validity when used with Aβ, suggesting direct markers of cell apoptosis/death should be used (Benilova *et al.*, 2012, Wogulis *et al.*, 2005). Further support for the role in HSP27 and αB crystallin in prevention of fibril formation, come from evidence that the levels of these sHSPs negatively correlate to the concentrations of ROS and $NO^{\cdot}$, both of which are produced abundantly as fibrils are formed (Reviewed - Ecroyd and Carver, 2009).

αB crystallin has also been linked to increased tau degradation, possibly via ubiquitination. The sHSP has also been shown to bind tau and NFTs, preventing their phosphorylation with via interacting with kinases or through enhancing dephosphorylation by phosphatises and potentially acting through ubiquitin ligase capabilities. These data suggest αB crystallin may have a beneficial role in attempting to prevent disease progression (Bjorkdahl *et al.*, 2008). Interestingly, and in contrast to a significant quantity of data obtained using samples from Alzheimer's disease patients, mouse models and *C. elegans* (Link, 2006), work with another AD mouse model has shown levels of αB crystallin to decrease with age and disease progression (Ojha *et al.*, 2011). Such data raise important questions regarding selection of appropriate models and appropriate promoters for the study of complex disorders, such as AD. These data emphasis the impact of species/strain background choices as well

as particular methodological approaches on experimental conclusions that are drawn. Despite a wealth of research into the role of αB crystallin in Alzheimer's disease and amyloid fibril formation, a definitive positive/negative role remains to be established. Results for the majority of groups agree that αB crystallin limits fibril formation but the toxicity of the alternately formed products is debated. There remains no standard method for fibril production *in vitro*, the appropriate molar concentration of Aβ to use culture, the use of $A\beta_{(1-40)}$ or $A\beta_{(1-42)}$, and methods used to assess neurotoxicity. The range of experimental differences limits the conclusions that can be applied in understanding the disease state (Ecroyd and Carver, 2009).

1.4 Primary Hypothesis

Beneficial effects of IR1072 in multiple model systems of ageing and neurodegeneration are generated via a complex protein-based signalling cascade.

This hypothesis has been formulated following a series of key findings regarding the biological effects of IR1072. As detailed in the introduction, mitochondria are believed to be critical in absorption and key initiators of the biological effects of infrared light. Previously undertaken research in the laboratory established altered activity of Complex II following IR1072 exposure in CD-1 mice. Therefore it was critical to investigate this property in further detail in the present study. Research conducted by our laboratory had also previously established that chronic IR1072 exposure reduced the number of small amyloid plaques present in the TASTPM brain (Grillo *et al.*, 2013). Therefore it was logical to examine the heat shock protein family, a family of proteins known to be responsible for the removal of cellular aggregates, including β-amyloid. Another component of this primary hypothesis was to examine molecular changes underpinning observed improved working memory in CD-1 mice exposed to IR1072 (Michalikova *et al.*, 2008). Research conducted using lymphocytes had previously demonstrated protective effects of IR1072 against UVA-induced cytotoxicity (Bradford *et al.*, 2005); the primary hypothesis for this present study also required examination of whether IR1072 was able to protect neurons against disease related cytotoxicity; induced through oxidative-stress and β-amyloid exposure.

1.4.1 Key aims to address the primary hypothesis

1. Determine whether IR1072 exposure is sufficient to protect against toxic, disease-related insults in an *in vitro* neuronal culture system, assess the effects on cell proliferation and ATP production as a measure of mitochondria activity.
2. Determine whether the oxidative phosphorylation activity of electron transport chain components are altered by IR1072 exposure.
3. Assess the effects of IR1072 exposure on the levels of heat shock proteins and disease-related proteins via in a premature ageing mouse model, CD-1, and an Alzheimer's disease mouse model, TASTPM, via western blotting and immunohistochemistry.
4. Investigate the effect of age and sex on the photomodulatory effects of IR1072 in CD-1 mice and TASTPM mice, respectively through western blotting and immunohistochemistry.
5. Examine the effects of ageing on the expression levels of chaperone proteins and disease-related proteins in both the CD-1 and TASTPM strains to further understand the disease state.
6. Utilise the nematode *Caenorhabditis elegans* to understand/elucidate pathways essential to the biological effects of IR1072 and to understand how this information interplays with mammalian data.

Chapter 2: Methods and Materials

2.1 Animals

All mouse (*Mus musculus*) strains used in experiments were maintained in the Life Sciences Support Unit (LSSU), within Durham University. All mice had unrestricted access to food and water and were kept in a quiet same sex environment, under a 12 hour light/dark cycle. All procedures, including experimental, animal husbandry and breeding, were conducted in agreement with the UK Animal (Scientific Procedures) Act of 1986. PPL number: 40/3390.

CD-1 mice are the in-house mouse strain maintained at the Life Science Support Unit of Durham University.

TASTPM mice (heterozygous double transgenic mice (TASTPM) with the Swedish Amyloid Precursor Protein (K670N; M671L) double familial mutation (Thy-1-APP695Sw, Line 10 (TAS10) plus the PS1 (M146V) mutation (Thy-1-PS-1M146V) were backcrossed onto a pure C57BL/6 background originally obtained from GlaxoSmithKline (Harlow, Essex, UK) where a breeding programme was set up within the LSSU at Durham University.

2.2 *In vivo* IR Treatments and Apparatus

The treatment apparatus is comprised of LED arrays which emit infra red light at 1072 nm ± 25 nm. The arrays are fitted together to form a box in which the animal is enclosed for the duration of the exposure. This manner of treatment

ensures the animal will be exposed to IR1072 from every direction. The LEDs are pulsed at 600 Hz, with a duty cycle of 300 microseconds, 5 mW/cm^2. Thermal drift was prevented by the fitting of a standard cooling fan to the equipment, thus room temperature was maintained, temperature was monitored at all times. LED arrays at the same specification were used for *in vitro* work and work with *C. elegans*. Sham treatments were conducted using replica equipment which was fitted with LED arrays but did not emit any light, of any wavelength, when turned on. LED arrays were supplied by Virulite Distribution Ltd, UK and were validated by both Dr Gordon Dougal (Virulite Distribution Ltd, UK) and the Durham University Physics Department (Dr Andrew Beeby).

2.2.1 Acute IR1072 Treatments

CD-1 or TASTPM mice were exposed to IR1072 or Sham treatments, for six minutes per day, over a 10 day period. Tissue (liver and/or brain) was then immediately taken for preparation for use in mitochondrial studies, immunoblotting or immunohistochemistry.

2.2.2 Chronic IR1072 Treatments

CD-1 or TASTPM mice were exposed to IR1072 or Sham exposures for six minutes a day, for two consecutive days, twice a week over a 5-6 month period. The weights of the mice were monitored during this time period. Tissue (liver and/or brain) was taken to be prepared for immunoblotting, immunohistochemistry or mitochondrial respiratory studies.

2.3 Immunoblotting

2.3.1 Sample Preparation

CD-1 or TASTPM mice were stunned and sacrificed humanely using a Schedule 1 technique, brain tissue dissected, the left hemisphere removed and snap frozen at –20°C. Brains were homogenised individually in a glass/glass dounce homogeniser using 5 ml homogenisation buffer (50 mM Tris-Base, 5 mM ethylenediaminetetraacetic acid (EDTA), 5 mM ethyleneglycotetraacetic acid (EGTA) and 150 µM Protease Inhibitor Cocktail III, pH 7.4).

Protein concentrations were determined using a Lowry Protein Assay (Lowry *et al.*, 1951) using bovine serum albumin (BSA) as a protein standard. A stock solution of BSA (10 mg/ml) was diluted using distilled water to give a range of protein concentrations, 0-100 µg/ml, in triplicate. Protein samples of 5 µl and 10 µl aliquots, made up to 100 µl using distilled water, were also assayed in triplicate. Lowry reagent A (2% (w/v) sodium carbonate, 0.1 M sodium hydroxide, 5% (w/v) sodium dodecyl sulphate (SDS)), Lowry reagent B (2% (w/v) sodium potassium tartrate) and Lowry reagent C (1% (w/v) copper sulphate) were mixed to a ratio of 100:1:1, respectively.

0.5 ml of the Lowry reagent mixture was added to each sample and to the BSA protein standards; each was vortexed and incubated for 10 minutes at room temperature. 50 µl of Folin-Ciocalteau phenol reagent (1:1, Folin:dH_2O (distilled water)) was added to each sample and standards, each eppendorf vortexed and incubated for 30 minutes at room temperature in the dark. After this time, 0.5 ml of distilled water was added to each eppendorf to terminate the reaction.

A Jenway Genova spectrophotometer was used to measure absorbance at λ=770 nm for each sample. A standard curve was plotted of λ=770 nm absorbance for BSA standards which was then used to determine unknown protein concentrations.

Samples were prepared for immunoblotting in 3x sample buffer (30 mM NaH_2PO_4, 30% (v/v) glycerol, 0.05% (w/v) Bromophenol blue, 7.5% (w/v) SDS, in dH_2O), DTT (Dithiothreitol, 23.5 mM final concentration, from a 200 mM stock solution made with dH_2O) with 10-50 µg of protein and made up to a final volume of 15 µl with dH_2O.

Samples were thoroughly vortexed, centrifuged at 13,000 rpm for one minute, incubated for five minutes at 95°C, centrifuged at 13,000 rpm for one minute and thoroughly vortexed again. Samples were then stored at -20°C or applied to an SDS-PAGE (polyacrylamide gel electrophoresis) gel for electrophoresis.

2.3.2 Immunoblotting

Samples underwent SDS-PAGE (Bradford *et al.*, 2005), wells were formed for loading samples using a 0.75 mm 10 well comb and formed from 6.5% SDS-PAGE stacking gel (56.0% (v/v) distilled water, 24.7% stacking gel buffer (0.5 mM Tris-base, 8 mM EDTA, 0.4% (w/v) SDS), 16.1% (v/v) acrylamide (40% stock, 29:1, acrylamide:bis-acrylamide), 2% ammonium persulphate (stock 1 mM made up with dH_2O) and 0.25% TEMED (Tetramethylethylenediamine (v/v)). After stacking gel had set, the comb was removed and the wells washed with water.

10% acrylamide resolving gels (49.73% (v/v) dH_2O, 24.86% (v/v) acrylamide (40%, 29:1, acrylamide:bis-acrylamide), 24.86% (v/v) running gel buffer (1.5 mM Tris-base, 8 mM EDTA, 0.4% (w/v) SDS), 0.5% ammonium persulphate (1 mM stock made with dH_2O) and 0.05% TEMED); 15% acrylamide resolving gels (37.3% (v/v) dH_2O, 37.29% (v/v) acrylamide (40%, 29:1, acrylamide:bis-acrylamide), 24.86% (v/v) running gel buffer (1.5 mM Tris-base, 8 mM EDTA, 0.4% (w/v) SDS), 0.5% ammonium persulphate (1 mM stock made with dH_2O) and 0.05% TEMED), or 7.5% acrylamide resolving gels (55.94% (v/v) dH_2O, 18.65% (v/v) acrylamide (40%, 29:1, acrylamide:bis-acrylamide), 24.86% (v/v) running gel buffer (1.5 mM Tris-base, 8 mM EDTA, 0.4% (w/v) SDS), 0.5% ammonium persulphate (1 mM stock made with dH_2O) and 0.05% TEMED) were used.

Resolving gels were left to set for 30 minutes prior to use, following this gels were placed in Hoefer Mighty Small II SE 260 vertical slab gel electrophoresis tanks (Hoefer, Germany) and the tanks were filled with electrode buffer (50 mM Tris-base, 384 mM glycine, 1.8 mM EDTA, 0.1% SDS (w/v) pH 8.8). Previously prepared 15 µl samples and pre-stained standard (10-250 kDa) were loaded into stacking gel wells using a 50 µl Hamilton syringe.

Electrophoresis was conducted at 180 V and 10 mA, until samples had entered the resolving gel, after which mA were increased to 15 mA until the 10 kDa marker reached the bottom of the gel.

Protein within the resolving gel was transferred onto nitrocellulose membrane by using a transfer cassette composed of sponge, two sheets of blotting card, nitrocellulose membrane (0.45 µm pore size), SDS-PAGE gel, two sheets of

blotting card and another sponge, all of which were soaked in transfer buffer previously, bar the SDS-PAGE gel. Air bubbles were removed during the construction of the cassette by rolling a 50 ml Falcon tube over each layer, bar directly rolling the nitrocellulose and acrylamide. Transfer of proteins onto nitrocellulose membrane was performed using transfer buffer (25 mM Tris-Base, 192 mM Glycine, 20% Methanol (v/v)) and a Hoefer TE Series transfer unit (Hoefer, Germany), set at 50 V, <200 mA, for 2.5 hours (or less, depending on protein size) kept cold using ice and cool packs.

Following transfer, the nitrocellulose was incubated in 10 ml blocking buffer (5% (w/v) dried milk powder, 0.2% (v/v) Tween-20, 100 µl 2 M NaOH, in TBS (Tris Buffered Saline (50 mM Tris-base, 0.9% (w/v) sodium chloride, pH 7.4)), for one hour at room temperature, with gentle agitation.

Nitrocellulose was the incubated with primary antibody (see table 2.1) in incubation buffer (TBS pH 7.4, 2.5% dried milk powder) at 4°C for antibody specific incubation times (see table 2.1) with gentle agitation. Following the incubation period, the nitrocellulose was washed four times for 10 minutes each, in 10 ml wash buffer (TBS pH 7.4, 2.5% dried milk powder, 0.2% Tween-20) at room temperature with gentle agitation. Nitrocellulose was then incubated for one hour at room temperature in incubation buffer containing 1:2000 dilution of HRP (horseradish peroxidase) linked anti-mouse or anti-rabbit (see table 2.1) antibody with gentle agitation. Excess secondary antibody was removed by washing as described previously. Nitrocellulose was then rinsed in TBS and incubated in 10 ml luminol solution (Solution A: Solution B 1:1, (Solution A, 100 mM Tris-base pH 8.5, 25 mM luminol, 396 µM p-Coumaric acid. Solution B, 100 mM Tris-base pH 8.5, 6.27 mM H_2O_2). Luminol was then drained from the

nitrocellulose and wrapped in cling film, after which it was taped into a film cassette. The nitrocellulose was then exposed to Hyperfilm™ for various times, the hyperfilm was then developed using Kodak-D19 developer and fixed for five minutes in Kodak Unifix fixative.

The immunoreactive signals from each lane were quantified using ImageJ (version 1.43, National Institute of Health, USA). Optical density of the labelled bands was normalised against the background density. Protein levels were standardised using anti-mouse β-actin primary antibody (1:2000 dilution, Sigma, UK).

2.3.3 Protocol for Phosphorylated Antibodies

Method was followed as stated previously in 2.3.2, until the end of the transfer stage when membranes were blocked in 10 ml blocking solution (5% (w/v) BSA, 0.1% (v/v) Tween-20, in TBS) for one hour at room temperature. Subsequently antibodies were incubated with membrane in a 2.5% (w/v) BSA, 0.1% (v/v) Tween-20 TBS solution for 3 days at 4^{o}C, with gentle agitation. Membranes were then subjected to four 10 minute washes using a 0.1% (v/v) Tween-20 TBS solution. Secondary antibody was incubated at 1:1000 dilution of HRP linked anti-mouse or anti-rabbit (see table 2.1) antibody, in a 2.5% (w/v) BSA, 0.1% (v/v) Tween-20 TBS solution for one hour at room temperature, with gentle shaking. Excess secondary antibody was removed by washing the membrane four times, each for 10 minutes in 0.1% (v/v) Tween-20 TBS buffer. Nitrocellulose membrane was then incubated for five minutes in Pierce® SuperSignal West Pico Chemiluminescent Substrate, mixed 1:1. Excess

developing solution was then removed from the membrane, the membrane enclosed in cling film and taped into a cassette, exposed to Hyperfilm™, developed using Kodak-D19 developer, then fixed for five minutes in Kodak Unifix fixative.

Membranes were rinsed in stripping buffer (200 mM glycine, 0.1% SDS (w/v), 1% Tween-20 (v/v), pH 2.2) before incubation in 10 ml stripping buffer for 10 minutes with gentle shaking. Following this, the membrane was washed twice, each for 10 minutes in TBS. Subsequently, membranes were washed twice with 0.1% (v/v) Tween-20 TBS solution for five minutes per wash. Following this the membrane was blocked for one hour, at room temperature with gentle shaking, in 10 ml blocking buffer (5% (w/v) dried milk powder, 0.02% (v/v) Tween-20, 100 µl 2 M NaOH, in TBS. The membrane was then incubated with anti-mouse β-actin primary antibody (1:5000 dilution, Sigma Aldrich, UK) to standardise protein levels, following the method described in 2.3.2.

Table 2.1. Antibody Concentrations and Conditions

Antibody	Predicted Weight (kDa)	Acrylamide Gel %	Monoclonal/ polyclonal	Concentration	Secondary	Incubation (Days)	Source	Peptide Blocking Agent
APP	90	10	Polyclonal	1:1000	Rabbit	2	Cell Signaling	Marvel
AT8	79	10	Monoclonal	1:50	Mouse	2	ThermoFisher	BSA
GluA2 (N19)	100	7.5	Polyclonal	1:2000	Goat (1:5000)	1	Santa Cruz	Chicken Albumin
GSK-3β	50	10	Polyclonal	1:10,000	Rabbit	1	Sigma Aldrich	Marvel
HSF1	66	10	Polyclonal	1:200	Rabbit	2	ProteinTech	Marvel
HSP105	105	7.5	Polyclonal	1:250	Rabbit	2	Cell Signaling	Marvel
HSP70	70	10	Polyclonal	1:125	Rabbit	2	Cell Signaling	Marvel
HSP27	28	15	Polyclonal	1:100	Rabbit	3	Cell Signaling	Marvel
PS1	53	10	Polyclonal	1:300	Rabbit	2	AbCam	BSA
P-HSP27 (Ser82)	27	15	Polyclonal	1:100	Rabbit	3	Cell Signaling	BSA
P-Tau (Ser519)	50	10	Monoclonal	1:5000	Rabbit	1	AbCam	BSA
SDHC	19	15	Polyclonal	1:1000	Rabbit	2	ProteinTech	Marvel
TARP γ2	37	10	Polyclonal	0.25 µg/ml	Rabbit	1	In house	Marvel
TARP γ8	50	10	Polyclonal	0.25 µg/ml	Rabbit	1	In house	Marvel
THY-1	22	15	Polyclonal	1:200	Rabbit	2	Cell Signaling	BSA
αB Crystallin	20	15	Monoclonal	1:100	Mouse	2	Roy Quinlan	Marvel
β-amyloid$_{(1-40)}$	87	10	Polyclonal	1:500	Rabbit	3	AbCam	BSA
β-amyloid$_{(1-42)}$	87	10	Polyclonal	1:200	Rabbit	3	AbCam	BSA
β-actin	43	-	Monoclonal	1:2000	Mouse	1	Sigma Aldrich	Marvel

2.4 Immunohistochemistry

2.4.1 Tissue Preparation

CD-1 or TASTPM mice were stunned, decapitated and brains rapidly dissected. The right hemisphere was removed and placed in a paraformaldehyde fixative solution (4% paraformaldehyde, 0.1 M Na_2PO_4, 0.1 M NaH_2PO_4, pH 7.4) for one week. After which the brains were primarily dehydrated in 10% sucrose overnight followed by 20% sucrose and 30% sucrose sequentially, made up with PBS (phosphate buffered saline, diluted from 10x stock solution, pH 7.4). Once the tissue was dehydrated, the brains were snap-frozen in isopentane at -70°C for one minute, and then stored at -80°C. Hemispheres were cut using a Leica model CM 3050S Cryostat at -25°C into 25 µm sagittal sections. The sections were then transferred into 24-well plates containing TBS 0.02% (w/v) sodium azide and stored at 4°C.

2.4.2 Immunohistochemical Protocol

To prevent endogenous peroxidase activity, samples were incubated at room temperature for 30 minutes in a solution of TBS, 10% (v/v) methanol and 3% (v/v) hydrogen peroxide (30% stock). Samples were then washed three times for five minutes in TBS-T, 0.2% (v/v) Triton X-100 in TBS. After this time sections were incubated for 30 minutes at room temperature in 0.2% (w/v) glycine, made in TBS. This was performed to quench excess paraformaldehyde.

Sections were subsequently blocked for one hour in 10% FCS (v/v) (Foetal Calf Serum) made in TBS-T. This was followed by incubation with the primary antibody in 1% (v/v) FCS and TBS solution; anti-GSK-3β was used at 1 µg/ml and kept at 4°C overnight. Following incubation with the primary antibody, sections were allowed to reach room temperature for one hour. Sections were then washed three times, each for five minutes in TBS-T. Consequently, sections were incubated at room temperature for two hours with 50 µl biotinylated anti-rabbit secondary antibody (Vector Laboratories, UK, part of VectorStain ABC Kit) in a solution of 1% (v/v) FCS and TBS. Sections were then washed three times, each for five minutes in TBS-T. ABC reagent (Vector Laboratories) was mixed 30 minutes before use and constituted of 100 µl of reagent A, 100 µl reagent B in 5 ml TBS. Sections were incubated in ABC reagent for one hour at room temperature. Sections were subsequently washed three times for five minutes each in TBS-T. This was followed by two subsequent washes for five minutes in TBS.

Samples were developed using 3,3'-Diaminobenzidine (DAB) solution (200 µl Buffer solution, 100 µl DAB and 100 µl H_2O_2 in 5 ml dH_2O; DAB peroxidase substrate kit, Vector Laboratories). After this point, developing was stopped by the addition of dH_2O and DAB solution removed. Sections were then rinsed three times in dH_2O. Sections were mounted, air-dried and coverslipped using DPX mountant and glass coverslips.

2.4.3 Protocol for Mouse on Mouse antibodies

For the anti-AT8 antibody (ThermoScientific, Fisher, UK), a Vector® M.O.M™ Kit (Vector Laboratories) was used as the primary antibody had been raised in a mouse and mouse tissue was being probed.

The initial steps were similar to the standard method; 2.4.2 was followed until the blocking stage. After which antigen retrieval was then performed on sections by incubating sections for 30 minutes in 50 mM Sodium Citrate, pH 8.4 and room temperature. This was followed by incubation with fresh 50 mM Sodium Citrate, pH 8.4, at 80°C for 30 minutes. Sections were then washed for 15 minutes with TBS-T. Samples were blocked for one hour using M.O.M™ Mouse Ig Blocking Reagent (4% (v/v) stock solution, diluted in TBS) with gentle shaking. Sections were washed twice for two minutes using TBS before incubation in M.O.M™ working diluent (8% (v/v) supplied protein concentrate stock solution in TBS) for five minutes. Anti-AT8 antibody was diluted to give a concentration of 1 µg/ml in the M.O.M™ working diluent and incubated overnight at 4°C, with gentle agitation. Subsequently, sections were washed twice for two minutes in TBS and incubated for 10 minutes with biotinylated secondary antibody (0.4% (v/v) M.O.M™ Biotinylated Anti-Mouse IgG, 8% (v/v) supplied protein concentrate stock solution in TBS). Samples were again washed twice for two minutes in TBS before application of ABC reagent (Vector Laboratories, 4% (v/v) Reagent A, 4% (v/v) Reagent B in TBS) which was created 30 minutes before use and allowed to mix. Sections were incubated in ABC reagent for five minutes at room temperature and consequently washed twice for two minutes in TBS before developing.

Samples were developed using DAB solution (4% (v/v) Buffer solution, 2% (v/v) DAB and 2% (v/v) H_2O_2 in dH_2O; DAB peroxidase substrate kit (Vector Laboratories, UK)). After this point, developing was stopped by the addition of dH_2O and DAB solution removed. Sections were then rinsed three times in dH_2O. Sections were mounted, air-dried and coverslipped using DPX mountant and glass coverslips. Sections were viewed on a Nikon Eclipse E400 microscope, where images were photographed using Progen Eyepiece 3 mega-pixel camera in TSView 7, Tuscen Image Technology Co., Ltd., China.

2.5 Mitochondrial Respiratory Studies

2.5.1 Mitochondrial Isolation

Mice were stunned and decapitated, brain tissue removed and kept cold on ice in isolation buffer (220 mM mannitol, 60 mM sucrose, 5 mM Tris-base, 1 mg/ml BSA (essentially fatty acid free), 0.5 mM EGTA, pH 7.4). Liver tissue was also removed, kept cold on ice and in a separate isolation buffer (250 mM Sucrose, 3.4 mM Tris-base, pH 7.4). Tissues were rinsed three times in their respective isolation buffers to remove excess blood. Tissues were roughly chopped using scissors and subsequently rinsed twice in a small volume (<5 ml) of isolation buffer using a Pasteur pipette. Tissue was homogenised gently three-four times using a loose pestle in a 7 ml dounce glass/glass homogeniser containing 5 ml of ice-cold isolation buffer. A smooth suspension was gained by further homogenising the tissue using a tight pestle seven-eight times. Brain and liver homogenates were then transferred to clean JA20 tubes, balanced with isolation buffer, and centrifuged using a Beckman JA20 rotor at 2000 rpm for 10

minutes, at 0-4°C. Subsequently, the pellet was discarded and the supernatant further centrifuged at 10,000 rpm for 10 minutes, at 0-4°C.

The liver preparation supernatant was discarded and the pellet resuspended in chamber buffer (220 mM mannitol, 60 mM Sucrose, 5 mM Tris-Base, 1 mg/ml BSA (essentially fatty acid free) pH 7.4) at 10,000 rpm for 10 minutes at 0-4°C. After this, the supernatant was discarded and the remaining pellet resuspended gently in approximately 0.5 ml chamber buffer at room temperature, ready for oxidative phosphorylation experiments.

For the brain suspension, the pellet was resuspended in approximately 9 ml of ice-cold Percoll® solution (250 mM Sucrose, 5 mM Tris-HCl, 0.1 mM EGTA, 18% Percoll®, pH 7.4). The brain tissue was then centrifuged at 10,000 rpm for 45 minutes.

After centrifugation two layers were visible in the JA20 tube, the top layer containing synaptosomes and the bottom containing a loose mitochondrial pellet. Using a Pasteur pipette, the top layer was removed and placed in a clean JA20 tube. The loose mitochondrial pellet was then removed using a Pasteur pipette and placed in a clean JA20 tube. Both were resuspended in room temperature chamber buffer and centrifuged at 10,000 rpm for 10 minutes in order to remove Percoll®. Subsequently, the supernatant was removed and discarded from both JA20 tubes. The pellets were individually resuspended gently using Pasteur pipettes in approximately 8 ml of chamber buffer and centrifuged for 10 minutes at 10,000 rpm. Finally, the supernatant was removed, leaving approximately 200 µl of synaptosomes and mitochondria. Synaptosomes were frozen and the mitochondria were used immediately in

oxidative phosphorylation studies. Protein concentrations were determined spectrophotometrically using the Lowry Protein Assay (See 2.3.1.; Lowry *et al.*, 1951).

2.5.2 Oxidative Phosphorylation Protocol

A Clark-type oxygen electrode was used to polarographically measure mitochondrial oxygen consumption (Sweetman and Weetman, 1969) with a maximum bath volume of 1 ml (Rank Bros, Bottisham, UK). A Kipp and Zonen flat bed recorder was calibrated to provide a chart speed of 0.5 mm/sec and a full-scale deflection of 10 mV to record changes in oxygen consumption.

The reaction chamber had a final volume of 0.3 ml, made up of chamber buffer plus 5 mM KH_2PO_4, saturated with oxygen (139 ng O atoms/ml). The experiment began with the addition of liver (0.9-1.2 mg) or brain (0.3-0.5 mg) mitochondria protein to measure oxidative respiration and the chamber sealed.

Endogenous respiration was measured for one minute, after this time substrate was added to the chamber and the chamber re-sealed. Substrates were 5 mM succinate or 5 mM glutamate plus 5 mM malate, added to measure state 4 respiration, where the mitochondria respire in the presence of excess oxygen and excess substrate, in the absence of ADP.

After recording state 4 respiration for 1 minute, ADP (167 μM) was added in order to measure state 3 respiration, at this point substrate, oxygen and ADP are all in excess. As the ADP becomes phosphorylated, state 4 respiration

returns, leaving oxygen and substrate in excess only (Chance and Williams, 1956a).

RCI (Respiratory Control Index) was calculated by dividing state 3 respiration rate by return to state 4 respiration rate, giving a measure of the integrity of mitochondria and of oxidation coupling to ATP synthesis in the respiratory chain. Values greater than 3 and 2 for substrates, glutamate plus malate and succinate respectively, indicate tightly coupled mitochondria (Chance and Williams, 1956a).

Glutamate (5 mM) plus Malate (5 mM) Succinate (5 mM)

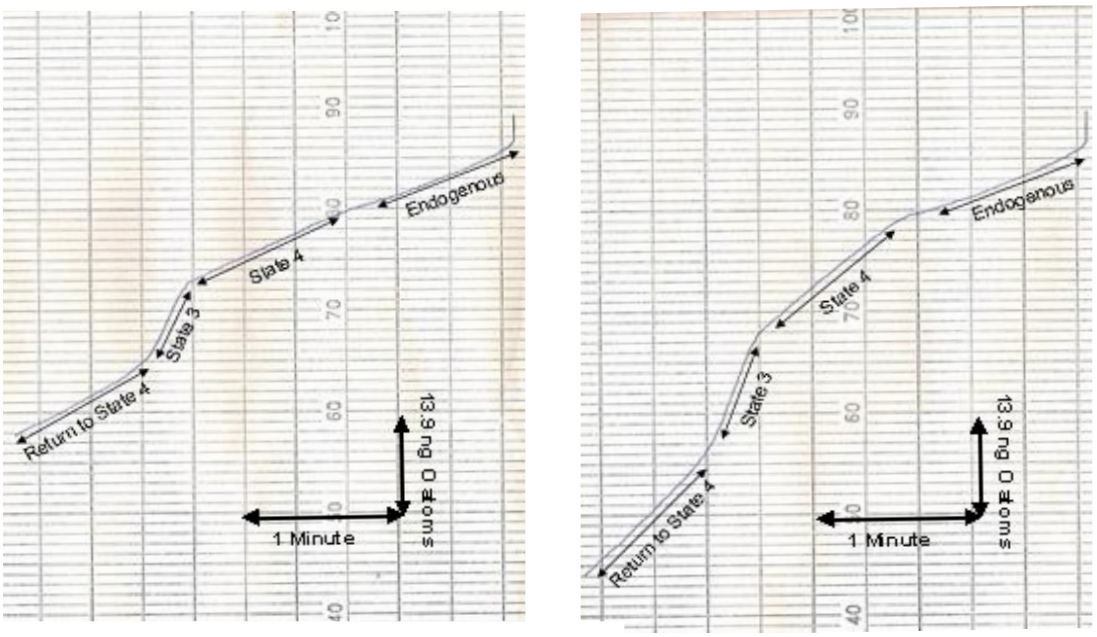

Figure 2.1. Examples of Oxidative Phosphorylation traces for Complex I and II. Traces generated by measuring the endogenous respiration, mitochondria only, for one minute before the addition of any substrate, one minute after adding glutamate (5 mM) plus malate (5 mM; Complex I) or succinate (5 mM; Complex II) which is noted as state 4 respiration. State 3 respiration is measured following the addition of ADP (167 µM) and as ADP becomes phosphorylated, respiration returns to state 4, respiration is measured until it has completely returned to State 4 and is then also recorded for one minute.

2.6 Neuronal Cultures

2.6.1 Cell maintenance

CAD (Cath.a differentiated) murine CNS (central nervous system) catecholaminergic cell line were maintained in 75 cm^3 (Sarstedt, UK) flasks in Gibco® DMEM (Dulbecco's Modified Eagle's Medium) /F12 +GlutaMAX® +10% FCS.

2.6.2 *In vitro* IR1072 Treatments

The treatment apparatus is composed of LED arrays which emit infra red light at 1072 nm ± 25 nm. The arrays are fitted together to be held above the cell culture plate being irradiated, see figure 2.2. The LEDs are pulsed at 600 Hz, with a duty cycle of 300 microseconds, 5 mW/cm^2.

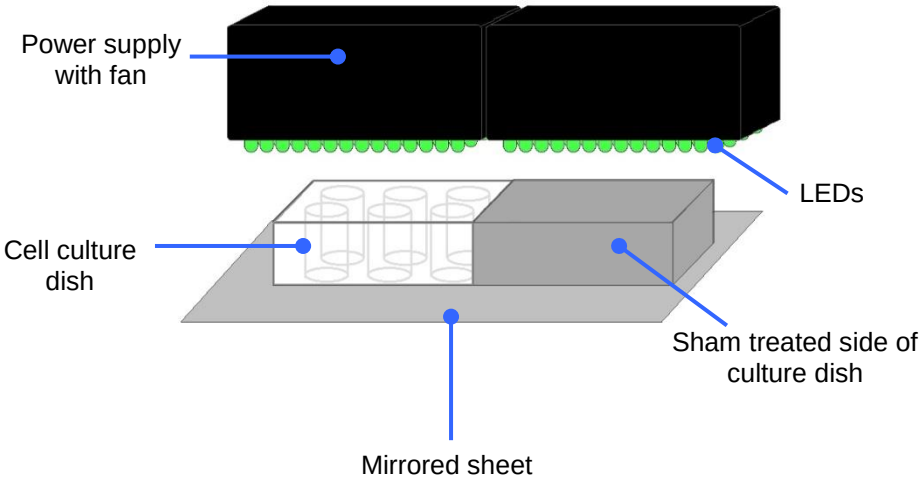

Figure 2.2. IR1072 treatment apparatus used in tissue culture experiments

2.6.2.1 In vitro IR1072 preconditioning

CAD cells were seeded in 96 well plates (Sarstedt, UK) and grown at 37°C, 5% CO_2, for 72 hours before use.

Cells were exposed to five sets of three minute treatments of IR1072 or Sham treatments, with 30 minutes between each exposure. Cells were then exposed to hydrogen peroxide for four hours at a final concentration of 100, 75 or 50 µM,

with PBS as a volume control. After this a MTT assay was performed (see 2.6.3).

2.6.2.2 In vitro IR1072 exposure plus Hydrogen Peroxide insult

CAD cells were seeded in 96 well plates (Sarstedt, UK) and grown at 37°C, 5% CO_2, for 72 hours before use. Cells were exposed to 150 or 50 µM H_2O_2 in DMEM/F12 + GlutaMAX® + 10% FCS or to a PBS volume control in DMEM/F12 + GlutaMAX® + 10% FCS. Immediately after the addition of the media containing H_2O_2 or PBS, cells were exposed to five sets of three minute IR1072 treatments, 30 minutes apart, for Sham treated. Four hours after the addition of the media containing H_2O_2, an MTT assay was performed (see 2.6.3).

2.6.3 MTT Assay

MTT (3-(4,5-dimethylthiazol-2-yl)-2,5-diphenyltetrazolium bromide) uses mitochondrial dehydrogenase activity as a measure of cell viability. 10 µl of MTT (5 mg/ml, in PBS, sterile filtered) was added to each well and incubated for 2.5 hours at 37°C. After this time, the media containing MTT was removed and 100 µl of isopropanol added to each well. Following dissolution of the formazan crystals, the density of each well was measured spectrophotometrically at 595 nm using a Multiskan Ascent Plate Reader, Version 2.6. Isopropanol alone was used as a density control.

2.6.4 CytoTox 96 Non-radioactive Assay (Promega, UK)

CytoTox 96 assay kit quantifies LDH (lactate dehydrogenase) levels as a measure of cell lysis (necrosis).

Media was removed from cells and centrifuged at 13,000 rpm for two minutes. The supernatant containing the LDH was retained and the pellet resuspended in PBS, using the same volume removed from the cells, and placed back into the respective well of the 24 well plate. The 24 well plate was then frozen for two hours at -20°C to lyse all remaining cells. Cells were subsequently thawed and centrifuged at 13,000 rpm for two minutes; again the supernatant was retained as a measure of total remaining LDH. Dilutions; 1:10 and 1:20, were made of each supernatant using PBS as the diluent with DMEM/F12 plus 10% FCS used to calibrate the assay. 50 µl of substrate mix was added to 50 µl of each dilution prior to incubation for 30 minutes at room temperature in the dark. Neat, 1:10 and 1:20 dilutions were all completed in triplicate. Following this, 50 µl of stop solution was added to each well and the absorbance measured at 490 nm on a Multiskan Ascent Plate Reader, Version 2.6. Cell lysis, via LDH release in the media supernatant, was calculated as a percentage of the sum of total LDH absorbance, combining the absorbance of positive control freeze-thawed cells and absorbance of media containing LDH.

2.6.5 ATP Determination Assay (A22066, Invitrogen, USA)

Using 24 well plates, CAD cells were passaged and maintained in DMEM/F12 +GlutaMAX® +10% FCS and maintained at 37°C, 5% CO_2, for 72 hours. After

this time, cells were exposed to IR conditioning, consisting of five sets of three minute IR1072 or sham exposures with 30 minutes between each treatment. ATP was either assayed immediately after the final IR1072 exposure or the cells were returned to the incubator for four hours. Media was removed and replaced with 300 µl of cell lysis buffer (100 mM Tris-HCl, pH 7.7, 2 M NaCl, 20 mM EDTA, 0.2% (v/v) Triton-X100) and stored at 4°C for one hour. Buffer from each well was then centrifuged for 15 minutes at 13,200 rpm to remove cell debris. A standard reaction solution was made, as directed in the assay instructions. Using white Greiner® 96 well CellStar® UClear Bottom plates, 10 µl of the supernatant from each sample was added to 90 µl of this solution and incubated for 15 minutes. After this time the luminescence was measured on a MicroBeta® 1450 TriLux Luminescence Counter Workstation Version 3.2 and ATP concentration determined from a standard curve of [ATP] vs. luminescence, performed each time an assay was completed as instructed by the assay kit.

2.6.6 Immunocytofluorescence

Using 24 well plates, sterile 13 mm glass coverslips were poly-d-lysine (Sigma, UK) coated at room temperature for 12 hours, under UV light in sterile conditions. Wells were rinsed twice with sterile PBS and CAD cells passaged into 24 well plates in DMEM/F12 +10% FCS and maintained for at 37°C, 5% CO_2, for 72 hours.

After 72 hours, cells reached 70% confluence; media was replaced and cells were exposed to IR conditioning. This consisted of five sets of three minute

IR1072 or sham exposures with 30 minutes between each treatment. Following the final treatment, cells were returned to the incubator for four hours. After this time, the media was removed from the wells and coverslips washed with PBS-T (PBS with 0.05% (v/v) Tween-20) for five minutes, twice. Cells were fixed in 4% paraformaldehyde for 15 minutes and then washed twice, as stated previously.

Cells were then permeabilised using 0.5% (v/v) Triton X-100 in PBS for 10 minutes and washed a further time. Cells were then blocked using PBG (1% BSA (w/v; Fraction V, minimum 96% lyophilized powder), 0.5% (v/v) cold water fish skin gelatin in PBS, pH 7.4) for 15 minutes, after which the primary antibody was diluted in PBG; 1:400 anti-Ki67, and cells were incubated with the primary antibody for one hour at room temperature. Cells were then washed three times using PBS-T, each for five minutes and then incubated with the secondary antibodies (1:100 anti-DAPI (4',6-diamidino-2-phenylindole) and 1:500 anti-rabbit Alexa fluor 488) for one hour. Cells were then washed five times with PBS-T, as previously stated, mounted with Mowiol (Calbiochem, UK) and left to dry overnight at room temperature in the dark, before storage at 4^{o}C. Cells were inspected using a Carl Zeiss Axioskop 2 microscope equipped for epifluorescence. Images were captured using a Hamamatsu Orca 285 CCD camera controlled by Improvision Volocity software version 6.

2.6.7 Preparation of β-amyloid Structures for use in Neuronal Cultures

Human β-amyloid$_{(1-42)}$ peptide, Ascent Scientific, UK, was dissolved in DMSO (dimethyl sulphoxide) at 1 mg/ml and stored at -80°C until use.

Prior to use, the molar concentration of the peptide was calculated and diluted to 200 μM using sterile PBS. The peptide was then incubated for 72 hours at 37°C, 5% CO_2, without agitation. The peptide was then diluted to the required concentration using DMEM/F12 plus GlutaMAX® +10% FCS, inverted and gently added to neuronal cultures, with DMSO in DMEM/F12 plus GlutaMAX® +10% FCS as a control volume in control neuronal cultures.

2.6.7.1 IR1072 Exposure of Cultures and Aβ

24 hours after seeding in 24 well plates, cells were exposed to five sets of 3 minute IR1072 treatments or sham treated, with 30 minutes between each exposure. 24 hours later, medium was removed and replaced with that containing Aβ or DMSO:PBS, five sets of three minute IR1072 or sham exposures immediately followed. 24 hours after media change, cells were exposed to five sets of 3 minute IR1072 treatments or sham treated, with 30 minutes between each exposure. 24 hours after this the CytoTox 96 non-radioactive assay was performed (see 2.6.4). Between each exposure and after each set of exposures cells were returned to the incubator and maintained at 37°C, 5% CO_2.

2.6.8 Electron Microscopy

Electron micrographs were obtained (figure 2.3) to determine the structure of the β-amyloid peptide following fibril formation as described in 2.6.7. A sample of 200 μM β-amyloid$_{(1-42)}$ peptide was removed, prior to the use of the peptide in

neuronal cultures. Samples were negative stained with 2% uranyl acetate (w/v), in distilled water, onto 400 mesh formvar coated copper grids and air dried. Samples were viewed using a Hitachi H7600 Transmission Electron Microscope. Mrs Christine Richardson conducted all electron microscopy in the Histology laboratory within the University of Durham.

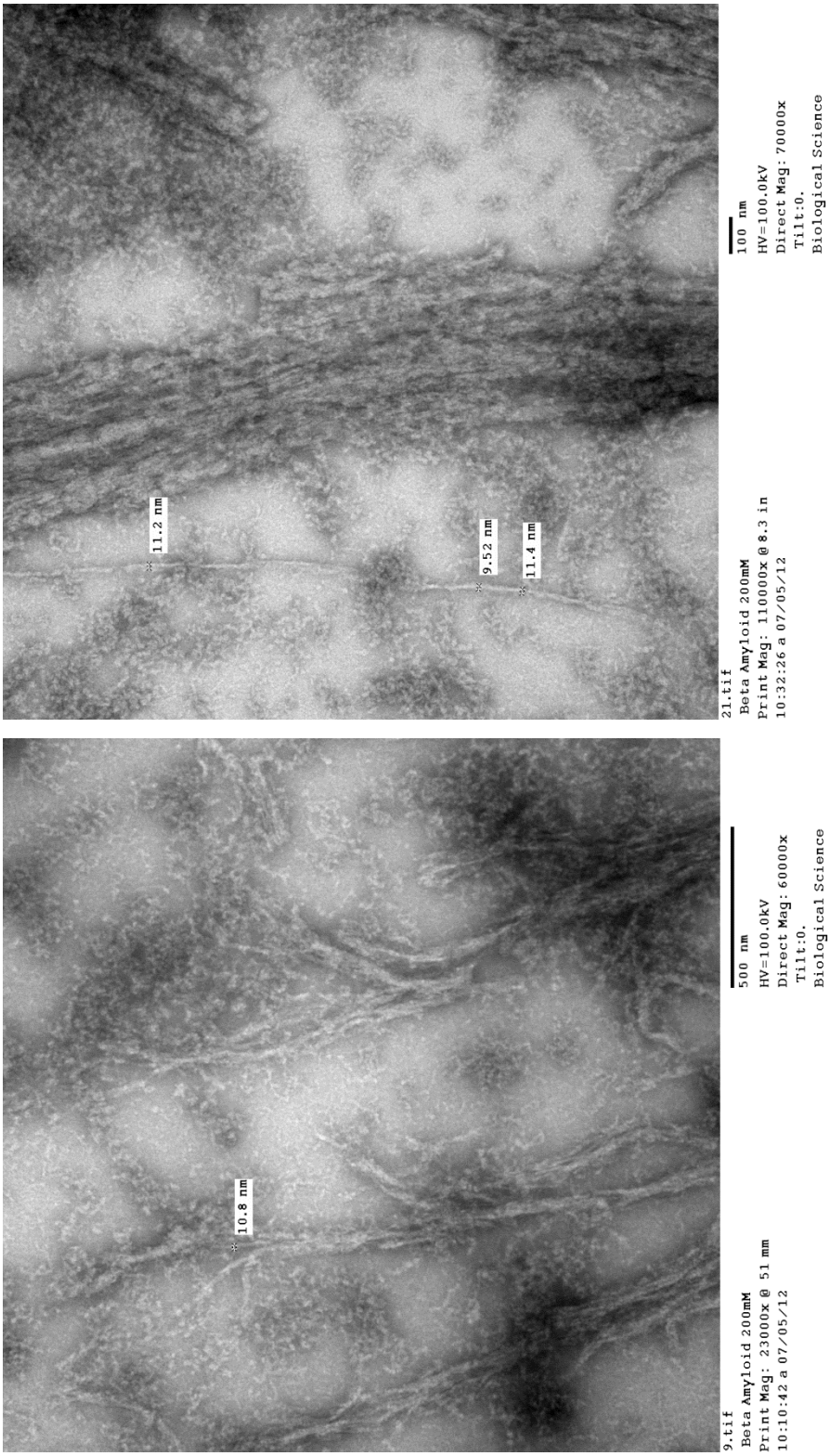

Figure 2.3. Representative electron micrographs of β-amyloid $_{(1-42)}$ fibrils/oligomers. Fibrils/Oligomers formed by the method stated in 2.6.7 and imaged as in 2.6.8. Scale bar on image A) 100 nm, B) 500 nm. Labelling of fibrils is defined in nm.

2.7 Statistical Analysis

All data were analysed using Microsoft Excel 2007 and GraphPad Prism Version 5, GraphPad Software Inc. All data were verified to be normally distributed. All data are displayed as mean ± standard error of the mean (SEM).

For CD-1 and TASTPM timeline data, data were subjected to one-way ANOVA analysis of variance, with a Bonferroni post-hoc test.

For comparing sham and IR1072 conditions, data were subjected to an unpaired two-tailed Student's T-test.

When examining the effect of IR1072 exposure and β-amyloid concentration on cell death in CAD cells; a two-way ANOVA analysis of variance was conducted, with a Bonferroni post-hoc test.

Significance denoted as $p<0.1$ representing a trend towards a significant difference between conditions, whereas $*p<0.05$, $**p<0.01$, $***p<0.001$ represent a significant difference between conditions.

2.8 Nematode Strains and Maintenance

A Leica Model MZ9.5 was used for all light microscopy.

SS104, *glp-4 (bn2)I*, nematodes were used for lifespan experiments and protein extraction assays. The SS104 are fertile at 15°C, but infertile when kept at 25°C.

Table 2.2. Summary of Nematode Strains Used in This Investigation

Strain Name	Genotype	Gene/Protein Effected	Mutation/Modification	Cutorial Remarks
CL2070	*dvIs70 Is[hsp-16.2::gfp; rol-6(su1006)]*	HSP16.2	HSP16.2 expressed via a GFP-tagged promoter	Used for lifespan studies and to determine if IR1072 exposure initiated HSP16.2 via imaging GFP levels
GR1307	*daf-16 (mgDf50) I*	*daf-16*	Eliminates gene coding region	Used for lifespan studies
N2	-	-	-	Wild type strain, used for lifespan studies
PS3551	*hsf-1(sy441) I*	*hsf-1*	Substitution, cytosine for thymine in coding sequence	HSF-1 expressed is non-functional, used for lifespan experiments
RB1104	*hsp-3 (ok1083) X*	*hsp-3*	Homozygous for *hsp-3* deletion	Used for lifespan studies
SJ4005	*zcIs4 (hsp-4::GFP)*	HSP4	HSP4 expressed via a GFP-tagged promoter	Used determine if IR1072 exposure initiated HSP4 via imaging GFP levels
SJ4100	*zcIs13 hsp-6::gfp*	HSP6	HSP6 expressed via a GFP-tagged promoter	Used for lifespan studies and to determine if IR1072 exposure initiated HSP6 via imaging GFP levels
SS104	*glp-4 (bn2)I*	Abnormal germ line proliferation	Temperature-induced sterility	Nematodes are fertile at 15°C, but infertile when kept at 25°C, used for lifespan studies and protein extraction

2.8.1 Nematode Growth Medium

NGM (nematode growth medium) was made using 1.5 g/l NaCl, 2.5 g/l peptone (NZ- Soy BL7, enzymatic hydrolysate) and 17 g/l agar in distilled water. Following sterilisation, 1 ml/l cholesterol (5 mg/ml in ethanol) was added followed by freshly sterilised 1 ml/l 1 M calcium chloride, 1 ml/l 1 M magnesium sulphate and 25 ml/l 1 M potassium phosphate (pH 6.0).

5 ml NGM was aliquoted per 35 mm plate under sterile conditions and allowed to set, prior to storage at 4°C until use.

2.8.2 M9 Buffer

M9 buffer was used in all bacterial viability assays and egg preparation (2.8.6), the solution was freshly produced and sterilised (via autoclaving) before each use. M9 (22 mM KH_2PO_4, 41 mM $Na_2HPO_4.2H_2O$, 85 mM NaCl) was separated into 250 ml aliquots, autoclaved and allowed to cool. 1 ml of 1 M $MgSO_4$ was added, per 250 ml aliquot, under sterile conditions prior to use.

2.8.3 Bacterial maintenance

All strains of OP50 bacteria (*E. coli*) were maintained in cultures kept at 4°C. Fresh bacterial cultures were grown by adding 35 ml LB (Luria-Bertani) media (10 g/l tryptone, 5 g/l yeast extract, 10 g/l sodium chloride, made up with dH_2O and autoclaved) to a 50 ml falcon tube. In sterile conditions, an inoculating loop was used to taken a sample of OP50 from either frozen or clean, refrigerated

cultures. These were then grown overnight at 37°C, whilst being continually agitated at 215 rpm.

2.8.4 Seeding plates

60 mm plates were seeded with 100 µl of OP50 under sterile conditions. The plates were then left to dry overnight at room temperature. This was performed 2-3 days before the use of the plates.

2.8.5 Chunking/strain maintenance

In order to maintain a high number of worms, plates were initially seeded, as described in 2.8.4. Following seeding, a sterile environment was created using a Bunsen burner, a small cube of agar was cut from starved plates of nematodes using a sterilised scalpel. These cubes were then transferred, worm side down, onto plates seeded 1-2 days previously. The cubes were placed adjacent to the bacterial lawn and then transferred to an incubator.

2.8.6 Egg Bleaching

This was performed using gravid worms. Individual plates were washed with 2 ml of M9 buffer; this was then pipetted into eppendorfs using a large pipette tip. The adult worms were then left for two minutes to settle into a loose pellet in the eppendorf, the excess solution was then removed leaving approximately 200 µl of solution and the loose worm pellet. 125 µl of bleach solution (7:8, Sodium

hypochlorite:4 M NaOH) was added to each eppendorf. The eppendorfs were then shaken continually for approximately five minutes, cessation of shaking occurred when loss of definition of the worms was observed. Eppendorfs were then filled to 1 ml with M9 buffer and centrifuged for 2,400 rpm for 90 seconds. After this time, the supernatant was removed and M9 used to fill the eppendorf to 1.5 ml, this was then vigorously shaken to dislodge the pellet. Again, the eppendorfs were centrifuged for 90 seconds at 2,400 rpm. The supernatant was removed, leaving approximately 50 µl of solution. The number of eggs was judged by eye under the microscope and more M9 buffer added to the eppendorf or the solution aliquoted onto seeded plates, dependent on the observable egg number. Plates were then stored at 15°C.

2.8.7 Egg Lay

Worms which had undergone method step 2.8.6 were grown until gravid, at this point gravid worms were transferred onto plates which had been previously seeded and stored at 25°C (15°C for SS104, *glp-4 (bn2)I* strain) for four hours. Subsequently the gravid worms were removed and the plates now containing eggs were kept at 25°C, except for work completed with the SS104 strain whereby the plates containing eggs were kept at 15°C for two to three days and then shifted to 25°C to induce sterility for timeline experiments. When the worms reached late L3/early L4 stages (as shown in figure 7.2) they were picked and transferred onto fresh plates for the lifespan protocol.

In non-sterile strains, the nematodes were transferred onto fresh, seeded 60 mm plates daily for a period of seven days following the initiation of egg laying

in the nematodes selected for the lifespan, in order to minimise the interference of progeny.

2.9 IR1072 Exposure of *C. elegans*

2.9.1 Apparatus and Protocol

Initial experiments were conducted using IR1072 apparatus consisting of 1072 nm near infrared LED array, which enclosed the 35 mm petri dishes, containing a known number of *C. elegans*. Irradiation was facilitated using 1072 nm LEDs pulsing at 600 Hz and a duty cycle of 300 microseconds, 5 mW/cm^2. Temperature was monitored and the apparatus was fitted with a standard cooling fan, to ensure thermal drift from peak wavelength was not achieved and as to not to heat shock *C. elegans*. Initial experiments were conducted using three, six and 12 minute cycles of exposure.

Further IR1072 experiments were conducted using a second apparatus; this consisted of six individual 1072 nm near infrared LED arrays fixed together horizontally. The 60 mm plates were positioned beneath the arrays and upon mirrored sheets to facilitate irradiation from every possible direction. Irradiation was again administered using 1072 nm LEDs pulsing at 600 Hz and a duty cycle of 300 microseconds, 5 mW/cm^2. Each array was fitted with an individual standard cooling fan. All experiments were conducted at 25°C within an LTE Qualicool™ incubator (LTE Scientific Ltd, Oldham, UK) and temperature was also monitored using a digital thermometer. Exposure cycle was 12 minutes every three hours for 24 hours. This was then repeated every three days. For

experimental set up, see figure 2.4. Both apparatus were supplied by Virulite Distribution Limited, County Durham, UK.

2.9.2 Preliminary Chronic IR Treatment Protocol

Initial experiments conducted with *C. elegans* included exposure to IR1072 treatments for three, six or 12 minutes daily until the *C. elegans* reached the end of their lifespan. Sham treatments conducted involved wrapping the petri dishes containing the *C. elegans* in aluminium foil, and exposing the *C. elegans* to IR1072 for three, six or 12 minute sessions. During the daily exposures the temperature of the internal box was monitored.

2.9.3 Secondary Chronic IR Treatment Protocol

Secondary *C. elegans* experiments were conducted using 12 minute exposure times every four hours, for 24 hours, conducted every three days until the end of the *C. elegans* lifespan. Again, the Sham treated dishes were wrapped in aluminium foil for the exposure duration. These experiments were undertaken within an incubator, maintained at 25°C.

2.9.4 Tertiary Chronic IR Treatment Protocol

Tertiary *C. elegans* lifespans were conducted using an alternate treatment protocol to limit any potential interference of intermittent heating of the nematodes caused by the equipment. This protocol consisted of a cycle of 50

seconds of IR exposure followed by a 100 second period of no exposure. This cycle was repeated for 24 hours, every three days for the duration of the lifespan.

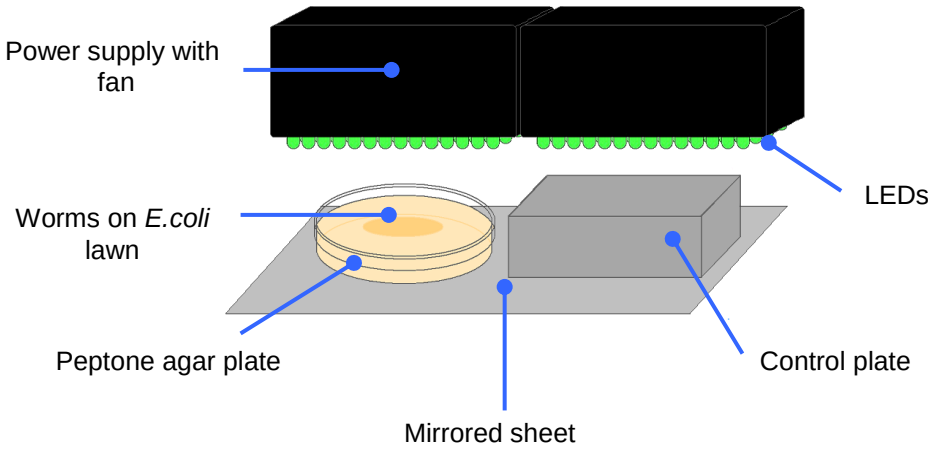

Figure 2. 4. *C. elegans* IR1072 treatment apparatus

2.9.5 Lifespan and Data Analysis

In all lifespan experiments the *C. elegans* were counted every second day, following the first week of the experiment and transferred to fresh 60 mm peptone plates every three to four days to prevent the onset of starvation and to limit effects of agar dehydration. All lifespan experiments were conducted at 25°C in a temperature controlled incubator. Lifespan data were analysed using JMP® Version 8.02 statistical software, (SAS Institute Inc, USA), where applicable data was fitted to the Kaplan-Meier survival model, with statistical significance determined using Log-Rank and Wilcoxon analysis.

2.9.6 Kanamycin Treated OP50 IR1072 Treatment Protocol

These experiments were carried out in the same manner as the above protocol, however *C. elegans* were transferred onto kanamycin treated OP50 (80 µl 10 mM kanamycin on 100 µl OP50 lawn, as described by Garigan *et al.*, 2002) for the duration of the lifespan. Lifespans were conducted as described in 2.9.5.

2.10 IR1072 and Bacterial Viability

2.10.1 Experimental Design

Six 60 mm NGM plates were seeded with 100 µl of OP50 bacteria. 24 hours later, two plates were treated with IR1072 irradiation for the following 24 hours at 25°C, two plates were treated with 80 µl of kanamycin (10 mM) and kept at 25°C and the remaining two plates were controls and also kept at 25°C for 24 hours.

2.10.2 Determining Viability

All six plates were removed from 25°C incubator and 1 ml of M9 (plus $MgSO_4$) added to each plate surface, under sterile conditions. A sterilised glass spreader was used to scrape the *E. coli* lawn into the buffer solution. The solution was then removed from the plate surface and aliquoted into an eppendorf. This was repeated for each plate and a freshly sterilised glass spreader was used each time.

The stock bacterial solutions were also diluted one in five, in duplicate for each plate, in order to determine the approximate number of colony forming units (CFUs) of the OP50 from each plate in each condition. The optical density at λ=600 nm was measured using a Jenway Genova spectrophotometer, where an absorbance of 1 = $8x10^8$ CFU per ml.

The stock solutions were then diluted to approximately the same concentration of CFUs using M9 (plus $MgSO_4$) and then a range of dilutions were created; 10^{-2}, 10^{-4}, 10^{-6}, 10^{-7}, 10^{-8}, 10^{-9}, 10^{-10}, in duplicate, for each plate. These dilutions were each vortexed and 100 µl from each dilution was pipetted onto a fresh 60 mm NGM plate and spread using a sterilised glass spreader. Two additional 60 mm plates were used to aliquot 100 µl of M9 (plus $MgSO_4$) buffer. See table 2.3. The 60 mm plates were then stored at 37°C overnight, 18 hours later the plates were removed and the number of colonies on each plate were counted.

Control				IR				Kanamycin			
Plate 1		Plate 2		Plate 1		Plate 2		Plate 1		Plate 2	
10^{-2}	10^{-2}	10^{-2}	10^{-2}	10^{-2}	10^{-2}	10^{-2}	10^{-2}	10^{-2}	10^{-2}	10^{-2}	10^{-2}
10^{-4}	10^{-4}	10^{-4}	10^{-4}	10^{-4}	10^{-4}	10^{-4}	10^{-4}	10^{-4}	10^{-4}	10^{-4}	10^{-4}
10^{-6}	10^{-6}	10^{-6}	10^{-6}	10^{-6}	10^{-6}	10^{-6}	10^{-6}	10^{-6}	10^{-6}	10^{-6}	10^{-6}
10^{-7}	10^{-7}	10^{-7}	10^{-7}	10^{-7}	10^{-7}	10^{-7}	10^{-7}	10^{-7}	10^{-7}	10^{-7}	10^{-7}
10^{-8}	10^{-8}	10^{-8}	10^{-8}	10^{-8}	10^{-8}	10^{-8}	10^{-8}	10^{-8}	10^{-8}	10^{-8}	10^{-8}
10^{-9}	10^{-9}	10^{-9}	10^{-9}	10^{-9}	10^{-9}	10^{-9}	10^{-9}	10^{-9}	10^{-9}	10^{-9}	10^{-9}
10^{-10}	10^{-10}	10^{-10}	10^{-10}	10^{-10}	10^{-10}	10^{-10}	10^{-10}	10^{-10}	10^{-10}	10^{-10}	10^{-10}

Table 1.3. Bacterial Viability Assay Dilutions

= 3 conditions (14 total dilutions per original plate x 2 original plates) + 2 M9 (plus $MgSO_4$) control plates; total of 86 plates

2.11 Nematode protein extraction for Spectrophotometer Analysis

40 x 60 mm plates of NGM were seeded with 100 µl OP50 bacteria and left for 48 hours, subsequently the plates were chunked onto (as described in 2.8.5) using plates with established SS104, *glp-4 (bn2)I* populations. The plates were then left at 15°C for five days.

After five days, the nematodes were washed into falcon tubes using M9 buffer (see 2.8.2) and gently centrifuged for two minutes to form a loose pellet. Excess M9 buffer was removed and nematode pellets snap frozen in liquid nitrogen for five minutes. Pellets were then thawed quickly in a 60°C water bath, and once thawed the falcons were immediately placed onto ice and lysis buffer (50 mM Tris HCl, 50 mM KCl, 10 mM EDTA, 1:100 Protease inhibitor cocktail III, 10 mM Na_3VO_4, 5 mM NaF, pH 8.0) added in an equal volume to that of the pellet. Worm pellets were then separated into 200 µl aliquots, kept on ice, and

sonicated three times for 10 second periods. Homogenate was left to stand on ice for 30 minutes and then centrifuged for 30 minutes at 13,200 rpm at 4^{o}C. Supernatant was subsequently removed and retained. Protein content of extraction was measure using a Lowry assay, described as in (2.3.1), with the exception that in using the lysis buffer in the preparation of the standards, the buffer was diluted 10 times due to high Tris HCl and EDTA content of buffer.

A Shimadzu UV-3600 UV-VIS-NIR Spectrophotometer (Shimadzu U.K. Ltd, Milton Keynes, UK) was calibrated using lysis buffer as a baseline. The absorbance spectra of samples, diluted to 1 mg/ml, were then measured from 1500 nm-600 nm. The spectrum of each sample was measured three times, with the sample being carefully resuspended before each reading.

2.12 Mitochondria extraction for Spectrophotometer Analysis

2.12.1 Absorbance Profile of Isolated Irradiated Mitochondria

Mitochondria were isolated from the liver and brain of four male, CD-1 mice at 5 months of age, as described in 2.5.1. A Lowry was performed on the isolated mitochondria, as described in 2.3.1, and the pure mitochondrial preparations were diluted to 1 mg/ml using ice-cold Chamber buffer and kept on ice at all times. A Shimadzu UV-3600 UV-VIS-NIR Spectrophotometer was calibrated using chamber buffer (see 2.5.1) as a baseline. The absorbance spectra of samples were then measured from 1500 nm-600 nm. The spectrum of each sample was measured three times, with the sample being carefully resuspended before each reading.

The mitochondria preparations were then exposed to five 6 minute exposures of IR1072, timed 30 minutes apart. The irradiation was carried out by aliquoting the mitochondria preparation to a 35 mm petri dish. Between IR1072 exposures, the mitochondria were returned to a cuvette and kept on ice. The absorbance profile of the mitochondria was recorded three times immediately prior to the following IR exposure. This was repeated for both the brain and liver mitochondrial preparations. Using Microsoft Excel 2007 the absorbances were corrected for baseline readings and the average of each reading plotted.

2.12.2 Absorbance Profile of Mitochondria Irradiated for 10 days *in vivo*

4 male three month old CD-1 mice were irradiated for six minutes a day for a period of 10 days, as described in 2.2.1. Mitochondria were isolated from the liver and brain, as described in 2.5.1.

A Lowry was performed on the isolated mitochondria, as described in 2.3.1, and the pure mitochondrial preparations were diluted to 1 mg/ml using ice-cold Chamber buffer and kept on ice at all times. A Shimadzu UV-3600 UV-VIS-NIR Spectrophotometer was calibrated using Chamber buffer (see 2.5.1) as a baseline. The absorbance spectra of samples were then measured from 1500 nm - 600 nm. The spectrum of each sample was measured three times, with the sample being carefully resuspended before each reading.

Chapter 3: Acute IR1072 Treatments - Effects *in vitro* using murine neuronal-derived cultures

3.1 Introduction

3.1.1 *In vitro* model system – neuronal cultures

Neuronal cultures provide a useful, simplified model system to enable direct investigation of a biological system under controlled and reproducible conditions which can only be controlled to a limited extent in whole animal models. The defined system allows for any variations in outcome to be attributed to particular components of the system which can be manipulated. *In vitro* systems provide a relatively low-cost, non-time consuming method with high replicability; they also enable the ability to work at high *n* numbers, resulting in a reduced need for animals in scientific procedures, allaying some ethical issues associated with biological research (Hartung *et al.*, 2002, Qi *et al.*, 1997).

Neuronal culture systems present a unique method to study every facet of neural processes; including synapse formation, differentiation, functionality, and to apply these investigations in understanding/manipulating potential therapies.

For the purpose of these investigations, CAD (Cath.a-differentiated) cells were used. CAD cells are a catecholaminergic cell line, derived from the Cath.a cell line which was procured from a brain tumour that had developed in a transgenic mouse model. Cath.a cells express a range of neuronal markers including synaptophysin and Na^+, Ca^{2+} and K^+ voltage gated channels, synapse specific markers including SNAP25 (synaptosomal-associated protein 25), and have

been shown to produce dopamine and noradrenaline (Qi *et al.*, 1997). CAD cells differ from Cath.a cells as they spontaneously lost their oncogene, SV40 T antigen, during propagation after the cells had committed to a neuronal phenotype (Qi *et al.*, 1997).

Differentiation is able to be induced in the CAD cell line through the withdrawal of serum from culture media, and cells will not fully differentiate in serum-containing culture media, they proliferatively double in 18-22 hours. They do partially differentiate in serum-containing media, but do not show significant numbers of processes. The CAD cell line express markers associated with mature neurons and ultrastructurally resemble neurites (Qi *et al.*, 1997).

3.1.2 Hydrogen Peroxide and β-amyloid as Neuronal Insults

Production of reactive oxygen species, including hydrogen peroxide, are a natural by-product of oxidative phosphorylation and at low levels can act as signalling molecules for a variety of cellular processes (See Introduction, 1.8). However high levels of ROS are detrimental and Aβ oligomers have been reported to cause oxidative damage via production of hydrogen peroxide and Aβ structures form. This in turn further damages the cell and mitochondrial membrane potential, disrupting the ETC and ultimately resulting in the release of Cytochrome *c* and apoptosis (Beere, 2005, Tabner *et al.*, 2005); therefore using hydrogen peroxide to induce neuronal damage was chosen to model this aspect of Alzheimer's disease.

The Aβ peptide is the predominate protein aggregate associated with Alzheimer's disease but a great deal remains to be determined about its role in neuronal death, including whether its presence continually drives cell death or if a certain concentration needs to be reached to trigger apoptosis. A number of model systems have been established to investigate the effect of Aβ on neuronal systems, including hippocampal slices, primary cultures and continuous cell lines. A number of methods are used for the creation of toxic Aβ structures from synthetic peptides, with a wide range of permutations exacted to push structure formation towards fibrillar or oligomeric. An aim for this investigation was to create an Alzheimer's disease model system *in vitro* to explore whether IR1072 had any effect on Aβ induced cell toxicity. A wide number of studies were reviewed before the protocol for Aβ fibril/oligomer production was decided upon that is described in 2.6.7 (El-Agnaf *et al.*, 2001, Isobe *et al.*, 2000, Kayed *et al.*, 2003, King *et al.*, 2009, Kranenburg *et al.*, 2005, Kudva *et al.*, 1997, Lorenzo and Yankner, 1994).

For this investigation, a treatment protocol was devised based upon work by Bradford, 2005, who tested a range of IR treatment protocols on cell viability in human lymphocytes, and found that cells irradiated with IR1072 using a 5 x 3 min treatment protocol showed a significantly higher viability than that of cells irradiated with other IR wavelengths using the same protocol (Bradford *et al.*, 2005). Burroughs & Chazot, (unpublished), also found the same treatment protocol was sufficient to elicit 90% protection against mild excitotoxic glutamate insults in rat primary neuronal cultures. Another aim of this investigation was to determine whether IR1072 exposure could also protect against hydrogen

peroxide based insults and to determine whether IR1072 exposure alone had any effect on neuronal viability.

3.2 Results

All data were processed using Microsoft Office Excel 2007 and statistical analyses were carried out using GraphPad Prism Version 5, GraphPad Software Inc.

3.2.1 IR1072 Preconditioning, followed by H_2O_2 exposure

CAD cells were maintained as described in 2.6.1. CAD cells were either sham treated or treated with five sets of 3 minute IR1072 exposures, 30 minutes apart. Immediately after this time, hydrogen peroxide was added to the media to give final concentrations of 50 µM, 75 µM or 100 µM, with PBS used as a volume control. The cells were then incubated for four hours at 37°C, 5% CO_2. After this time a MTT assay was performed (see 2.6.3). Figure 3.1. Part A) shows 100 µM H_2O_2, Part B) shows 75 µM H_2O_2 and Part C) shows 50 µM H_2O_2.

3.2.1.1 Exposure of IR1072 Preconditioned CAD cells to 100 µM Hydrogen Peroxide

In the presence of 100 µM hydrogen peroxide, figure 3.1, part A, sham-preconditioned neuronal cultures displayed a 32.69% decrease in cell viability

compared to control sham cultures which received PBS. In the presence of 100 μM hydrogen peroxide, IR1072-preconditioned neuronal cultures displayed a 26.18% decrease in cell viability, compared to control IR1072 cultures that received PBS. A 6.64% trend for increased cell viability was found in IR1072-preconditioned neuronal cultures which received PBS compared to sham-preconditioned cultures that also received PBS. A 16.19% increase in cell viability in IR1072-preconditioned neuronal cultures which received 100 μM hydrogen peroxide was found compared to sham-preconditioned cultures that also received hydrogen peroxide.

Data compared using an unpaired two tailed Student's T-test. Data represent mean ± SEM.

3.2.1.2 Exposure of IR1072 Preconditioned CAD cells to 75 μM Hydrogen Peroxide

In the presence of 75 μM hydrogen peroxide, figure 3.1, part B, sham-preconditioned neuronal cultures displayed a 31.70% decrease in cell viability, compared to control sham cultures which received PBS. In the presence of 75 μM hydrogen peroxide IR1072-preconditioned neuronal cultures displayed a 19.30% decrease in cell viability, compared to control IR1072 cultures that received PBS. A 3.24% trend for increased cell viability in IR1072-preconditioned neuronal cultures which received PBS was found, compared to sham-preconditioned cultures that also received PBS. A 17.99% increase in cell viability in IR1072-preconditioned neuronal cultures which received 75 μM

hydrogen peroxide was found compared to sham-preconditioned cultures that also received hydrogen peroxide.

Data compared using an unpaired two tailed Student's T-test. Data represent mean ± SEM.

3.2.1.3 Exposure of IR1072 Preconditioned CAD cells to 50 μM Hydrogen Peroxide

In the presence of 50 μM hydrogen peroxide, figure 3.1, part C, sham-preconditioned neuronal cultures displayed a 27.39% decrease in cell viability, compared to control sham cultures which received PBS. In the presence of 50 μM hydrogen peroxide IR1072-preconditioned neuronal cultures displayed a 10.59% trend for decreased cell viability, compared to control IR1072 cultures that received PBS. No difference in cell viability in IR1072-preconditioned neuronal cultures which received PBS was found compared to sham-preconditioned cultures that also received PBS. A significant 29.05% increase in cell viability in IR1072-preconditioned neuronal cultures which received 50 μM hydrogen peroxide was found compared to sham-preconditioned cultures that also received hydrogen peroxide.

Data compared using an unpaired two tailed Student's T-test. Data represent mean ± SEM.

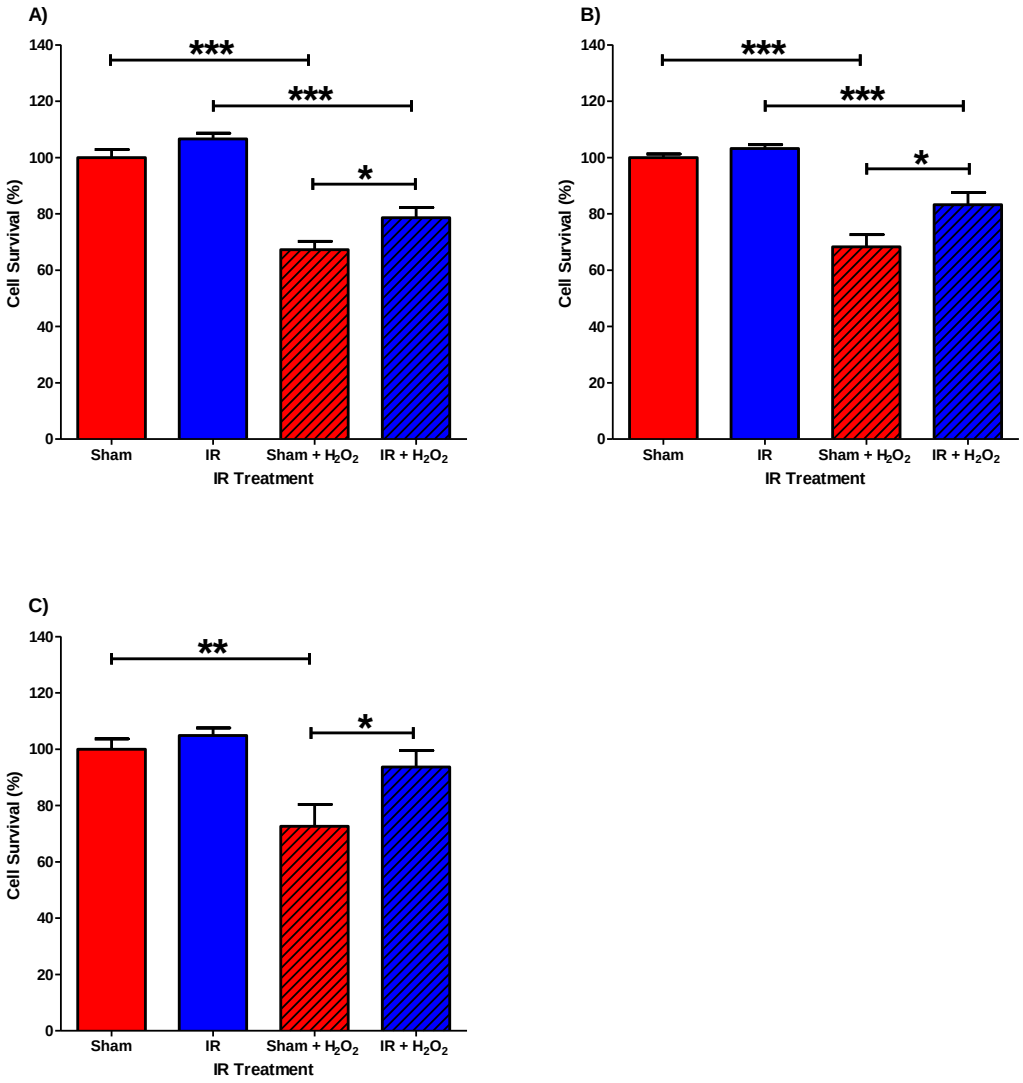

Figure 3.1. Preconditioning CAD Cells with IR1072 A) 100 µM hydrogen peroxide; B) 75 µM hydrogen peroxide, C) 50 µM hydrogen peroxide. Cell viability determined using an MTT assay, (Sham cultures, without hydrogen peroxide represent 100%). Mean values ± SEM, n= 24 from one culture, for A) and C); n=72, from 3 cultures, for B); *p<0.05, **p<0.01, ***p<0.001.

3.2.2 Exposure of CAD Cultures to H_2O_2, Followed by IR1072 Treatment

CAD cells were passaged into 24 well plates, as described in 2.6.1. DMEM/F12 +GlutaMAX® +10% FCS was removed from the cells and replaced with fresh media containing hydrogen peroxide at a range of concentrations (150 µM or 50 µM), or PBS as a control. Cells were then immediately exposed to five sets of 3 minute IR1072 treatments, 30 minutes apart or Sham-treated. Cells were then incubated at 37°C, 5% CO_2 for four hours, after which an MTT assay was performed (see 2.6.3).

3.2.2.1 Exposure of CAD Cultures 150 µM Hydrogen Peroxide, Followed by IR1072 Conditioning

In the presence of 150 µM hydrogen peroxide, figure 3.2, part A, sham-treated neuronal cultures displayed a 69.11% decrease in cell viability compared to control sham cultures which received PBS. In the presence of 150 µM hydrogen peroxide, IR1072-treated neuronal cultures displayed a 72.07% decrease in cell viability compared to control IR1072 cultures that received PBS (Figure 3.2, part A). No difference in cell viability in IR1072-treated neuronal cultures which received PBS was found compared to sham-treated cultures that also received PBS. No significant difference was found between IR1072-treated cultures which received 150 µM hydrogen peroxide was found compared to sham-treated cultures that also received hydrogen peroxide.

Data compared using an unpaired two tailed Student's T-test. Data represent mean ± SEM.

3.2.2.2 Exposure of CAD Cultures 50 μM Hydrogen Peroxide, Followed by IR1072 Conditioning

In the presence of 50 μM hydrogen peroxide, figure 3.2, part B, sham-treated neuronal cultures displayed a 17.23% decrease in cell viability compared to control sham cultures which received PBS. In the presence of 50 μM hydrogen peroxide, IR1072-treated neuronal cultures displayed a 17.28% trend for decreased cell viability, compared to control IR1072 cultures that received PBS. A 21.27% increase in viability was found between IR1072-treated CAD cultures and Sham-treated cultures which both received PBS. A 25.65% increase in cell viability was also found in IR1072-treated neuronal cultures, in the presence of 50 μM hydrogen peroxide, compared to sham-treated cultures that also received 50 μM hydrogen peroxide.

Data compared using an unpaired two tailed Student's T-test. Data represent mean ± SEM.

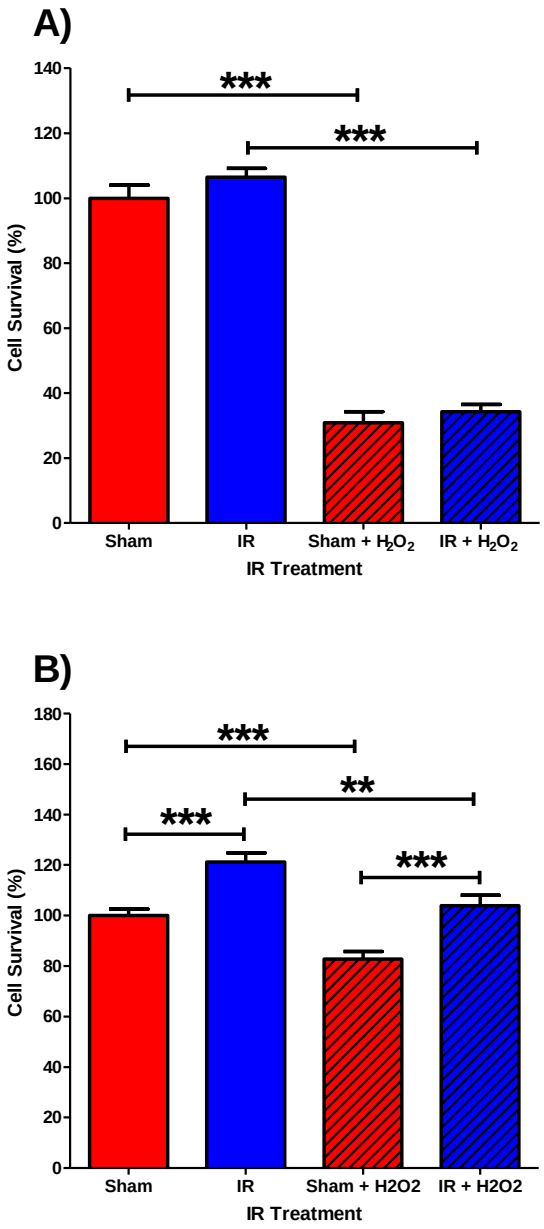

Figure 3.2. CAD Cells Sham-treated or IR1072 treated, following the addition of hydrogen peroxide. A) 150 μM hydrogen peroxide; B) 50 μM hydrogen peroxide. Cell viability determined using an MTT assay, (sham cultures, without hydrogen peroxide, represent 100%). Mean values ± SEM, n= 24 from one culture, for A); n=48, from two cultures, for B); **p<0.01, ***p<0.001.

3.2.3 Effect of IR1072 Exposure on CAD Cell Viability

As CAD cultures were seeded from the same stock solution of cells, cell density was identical at the time of passage. Therefore the observation of increased and trends towards increased MTT absorbance in IR1072 exposed cultures, shown in 3.2.1 and 3.2.2, compared to sham-treated controls was unexpected. This was explored further by sham-treating or exposing new CAD cultures to five sets of 3 minute IR1072 treatments, 30 minutes apart. The cells were then incubated for four hours at 37°C, 5% CO_2. After this time a MTT assay was performed (see 2.6.3). A highly significant difference was observed between Sham treated control cultures and IR treated cultures which show a 17.68% increase in cell survival, see figure 3.3.

Data compared using an unpaired two tailed Student's T-test. Data represent mean ± SEM.

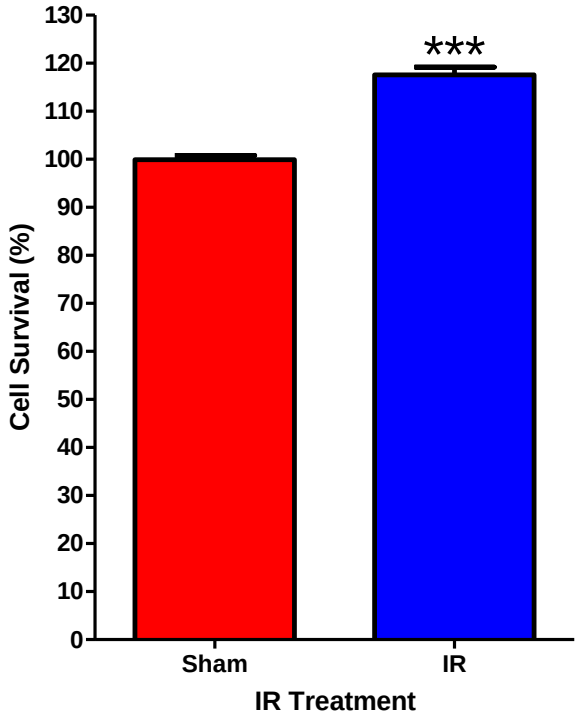

Figure 3.3. Cell viability of CAD Cells Sham-treated or IR1072 treated, viability determined using an MTT assay. Sham cultures represent 100% viability. Mean values ± SEM, n= 384 from eight cultures; ***p<0.001.

3.2.4. The Effect of IR1072 Exposure on CAD Cell Proliferation

In order to determine whether the increased number of viable cells found in 3.2.3, following exposure to IR1072 was due to LLLT preventing cell death/cell turnover or causing cells to actively proliferate immunocytofluorescence was performed as described in 2.6.6. Cells were stained with Ki67, a protein strictly associated with cell proliferation. Ki67 is present during all active phases of the cell cycle but is not present in resting cells. After the breakdown of the nuclear membrane, Ki67 can be found at low levels in the cytoplasm but at interphase, Ki67 is exclusively and densely found in the nucleus and during mitosis found on the surface of the chromosomes (Scholzen and Gerdes, 2000).

CAD cells were grown for 72 hours in 24 well plates and treated as described in 2.6.5. IR1072-treated neuronal cultures displayed no significant difference in the percentage of cells that stained positive for Ki67 when compared to sham-treated neuronal cultures. A total of 6236 cells were counted in the Sham-treaded condition, with 818 staining for Ki67. In the IR1072 exposed condition a total of 5701 cells were counted with 873 staining positive for Ki67. Examples of immunocytofluorescence for both conditions are shown in figure 3.4, with figure 3.5 showing statistical analysis of staining.

Data compared using an unpaired two tailed Student's T-test. Data represent mean ± SEM.

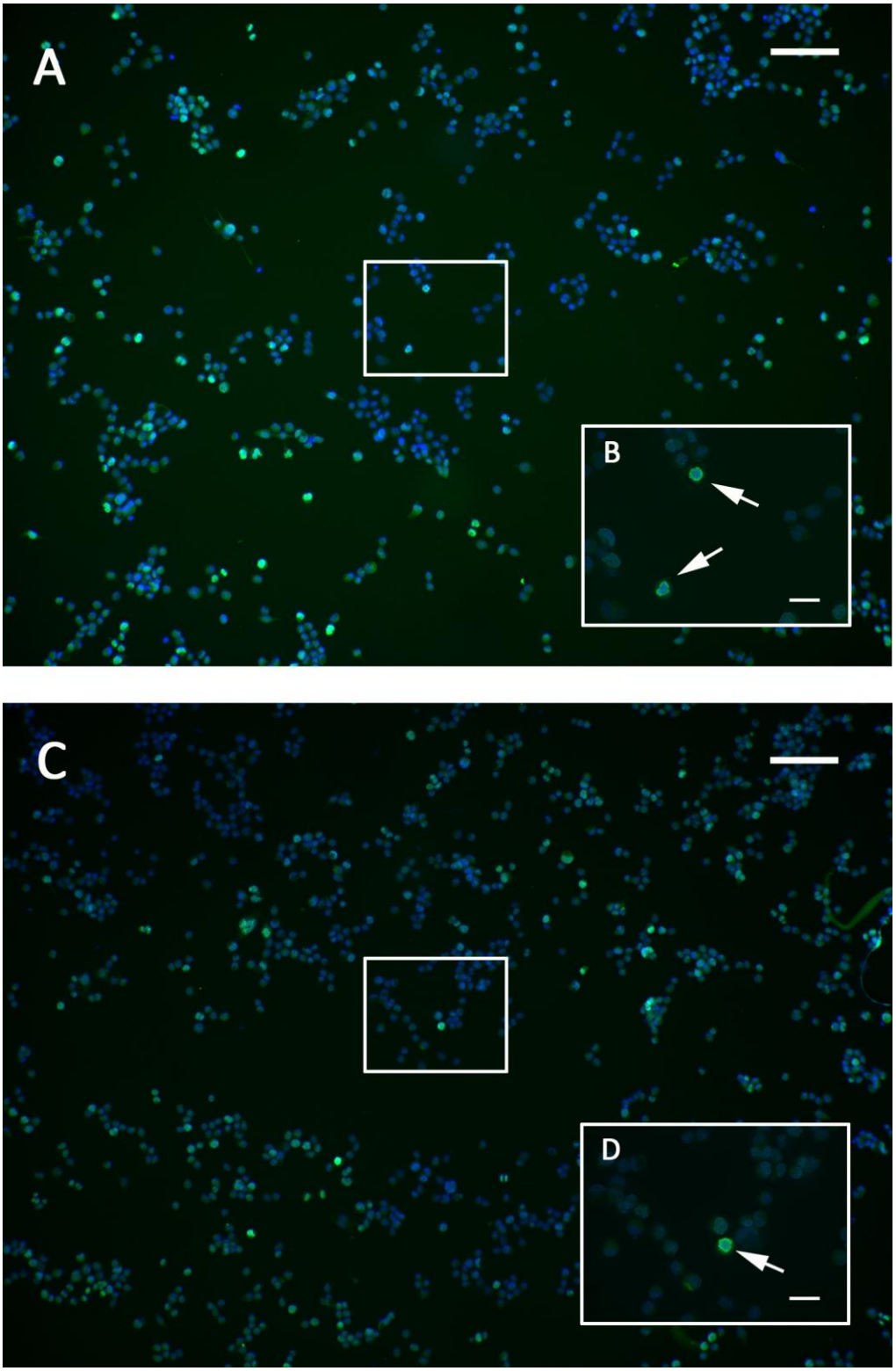

Figure 3.4. A) Sham treated CAD cells B) Magnified image of cells highlighted in the white box in figure A, arrows indicate Ki67 positive cells. C) IR Treated CAD cells D) Magnified image of cells highlighted by the white box in figure C. Figures A and C, scale bar 100 µm. Figures B and D, scale bar 20 µm.

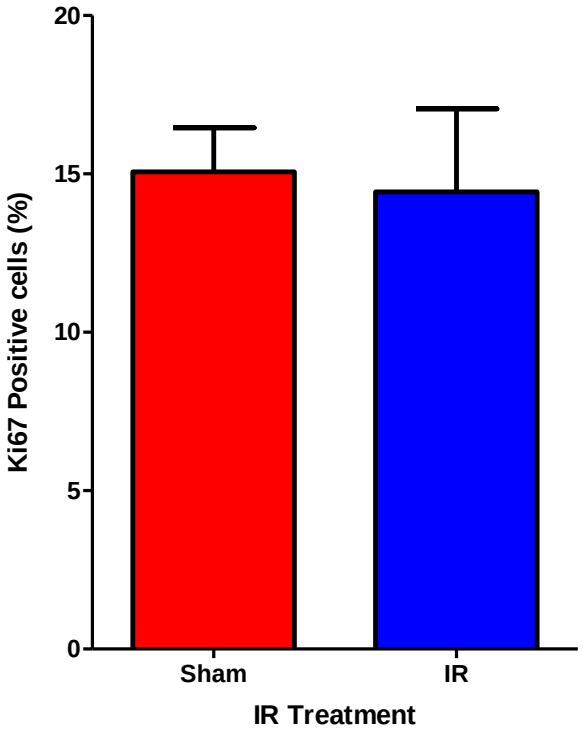

Figure 3.5. Graph to compare the effect of IR1072 exposure on cell proliferation against that of Sham-treated cultures, using Ki67 as a marker. Values are given as percentages of the total number of cells counted. There is no significant difference between the conditions. Data shown mean value ± SEM, n=6 replicates.

3.2.5 Effect of IR1072 Exposure on ATP Production in CAD Cells

A number of studies into the effects of photobiomodulation of biological systems suggest that mitochondria act as the primary photoacceptors for NIR. This has been supported by reports of increased activity of members of the electron transport chain; cytochrome *c* oxidase and Complex II, increased ATP and ROS production, increased mitochondrial membrane potential and mitochondrial velocity in response to LLLT (Desmet *et al.*, 2006, Gao and Xing, 2009, Karu, 2008, Silveira *et al.*, 2007, Trimmer *et al.*, 2009, Tsai *et al.*, 2001, Wong-Riley *et al.*, 2005).

Altered activity of components of the ETC in the mitochondria following IR1072 is reported later in this document, see Chapter 4, thus the CAD cell system was utilised to investigate whether IR1072 had any specific effects on ETC activity via measuring ATP levels, the product of the electron transport chain.

CAD cell cultures were grown and treated as described in 2.6.5, ATP concentrations were determined from a standard curve constructed from the concentration of known ATP standards. ATP concentrations were normalised against approximate cell density, calculated by performing LDH assays, see 2.6.4, on adjacent wells. This was performed as IR1072 exposure had been found to prevent cell death/turnover previously, see 3.2.3.

3.2.5.1 Measurement of ATP Concentrations Immediately Following IR1072 Exposure

CAD Cultures were passaged into 24 well plates and grown for 72 hours. After this time, cultures were either Sham-treated of exposed to five sets of 3 minute IR1072 exposures, 30 minutes apart. Immediately after this time, an ATP assay was performed on six wells in each condition; see 2.6.5, and an LDH assay, see 2.6.4, on the remaining six wells in each condition. ATP luminescence values were normalised against the absorbance values of LDH of freeze-thawed cells only (LDH measurements of the media were not accounted for as this is a measure of dead cells, freeze-thawed LDH absorbances refer to cells alive at the start of the assay, therefore those cells capable of ATP production).

There was no significant difference in ATP concentration in IR-treated CAD cultures compared to Sham-treated controls (n=6 for both conditions). This is shown in figure 3.6., part A. Data compared using an unpaired two tailed Student's T-test. Data represent mean ± SEM.

3.2.5.2 Measurement of ATP Concentration Four Hours after IR1072 Exposure

CAD Cultures were passaged into 24 well plates and grown for 72 hours. After this time, cultures were either Sham-treated of exposed to five sets of 3 minute IR1072 exposures, 30 minutes apart. After the final exposure, cells were returned to the incubator and kept at 37°C, 5% CO_2, for four hours. After this time, an ATP assay was performed on six wells in each condition; see 2.6.5,

and an LDH assay, see 2.6.4, on the remaining six wells in each condition. ATP luminescence values were normalised against the absorbance values of LDH of freeze-thawed cells only.

There was no significant difference in ATP concentration in IR-treated CAD cultures compared to Sham-treated controls (n=6 for both conditions). This is shown in figure 3.6., part B. Data compared using an unpaired two tailed Student's T-test. Data represent mean ± SEM.

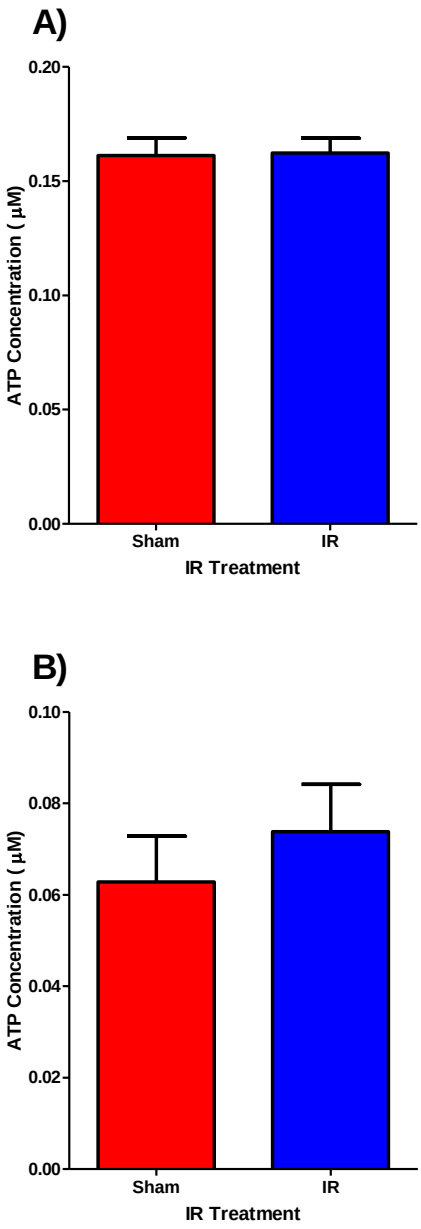

Figure 3.6. Column graphs to show that exposure of cultures to IR1072 has no significant effect on ATP concentration, compared to the ATP concentration in Sham-treated control cultures. A) shows [ATP] measured immediately after IR or sham exposures p=0.914. B) Shows [ATP] four hours after IR/Sham exposures, p=0.463. n=6 replicates from one culture for both A) and B).

3.2.6 IR1072 Exposure Protects CAD Cells From β-amyloid Induced Toxicity

24 hours after cells were passaged into 24 well plates they were exposed to five sets of three minute IR1072 or Sham treatments, 30 minutes apart, cells then were returned to the incubator. 24 hours after this time, media was removed and replaced with DMEM/F12 +GlutaMAX® +10% FCS containing the β-amyloid$_{(1-42)}$ (Aβ) peptide. Peptide Aβ was prepared as described in 2.6.7, the formation of a mixture of fibrils and oligomers confirmed through transmission electron microscopy (as described in 2.6.8), figure 2.3 shows example electron micrographs of Aβ structures formed.

Cells were exposed to a final concentration of 0.5, 1, 2.5, 3.5, 4.5, 5, 10 or 25 μM of Aβ, using a volume of DMSO:PBS in DMEM/F12 +GlutaMAX® +10% FCS (ratio the same as that in Aβ cultures) as a control. Immediately after, cells were exposed to a second set of five 3 minute IR1072 or Sham exposures and returned to the incubator. 24 hours after the addition of Aβ, the cells were again exposed to five sets of 3 minute IR1072 or Sham treatments, 30 minutes apart, and again returned to the incubator. 24 hours after the third set of IR1072 or Sham exposures a CytoTox 96® Non-radioactive assay, measuring LDH release, was performed on the cultures, as defined in 2.6.4.

Data were analysed using a two-way ANOVA analysis of variance, narrative of the results is shown below. Data shown as mean ± SEM in figure 3.7.

IR Treatment accounts for 2.49% of the total variance, ***$p<0.0001$. If IR treatment has no effect overall, there is a less than 0.1% chance of randomly

observing this effect in an experiment this size, or larger. The effect of IR treatment is considered extremely significant.

Aβ concentration accounts for approximately 80.04% of the total variance, ***p<0.0001. If Aβ concentration has no effect overall, there is a less that 0.1% chance of randomly observing an effect in an experiment of this size, or larger. The effect of concentration is considered extremely significant.

Exposure to IR1072 had no significant effect, compared to sham treated controls, against cell death when cells were exposed to PBS, 0.5 μM or 1 μM $A\beta_{42}$. However, there was a trend for a reduction in cell death in the IR1072 treated condition, compared to sham treated controls ($p<0.1$) at 2.5 μM and 3.5 μM $A\beta_{42}$.

At 4.5 μM Aβ, treatment of CAD cells with IR1072 elicited a statistically significant reduction in cell death of 23.13%, compared to sham treated controls.

Concentrations of Aβ at 5 μM, 10 μM and 25 μM were exceedingly toxic to Sham treated cells. However, despite the high concentrations of Aβ treated of cells with IR1072 significantly reduced cell death by 23.94%, 24.13% and 16.43%, respectively.

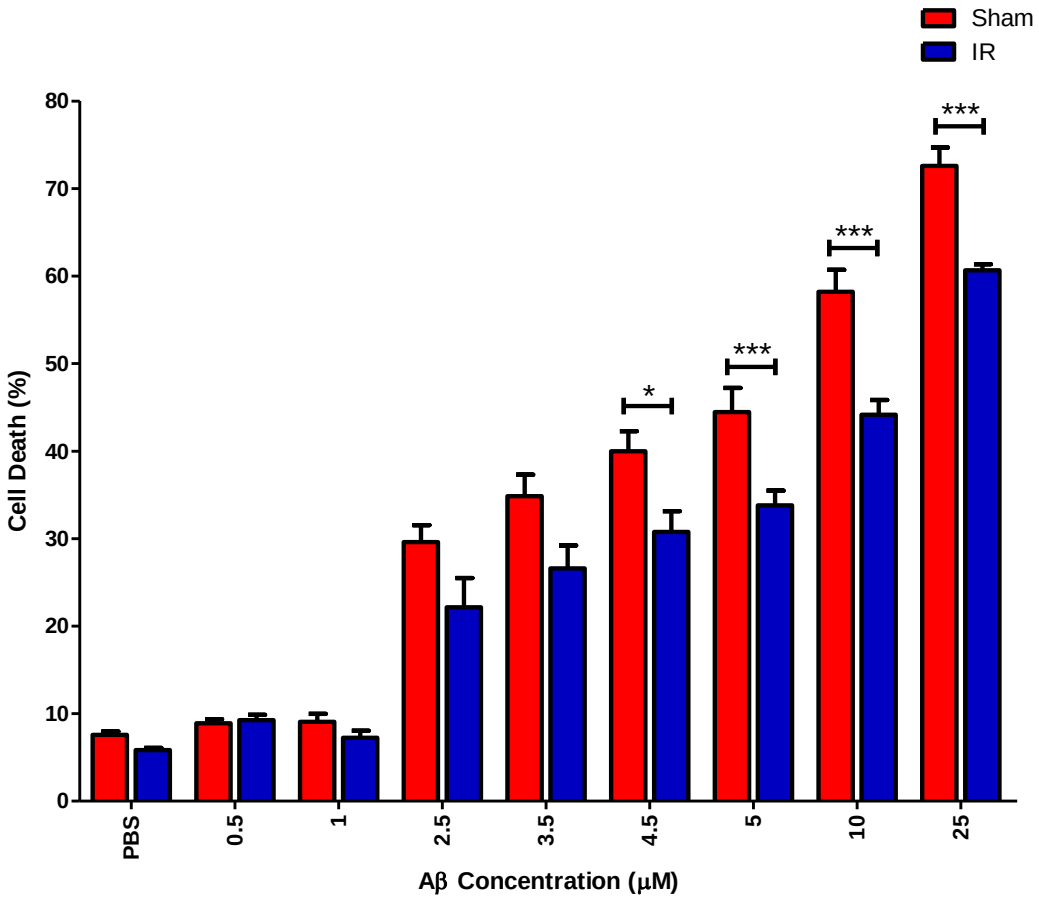

Figure 3.7. A column graph to compare the effect of IR1072 exposure against Sham-treatment on Aβ induced cell death. Cell death determined via measuring the concentration of LDH release into media and expressed a percentage of the number of total cells present in culture. Mean values ± SEM. *p<0.05, **p<0.01, ***p<0.001.

Neuronal CAD cell protection afforded by IR1072 preconditioning, compared to sham-treated controls when cell toxicity is induced through Aβ exposure					
Aβ (μM)	n =	P Value	Increase or decrease in cell death	Percentage change in cell death (%)	Percentage of cell protection induced (%)
PBS Only	18	-	-	-	-
0.5	6	-	-	-	-
1	6	-	-	-	-
2.5	6	NS	↓	7.45	25.17
3.5	6	NS	↓	8.26	23.70
4.5	6	*<0.05	↓	9.24	23.13
5	6	***<0.001	↓	10.64	23.94
10	6	***<0.001	↓	8.02	24.13
25	6	***<0.001	↓	11.93	16.43

Table 3.1. Data with a trend toward significant differences are shaded blue ($p<0.1$). Data with statistically significant altered protection levels are shaded green. Data were analysed using a Two-way ANOVA analysis of variance. Arrows indicate direction of altered expression, (↑, increase; ↓, decrease), '-' indicates no significant change. Abbreviations: Aβ, β-amyloid$_{(1-42)}$; N/C, No Change; PBS, phosphate buffered saline.

3.3 Discussion

The level of protection achieved through IR1072 preconditioning against hydrogen peroxide insults appeared to be dependent on the severity of the subsequent insult. The higher the concentration of hydrogen peroxide, the less IR1072 exposure was able to protect against insults. Previous work in our laboratory using glutamate as an excitotoxic insult also found IR1072 preconditioning was neuroprotective in a severity-dependent manner in primary cultures (Burroughs, 2010).

IR1072 conditioning of CAD cultures following the addition of hydrogen peroxide also elicited neuroprotective effects, in an insult dependent manner. It was also interesting to note that the level of neuroprotection observed was greater than that observed when cultures were preconditioned with IR1072 before addition of hydrogen peroxide, despite exposure to higher concentrations of hydrogen peroxide. These data suggest that IR1072 preconditioning may not be required for a profound level of neuroprotection. It also shows that IR1072 is still able to elicit biological effects despite severe toxic conditions.

More research needs to be conducted to determine the concentrations of hydrogen peroxide that IR1072 can protect against and to what degree preconditioning can be protective against these concentrations, and whether protection observed through IR1072 exposure without preconditioning can be augmented. Research also needs to be conducted into the role of IR1072 against a greater range of insults; such as serum deprivation, rotenone or cyanide exposure. LLLT has also been previously shown to be promote cell survival and protect against UVA (Bradford *et al.*, 2005), methanol-derived

formate (Eells *et al.*, 2003), MPP+ (1-methyl-4-phenylpyridium) and rotenone exposure (Liang *et al.*, 2008), amongst other insults, *in vitro*.

LLLT has previously been shown to be protective against potassium cyanide induced cell death in visual cortical neurons that had been preconditioned with NIR at 670 nm for 10 minutes, at a total energy density of 30 J/cm^2. Liang (2006) also found that the degree of protection depended on the severity of the insult, with approximately 50% protection achieved at 100 μM potassium cyanide and 33% at 300 μM. The authors found that LLLT was protecting visual cortical neurons via increased Bcl-2 levels and decreased Caspase-3 and BAX levels, suggesting direct interaction of LLLT with apoptotic pathways (Liang *et al.*, 2006). Preconditioning of striatal and cortical neurons with LLLT at 670 nm, twice a day for 80 seconds, protected against rotenone- (56% and 66%, respectively) and MPP^+ induced apoptosis (37% and 47%, respectively). Inhibition of ATP production by MPP^+ was also significantly reversed through LLLT preconditioning; rising from 48% to 70% of control levels (Ying *et al.*, 2008).

Increased CAD cell viability in conditions where IR1072 exposure was the only variable was somewhat surprising. Cell proliferation following LLLT has been reported in multiple cell culture systems and cell types; including osteoblasts (Kreisler *et al.*, 2003, Pires Oliveira *et al.*, 2008, Ueda and Shimizu, 2003), fibroblasts (Hawkins and Abrahamse, 2006, Taniguchi *et al.*, 2009, Vinck *et al.*, 2003), muscle cells and epithelial cells (Sommer *et al.*, 2001, Whelan *et al.*, 2001). However, it had not been reported in neuronal cells, therefore it was important to determine whether IR1072 exposure was causing the CAD cultures

to actively proliferate or whether the increased viability was due to decreased cell-turnover which occurs naturally in any culture system.

Following the discovery of significantly increased cell viability in IR1072 treated CAD cells, compared to sham treated cultures, Ki67 was used to stain cells. These data (Figure 3.4 and 3.5) clearly demonstrate no significant difference in proliferation between the IR1072 condition and the sham-treated condition. Further to this, ATP concentrations in sham and IR1072 treated cultures were also examined to determine whether this was a factor in the increased cell viability, as increased ATP levels and mitochondrial electron transport activity have been specifically reported following LLLT (see introduction 1.1.6). However, no significant change in ATP concentration was found when the two conditions were compared. This suggests that IR1072 doesn't alter ATP production, or further IR1072 exposures are required to see a significant alteration in ATP levels. Repeated daily exposures may also be required to see long term changes in level. It would also be of interest to measure ADP levels, ATP production could be increased following IR1072 exposure but if consumption is also increased, no net change in ATP levels would be identified. It would also be difficult to identify changes in ATP if the alterations are only transient, the detection system used would not be sensitive enough to detect such alterations. Therefore, through concomitantly measuring ADP concentration a better profile of electron transport chain activity during/after LLLT could be obtained.

There are a significant number of techniques which are in use to form Aβ structures from synthetic Aβ peptide. The advantage of 'growing' Aβ structures *in vitro* lies in the fact that conditions can be tightly controlled and manipulated

to create a particular structure or a mixture of structures. However, there is not a ‘standard’ method for the formation of Aβ oligomers or aggregates; this has resulted in the ability of aggregates formed in different conditions to have significantly different efficacies despite being formed from the same starting peptide (Benilova *et al.*, 2012, Haass and Selkoe, 2007). Methodologies are available for generating Aβ structures from synthetic peptides, with a number of conditions manipulated to force the formation towards fibrillar or oligomeric structures (El-Agnaf *et al.*, 2001, Isobe *et al.*, 2000, Kayed *et al.*, 2003, King *et al.*, 2009, Kranenburg *et al.*, 2005, Kudva *et al.*, 1997, Lorenzo and Yankner, 1994). An aim for this investigation was to create an Alzheimer’s disease model system *in vitro*, and to create a relatively simple method through which a range of Aβ-derived structures could be formed which perhaps more closely represent what is clinically present in the Alzheimer’s disease brain. Fibrils formed through the method described in 2.6.7, were approximately 10 nm in diameter, in same range as diameters previously reported *in vitro* (Hartley *et al.*, 1999, Lorenzo and Yankner, 1994), with diffuse oligomeric-type structures forming alongside fibrils, visible in figure 2.3.

A secondary aim was to investigate whether this synthetic Aβ had any effect on cell death, and if IR1072 exposure altered the degree of Aβ-induced cell toxicity. IR1072 exposure was found to consistently and significantly reduce cell death caused by Aβ, by up to 25%, over the range of Aβ concentrations (0.5-25 μM) used. The lack of a significant level of cell death at low concentrations of Aβ (0.5-1 μM) demonstrates that it is not the mere presence of Aβ that is toxic to cells and that an insult threshold must be achieved before a significant level of cell death is observed, supporting data which have shown patients that despite

expressing low levels of Aβ, never develop clinically diagnosable Alzheimer's disease (Haass and Selkoe, 2007).

The lack of a significant neuroprotective effect of LLLT at low Aβ concentrations (0.5-2.5 μM) is interesting; it suggests that Aβ levels have to reach a damaging level before neuroprotective effects induced by IR1072 become activated. The range of Aβ concentrations used would not necessarily be found *in vivo*. However, the use of potentially unrealistic concentrations *in vitro* is a necessary experimental limitation, as synthetic Aβ peptides have been reported to be less neurotoxic than cell-derived Aβ (Benilova *et al.*, 2012). Nevertheless, there is evidence to suggest cellular concentrations of Aβ can reach micromolar levels in vesicular compartments; therefore concentrations used in this investigation do have biological relevance (Hu *et al.*, 2009).

In conjunction with other results indicating a role for heat shock proteins in the neuroprotective effects observed following IR1072 exposure, the methodology for the production of toxic Aβ structures could be explored further through utilising the continuous culture system. Further characterisation of the CAD cell line is needed to determine which HSPs are lacking and which are expressed. Indeed, HSP27 has been shown to protect against hydrogen peroxide insults through regulation of glutathione levels (Preville *et al.*, 1999), a potential mechanism occurring here. Our laboratory has determined that neither differentiated nor undifferentiated CAD cells express αB crystallin (Chazot *et al*., unpublished), but little is known regarding other HSPs. The ability to transfect cultures with extra copies of heat shock protein machinery, to investigate whether the neuroprotective effects can be potentiated, is an important starting point following further characterisation.

In vitro systems are important and useful investigative tools; they do however have disadvantages, particularly with the use of continuous cell lines, such as the CAD cell line. Continuous cell lines are typically poorly differentiated and have been shown to lose many of the original phenotypic characteristics of the original *in vivo* cell type. Immortalised cell lines are characteristically homogenous, compared to primary cultures, and the results from such cultures are much easier to standardise (Hartung *et al.*, 2002). The CAD cell line used in this investigation was homogenous and CAD cell cultures have previously been shown to lack the expression of glia specific markers such as GFAP (Qi *et al.*, 1997).

The brain is an intricate organ, comprised of a complex population of cells, with subpopulations possessing different characteristics whose expression is not usually limited to discrete locations. This adds extra layers of complexity to an organ which is relatively poorly understood. Therefore the use of cultured neurons, whether primary or continuous, has limitations in that these neuronal populations lack the diversity of the cell types found in the brain. An advantage of continuous culture is that many of the cell lines can be manipulated to differentiate into more favourable cell types, through the addition or removal of growth factors. Cath.a cells, from which the CAD cells are derived, are classed as a CNS catecholaminergic cell line despite lacking significant numbers of neurites. However, CAD cells do express neuron-specific proteins, synaptic vesicles and visible processes (Qi *et al.*, 1997).

In the studies conducted in this chapter, CAD cells were not fully differentiated – CAD cells show a unique ability to reversibly morphologically differentiate on the withdrawal of serum from the culture medium. All experiments in this chapter

were conducted in DMEM/F12 +GlutaMAX®, plus 10% foetal calf serum. In serum containing media the cell population will double over 18-22 hours, which dramatically drops upon serum removal (Qi *et al.*, 1997). In the presence of serum, CAD cells only display short processes and lose some of the morphology associated with neurons, however they do still express neuronal markers such as tyrosine hydroxylase and synaptotagmin (Qi *et al.*, 1997). Although processes were visible in the cultures used when viewed under the microscope, it may be beneficial to repeat the experiments detailed in this chapter with fully differentiated CAD cultures to determine if a mature neuron is still able to be sufficiently protected from Aβ an hydrogen peroxide toxicity by IR1072.

Overall this investigation has established that acute IR1072 exposure is neuroprotective against both H_2O_2 and Aβ insults. The degree of neuroprotection appears to be dependent upon the severity of the insult. With IR1072 preconditioning, the *in vitro* system appears to be able to withstand more significant insults than when cultures are exposed to IR1072 after exposure to an insult. The apparent neuroprotective response from IR1072 exposure to toxicity does not appear to occur as a result of increased cell proliferation, nor does it appear to be attributed to increased ATP production following IR1072 exposure. The ability for acute IR1072 exposure to significantly protect against cell toxicity caused by two molecules/species associated with propagation of the disease state in Alzheimer's disease provides an exciting insight into the neuroprotective potential for IR1072 in disease management.

The remaining chapters focus on the use of IR1072 *in vivo* systems. It is important to investigate the effects of IR1072 in an *in vivo* system to provide insight into the mechanisms of action through which IR1072 has been shown to be neuroprotective when neurons are exposed to a number of insults. An important mechanism to investigate relates to mitochondria, as these organelles have been proposed to act as the primary photoacceptor for NIR. The principle aim of the following chapter is to determine whether acute IR1072 exposure alters activities of certain mitochondrial electron chain complexes, and whether these data correlate to the absence of increased ATP concentrations observed in the present chapter.

Chapter 4: Acute IR1072 Treatments - Effects *in vivo* on mitochondrial respiration rates

4.1 Introduction

4.1.1 *In vivo* model system- Mitochondria

Mice were irradiated as described in 2.2.1, using the same methods used as described by Michalikova (2008) and Burroughs (2010). To further investigate the effects of acute of IR1072 on Complex I and II respiratory chain activity, oxidative phosphorylation was measured using the polarographic method in mitochondria isolated from both male and female CD-1 mouse liver and brain tissue, at 3 months of age, in sham and IR1072-preconditioned animals.

Mitochondria were isolated in this investigation from both the liver and the brain. In order to obtain sufficient mitochondria for experimental repeats, a minimum of three mice were used for each preparation. A Clark-type electrode was used to measure oxygen consumption polarographically (Sweetman and Weetman, 1969). The polarographic method of measuring respiratory rates in both cells and isolated organelles, such as mitochondria, was first reported in 1956 by Chance & Williams. This method enabled measurement of the rate of oxygen consumption in the presence of a range of substrates and in the absence and presence of phosphate. Work by Chance & Williams also resulted in the discovery of three energy conservation sites in the electron transport chain (Chance and Williams, 1956a, Ernster, 1993).

The ratio between the active state of respiration (state 3) and controlled respiration, after all ADP has been phosphorylated, (return to state 4) is known as the respiratory control coefficient or index (RCI). This ratio allows the experimenter to determine the strength of mitochondrial membrane coupling. The greater the RCI, the more tightly coupled the mitochondrial preparation. The mitochondria membrane needs to be tightly coupled in order for the electron transport chain to act efficiently and to phosphorylate ADP to ATP (Campello *et al.*, 1964).

Substrates, glutamate plus malate and succinate, measure the oxidative phosphorylation activity of Complex I and Complex II respectively (Chance and Williams, 1956b). Earlier work in our laboratory has demonstrated that daily, whole animal exposure, sessions of six minute IR1072 periods, over a 10 day period is sufficient to improve working memory in both male and female CD-1 mice. IR exposed aged (12 months) CD-1 mice showed increased consideration in their decision making and demonstrated a significantly improved cognitive performance, comparable to that of young (4 month) CD-1 mice (Michalikova *et al.*, 2008). Previously our laboratory has also reported that acute IR1072 treated 7 month old male CD-1 mice displayed higher Complex II activity (at state 4, state 3 and return to state 4 respiration rates) in isolated brain mitochondria compared to sham treated controls (*$p<0.05$). However there was no difference in endogenous respiration (Burroughs, 2010).

4.2 Results: Acute IR1072-preconditioning in CD-1 mice: Mitochondrial respiratory studies

4.2.1 Oxidative Phosphorylation Measurements of Three Month old CD-1 Mice: Liver

4.2.1.1 Complex I – Glutamate plus Malate

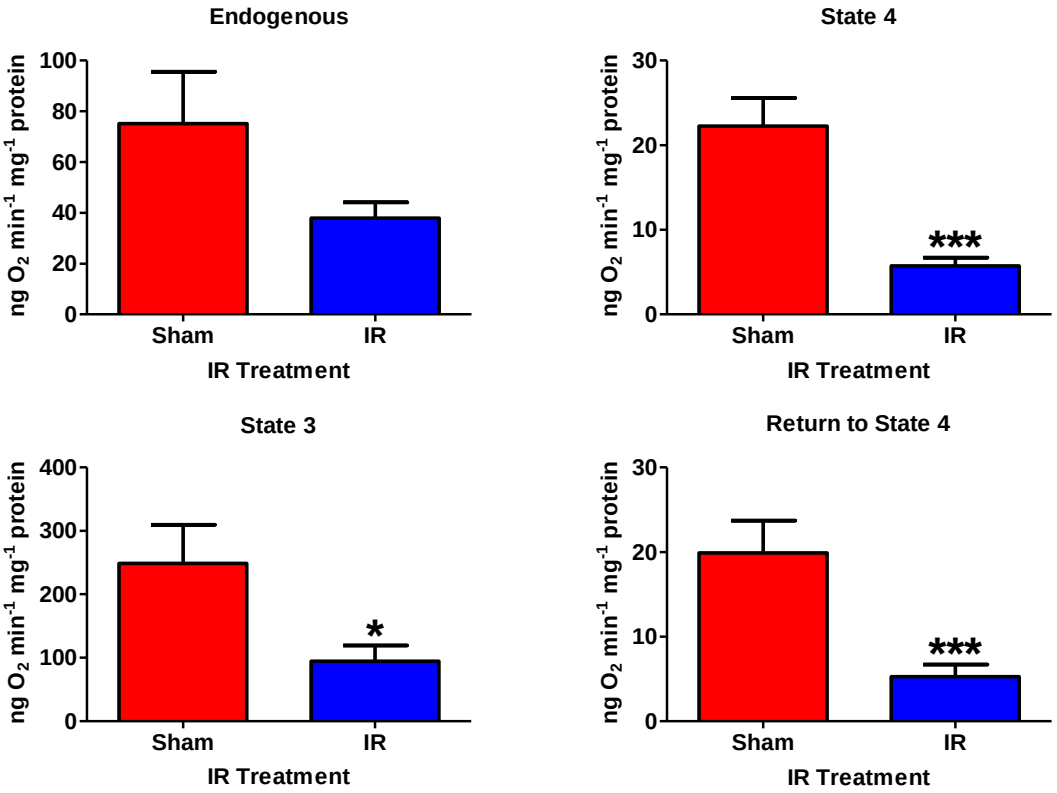

Figure 4.1. Effect of acute sham or IR exposure on glutamate plus malate respiratory rates in 3 month old CD-1 mouse liver mitochondria (*in vivo*). Mean values ± SEM, n = 4, *p<0.05, ***p<0.001.

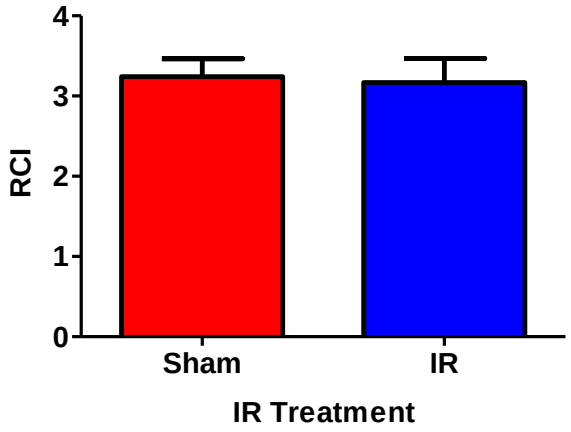

Figure 4.2. Effect of acute sham or IR exposure on glutamate plus malate RCI in 3 month old CD-1 mouse liver mitochondria (*in vivo*). Mean values ± SEM, n = 4.

Effect of acute IR1072 preconditioning on Complex I activities in mitochondria isolated from liver, compared to age-matched sham-treated controls, n=4				
Respiratory rate (ng O_2 min^{-1} mg $protein^{-1}$)	P Value	Result: ↑/↓	Percentage change (%)	Figure
Endogenous	0.084	↓	49.54	4.1
State 4	<0.0001	↓	74.28	4.1
State 3	0.022	↓	61.88	4.1
Return to State 4	0.001	↓	73.44	4.1
RCI	0.846	-	-	4.2

Table 4.1. Data with a trend in altered activity are shaded blue ($p<0.1$), data with statistically significant altered activity levels ($p<0.05$) are shaded green. Arrows indicate direction of altered expression, (↑, increase; ↓, decrease), '-' indicates no significant change. *$p<0.05$; **$p<0.01$. Abbreviations: RCI, respiratory control index.

4.2.1.2 Complex II – Succinate

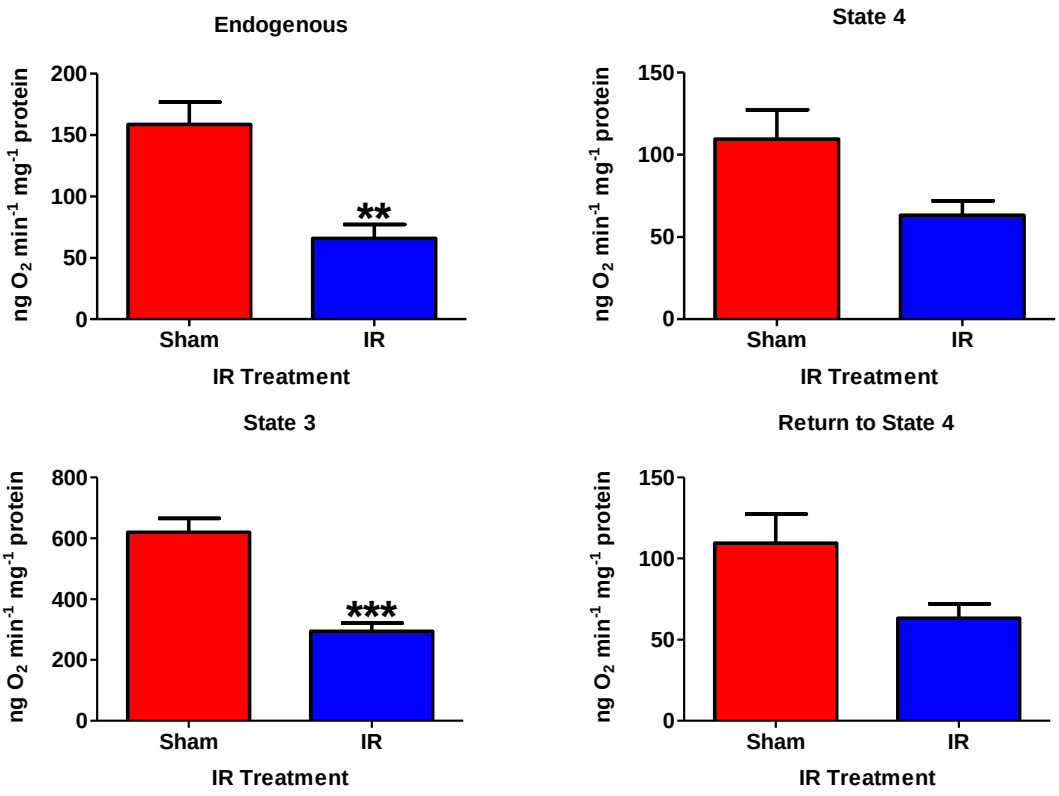

Figure 4.3. Effect of acute sham or IR exposure on succinate respiratory rates in 3 month old CD-1 mouse liver mitochondria (*in vivo*). Mean values ± SEM, n = 4, **p<0.01, ***p<0.001.

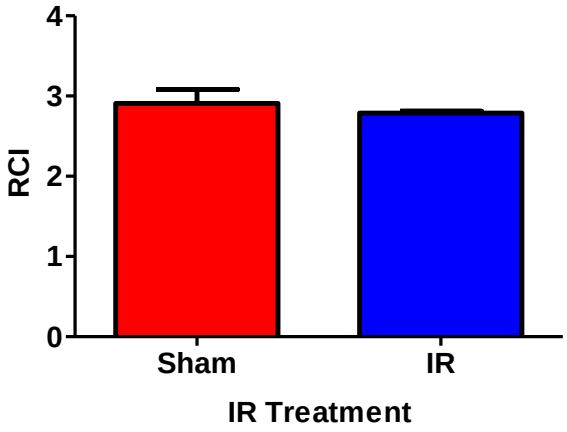

Figure 4.4. Effect of acute sham or IR exposure on succinate RCI in 3 month old CD-1 mouse liver mitochondria (*in vivo*). Mean values ± SEM, n = 4.

Effect of acute IR1072 preconditioning on Complex II activities in mitochondria isolated from liver, compared to age-matched sham-treated controls, n=4				
Respiratory rate (ng O_2 min^{-1} mg $protein^{-1}$)	P Value	Result: ↑/↓	Percentage change (%)	Figure
Endogenous	**0.005	↓	-58.50	4.3
State 4	0.058	↓	-42.34	4.3
State 3	***0.001	↓	-52.57	4.3
Return to State 4	0.058	↓	-42.34	4.3
RCI	0.528	-	-	4.4

Table 4.2. Data with a trend in altered activity are shaded blue (p<0.1), data with statistically significant altered activity levels (p<0.05) are shaded green. Arrows indicate direction of altered expression, (↑, increase; ↓, decrease), '-' indicates no significant change. *p<0.05; **p<0.01, ***p<0.001. Abbreviations: RCI, respiratory control index.

4.2.2 Oxidative Phosphorylation Measurements of Three Month old CD-1 Mice: Brain

4.2.2.1 Complex I – Glutamate plus Malate

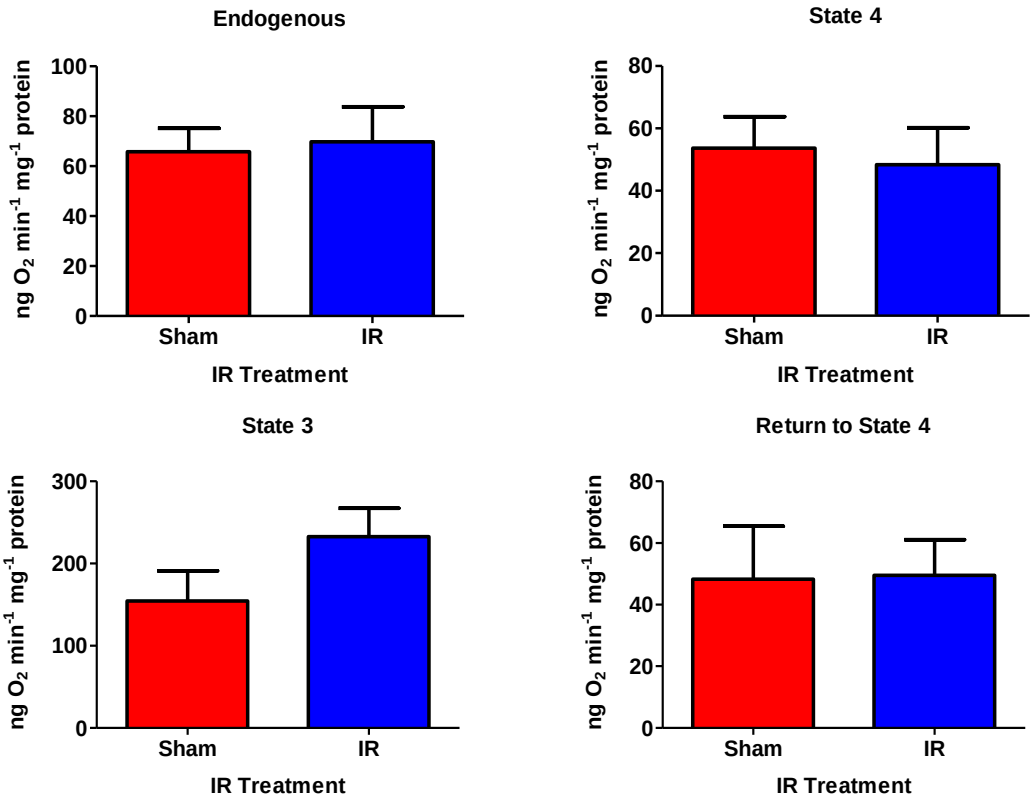

Figure 4.5. Effect of acute sham or IR exposure on glutamate plus malate respiratory rates in 3 month old CD-1 mouse brain mitochondria (*in vivo*). Mean values ± SEM, n = 4.

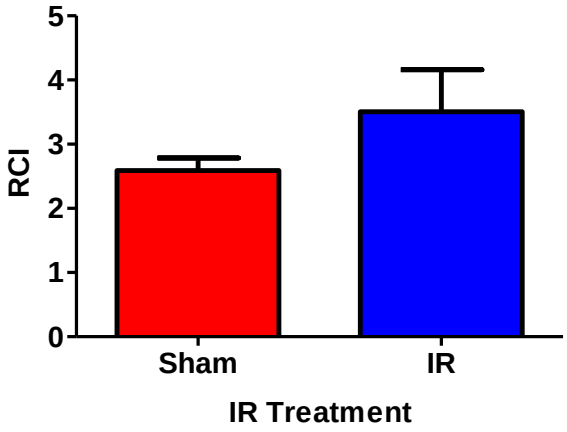

Figure 4.6. Effect of acute sham or IR exposure on glutamate plus malate RCI in 3 month old CD-1 mouse brain mitochondria (*in vivo*). Mean values ± SEM, n = 4.

Effect of acute IR1072 preconditioning on Complex I activities in mitochondria isolated from brain, compared to age-matched sham-treated controls, n=4				
Respiratory rate (ng O_2 min^{-1} mg $protein^{-1}$)	P Value	Result: ↑/↓	Percentage change (%)	Figure
Endogenous	0.811	-	-	4.5
State 4	0.734	-	-	4.5
State 3	0.150	-	-	4.5
Return to State 4	0.956	-	-	4.5
RCI	0.155	-	-	4.6

Table 4.0.3. Abbreviations: RCI, respiratory control index, '-' indicates no significant change.

4.2.2.2 Complex II – Succinate

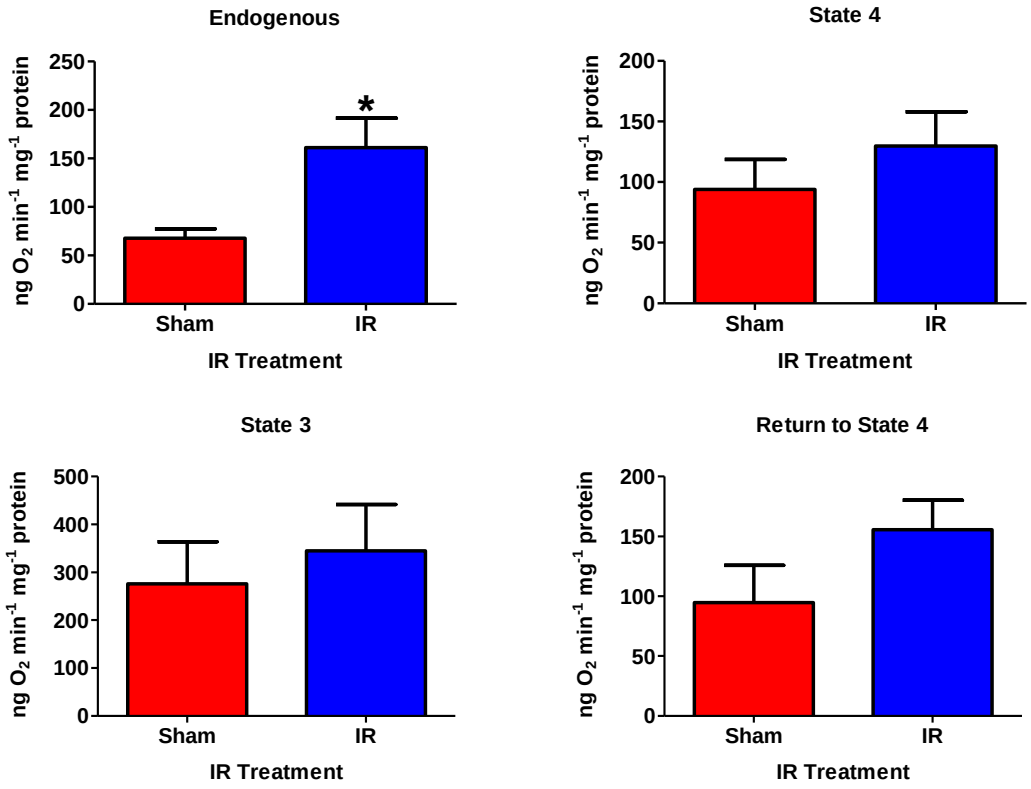

Figure 4.7. Effect of acute sham or IR exposure on succinate respiratory rates in 3 month old CD-1 mouse brain mitochondria (*in vivo*). Mean values ± SEM, n = 4.

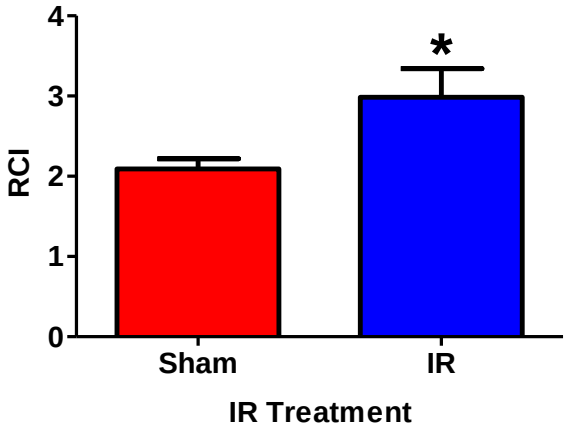

Figure 4.8. Effect of acute sham or IR exposure on succinate RCI in 3 month old CD-1 mouse brain mitochondria (*in vivo*). Mean values ± SEM, n = 4.

Effect of acute IR1072 preconditioning on Complex II activities in mitochondria isolated from brain, compared to age-matched sham-treated controls, n=4				
Respiratory rate (ng O_2 min^{-1} mg $protein^{-1}$)	P Value	Result: ↑/↓	Percentage change (%)	Figure
Endogenous	0.011	↑	137.93	4.7
State 4	0.398	-	-	4.7
State 3	0.642	-	-	4.7
Return to State 4	0.217	-	-	4.7
RCI	0.024	↑	42.80	4.8

Table 4.4. Data with statistically significant altered activity levels ($p<0.05$) are shaded green. Arrows indicate direction of altered expression, (↑, increase; ↓, decrease), '-' indicates no significant change. *$p<0.05$; **$p<0.01$. Abbreviations: RCI, respiratory control index.

4.3 Results: Absorption Spectra of Isolated Mitochondria

4.3.1 Absorbance Profile of Isolated Irradiated Mitochondria

Mitochondria were isolated as described in 2.5.1, and a Lowry assay performed (see 2.3.1). Each sample was then diluted to 1 mg/ml. Mitochondrial absorbance spectrum was measured on three occasions, from 1500 nm to 600 nm, and mitochondria were irradiated at 1072 nm as detailed in 2.12.1. Average absorbances (after correction for baseline values) plotted in figure 4.9 and 4.10, n = 3. The shaded area in the figure refers to the bandwidth of light emitted by the IR1072 LEDs, which have a bandwidth of 25 nm.

4.3.2 Absorbance Profile of Mitochondria Irradiated for 10 days *in vivo*

Mice were irradiated as described in 2.2.1 and mitochondria were isolated from the brain and liver of 3 month old D-1 mice as described in 2.5.1, and a Lowry assay performed (see 2.3.1). Each sample was then diluted to 1 mg/ml. Mitochondrial absorbance spectrum was measured three times, from 1500 nm to 600 nm, and mitochondria were irradiated at 1072 nm as detailed in 2.12.1. Average absorbance (after correction for baseline values) is plotted in figure 4.11, n = 4. The shaded area in the figure refers to the bandwidth of light emitted by the IR1072 LEDs, which have a bandwidth of 25 nm.

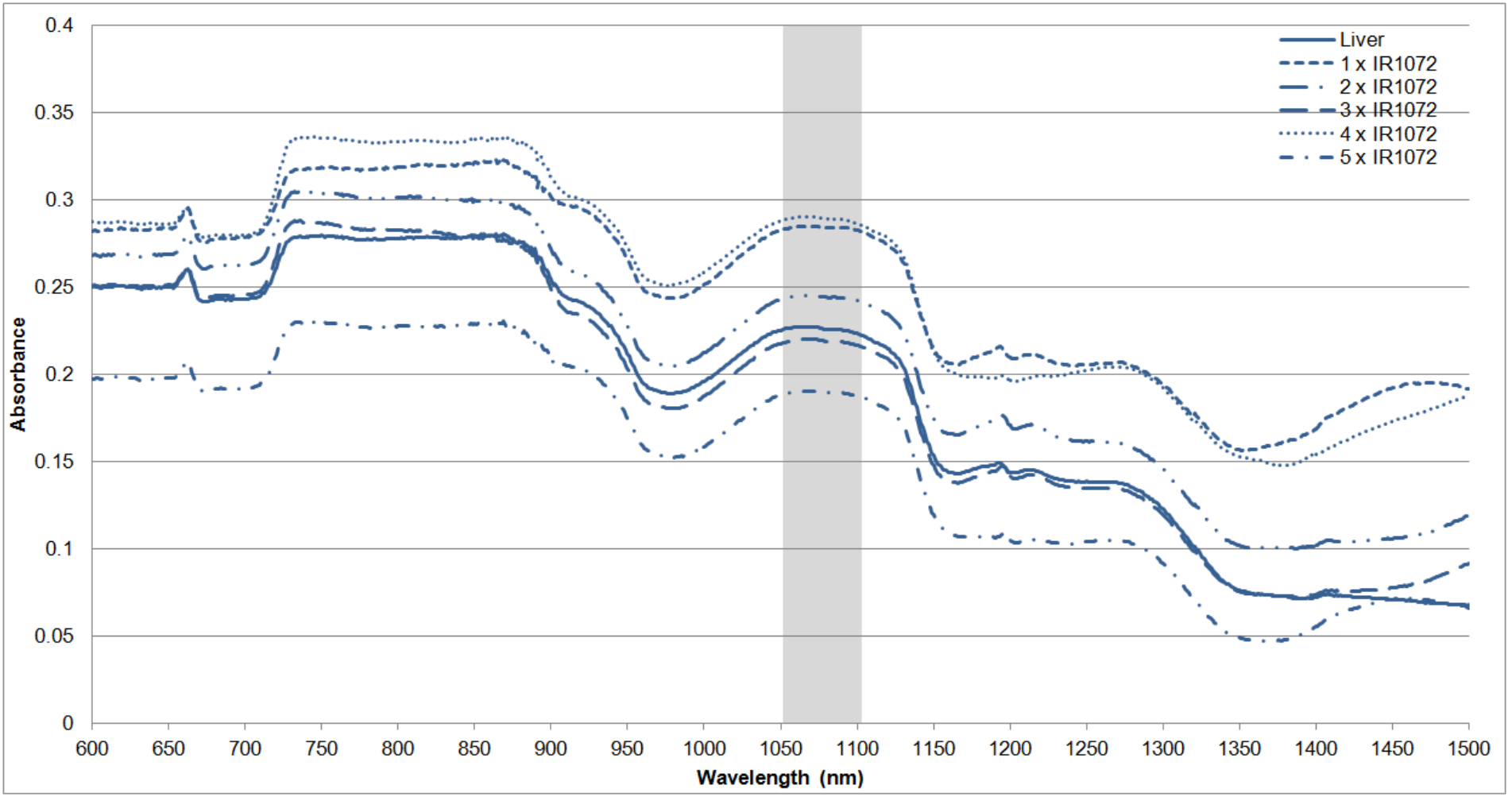

Figure 4.9. Absorption spectra of isolated liver mitochondria, irradiated *in vitro.* Shaded area indicated bandwidth of IR1072 LEDs.

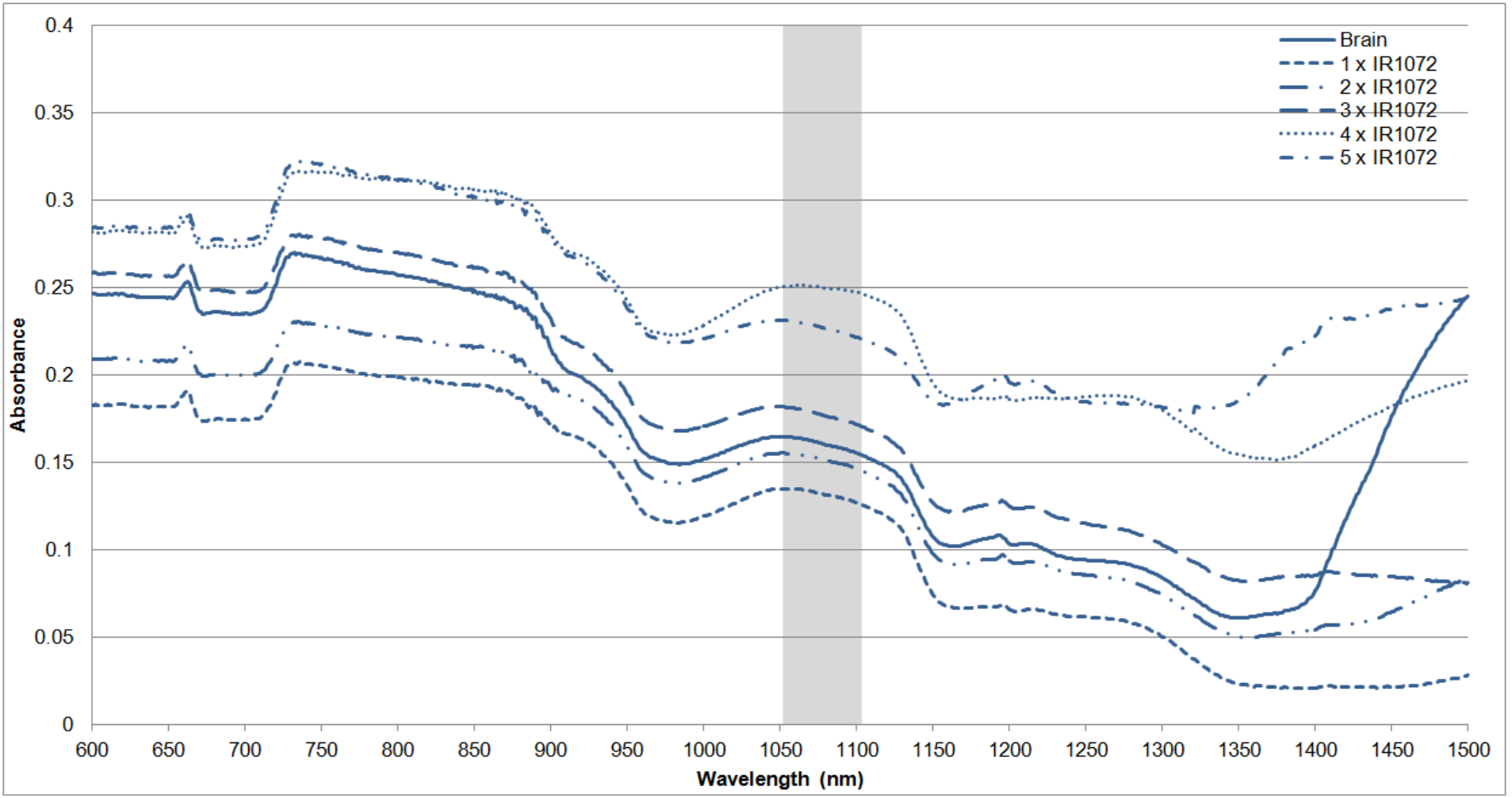

Figure 4.10. Absorption spectra of isolated brain mitochondria, irradiated *in vitro.* Shaded area indicated bandwidth of IR1072 LEDs.

Figure 4.11. Absorption spectra of isolated liver mitochondria, sham or IR irradiated *in vivo.*

4.4 Discussion

The aim of this line of research was to investigate whether acute IR1072 exposure had any effect on the activity of Complex I and/or Complex II in the ETC, of isolated mitochondria from both male and female CD-1 mice at three months of age.

A minimum of three mouse brains are required for each preparation in order to isolate a sufficient quantity of mitochondria for adequate experimental repeats. Therefore, it was only possible to complete two repeats for each sex for each substrate condition. These investigations were completed to further previous work in our laboratory which had investigated the effect of acute IR1072 exposure on 7 month old male CD-1 mice (Burroughs, 2010).

As it has been widely reported that mitochondria act as the primary absorption site for LLLT, with cytochrome *c* oxidase as the proposed principle photoacceptor for NIR (Gao and Xing, 2009, Karu, 1999, Karu *et al.*, 2004, Karu *et al.*, 2005), it was important to investigate mitochondrial respiratory activity following IR1072 exposure. It has previously been reported that up to 50% of NIR is able to be absorbed by mitochondrial chromophores (such as cytochrome *c* oxidase) in the liver (Beauvoit *et al.*, 1995, Beauvoit *et al.*, 1994), therefore it was of interest to investigate liver, as well as brain, mitochondria. As the IR treatment apparatus facilitated irradiation at every conceivable angle of the entire CD-1 mouse, investigation of oxidative phosphorylation of mitochondrial isolated from the liver and brain of animals was the principle target of these investigations.

In order to measure activity of particular components of the ETC, glutamate plus malate and succinate were used to measure the activity of complex I and complex II respectively (Burroughs, 2010, Chance and Williams, 1956b, Markham *et al.*, 2004). Measuring different complexes using oxidative phosphorylation allows determination of both the degree of mitochondrial coupling and to investigate where any alterations in the ETC activity occur, if any, following acute IR1072 exposure. As mentioned previously, the RCI gives a measure of mitochondrial coupling. A high RCI value dictates tightly coupled mitochondria, values for adequately coupled mitochondria for Complex I and Complex II are given in table 4.9.

	IR Treatment Condition	Glutamate + Malate (Complex I)	Succinate (Complex II)
Chance & Williams, 1956a	-	>3	>2
3 month old Male CD-1 mice - Liver	Sham	3.242 ± 0.228	2.908 ± 0.175
	IR	3.168 ± 0.300	2.790 ± 0.024
3 month old Male CD-1 mice - Brain	Sham	2.590 ± 0.195	2.091 ± 0128
	IR	3.506 ± 0.654	2.986 ± 0.355

Table 4.5. RCI values generated through respiratory studies in this investigation, compared to the values of Chance & Williams (1956a), which indicate tightly coupled mitochondria. Cells shaded green indicate loosely coupled mitochondria.

For the respiratory studies performed with mitochondria isolated from CD-1 mice, the value highlighted in table 4.5 indicates more loosely coupled mitochondria and thus oxidative phosphorylation results less reliable. However, there are reports in mice and nematodes that show reduced mitochondrial coupling to be protective, by having a more loosely coupled membrane, the

electron transport chain is less efficient but lower levels of ROS are produced, a normal by-product of respiration, and this in turn has been attributed to increased lifespan (Lemire *et al.*, 2009).

However, all other RCI values were all above 3 or 2 for glutamate plus malate and succinate, respectively, indicating tightly coupled mitochondria and therefore more reliable oxidative phosphorylation readings (Campello *et al.*, 1964, Chance and Williams, 1956b). Acute IR1072 exposure did not affect mitochondria coupling, except in Complex II in brain mitochondria. This suggests that IR1072 exposure may result in a more efficient ETC and therefore lead to the increased ATP levels commonly reported following IR exposure – although only preliminary experiments into ATP levels following IR1072 were conducted in this investigation (see Chapter 3). This could be supported through investigation of SDHC (succinate dehydrogenase Complex II) levels, a membrane coupled component of the electron transport chain. It is possible that the RCI for the sham-treated mice is low due to the length of time isolation requires. Long preparatory methods adversely effects mitochondrial coupling. Brain mitochondria are particularly predisposed to low coupling values, due to long Percoll® filtration steps to remove synaptosomes (Markham *et al.*, 2004).

These respiratory studies found that acute IR1072 showed significantly decreased endogenous respiratory rates in liver mitochondria for both Complex I and II, with significantly increased Complex II in brain mitochondria, perhaps as a result of a greater degree of mitochondrial membrane coupling.

Interestingly, following acute IR1072 exposure both Complex I and II activity were significantly reduced in mitochondria isolated from the liver, however this

was more profound in Complex I than Complex II. These results were somewhat unexpected as previous work in our laboratory has found that neither Complex I or Complex II activity were altered in 7 month old mouse liver mitochondria (Burroughs, 2010).

Significantly, mice at 3 months of age also showed significantly increased Complex II activity in brain mitochondria, when exposed to acute IR1072. In conjunction with the results reported by Burroughs, 2010, the results from this study demonstrate consistent upregulation of Complex II following acute IR1072 exposure, however results from 7 month old mice showed altered activity across all stages of oxidative phosphorylation. Supporting the suggestion that age affects the magnitude of effects of IR1072, as explored in Chapter 5.

It would be particularly interesting to conduct further investigations using male mice to repeat work by Michalikova, *et al.,* 2008, who found LLLT at 1072 nm significantly improved working memory in middle-aged female CD-1 mice. Female CD-1 mice have already been shown to have a significantly better working memory than age-matched male CD-1 mice at both 4 and 12 months (Ennaceur *et al.*, 2008, Michalikova *et al.*, 2008), therefore finding acute IR1072 exposure has reduced ETC activity in age-matched mice (male and female), it would be of particular significance to determine whether IR1072 potentiates/augments the working memory deficits these mice have already demonstrated through the altered Complex I and II activity reported here. Burroughs, 2010, chronically IR1072 treated CD-1 male mice and exposed the mice to a 3D radial maze. IR1072 treated mice showed improved working memory compared to sham-treated controls, but only in mice treated from 3 months of age and not those who started IR1072 exposure at 7 months of age –

again suggesting that younger mice may be more susceptible to acute IR1072 exposure (Burroughs, 2010). When mice reach a certain severity of learning deficit or state of amyloidosis, chronic IR1072 exposure may be required to have a significant impact. As detailed in chapter 5, more significant differences in a range of protein levels were found in older CD-1 mice exposed to chronic IR1072. In future it would be of interest to investigate the effects of chronic IR1072 exposure on mitochondrial complex activities.

It is perhaps surprising that there were significant alterations in Complex I activity in liver mitochondria, as it has previously been reported that NADH-dehydrogenase, a chromophore component of Complex I, which is believed to act as the principle photoacceptor in the blue-spectral region solely (Gao and Xing, 2009, Karu, 1988). Alterations in Complex I activity following NIR are not commonly reported, perhaps because investigations focus on the activity of cytochrome *c* oxidase (Complex IV) activity as this has been reported to act as the main photoacceptor in the red to near infrared light region (Gao and Xing, 2009, Karu, 1999). However significant effects of NIR on Complex I have been reported by several groups. NIR at 633 nm, has been shown to reverse rotenone-induced inhibition of Complex I in retinal nerves of rats in a dose dependent fashion, preventing nerve damage (Rojas *et al.*, 2008). Preconditioning of striatal and cortical neurons with NIR at 670 nm, has also been found to protect against apoptosis and inhibition of ATP synthesis; induced by MPP^+ which act through inhibiting Complex I activity (Liang *et al.*, 2008, Ying *et al.*, 2008). NIR, at 670 nm, has also been shown to reverse nitric oxide-mediated inhibition of oxygen consumption at Complex IV (NO competes with O_2 for the active site in cytochrome *c* oxidase) and Complex I, and thus

protect cardiomyocytes against hypoxia and re-oxygenation injury (Zhang *et al.*, 2009). Altered Complex I and II activity may be due to IR1072 affecting ΔΨm, notably increased ΔΨm has been shown to alter NADH-linked dehydrogenase reactions (Karu, 2008, Passarella *et al.*, 1984). This wealth of published data, as well as data found in this investigation, supports the principle that Complex I does not specifically act as a photoacceptor to the blue-spectral region, but also appears to be influenced by light in the red-near infrared region.

LLLT at 904 nm has been shown to increase Complex IV, perceived as the principle NIR photoacceptor, and Complex II activity in mitochondria at wound sites in Wistar rats (Silveira *et al.*, 2007). Indeed LLLT at 904 nm has since also been shown to increase the activity of Complex I, II, III and IV at sites of muscle damage in Wistar rats (Silveira *et al.*, 2009), supporting evidence found in this investigation and respiratory studies performed by Burroughs, 2010, who found increased Complex II activity in brain mitochondria in 7 month old CD-1 mice (Burroughs, 2010). This study found significantly increased Complex II activity in female CD-1 brain mitochondria following acute IR1072 exposure. Taken together, these data suggest that Complex I and Complex II activity are able to be manipulated by LLLT and may therefore result in alterations in ETC activity. Influence of electron transport chain activity by IR1072 may alter $\Delta\Psi_m$, ATP and reactive oxygen species production, all of which can result in induction of signalling pathways and increased energy availability (Reviewed - Gao and Xing, 2009). It has been proposed that intracellular gradients of ADP, established at the synapse due to high ATP consumption, can slow down the motility of mitochondria resulting in concentration of mitochondria at sites of high ATP requirement. ADP concentration is tightly linked to mitochondrial

respiration rates; with more ADP available, the ETC can produce more ATP which is quickly consumed. This may explain why increased ETC complex activity has been observed in the brain tissue, which consumes significantly more energy than liver tissue (Mironov, 2007), following irradiation at 1072 nm. These data suggest that neurons may be able to function better following irradiation, and this data perhaps explains why no change in ATP levels were reported in Chapter 3, as $\Delta\Psi_m$ gradients may only be apparent over small regions of high activity in neurons, occur in a transient manner and depend on ADP availability, but it does provide data to show longer term IR exposure has the potential to alter ETC activity.

The magnitude of the secondary effects of NIR absorption appears to differ across a range of studies; this is most likely due to the choice of wavelength, protocol and biological system used, as well as knowledge that different wavelengths appear to have different capabilities regarding modulating alternate components of the ETC. As in this investigation, a great deal of primary research into the NIR photoacceptor has relied on oxidative phosphorylation studies. These investigations isolate mitochondria from their cellular environment which in turn may alter parameters of the ETC; the lack of direct *in-situ* experimental support of these assays limits extrapolation and application of the results to other biological systems.

From the absorption spectra of mitochondria shown in figures 4.17 and 4.18, there appears to be a broad peak from 1150-1000 nm, which may relate to a particular protein/complex responsible for absorption of NIR at 1072 nm. This peak appears to be more prominent in liver mitochondria than brain mitochondria; as previously stated liver chromophores are thought to be

responsible for up to 50% of NIR absorption (Beauvoit *et al.*, 1995, Beauvoit *et al.*, 1994). The absorption profile of isolated mitochondria does not appear to be significantly different following irradiation, whether that occurs *in vitro* or *in vivo*. The absorption intensity does appear to significantly alter (see figures 4.17 and 4.18) following irradiation, after the first few exposures it appears to increase before decreasing to below 'control' or 'sham' levels in liver mitochondria. However, the opposing effect seems to occur in brain mitochondria, where the final absorption profile (five sets of IR1072 exposures *in vitro*) is above that of the 'control' level. In the absorption profile of liver mitochondria irradiated or sham-treated *in vivo*, there is a significant peak at approximately 1200 nm which is not present in the mitochondria previously isolated (see figure 4.19). As the peak is present in both sham and IR exposed mitochondria, this may be due to a contaminant. A significant amount of further research needs to be carried out in order to identify the proteins/complexes responsible to the peaks in the mitochondrial profiles and to determine whether quantities/activities of these proteins/complexes alter following IR exposure, techniques utilising mass spectroscopy could aid in this investigation.

As the predominant result from this chapter has been the discovery of reduced Complex I and II activity in the liver, with the observation of increased Complex II consistent with previous research, it would be beneficial to repeat these experiments and to directly measure ATP content of cells in order to establish whether IR1072 is altering ATP levels through altering Complex activity in both tissues. As the *in vitro* system used in Chapter 3 was a neuronal system, perhaps the result of no net change in ATP that was observed is only applicable to the activity of Complex I and II investigated in brain mitochondria – in this

chapter, only Complex II was reported to be increased. Therefore it would be of significant interest to determine both ATP and ADP levels in isolated mitochondria to investigate whether there is a change in the ATP:ADP ratio following IR1072 exposure. Further work could also be performed *in situ* through the use of fluorescent dyes, such as JC-1 (5,5',6,6'-tetrachloro-1,1',3,3' tetraethylbenzimidazolylcarbocyanine iodide), to monitor the effects of NIR on the mitochondrial membrane potential during and following LLLT in living cells (Johnson *et al.*, 1981, Mathur *et al.*, 2000). Using biochemical techniques, as described by Silveira, 2009, investigation of the effect of IR1072 on other components of the ETC, not previously studied would be useful, namely Complex IV (Silveira *et al.*, 2009). These experiments would provide a comprehensive overview of the effects of IR1072 on the ETC to examine whether these effects alter across age and sex of animals, as suggested from the findings reported in this chapter, as well as what effect longer term exposure protocols may induce.

These data have provided important insights into the role of age in the biological effects of IR1072 exposure, with younger mice demonstrating more activity alterations than older counterparts investigated previously, suggesting different magnitudes of biological effects are conceivable in whole animal systems. These data provide support that IR1072 is able to alter mitochondrial activity, whether this is via direct absorption through proposed photoacceptors or via an alternate mechanism remains unknown. However, the absorption profiles of isolated mitochondria clearly demonstrate that there appears to be molecule(s) present which absorbs at 1072 nm. These *in vivo* data provided important insights into photomodulatory effects in one mouse model, CD-1; it was

important to also investigate the effects of gender on electron transport chain activity in TASTPM mice; this is explored in chapter 6.

The next chapter centres on investigation of the effects of chronic IR1072 exposure in the CD-1 mouse strain which has premature learning deficits. The aim of this chapter was to build on previously published data which established IR1072 exposure improved the memory performance of CD-1 mice. This chapter aims to probe putative proteins and pathways involved in the biological effects of IR1072 absorption which may be responsible for the improved behavioural performance of the CD-1 strain.

Chapter 5: Age-dependent changes in protein expression and the effect of *in vivo* chronic IR1072 exposure on protein expression in CD-1 mice

5.1 Introduction

It has been reported that 50% of CD-1 mice die before they reach two years of age, with 50% of females surviving to 18 months, while 50% of males only living until 16 months (Ennaceur *et al.*, 2008, Homburger *et al.*, 1975). Amyloidosis is the most common cause of death in both male and female CD-1 mice, with its presence observed in 50% of mice, of both sexes. However, it has been found to arise in males at 8 months of age, whereas females do not display amyloid deposition until 12 months of age (Engelhardt *et al.*, 1993). Amyloidosis is the principle cause of death in the CD-1 strain. This systemic amyloidosis is postulated to be due to an underlying chronic inflammatory disorder (Engelhardt *et al.*, 1993, Frith and Chandra, 1991). Amyloid deposition is systemic, beginning with the duodenum, jejunum and ileum, death commonly following infiltration of kidney glomeruli, although all internal organs can be affected. The amyloid is similar to that found in humans, it is composed of wide, non-branching strands (Frith and Chandra, 1991). A significant number of CD-1 mice have also been repeatedly shown to develop abscesses, tumours and septicaemia; with neoplastic lesions more common in male mice (Engelhardt *et al.*, 1993).

Cognitive deficits in the CD-1 strain have previously been reported by Mizumori (1982), who demonstrated a lack of working memory in male mice of this strain when mice were faced with an enclosed radial maze at three months of age

(Mizumori *et al.*, 1982). This was further investigated using detailed behavioural analysis in both male and female CD-1 mice at 4 months and 12 months of age. These studies found that 4 month old female mice performed significantly better in the behavioural tests than age-matched males; with older mice consistently demonstrating a reduced capability to acquire a working memory when compared to their younger counterparts (Ennaceur *et al.*, 2008, Michalikova *et al.*, 2008). CD-1 mice were also shown to lack memory retention in 'land-based' maze tasks compared to other strains (Patil *et al.*, 2009). The CD-1 strain also show an impaired response to shock, the authors hypothesise that this is due to motor characteristics of the strain rather than cognitive issues, as they have also shown small amounts of 'freezing' behaviour when exposed to fear conditioning (Adams *et al.*, 2002).

A potential reason for the limited cognitive function seen in the CD-1 strain could be attributed to a reduced brain size, relative to that of other mouse strains. For example CD-1 mice show significantly smaller brain volumes, compared to age matched C57 mice, despite the C57 having smaller body mass. The cerebral cortex has been reported to be 10% smaller, and ventricular compartments 13% smaller in the CD-1 mouse, but with an approximately 4% larger striatum than C57 mice (Chen *et al.*, 2006). The smaller cortex of the CD-1 mouse may explain why the C57 strain consistently out-performs the CD-1 strain in memory-based tasks (Ennaceur *et al.*, 2006, Michalikova *et al.*, 2010, Patil *et al.*, 2009).

These data demonstrate that the CD-1 strain develops premature cognitive deficits, advocating the use of this strain in the study of ageing and in investigating the modulation of this process.

The aim of this chapter was to establish protein changes that occur during ageing of the CD-1 strain, which may contribute to their learning deficits which progress with age and premature death. Relatively little is known about protein expression in this mouse strain during ageing, additional research was required to further work previously undertaken in our laboratory, whereby male mice at 3, 10 and 12 months were investigated (Burroughs, 2010). A second aim was to determine whether chronic IR1072 treatment of young and old CD-1 mice, would alter protein expression and whether the magnitude of alteration was age-dependent, through the use of immunoblotting and immunohistochemistry.

Male mice were exposed to sham or IR1072 treatments as described in 2.2.2., from 2 months of age until 7 months of age (denoted as ‘Young’ mice) and from 7 months to 13 months of age (denoted as ‘Old’ mice).

5.2 Results

5.2.1 Immunoblotting Analysis

Data were analysed using ImageJ, version 1.43, National Institutes of Health, USA, and processed using Microsoft Office Excel 2007 and statistical analyses were carried out using GraphPad Prism Version 5, GraphPad Software Inc.

Data is summarised in table 5.1.

Male CD-1 mice at 12 months of age displayed a 55.51% reduction in HSP105 expression, compared to mice of 3 months of age. Mice of 10 months of age also demonstrated a 42.75% decrease in HSP105 expression when compared to mice of 3 months of age. However, there was no significant difference between the expression of HSP105 in 10 month old male CD-1 mice and mice of 12 months of age. Data shown in figure 5.1 and table 5.1.

Male CD-1 mice at 12 months of age showed a 39.40% decrease in HSP70 expression compared to mice of 3 months of age. Mice at 10 months of age also showed a 14.79% trend for a decrease in HSP70 expression compared to mice of 3 months of age. Mice at 12 months of age also showed a 28.89% decrease in HSP70 expression compared to mice of 10 months of age. Data shown in figure 5.2 and table 5.1.

Male CD-1 mice at 12 months of age showed a 45.40% decrease in TARP γ2 expression, compared to mice of 3 months of age. Mice of 10 months of age also showed a 40.61% reduction in TARP γ2 expression compared to mice at 3 months of age. All other comparisons were non-significant. Data shown in figure 5.3 and table 5.1.

All other proteins investigated were deemed not to alter with age.

All data were analysed using a one-way ANOVA with a Bonferroni's multiple comparison post test.

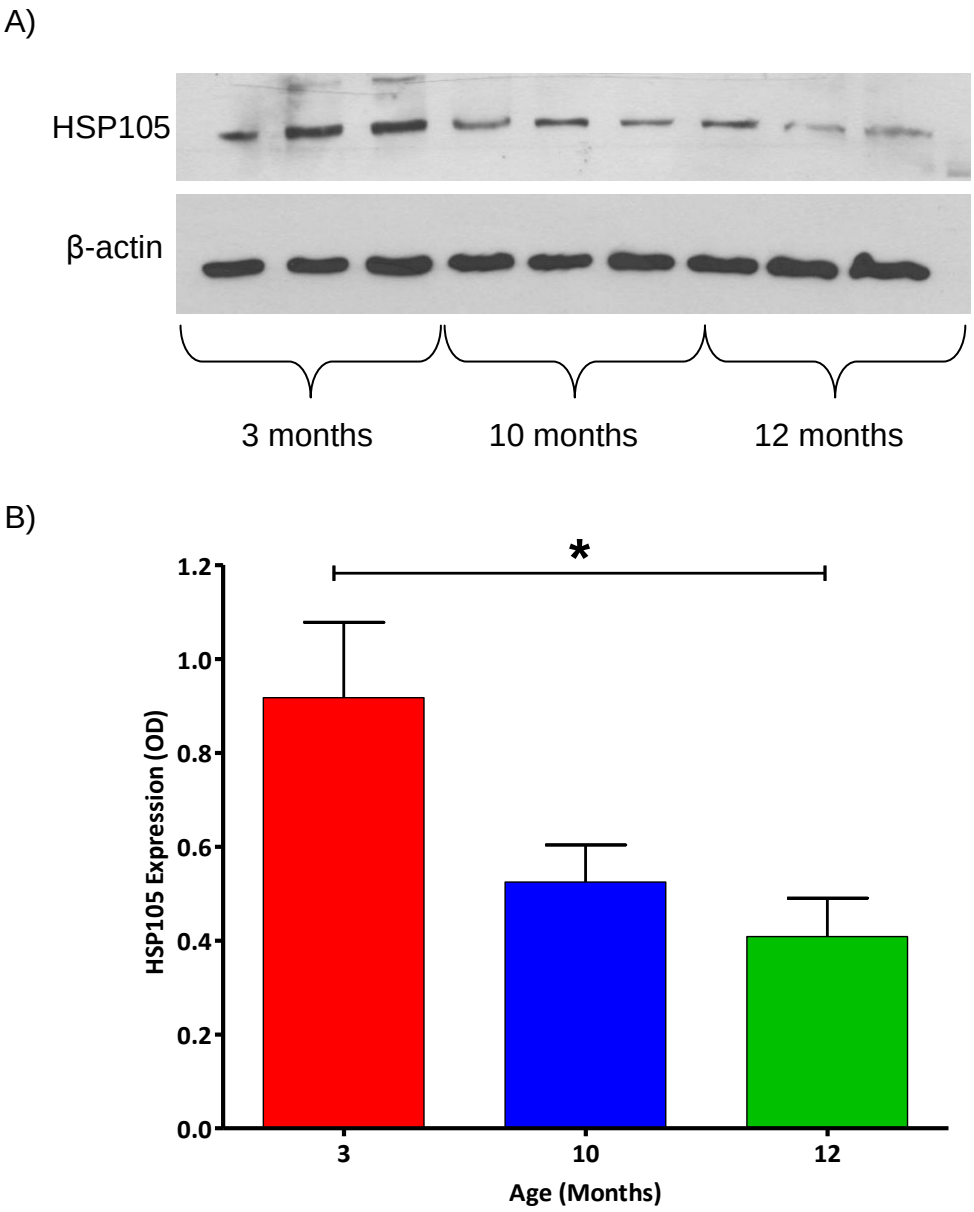

Figure 5.1. Age dependent alterations in HSP105 expression; shown in 3 month, 10 month and 12 month old male CD-1 mouse brains. A) is an immunoblot, each lane represents an individual mouse and B) shows the quantitative analyses of immunoblot data. Mean values ± SEM, n=3 at each age point, 12 month mice had a significant (*$p<0.05$) decrease in HSP105 expression, compared to 3 month CD-1 mice. All other comparisons were non-significant. Abbreviations: HSP105, Heat shock protein 105; OD, optical density.

A)

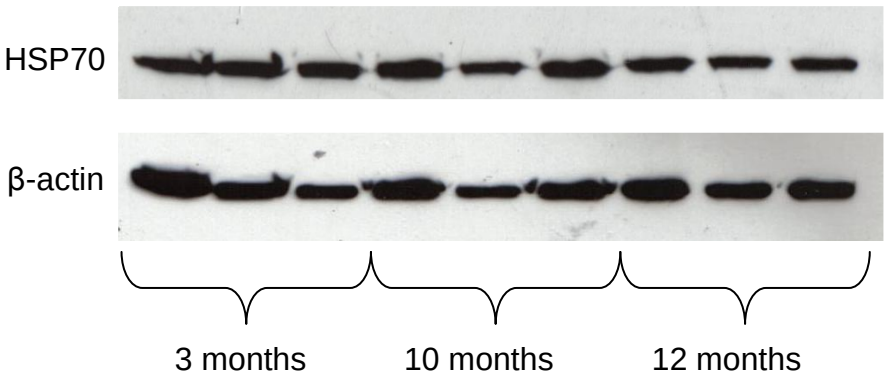

B)

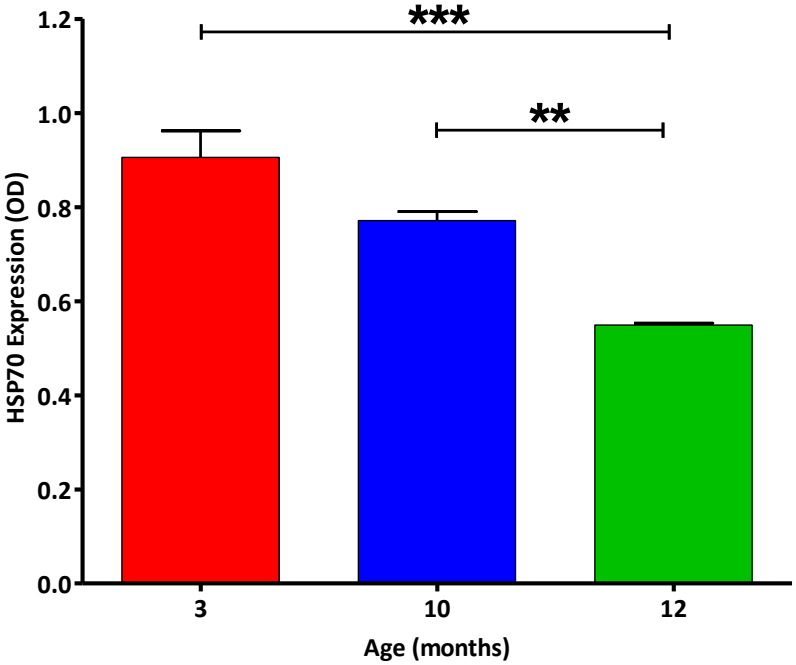

Figure 5.2. Age dependent alterations in HSP70 expression; shown in 3 month, 10 month and 12 month old male CD-1 mouse brains. A) is an immunoblot, each lane represents an individual mouse and B) shows the quantitative analyses of immunoblot data. Mean values ± SEM, n=3 at each age point. A significant reduction in HSP70 expression was found when comparing expression in 3 month old CD-1 mice to that of 12 month (*$p<0.05$) and 10 month to 12 month old CD-1 mice (***$p<0.001$). All other comparisons are non-significant. Abbreviations: HSP70, heat shock protein 70; OD, optical density.

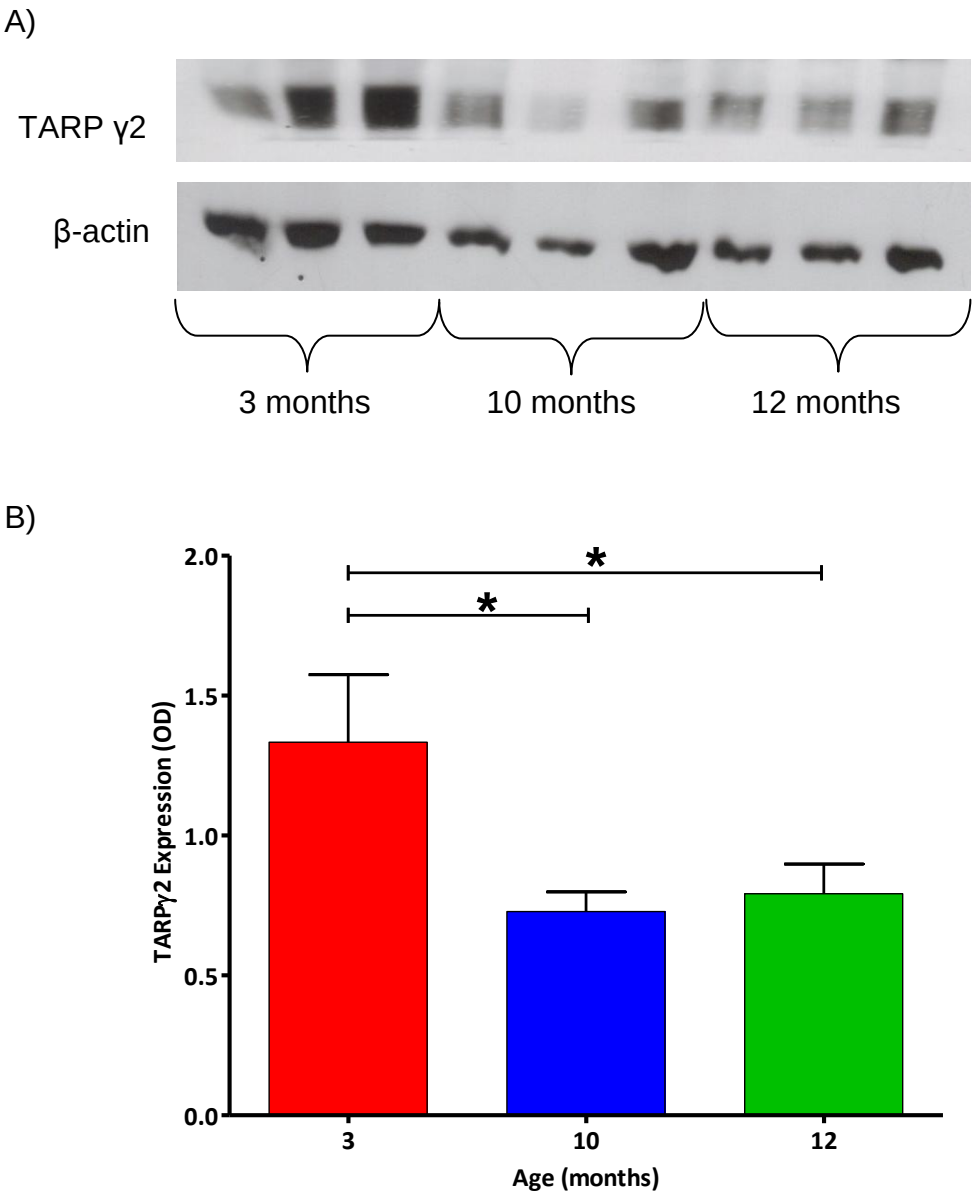

Figure 5.3. Age dependent alterations in TARP γ2 expression; shown in 3 month, 10 month and 12 month old male CD-1 mouse brains. A) is an immunoblot, each lane represents an individual mouse and B) shows the quantitative analyses of immunoblot data. Mean values ± SEM, n=3 at each age point. A significant reduction in TARP γ2 expression was found when comparing expression in 3 month old CD-1 mice to that of 10 month and 12 month old CD-1 mice (*$p<0.05$). All other comparisons are non-significant. Abbreviations: TARP γ2, Transmembrane AMPA regulatory protein γ2; OD, optical density.

Effect of age on protein expression in male CD-1 mice at 3, 10 and 12 months of age, n=3 for each condition						
Antibody/Protein	P Value	3 vs. 10	3 vs. 12	10 vs. 12	Result: ↑ or ↓	Figure
GSK-3β	0.890	-	-	-	-	Not shown
HSF1	Not determined					
HSP105	0.044	NS	*	-	↓	Figure 5.1
HSP70	0.001	NS	***	**	↓	Figure 5.2
P-HSP27	0.414	-	-	-	-	Not shown
αB crystallin	0.977	-	-	-	-	Not shown
TARP γ2	0.015	*	*	-	↓	Figure 5.3
TARP γ8	0.293	-	-	-	-	Not shown
MAPK	0.133	-	-	-	-	Not shown

Table 5.1. Data with a trend in altered expression levels are shaded blue ($p<0.1$), data with statistically significant altered expression levels ($p<0.05$) are shaded green. Arrows indicate direction of altered expression, (↑, increase; ↓, decrease), '-' indicates no significant change. *$p<0.05$, **$p<0.01$, ***$p<0.001$. Abbreviations: GSK-3β, glycogen synthase kinase-3β; HSF, heat shock factor; HSP, heat shock protein; MAPK, mitogen associated protein kinase; P-HSP, phosphorylated heat shock protein; TARP, transmembrane AMPA regulatory protein.

5.3 Chronic IR1072 treatment of CD-1 Male Mice

Male CD-1 mice were irradiated as outlined in 2.2.2, this chronic (five month) IR exposure was performed on mice from two months of age, designated as 'Young CD-1 mice', and mice from seven months of age, designated 'Old CD-1 mice'. Both age groups were exposed to the same treatment protocol and equipment. Sham mice were exposed to replica equipment, for the same time period, in the absence of IR1072. During the treatment period the weight of mice and temperature of equipment was monitored. Equipment as outlined in 2.2.2.

5.3.1 Young CD-1 Mice

5.3.1.1 Immunoblotting

Data were analysed using ImageJ, version 1.43, National Institutes of Health, USA, and processed using Microsoft Office Excel 2007 and statistical analyses were carried out using GraphPad Prism Version 5, GraphPad Software Inc. Data were analysed using a two-tailed student's T test. Data shown represent mean ± SEM, n= number of replicates.

Data is summarised in table 5.2.

IR1072 preconditioned male 7 month of age CD-1 mice showed a 92.68% increase in P-HSP27 expression, a 91.60% increase in TARP γ2 expression and a 458.26% increase in SDHC expression compared to age-matched sham treated controls.

A)

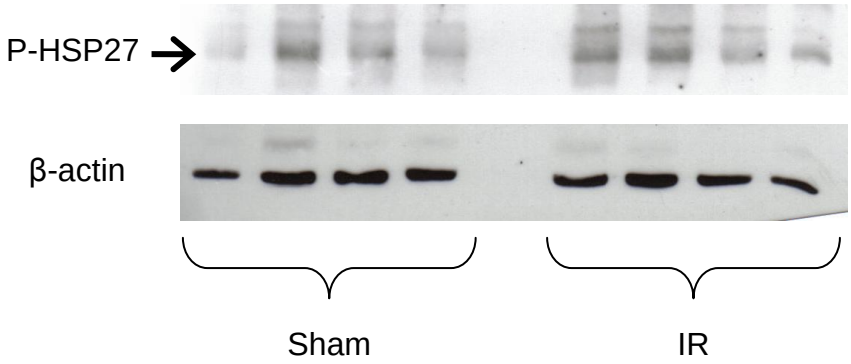

B)

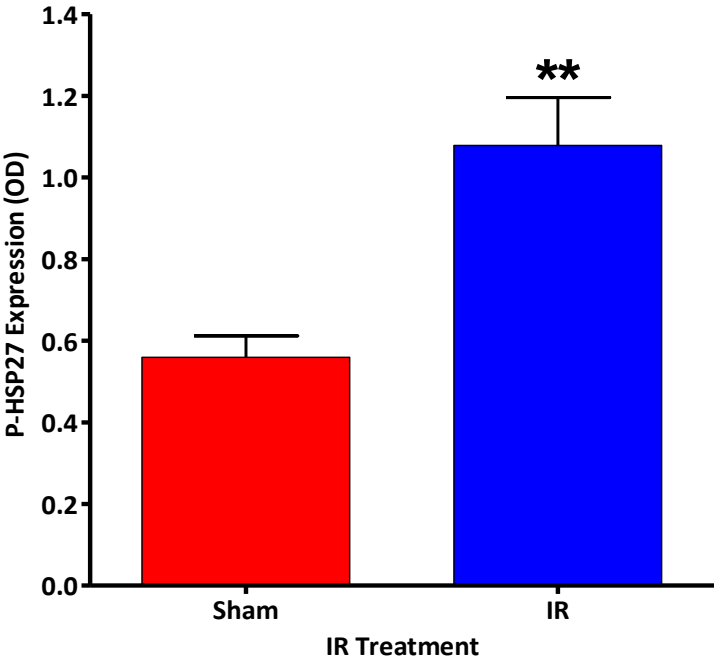

Figure 5.4. P-HSP27 expression in chronic preconditioned (*in vivo*) 7 month CD-1 male mice and Sham age matched controls. Each lane in A) demonstrates an individual mouse (n=4 for each condition) and B) represents quantitative analysis of P-HSP27 expression, demonstrating a significant increase in P-HSP27 expression following chronic IR1072 treatment, compared to sham treated animals, **p<0.01, Mean ± SEM. Abbreviations: P-HSP27, Phosphorylated-Heat shock protein 27; OD, optical density.

A)

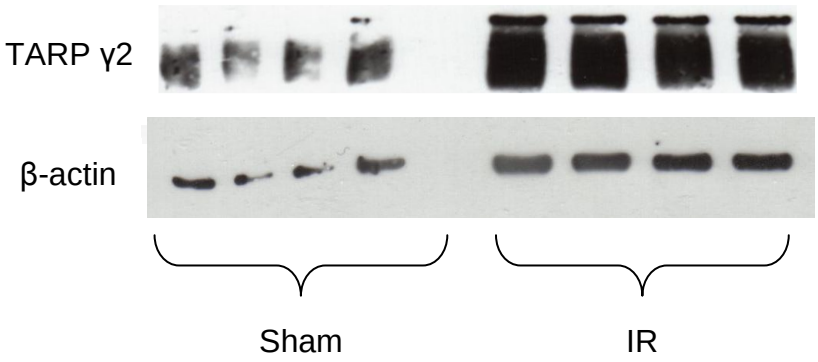

B)

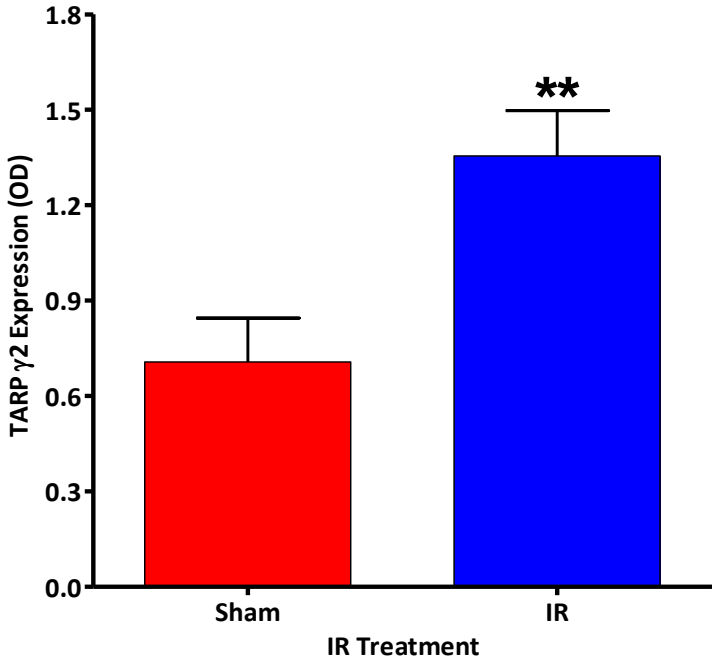

Figure 5.5. TARP γ2 expression in chronic IR1072 preconditioned (*in vivo*) 7 month CD-1 male mice and Sham age matched controls. Each lane in A) demonstrates an individual mouse (n=4 for each condition) and B) represents quantitative analysis of TARP γ2 expression, demonstrating a significant increase in TARP γ2 expression following chronic IR1072 treatment, compared to sham treated animals, **p<0.01, Mean ± SEM. Abbreviations: TARP γ2, Transmembrane AMPA receptor regulatory protein γ2; OD, optical density.

A)

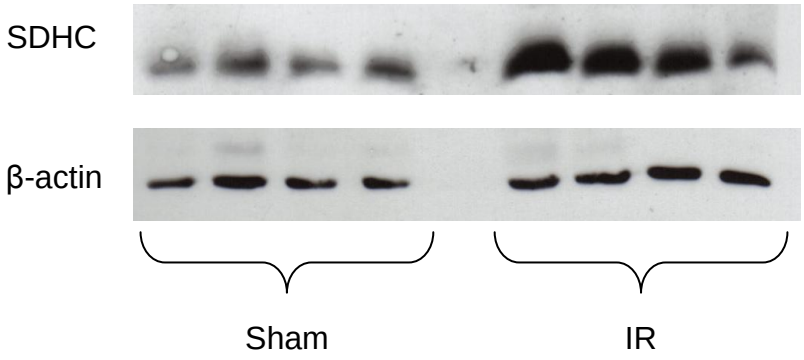

B)

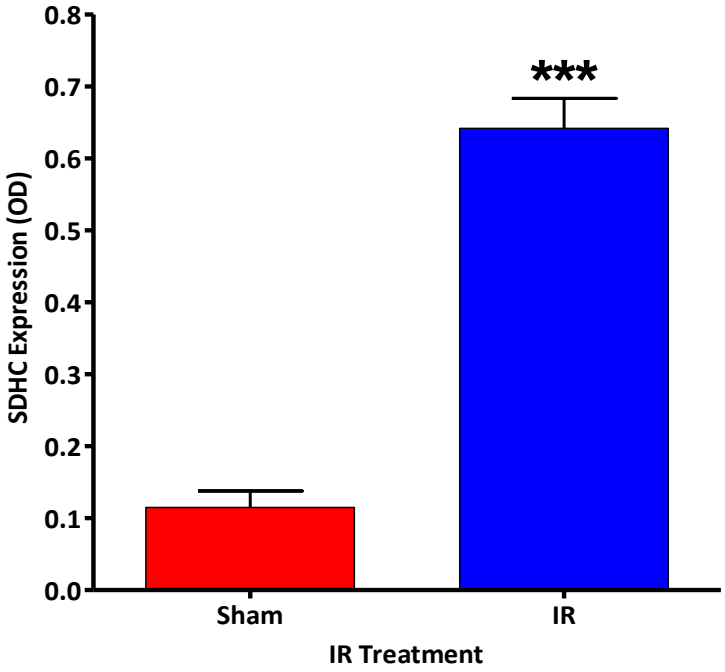

Figure 5.6. SDHC expression in chronic IR1072 preconditioned (*in vivo*) 7 month CD-1 male mice and Sham age matched controls. Each lane in A) demonstrates an individual mouse (n=4 for each condition) and B) represents quantitative analysis of SDHC expression, demonstrating a significant increase in SDHC expression following chronic IR1072 treatment, compared to sham treated animals, ***p<0.001, Mean ± SEM. Abbreviations: SDHC, Succinate dehydrogenase complex subunit C; OD, optical density.

Effect of Chronic IR1072 Preconditioning on protein expression in male CD-1 7 month old mice, compared to age matched sham-treated controls, n=4 for each condition			
Antibody/Protein	P Value	Result: increase or decrease	Figure
GSK-3β	0.520	-	Not shown
HSF1	0.502	-	Not shown
P-HSP27	**0.007	↑	Figure 5.4
αB crystallin	0.883	-	Not shown
TARP γ2	**0.009	↑	Figure 5.5
TARP γ8	0.350	-	Not shown
SDHC	***<0.001	↑	Figure 5.6
GluA2	Not determined		

Table 5.2. Data with a trend in altered expression levels are shaded blue ($p<0.1$), data with statistically significant altered expression levels ($p<0.05$) are shaded green. Arrows indicate direction of altered expression, (↑, increase; ↓, decrease), '-' indicates no significant change. *$p<0.05$, **$p<0.01$, ***$p<0.001$. Abbreviations: GluA2, glutamate receptor 2; GSK-3β, glycogen synthase kinase-3β; HSP, heat shock protein; P-HSP, phosphorylated heat shock protein; SDHC, succinate dehydrogenase Complex II; TARP, transmembrane AMPA regulatory protein.

5.3.2 Old CD-1 Mice

5.3.2.1 Immunoblotting

Data were analysed using ImageJ, version 1.43, National Institutes of Health, USA, and processed using Microsoft Office Excel 2007 and statistical analyses were carried out using GraphPad Prism Version 5, GraphPad Software Inc. Data were analysed using a two-tailed student's T test. Data shown represent mean ± SEM, n= number of replicates.

Data is summarised in table 5.3.

IR1072 preconditioned male 13 month of age CD-1 mice displayed a 51% reduction in HSF1, a 36.43% decrease in HSP70, a 43.13% reduction in αB crystallin and a 42.25% reduction in GluA2 expression compared to age-matched sham treated controls.

IR1072 preconditioned male 13 month of age CD-1 mice displayed a 329.69% increase in P-HSP27, a 48.75% increase in TARP γ2 expression compared to age-matched sham treated controls.

A)

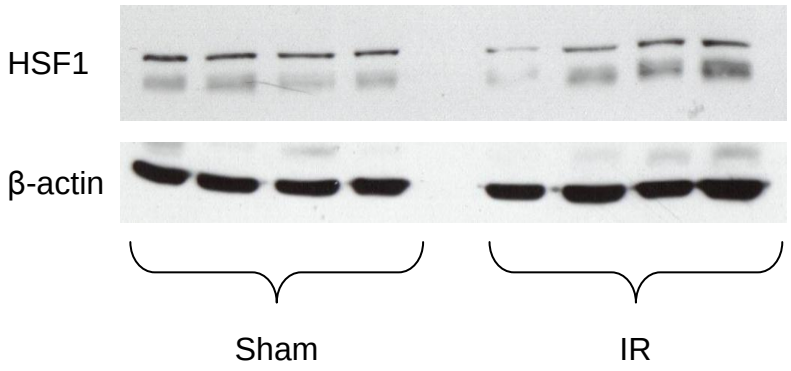

B)

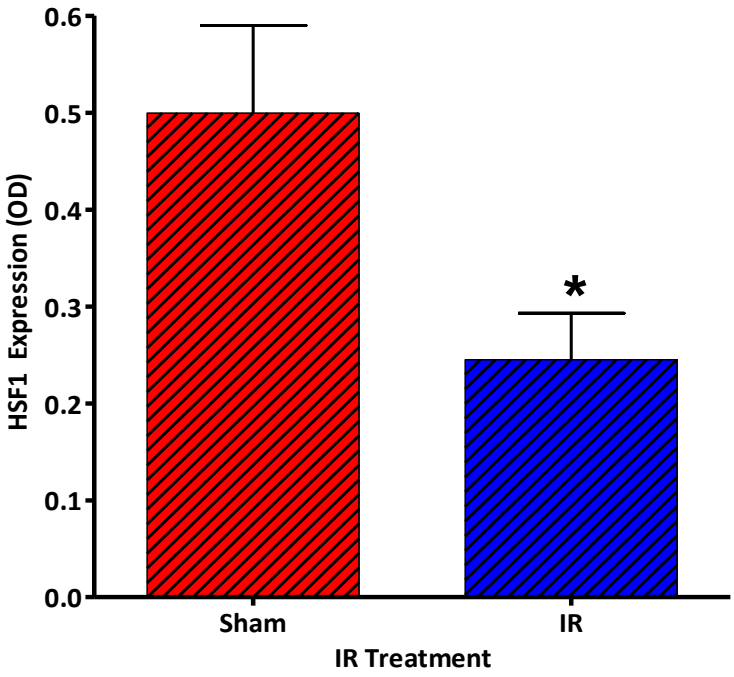

Figure 5.7. HSF1 expression in chronic IR1072 preconditioned (*in vivo*) 13 month CD-1 male mice and Sham age matched controls. Each lane in A) demonstrates an individual mouse (n=4 for each condition) and B) represents quantitative analysis of HSF1 expression, demonstrating a significant reduction in HSF1 expression following chronic IR1072 treatment, compared to sham treated animals, *p<0.05, Mean ± SEM. Abbreviations: HSF1, Heat shock factor 1; OD, optical density.

A)

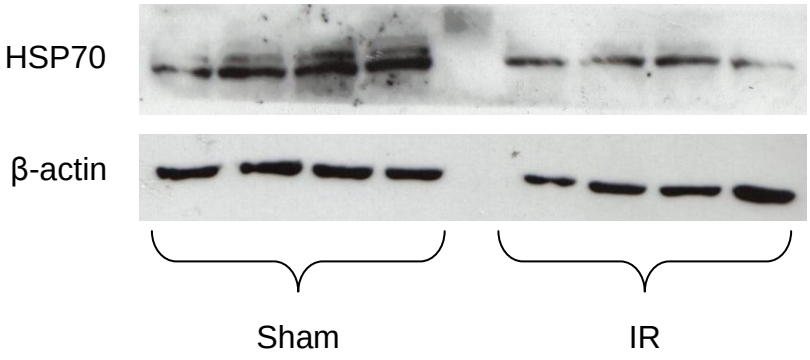

B)

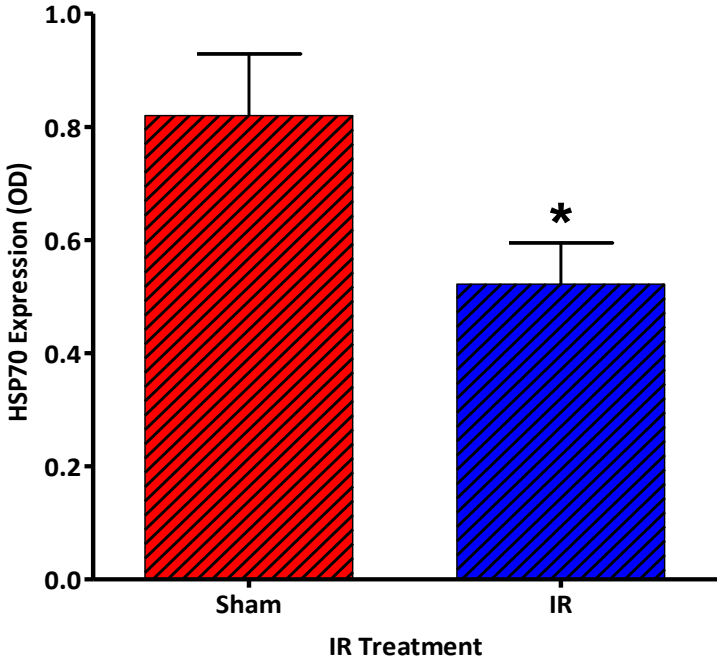

Figure 5.8. HSP70 expression in chronic IR1072 preconditioned (*in vivo*) 13 month CD-1 male mice and Sham age matched controls. Each lane in A) demonstrates an individual mouse (n=4 for each condition) and B) represents quantitative analysis of HSP70 expression, demonstrating a significant reduction in HSP70 expression following chronic IR1072 treatment, compared to sham treated animals, *p<0.05, Mean ± SEM. Abbreviations: HSP70, Heat shock protein 70; OD, optical density.

A)

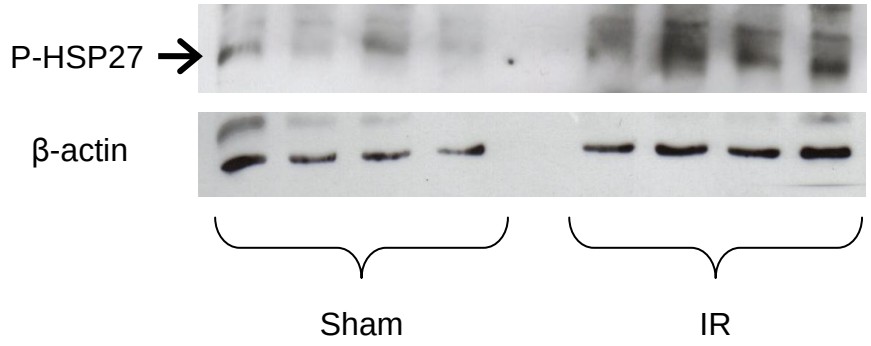

B)

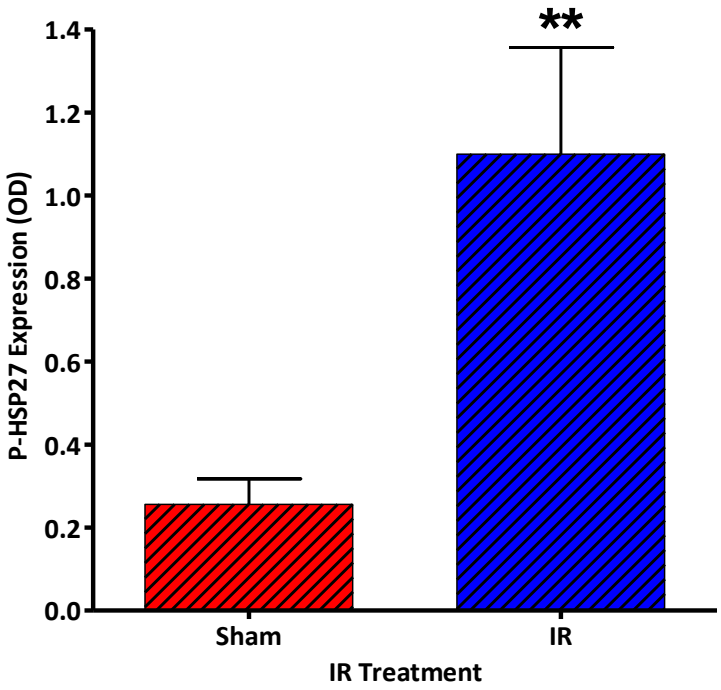

Figure 5.9. P-HSP27 expression in chronic IR1072 preconditioned (*in vivo*) 13 month CD-1 male mice and Sham age matched controls. Each lane in A) demonstrates an individual mouse (n=4 for each condition) and B) represents quantitative analysis of P-HSP27 expression, demonstrating a significant increase in P-HSP27 expression following chronic IR1072 treatment, compared to sham treated animals, **p<0.01, Mean ± SEM. Abbreviations: P-HSP27, Phosphorylated Heat shock protein 27; OD, optical density.

A)

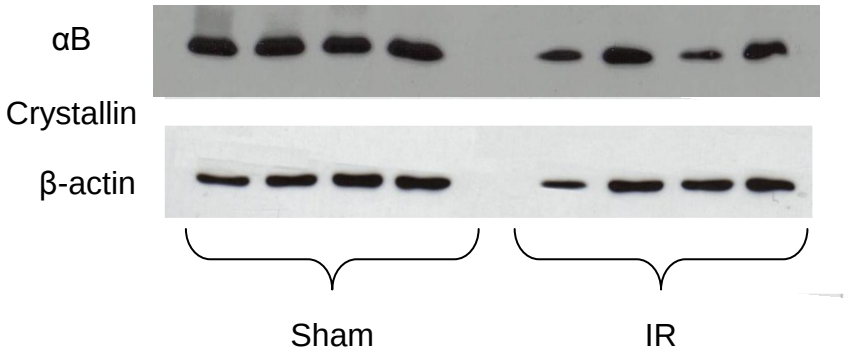

B)

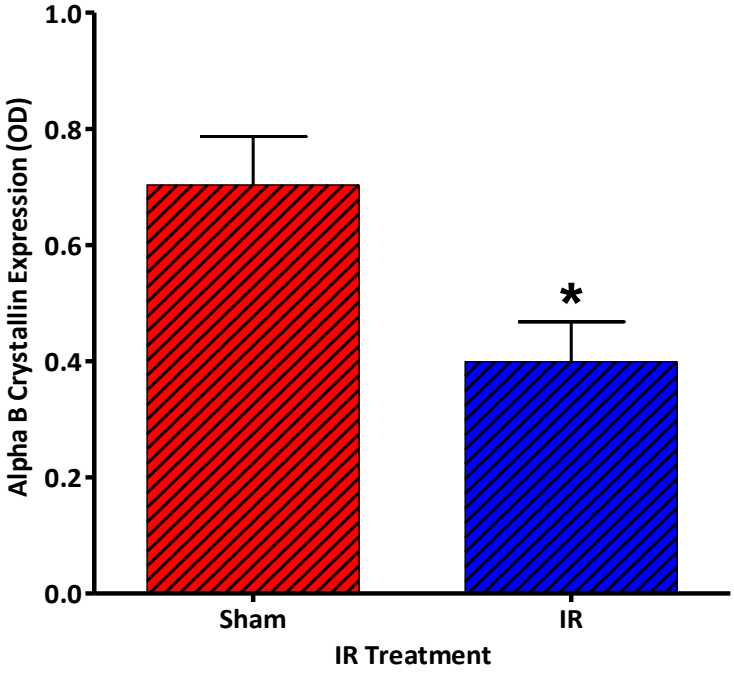

Figure 5.10. αB Crystallin expression in chronic IR1072 preconditioned (*in vivo*) 13 month CD-1 male mice and Sham age matched controls. Each lane in A) demonstrates an individual mouse (n=4 for each condition) and B) represents quantitative analysis of αB Crystallin expression, demonstrating a significant reduction in αB Crystallin expression following chronic IR1072 treatment, compared to sham treated animals, *p<0.05, Mean ± SEM. Abbreviations: OD, optical density.

A)

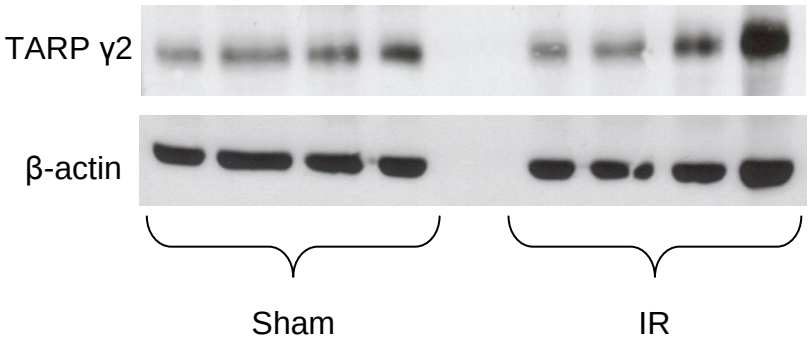

B)

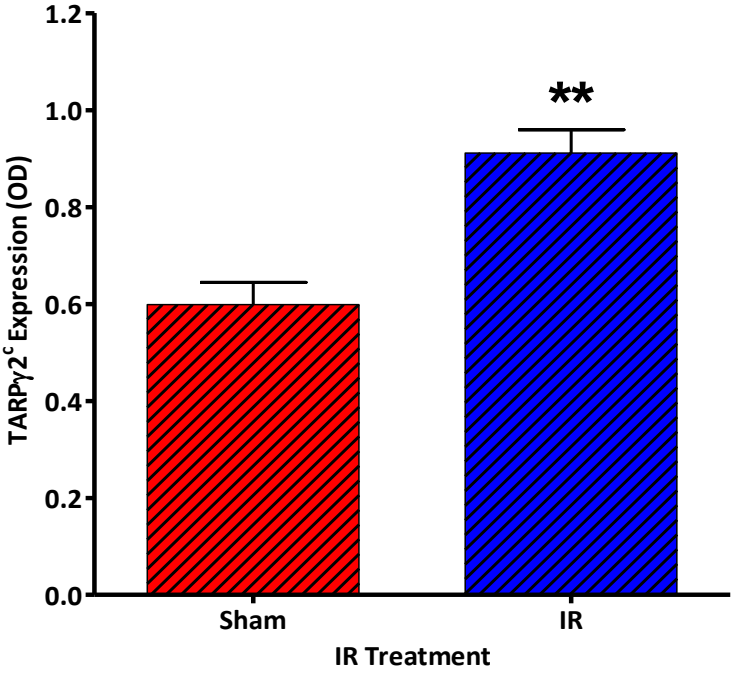

Figure 5.11. TARP γ2 expression in chronic IR1072 preconditioned (*in vivo*) 13 month CD-1 male mice and Sham age matched controls. Each lane in A) demonstrates an individual mouse (n=4 for each condition) and B) represents quantitative analysis of TARP γ2 expression, demonstrating a significant increase in TARP γ2 expression following chronic IR1072 treatment, compared to sham treated animals, **p<0.01, Mean ± SEM. Abbreviations: TARP γ2, Transmembrane AMPA regulatory protein; OD, optical density.

A)

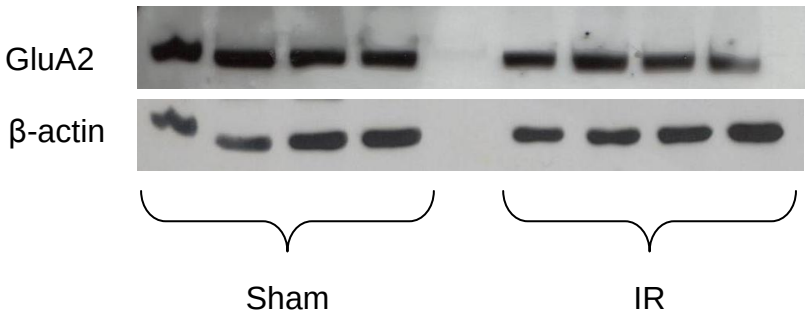

B)

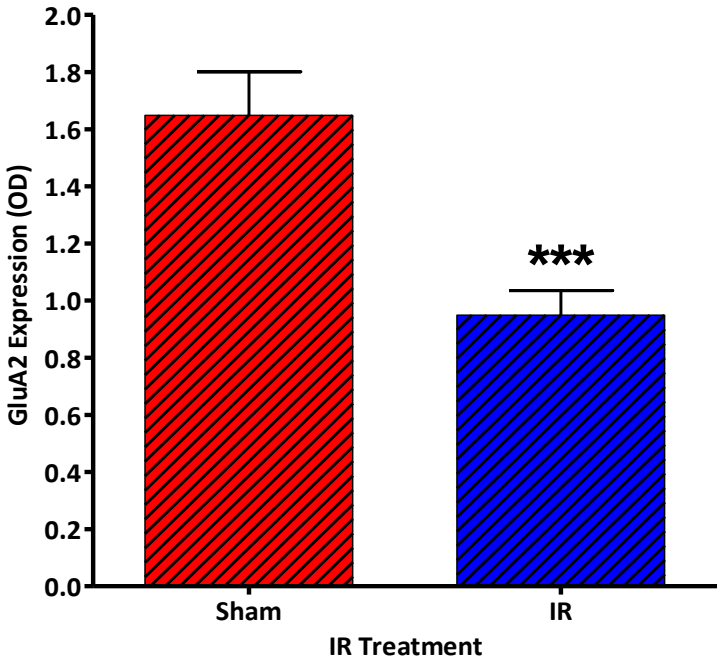

Figure 5.12. GluA2 expression in chronic IR1072 preconditioned (*in vivo*) 13 month CD-1 male mice and Sham age matched controls. Each lane in A) demonstrates an individual mouse (n=4 for each condition) and B) represents quantitative analysis of GluA2 expression, demonstrating a significant reduction in GluA2 expression following chronic IR1072 treatment, compared to sham treated animals, ***p<0.001, Mean ± SEM. Abbreviations: GluA2, AMPA glutamate receptor subunit 2; OD, optical density.

Effect of Chronic IR1072 Preconditioning on protein expression in male CD-1 13 month old mice, compared to age matched sham-treated controls, n=4 for each condition			
Antibody/Protein	P Value	Result: increase or decrease	Figure
GSK-3β	0.557	-	Not shown
HSF1	*0.026	↓	Figure 5.7
HSP105	0.131	-	Not shown
HSP70	*0.028	↓	Figure 5.8
P-HSP27	**0.007	↑	Figure 5.9
αB crystallin	*0.014	↓	Figure 5.10
TARP γ2	**0.006	↑	Figure 5.11
TARP γ8	0.418	-	Not shown
GluA2	***0.001	↓	Figure 5.12
SDHC	0.282	-	Not shown

Table 5.3. Data with a trend in altered expression levels are shaded blue ($p<0.1$), data with statistically significant altered expression levels ($p<0.05$) are shaded green. Arrows indicate direction of altered expression, (↑, increase; ↓, decrease), '-' indicates no significant change. *$p<0.05$; **$p<0.01$, ***$p<0.001$. Abbreviations: GluA2, glutamate receptor 2; GSK-3β, glycogen synthase kinase-3β; HSP, heat shock protein; P-HSP, phosphorylated heat shock protein; SDHC, succinate dehydrogenase Complex II; TARP, transmembrane AMPA regulatory protein.

5.4 Discussion

The aim of this chapter was to further elucidate proteins that alter with age of the CD-1 mouse, and to determine whether these proteins are also altered following chronic IR1072 exposure. Another aim of this chapter was to investigate whether protein changes altered in their profile and magnitude when comparing mice that began chronic IR1072 exposure at 2 months of age to those treated from 7 months of age.

Pathway	Protein	CD-1 Timeline (Age in months)			Effect of chronic IR1072 exposure	
		3 vs. 10	3 vs. 12	10 vs. 12	Young	Old
	GSK-3β	-	-	-	-	-
Chaperones	HSF1	Not determined			-	*↓
	HSP105	↓(NS)	↓	-	-	-
	HSP70	↓(NS)	***↓	**↓	*↓	*↓
	P-HSP27	-	-	-	**↑	**↑
	αB Crystallin	-	-	-	-	*↓
AMPA/ TARP	TARP γ2	*↓	*↓	↓ (NS)	**↑	**↑
	TARP γ8	-	-	-	-	-
	GluA2	Not shown ↓			N/D	***↓
	SDHC	Not determined			***↑	-
	MAPK	-	-	-	N/D	N/D

Table 5.4. Summary of all effects on ageing CD-1 mice and chronically IR treated mice, determined by western blotting. Abbreviations: AMPA, 2-amino-3-(3-hydroxy-5-methyl-isoxazol-4-yl)propanoic acid; GluA2, glutamate receptor 2; GSK-3β, glycogen synthase kinase-3 beta; HSF, heat shock factor; HSP, heat shock protein; P-HSP, phosphorylated heat shock protein; MAPK, mitogen associated protein kinase; SDHC, succinate dehydrogenase Complex II; TARP, transmembrane AMPA regulatory protein; NS, not significant trend; N/D, not determined. Purple shaded cells refer to results obtained previously in the laboratory. *p<0.05; **p<0.01, ***p<0.001, '-' indicates no significant change.

There were a number of changes that occurred in protein expression levels in ageing CD-1 mice; these included a decrease in HSP105, HSP70 and TARP γ2. These data further add to the profile of protein changes that occur during ageing of the CD-1 mouse, previously our laboratory has reported levels of HSP27, BDNF (brain derived neurotrophic factor) and GluA2 (Chazot *et al,* unpublished) also decrease with age and a range of other proteins, including P-HSP27, αB crystallin, HSP40, HSP60, HSP70 and HSP90 have been found to remain unchanged with age (Burroughs, 2010). The reduction in HSP70 and HSP105 during ageing, support the hypothesis of a reduced ability to induce HSP expression (Calderwood *et al.*, 2009, Soti and Csermely, 2003), whilst reduced GluA2 and TARP γ2 with age may explain the learning deficits observed in the CD-1 mice that become more apparent with age (Ennaceur *et al.*, 2008). From these data it could be implied that levels of HSF1 do not significantly alter during ageing of the CD-1 mouse, however it was not possible to directly investigate this due to lack of tissue, but it would be an interesting factor to investigate in the future.

However, chronic IR1072 exposure did appear to reduce HSF1 levels in old CD-1 mice, but there was no change in HSF1 levels in young mice that were irradiated. It is interesting to note that while a number of HSPs were reduced in expression in old CD-1 mice that were irradiated, including HSP70 and αB crystallin, levels of P-HSP27 were increased. In previous work HSP27, HSP40 and HSP60 have also been shown to be significantly increased in old CD-1 mice that were chronically irradiated (Burroughs, 2010). There remains work to be done regarding the role/function of HSF1 in the 'normal' state, definition of function has only been established using severe hypothermia and acute

stresses such as dietary restriction. This work has been done mainly in *C. elegans*, and the impact of HSF1 on mammalian longevity remains to be established (Anckar and Sistonen, 2011). These data suggest levels of HSF1 may not be a sufficiently sensitive measure of the capability of HSP expression or that HSP expression may be influenced by other mechanisms such as the STAT3 pathway (Saito *et al.*, 2009, Yamagishi *et al.*, 2009).

It is very interesting to note that an increased level of phosphorylated HSP27 was observed in both young and old CD-1 mice exposed to chronic IR1072. Phosphorylated HSP27 forms tetramers, which are able to target proteins towards ubiquitination, initially stabilising the aggregates before removing them. Functionality of P-HSP27 *in vivo* is difficult to determine as the phosphorylation status can change rapidly and alternately phosphorylated isoforms can exist at any one time (Rogalla *et al.*, 1999). As well as this, it is thought that the small oligomers of HSP27 that form following phosphorylation are the structures which interact with DAXX, preventing FAS-mediated cell death (see figure 1.12.; Beere, 2004, Garrido, 2002). Increased HSP27 is not only anti-apoptotic but is also able to activate and stabilise Akt to promote cell survival (Beere, 2004, 2005, Gao and Xing, 2009). Previous data showing increased HSP27, in both young and old CD-1 mice (Burroughs, 2010), supports data found in investigations with both the CD-1 strain and TASTPM strain following IR1072 exposure (see Chapter 6). HSP27 and the phosphorylated version have both been found to be consistently increased following chronic IR1072 exposure. Further work to investigate whether this is also the case for female CD-1 mice would be important to undertake. It was also interesting to find that the sHSP, αB crystallin, was decreased in old CD-1 mice that were chronically IR treated

but no change was found in young CD-1 mice that were irradiated, as well as no change in levels was found during ageing in the CD-1 line. The reduction in old CD-1 mice may be a result of decreased HSF1 levels that were also observed, however decreased αB crystallin has also been found in male and female TASTPM mice that have undergone chronic irradiation. It is therefore perhaps of more interest that young CD-1 mice showed no change in αB crystallin levels. The reduction in αB crystallin may be attributed to cell stress, the TASTPM strain already have a significant amyloid load at 7 months of age and the CD-1 strain have been reported to display increased amyloidosis with age (Engelhardt *et al.*, 1993), in the face of more stress, the response to IR1072 appears to be greater. The role of αB crystallin is not clear; it has been shown to exacerbate Aβ oligomer formation (Narayanan *et al.*, 2006, Stege *et al.*, 1999) but also increase tau degradation and dephosphorylation (Bjorkdahl *et al.*, 2008), as well as suppressing caspase-3 activation in apoptosis (Beere, 2004, 2005). However, more data suggest a negative role for the sHSP in disease progression (Mao *et al.*, 2001), therefore reduced αB crystallin may be a protective mechanism elicited by the cell, preventing exacerbation of the disease state.

This investigation found that chronic IR1072 exposure reduced HSP70 in old CD-1 mice, with previous reports showing reduction in young CD-1 mice also (Burroughs, 2010). Reduced HSP70 is particularly interesting in conjunction with reduced αB crystallin, as the two chaperones have been suggested to act synergistically *in vivo* to enable refolding of aggregates (Haslbeck *et al.*, 2005). This data suggests that in some conditions, IR1072 exposure may not be beneficial. Reduced HSP70 may result in limited chaperone capabilities,

diminished direction of proteins toward the ubiquitin-proteasome system and a dampened ability to prevent apoptosis via the extrinsic pathway (Mayer and Bukau, 2005, Mosser *et al.*, 1997, Ohtsuka and Suzuki, 2000, Turturici *et al.*, 2011). But no change was found in the levels of HSP105 following chronic irradiation, in young or old CD-1 mice, and HSP105 has been shown to compensate for HSP70 under certain cellular conditions and it has been shown to cause HSP70 to bind to substrates with a high affinity and in some conditions induce HSP70 expression. Therefore maintenance of HSP105 levels may aid in using the low levels of HSP70 in the best way for the cell (Saito *et al.*, 2009, Yamagishi *et al.*, 2004, Yamagishi *et al.*, 2003, Yamagishi *et al.*, 2000).

As differential effects of chronic IR1072 irradiation were found in male and female TASTPM mice (discussed in Chapter 6), it would be useful to repeat the age points investigated here with female CD-1 mice that have undergone the same treatment protocol to investigate whether this reduction is specific to CD-1 mice or whether it is a specific secondary effect to male CD-1 mice, as gender differences in HSP expression have been previously reported in a range of tissues (Voss *et al.*, 2003).

TARP γ2, also known as stargazin, is a transmembrane AMPA (α-amino-3-hydroxy-5-methyl-4-isoxazolepropionic acid) regulatory protein, one of a family of TARP proteins which are amongst a larger group of AMPA receptor binding partners, responsible for the trafficking and synaptic localisation of the glutamate ion-gated channel proteins which mediate excitatory neurotransmission (Donoghue, 2009, Vandenberghe *et al.*, 2005). Lack of TARP γ2 results in an absence of spontaneous AMPA receptor activity, demonstrating requirement of TARP γ2 in trafficking of AMPA receptors to the

cell surface although the precise mechanism of trafficking remains unknown. TARP γ2 is believed to be important in the correct folding of the AMPA receptor, (Vandenberghe *et al.*, 2005) but the principal role of TARP γ2 is thought to be acting as an auxiliary AMPA subunit, enabling interaction with scaffold proteins of the PSD (postsynaptic density; Bats *et al.*, 2007). Increased expression of TARP γ2, as observed in this investigation following chronic IR1072 exposure of CD-1 mice at both age points, has been shown to result in increased numbers of AMPA receptors, localising to the cell surface but the ratio of synaptic:non-synaptic AMPA receptors does not change. This data suggest that the size of the PSD limits the number of synaptic AMPA receptors which can be at the cell surface, and therefore the effect of upregulation on long term potentiation (LTP) may be limited (Bats *et al.*, 2007, Donoghue, 2009). The observed increase in TARP γ2 seen following chronic IR1072 exposure in CD-1 mice, suggests a potential for influence of LLLT over LTP. It is also interesting to note that levels of TARP γ2 and GluA2 decrease with age of the CD-1 mice, suggesting LTP becomes compromised with age, this could explain learning deficits which become apparent in behaviour tests with older CD-1 mice, compared to younger mice (Ennaceur *et al.*, 2008), therefore higher TARP γ2 levels would cause AMPA receptors to return to the PSD, increasing receptor activity. These data provide support for work with CD-1 mice previously conducted in our laboratory where acute treatment with IR1072 was sufficient to improve working memory in both male and female CD-1 mice. IR exposed aged (12 months) mice showed increased consideration in their decision making and demonstrated a significantly improved cognitive performance, tantamount to that of young (4 month) CD-1 mice (Michalikova *et al.*, 2008). This influence of

IR1072 over TARP γ2, and therefore potential LTP, is a very promising application. The reduction of GluA2 levels following IR1072 exposure in old CD-1 mice is a particularly interesting response. GluA2 is a subunit of the AMPA receptor, its presence determine the receptors permeability to calcium, sodium and potassium and is important in receptor trafficking and long-term depression. AMPA receptors are believed to express GluA1 in the absence of GluA2, rendering receptors sensitive to calcium, a sensitivity which can be heightened through increased TARP γ2 levels. GluA2 redundant receptors have been found in GABA-ergic inhibitory neurons, increasing excitability of the neurons ultimately with the potential to increase synaptic plasticity and LTP. Therefore in the future it would be of significant interest to determine where reduced GluA2 levels are compensated by amplified GluA1 levels (Bats *et al.*, 2007, Man, 2011).

The significant increase in SDHC, succinate dehydrogenase Complex II, following chronic IR1072 exposure is of particular interest as it is only present in CD-1 mice that were treated from 2 months of age, and not in those treated from 7 months of age. This suggests that younger mice may be more susceptible to the effects of IR1072 of mitochondria. The profound increase in SDHC, part of Complex II that is mitochondrial membrane bound, suggested that there may be an increase in electron transport chain complexes and potentially, activity and efficiency via increased coupling to the membrane. SDHC is very unstable when not membrane bound, suggesting the detected levels are membrane bound, and the greater the levels of SDHC, the more resistant the cell is to oxidative damage. Perhaps the increase in SDHC is not surprising, as increased Complex II activity has been previously reported in rats

irradiated at 904 nm (Silveira *et al.*, 2007). Work conducted in our laboratory has also found increased Complex II activity in IR1072-exposed CD-1 mice at 7 months of age (Burroughs, 2010) and this investigation has reported increased Complex II activity in mice at 3 months of age following acute irradiation. However, oxidative phosphorylation has not been investigated in mice which have undergone chronic IR1072 exposure; this would be of significant interest to complete as it would enable determination of whether the increased SDHC results in a functional improvement of Complex II activity. Data in this investigation has shown decreased activity of Complex I in male and female, mice at 3 months of age following acute IR1072 exposure. It would be of significant interest to look into the effect of chronic irradiation on young and old, as well as male and female CD-1 mice. It may be the case that the ETC in younger mice is more susceptible to irradiation but it may also be that a degree of stress is required to evoke a profound protective response from NIR. The majority of work undertaken with LLLT has utilised wounding or sub-lethal toxic insults (as detailed in Introduction 1.1.7) in order to determine the protective mechanisms of NIR. There has been very little work undertaken whereby a 'normal' system is exposed to LLLT and the effects examined, the work that has been performed has focussed on proliferation, namely in osteoblasts (Kreisler *et al.*, 2003, Pires Oliveira *et al.*, 2008, Ueda and Shimizu, 2003), fibroblasts (Taniguchi *et al.*, 2009, Vinck *et al.*, 2003), muscle cells and epithelial cells (Sommer *et al.*, 2001). The study of the effects of LLLT on the 'normal' system is an area requiring further examination; data reported in this investigation suggests that it is plausible that the magnitude of secondary effects of LLLT are dependent on the severity of the stress that the system is under. With

potentially more arduous stresses, such as accumulation of Aβ and phosphorylated tau in TASTPM mice, compared to the onset of amyloidosis in the CD-1 mice, resulting in initiation of a greater stress response. The stress of ageing in the CD-1 mice does appear to have an effect on the secondary effects of IR1072 as a greater number of the proteins examined were altered in the old CD-1 mice, compared to young CD-1 mice. This may also be due to progressive amyloidosis which occurs with age in the CD-1 mice, resulting in more cellular stress in older mice than younger mice and the higher level of stress triggers greater biological effects, secondary to LLLT.

These investigations have demonstrated that IR1072 exposure affects a number of proteins in the mammalian system that have been shown to have key roles in the maintenance of homeostasis within the cell; preventing the build up of toxic aggregates, encouraging cell survival or directing the cell towards apoptosis when deemed necessary. It was also interesting to find that the expression of a number of these proteins decrease with age in the CD-1 strain. Alterations were also observed in a regulatory protein, TARP γ2, required for LTP, which may explain improved learning and working-memory seen in the CD-1 strain following IR1072 exposure (Michalikova *et al.*, 2008), a protein which was also found to decrease with the age of the animals. Molecular changes may occur as a direct result of some of the altered mitochondrial electron transport chain complexes that were observed following IR1072 exposure, detailed in Chapter 4.

The next chapter utilises the data obtained from Chapter 5 to investigate whether IR1072 also modifies the expression levels of a number of proteins important in cell survival and LTP in a mouse model of Alzheimer's disease

(TASTPM) as well as the premature learning deficit CD-1 strain. It is important to determine whether the effects observed with the CD-1 strain are applicable to another dementia mouse model, which would support of a general mechanistic basis for photobiomodulation in a range of neurodegenerative diseases.

Chapter 6: Age-dependant changes in protein expression and the effect of chronic *in vivo* IR1072 exposure on protein expression in TASTPM mice

6.1 Introduction

The development of transgenic animal models of disease has provided useful tools to investigate the role of Aβ in AD progression and to provide knowledge to limit disease progression. Overexpression of APP, amyloid precursor protein, containing mutations associated with familial AD has allowed the study of AD pathology, behaviour and processing of Aβ in transgenic lines. A limitation of the use of transgenic lines is that they typically display exaggerated Aβ pathology and perhaps unsurprisingly, the use of familial mutations results in phenotypes which are more closely associated with familial AD which is much less common that sporadic forms (Balducci and Forloni, 2011). However, the major limitation of transgenic APP/PS1 (amyloid precursor protein/presenilin 1) lines is the lack of neuronal death and intracellular/extracellular NFTs which are frequently observed to be in AD patient samples. These characteristics are difficult to reproduce in animal models, demonstrating that there is still a significant level of development required to produce pathologically accurate transgenic systems (Balducci and Forloni, 2011, O'Brien and Wong, 2011).

The TASTPM transgenic line were created at GlaxoSmithKline (Harlow, UK) by crossing two transgenic lines, TAS10 and TPM, which expressed the Swedish double APP 695 and presenilin-1 M146V mutations, respectively but from the C57BL/6 background. Expression of both transgenes is driven by a THY-1 promoter (Howlett *et al.*, 2004). The TASTPM mouse line display a rapid age-

dependent increase the total level of $A\beta_{(1-40)}$ and $A\beta_{(1-42)}$, which ultimately results in plaque formation. The mice display a higher proportion of soluble Aβ when young and as the mice age, the proportion of insoluble Aβ increases, this is concomitant with the onset of observable Aβ plaques in the TASTPM brain (Hussain *et al.*, 2006). Intracellular and extracellular Aβ have been found in the TASTPM mouse (Howlett and Richardson, 2009). Plaque deposition is clear in the cortex of TASTPM mice from 3 months of age, with mature plaques evident from six months of age. At six months of age, plaques have established fibrillar cores surrounded by degenerating neurites and reactive glia and temporal lobe degeneration (Howlett *et al.*, 2004). At six months of age, cognitive function has also been shown to decline (Ennaceur & Chazot, unpublished). Female TASTPM mice have been shown to have a higher Aβ load than male age-matched mice, but this difference appears to have no bearing on differences in cognitive function between the sexes (Howlett *et al.*, 2004).

Many transgenic mouse models of Alzheimer's disease exist, a high proportion with similar mutations to the TASTPM strain, nevertheless little neuronal loss is commonly observed. This raises questions regarding the validity of these strains as models of the human disease. However, some neuronal loss is observed in TASTPM mice, this neuronal loss has been shown to correlate with total Aβ (40 amino acid and 42 amino acid) levels (Howlett, 2006); as well as observation of ultrastructural increases in synaptic distances (Richardson *et al.*, 2003), both relationships increase with animal age. Neuronal loss has been identified in the hippocampus in TASTPM mice, appearing to occur in a similar manner in the human AD brain, but to a lesser degree. An immune response to Aβ also appears to be present in the TASTPM strain, with microglia and

astrocytes found to colocalise with Aβ plaques and their pathology correlating to Aβ deposition and dystrophic neurites (Howlett *et al.*, 2008, Kurt *et al.*, 2001, Richardson *et al.*, 2003). Hyperphosphorylated tau is observable in small amounts from four months of age, closely associated with Aβ deposits; with the levels increasing with age, however, the formation of NFTs has not been observed (Howlett *et al.*, 2008). Paired-helical-like filaments have been observed in hippocampal neurons of TASTPM mice (Kurt *et al.*, 2003), but it is unclear whether the phosphorylation pattern is relatable to that observed in human AD. These data suggest that the TASTPM transgenic line are a suitable Aβ-model system to study the neurodegeneration that occurs in AD, albeit with a somewhat dampened inflammatory and tau tangle involvement.

Non-cognitive behaviour has also been studied in the TASTPM mice, however not in great detail. Male TASTPM mice have been reported to be more aggressive, such that single housing is needed. TASTPM mice also show locomotor hyperactivity as they age, reduced body weight despite increased feeding frequency and duration, premature death, disinhibition and alterations in circadian rhythm (Pugh *et al.*, 2007). The authors suggest some changes are a result of developmental problems rather than as a direct result of amyloid pathology, such as altered feeding patterns and weight loss. They do however; associate some changes with amyloid neuropathology, such as increased aggression and anxiety (Pugh *et al.*, 2007). The TASTPM mouse has been suggested to reproduce some of the human behavioural alterations seen in AD, including altered sleep patterns and aggression. However, comparables between mouse and human behaviour are not easily establish due to their complex nature (Graham, 2011).

The aim of this chapter was to further investigate protein level alterations during ageing in male TASTPM mice, and following chronic IR1072 exposure in both male and female TASTPM mice, including HSPs, APP and Aβ. Mice were exposed to sham or IR1072 treatments as described in 2.2.2., from 2 months of age.

6.2 Results

Data were analysed using ImageJ, version 1.43, National Institutes of Health, USA, and processed using Microsoft Office Excel 2007 and statistical analyses were carried out using GraphPad Prism Version 5, GraphPad Software Inc.

6.2.1 Immunoblot Analysis

Male TASTPM mice at 12 months of age demonstrated a 46.54% reduction in HSP105 expression compared to mice of 3 months of age. Mice of 7 months of age showed a 34.80% reduction compared to mice of 3 months of age. All other comparisons were non-significant. Data shown in figure 6.1 and table 6.1.

Male TASTPM mice at 12 months of age displayed a 199.53% increase in expression of αB crystallin compared to mice of 3 months of age. Mice at 7 months of age showed a 260.89% higher expression compared to mice of 3 months of age. There was no significant difference in expression of αB crystallin when comparing male TASTPM mice of 7 and 12 months of age. Data shown in figure 6.2 and table 6.1.

Male TASTPM mice at 7 months of age demonstrated a 40.35% reduction in TARP γ2 expression compared to mice of 3 months of age. Mice at 12 months of age showed a 20.10% decrease expression compared to mice at 3 months of age. There was no significant difference between TARP γ2 expression between mice of 7 and 12 months of age. Data show in figure 6.3 and table 6.1.

All data were analysed using a one-way ANOVA with a Bonferroni's multiple comparison post test and is summarised in table 6.1.

A)

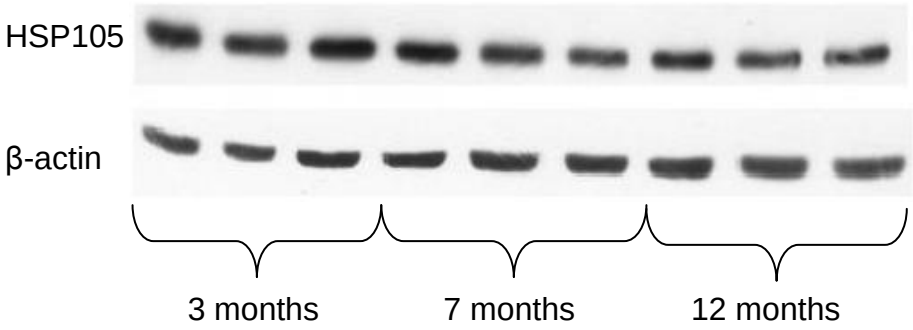

B)

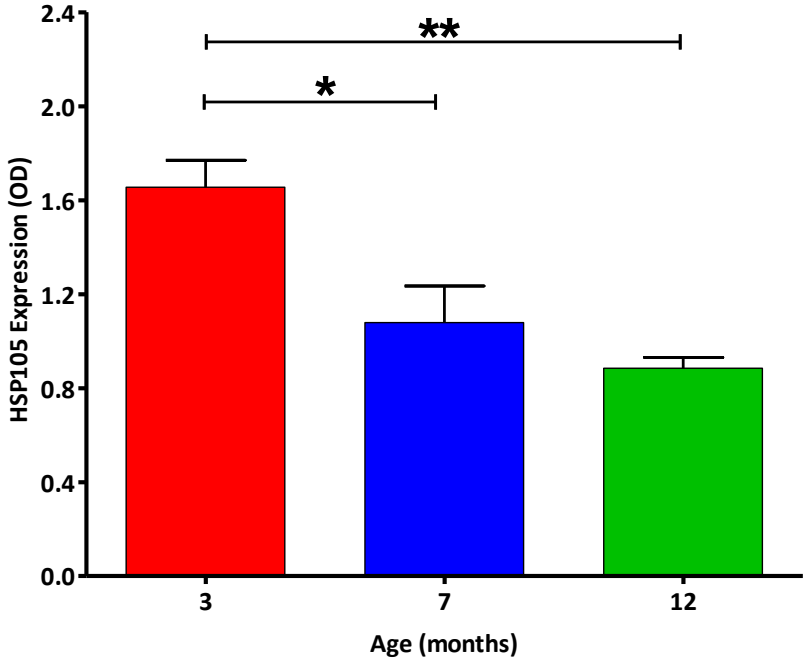

Figure 6.1. Age dependent alterations in HSP105 expression, shown in 3, 7 and 12 month old TASTPM male mouse brain. A) is an immunoblot where each lane represents an individual mouse and B) shows the quantitative analysis of immunoblot data. Mean values ± SEM, n=3 for each age point. A significant reduction was found between 3 month old mice to both 7 and 12 months mice (*p<0.05, **p<0.01 respectively). All other comparisons were non-significant. Abbreviations: HSP, heat shock protein; OD, optical density.

A)

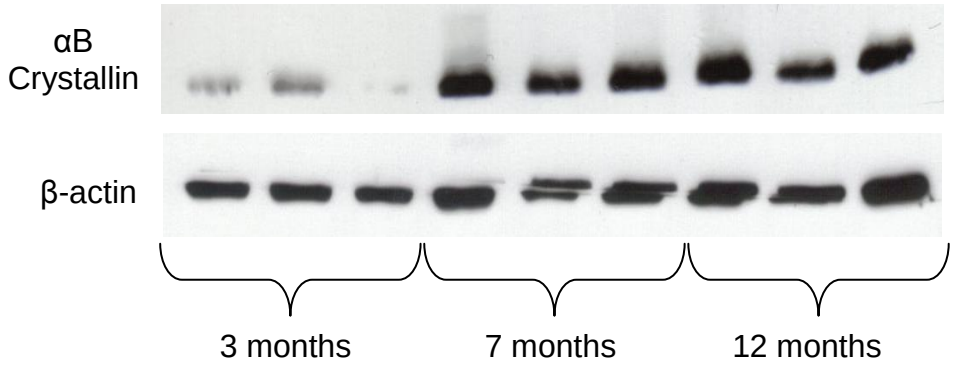

B)

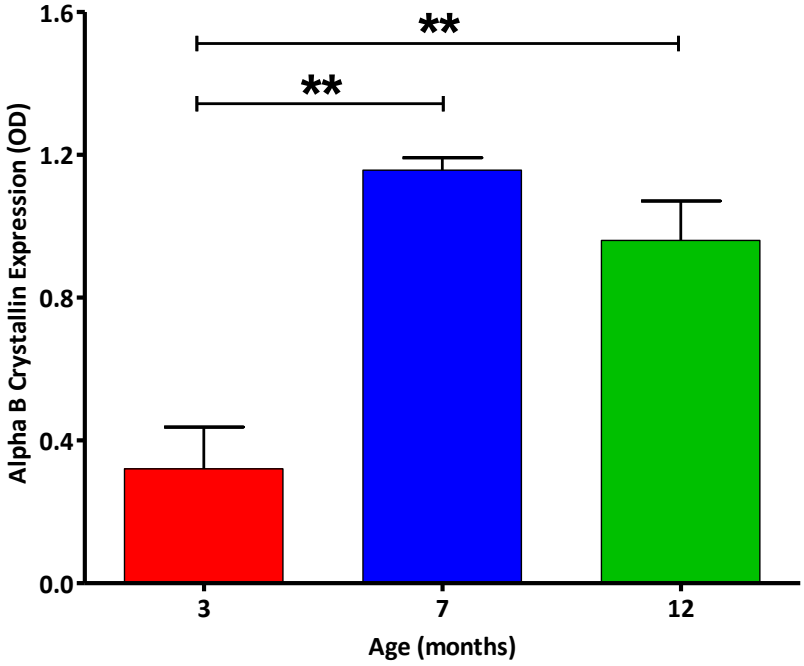

Figure 6.2. Age dependent alterations in αB Crystallin expression, shown in 3 months, 7 months and 12 months TASTPM mouse brains. A) is an immunoblot, each lane represents an individual mouse and B) shows the quantitative analyses of immunoblot data. Mean values ± SEM, n=3 at each age point. A significant increase in expression of αB crystallin is found when comparing 3 month old TASTPM mice to both 7 month and 12 month old TASTPM mice (**p<0.01). All other comparisons non-significant. Abbreviations: OD, optical density.

A)

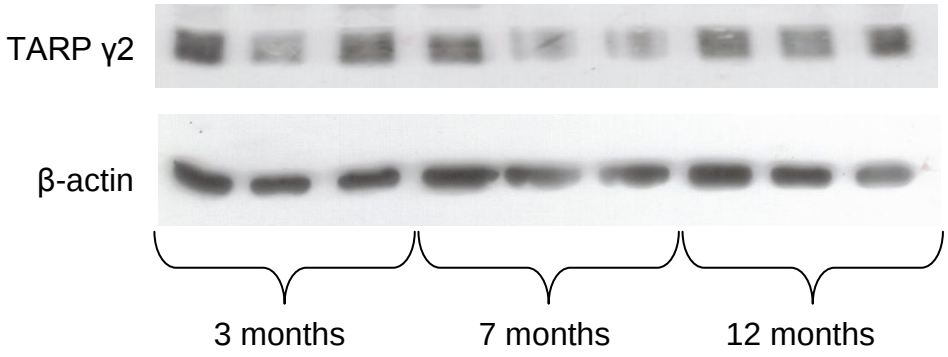

B)

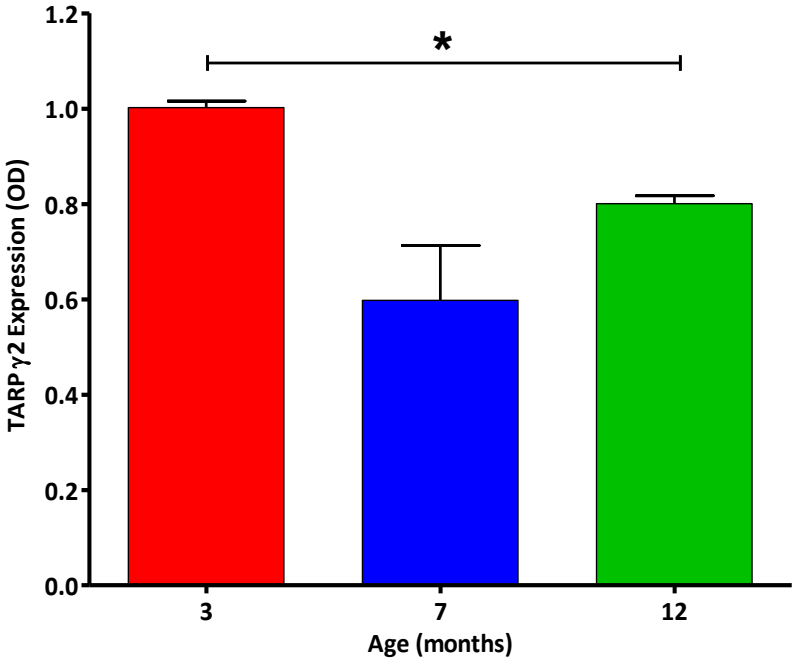

Figure 6.3. Age dependent alterations in TARP γ2 expression, shown in 3 months, 7 months and 12 months TASTPM mouse brains. A) is an immunoblot, each lane represents an individual mouse and B) shows the quantitative analyses of immunoblot data. Mean values ± SEM, n=3 at each age point. There is a trend for decreased expression at 7 months of age, compared to mice at 3 months ($p<0.1$), as well as a significantly decreased expression at 12 months of age compared to mice at 3 months of age (*$p<0.05$). All comparisons are non-significant. Abbreviations: TARP γ2, Transmembrane AMPA regulatory protein; OD, optical density.

Effect of age on protein expression in male TASTPM mice at 3, 7 and 12 months of age, n=3 for each condition						
Antibody/Protein	P Value	3 vs. 7	3 vs. 12	7 vs. 12	Result: ↑ or ↓	Figure
APP	0.242	-	-	-	-	Not shown
Aβ (1-40)	0.166	-	-	-	-	Not shown
Aβ (1-42)	Not determined					
Presenilin 1	Not determined					
AT8	0.371	-	-	-	-	Not shown
P-Tau (S519)	0.760	-	-	-	-	Not shown
GSK-3β	0.217	-	-	-	-	Not shown
HSF1	0.445	-	-	-	-	Not shown
HSP105	0.008	*	**	NS	↓	Figure 6.1
HSP27	0.460	-	-	-	-	Not shown
HSP70	0.479	-	-	-	-	Not shown
P-HSP27	0.180	-	-	-	-	Not shown
αB crystallin	0.002	**	**	NS	↑	Figure 6.2
TARP γ2	0.072	NS	*	-	↓	Figure 6.3
TARP γ8	0.109	-	-	-	-	Not shown
THY-1	Not determined					

Table 6.1. Data with a trend in altered expression levels are shaded blue ($p<0.1$), data with statistically significant altered expression levels ($p<0.05$) are shaded green. Arrows indicate direction of altered expression, (↑, increase; ↓, decrease), '-' indicates no significant change. *$p<0.05$, **$p<0.01$, ***$p<0.001$. Abbreviations: APP, amyloid precursor protein; Aβ, β-amyloid; AT8, hyperphosphorylated tau; GSK-3β, glycogen synthase kinase-3β; HSF, heat shock factor; HSP, heat shock protein; P-HSP, phosphorylated heat shock protein; P-tau, phosphorylated tau; TARP, transmembrane AMPA regulatory protein; NS, not significant.

6.3 Chronic IR treatment of TASTPM

There were difficulties in maintaining aged populations of TASTPM mice for longer than 7 months. Therefore chronic IR1072 treatment of mice was limited to when the mice reach 7 months of age. From 2 months of age, both male and female TASTPM mice were conditioned with IR1072 for six minute periods, for two consecutive days, twice a week for a total of five months. Sham mice were exposed to replica equipment, for the same time period, in the absence of IR1072. During the treatment period the weight of mice and temperature of equipment was monitored. Equipment is as detailed in 2.2.2.

6.3.1 Female TASTPM Mice

6.3.1.1 Immunoblotting

Data were analysed using a two-tailed student's T test. Data shown represent mean ± SEM, n= number of replicates. Data is summarised in table 6.2.

IR1072 preconditioned female TASTPM mice displayed an 80.44% reduction in APP (amyloid precursor protein) expression, a 79.89% decrease in β-amyloid$_{(1-42)}$ expression, a 78.41% lower αB crystallin expression and a 56.87% reduction in Presenilin-1 expression compared to age-matched sham treated controls.

IR1072 preconditioned female TASTPM mice displayed a 58.42% trend for decreased P-tau (S519) expression compared to age-matched sham treated controls.

IR1072 preconditioned female TASTPM mice demonstrated a 54.20% higher HSP105 expression, a 74.90% increase in HSP70 expression, 67.01% higher HSP27 expression, a 62.87% increase in P-HSP27 expression and a 654.34% increase in TARP γ2 expression compared to age-matched sham treated controls.

A)

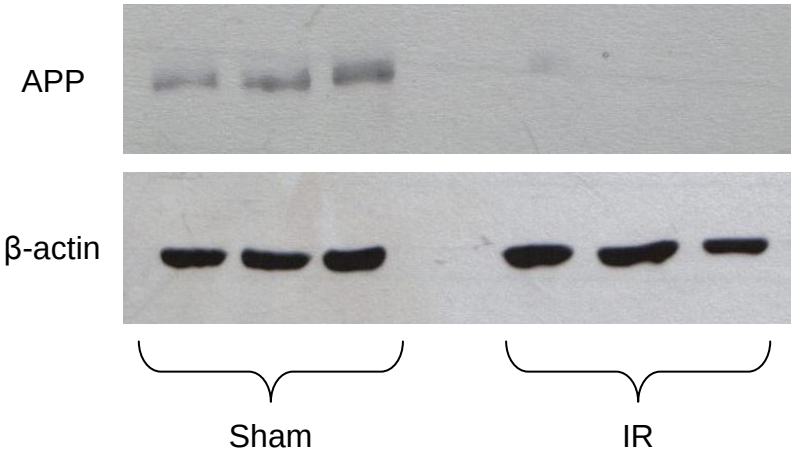

B)

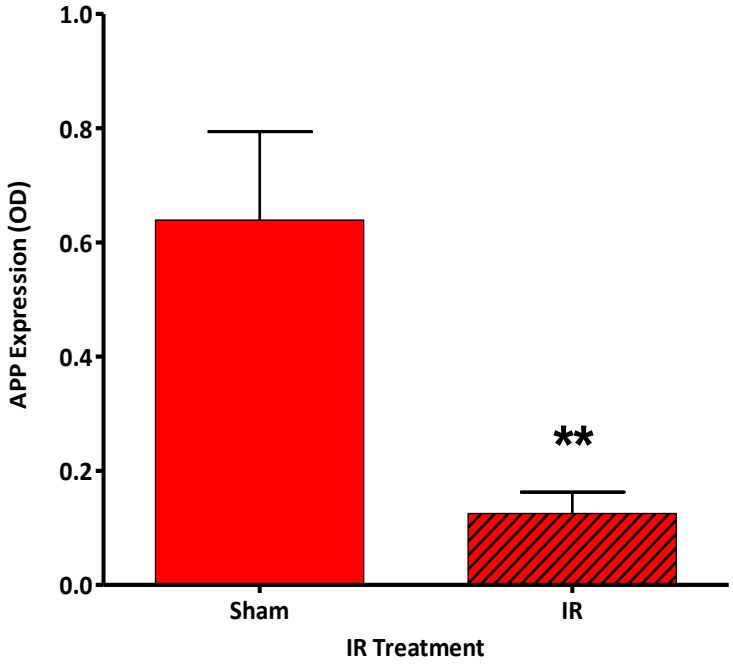

Figure 6.4. APP expression in chronic IR1072 preconditioned (*in vivo*) 7 month TASTPM Female mice and Sham age matched controls. Each lane in A) demonstrates an individual mouse (n=3 for each condition) and B) represents quantitative analysis of APP expression, demonstrating that chronic IR1072 exposure significantly decreases APP expression (**p<0.01). Mean values ± SEM. Abbreviations: APP, Amyloid precursor protein; OD, optical density.

A)

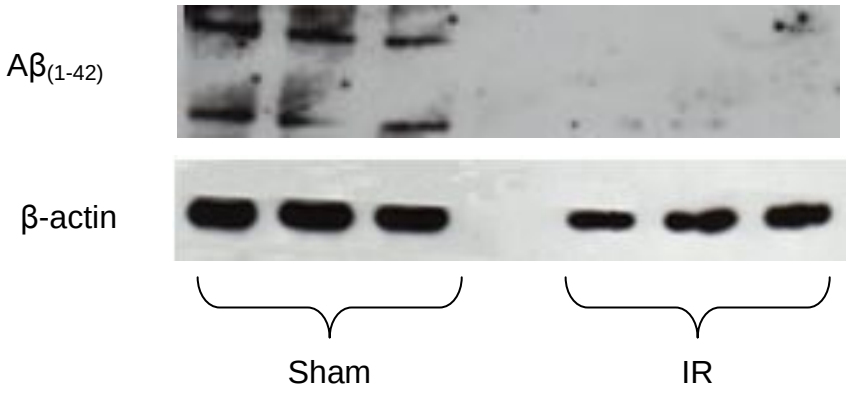

B)

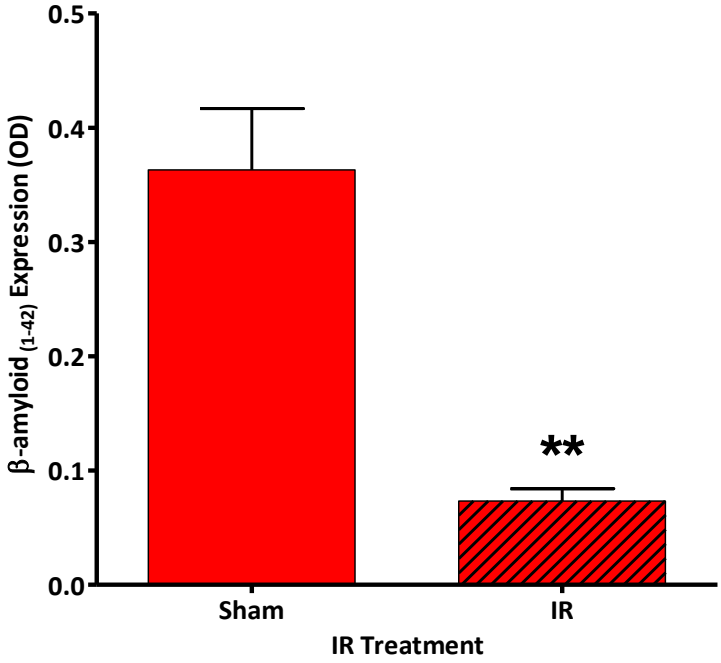

Figure 6.5. β-amyloid$_{(1-42)}$ expression in chronic IR1072 preconditioned (*in vivo*) 7 month TASTPM female mice and Sham age matched controls. Each lane in A) demonstrates an individual mouse (n=3 for each condition) and B) represents quantitative analysis of β-amyloid$_{(1-42)}$ expression, indicating that IR1072 treatment significantly decreases β-amyloid$_{(1-42)}$ expression in preconditioned animals (**p<0.01) Mean ± SEM. Abbreviations: Aβ, β-amyloid; OD, optical density.

A)

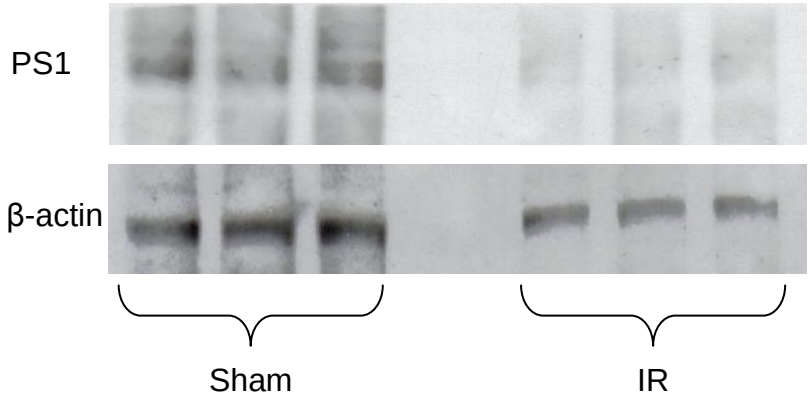

B)

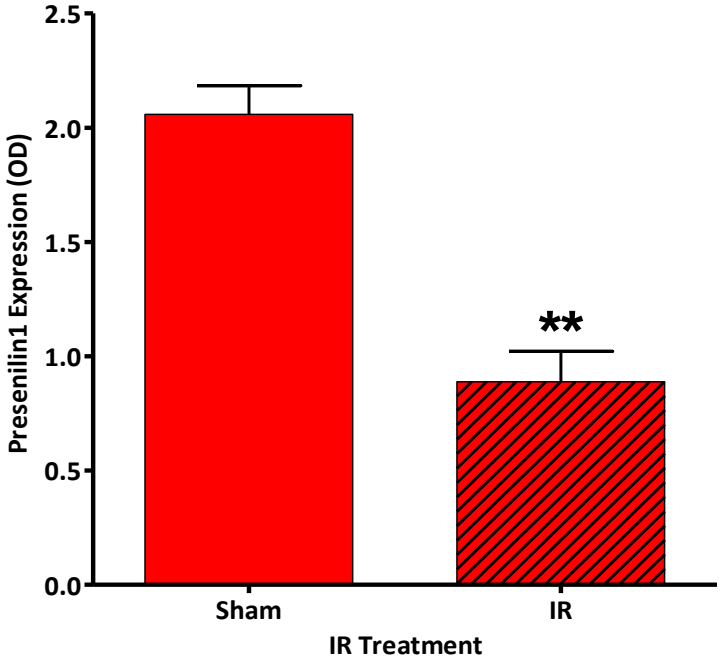

Figure 6.6. PS1 expression in chronic IR1072 preconditioned (*in vivo*) 7 month TASTPM female mice and Sham age matched controls. Each lane in A) demonstrates an individual mouse (n=3 for each condition) and B) represents quantitative analysis of PS1 expression, indicating that IR1072 treatment significantly decreases PS1 expression in preconditioned animals (**p<0.01) Mean ± SEM. Abbreviations: PS1, Presenilin 1; OD, optical density.

A)

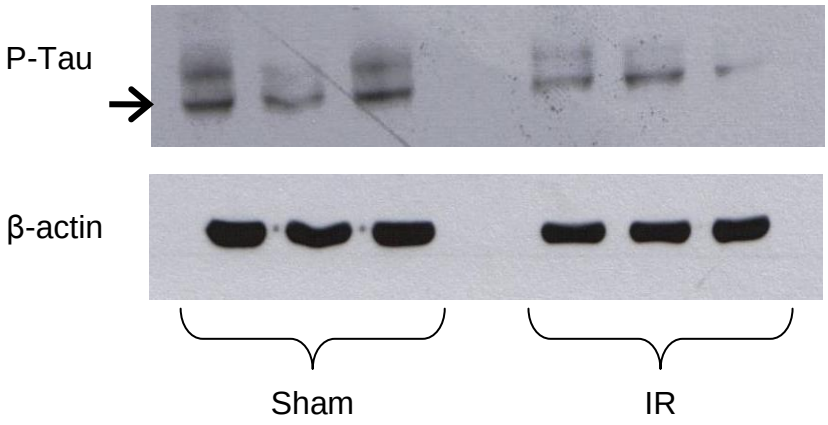

B)

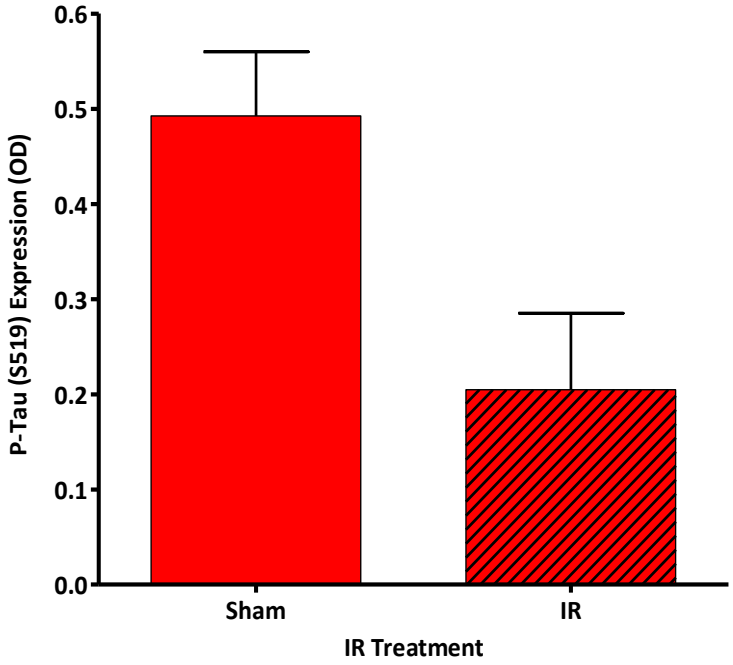

Figure 6.7. P-Tau (S519) expression in chronic IR1072 preconditioned (*in vivo*) 7 month TASTPM Female mice and Sham age matched controls. Each lane in A) demonstrates an individual mouse (n=3 for each condition) and B) represents quantitative analysis of P-Tau (S519) expression. There is a trend for decreased P-Tau (S519) expression in chronic IR preconditioned animals ($p<0.1$). Mean ± SEM. Abbreviations: P-Tau (S519), phosphorylated tau; OD, optical density.

A)

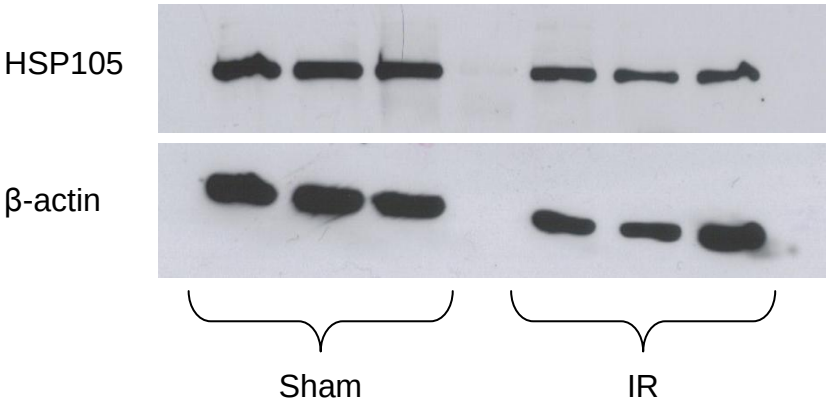

B)

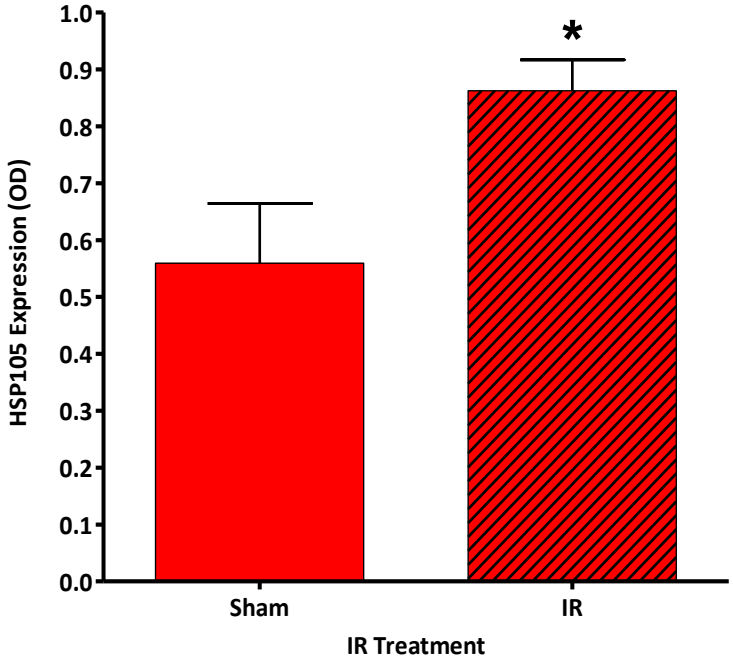

Figure 6.8. HSP105 expression in chronic IR1072 preconditioned (*in vivo*) 7 month TASTPM Female mice and Sham age matched controls. Each lane in A) demonstrates an individual mouse (n=3 for each condition) and B) represents quantitative analysis of HSP105 expression, indicating that IR1072 treatment significantly increases HSP105 expression in preconditioned animals (*p<0.05). Mean ± SEM. Abbreviations: HSP105, Heat shock protein 105; OD, optical density.

A)

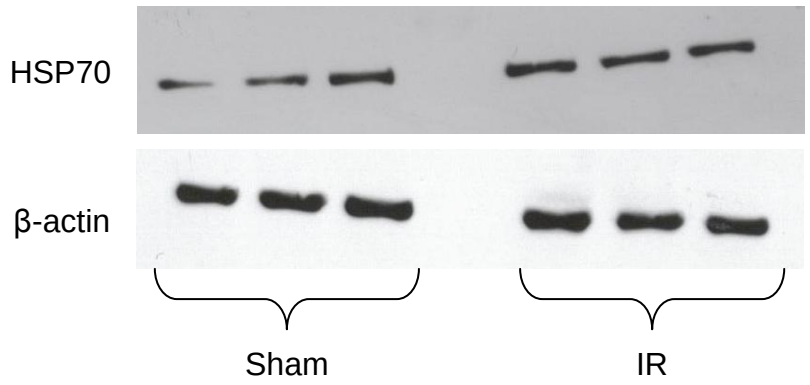

B)

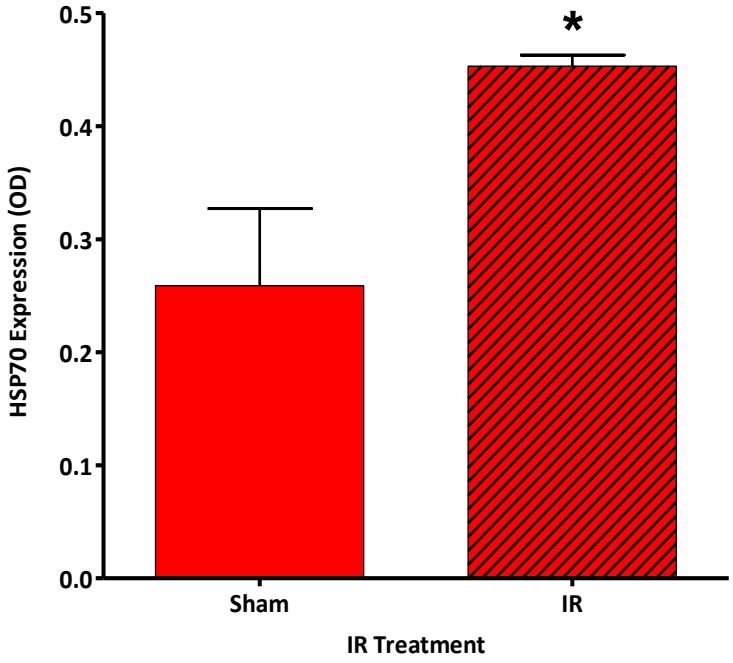

Figure 6.9. HSP70 expression in chronic IR1072 preconditioned (*in vivo*) 7 month TASTPM Female mice and Sham age matched controls. Each lane in A) demonstrates an individual mouse (n=3 for each condition) and B) represents quantitative analysis of HSP70 expression, indicating that IR1072 treatment significantly increased HSP70 expression in preconditioned animals (*p<0.05). Mean ± SEM. Abbreviations: HSP70, Heat shock protein 70; OD, optical density.

A)

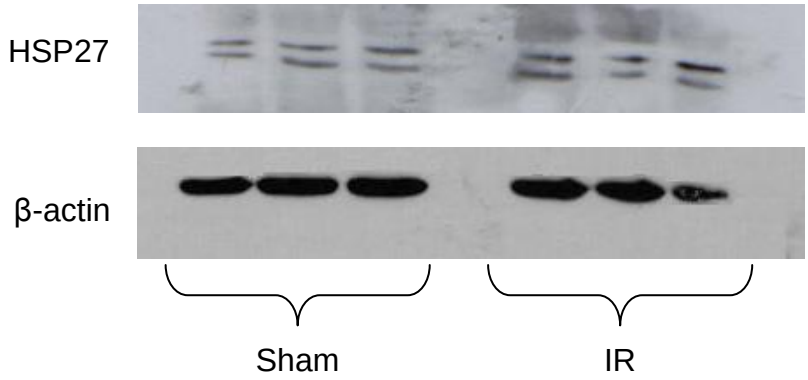

B)

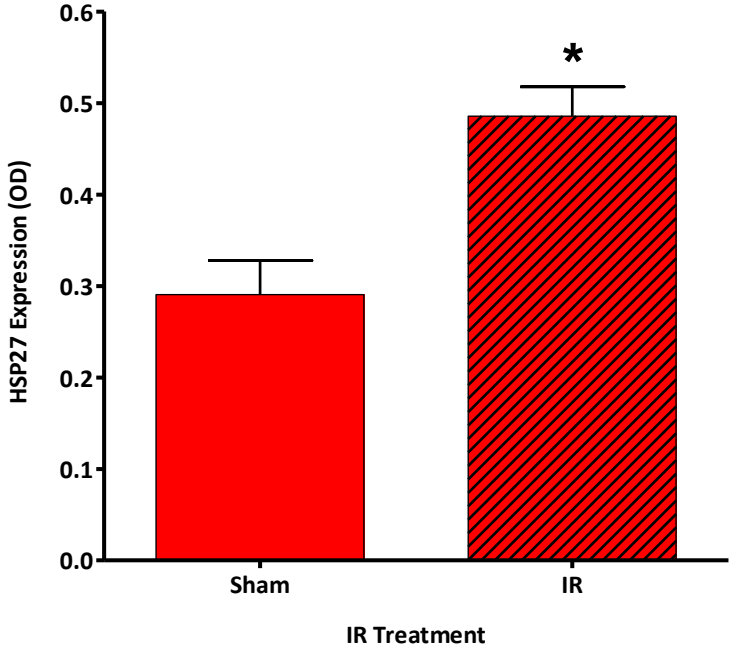

Figure 6.10. HSP27 expression in chronic IR1072 preconditioned (*in vivo*) 7 month TASTPM Female mice and Sham age matched controls. Each lane in A) demonstrates an individual mouse (n=3 for each condition) and B) represents quantitative analysis of HSP27 expression, IR1072 treated mice showed a significantly increased expression of sham treated age matched controls (*p<0.05) Mean ± SEM. Abbreviations: HSP27, Heat shock protein 27; OD, optical density.

A)

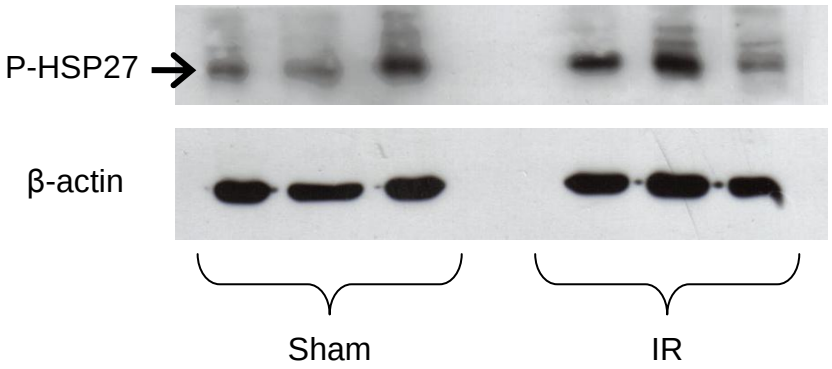

B)

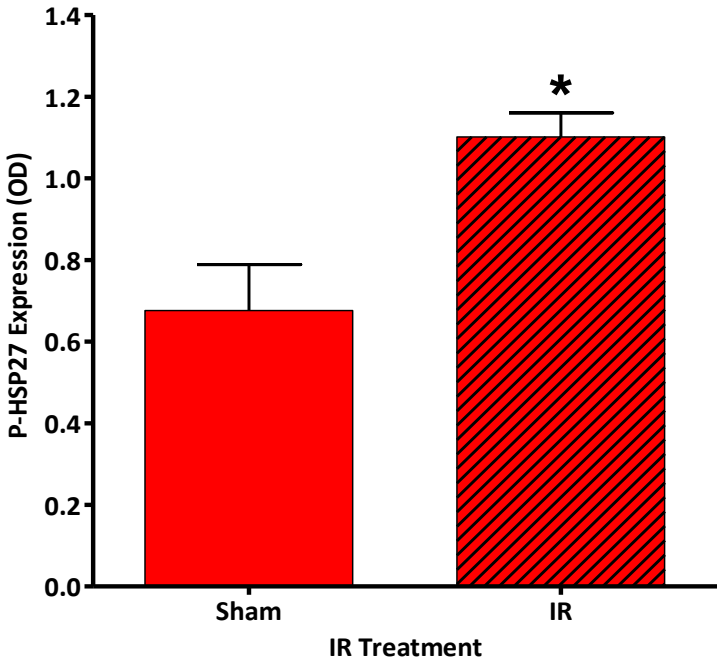

Figure 6.11. P-HSP27 expression in chronic IR1072 preconditioned (*in vivo*) 7 month TASTPM Female mice and Sham age matched controls. Each lane in A) demonstrates an individual mouse (n=3 for each condition) and B) represents quantitative analysis of P-HSP27, demonstrating a significant increase in expression following chronic IR treatment (*p<0.05). Mean ± SEM. Abbreviations: P-HSP27, Phosphorylated Heat Shock Protein 27; OD, optical density.

A)

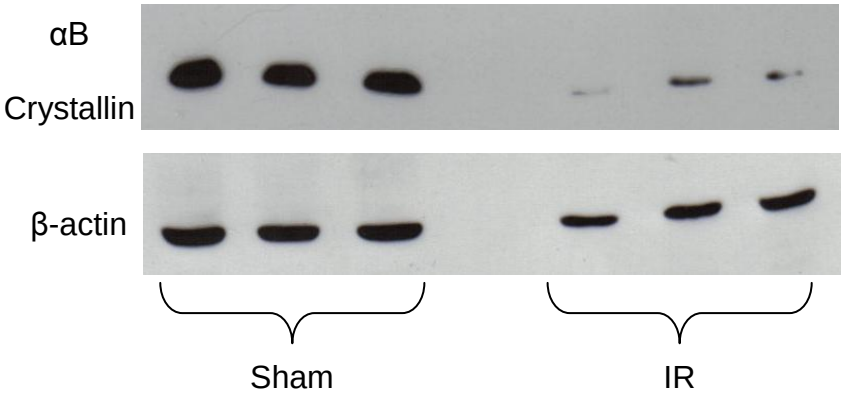

B)

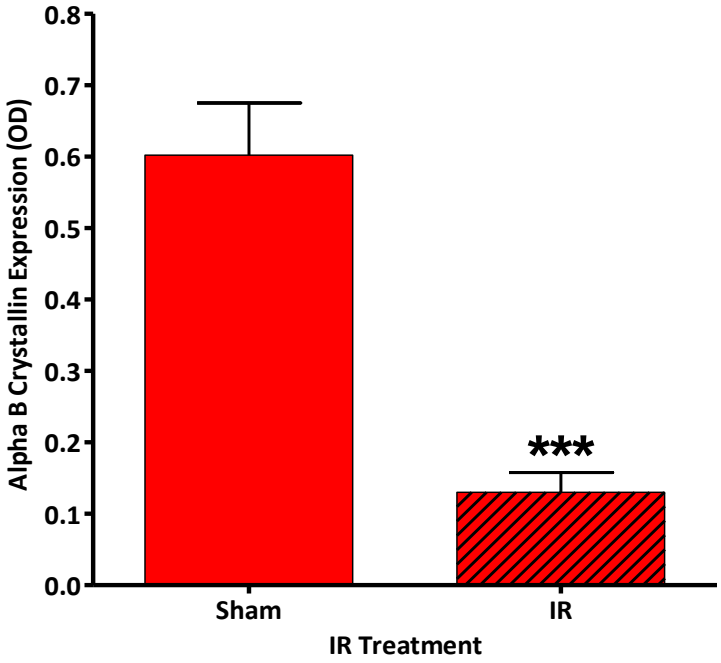

Figure 6.12. αB Crystallin expression in chronic IR1072 preconditioned (*in vivo*) 7 month TASTPM female mice and Sham age matched controls. Each lane in A) demonstrates an individual mouse (n=3 for each condition) and B) represents quantitative analysis of αB Crystallin expression, indicating that IR1072 treatment significantly increases αB Crystallin expression in preconditioned animals (***p<0.001) Mean ± SEM. Abbreviations: OD, optical density.

A)

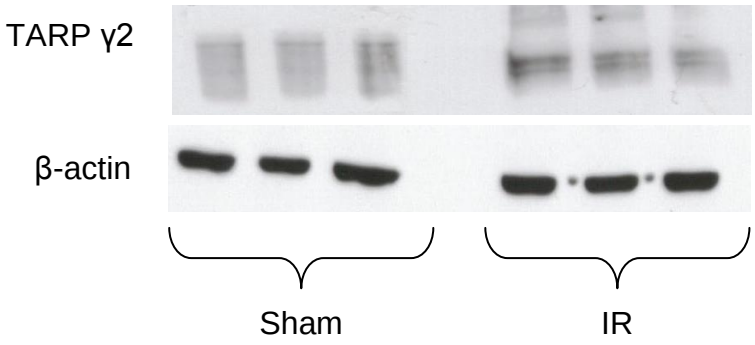

B)

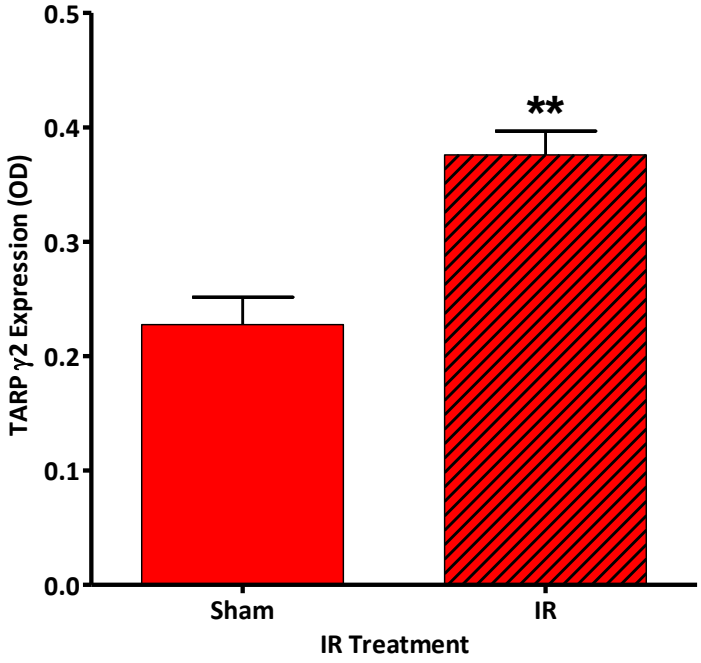

Figure 6.13. TARP γ2 expression in chronic IR1072 preconditioned (*in vivo*) 7 month TASTPM female mice and Sham age matched controls. Each lane in A) demonstrates an individual mouse (n=3 for each condition) and B) represents quantitative analysis of TARP γ2, demonstrating a significant increase in expression following chronic IR treatment (***p<0.001). Mean ± SEM. Abbreviations: TARP, Transmembrane AMPA regulatory protein; OD, optical density.

Effect of Chronic IR1072 Preconditioning on protein expression in female TASTPM mice, compared to age matched sham-treated controls, n=3 for each condition			
Antibody/Protein	P Value	Result: increase or decrease	Figure
APP	**0.009	↓	Figure 6.4
$A\beta_{(1-40)}$	0.770	-	Not shown
$A\beta_{(1-42)}$	**0.006	↓	Figure 6.5
Presenilin 1	**0.003	↓	Figure 6.6
AT8	0.982	-	Not shown
P-Tau (S519)	0.052	↓	Figure 6.7
GSK-3β	0.818	-	Not shown
HSF1	Not determined		
HSP105	*0.016	↑	Figure 6.8
HSP70	*0.048	↑	Figure 6.9
HSP27	*0.017	↑	Figure 6.10
P-HSP27	*0.029	↑	Figure 6.11
αB crystallin	***<0.001	↓	Figure 6.12
TARP γ2	***<0.001	↑	Figure 6.13
TARP γ8	0.188	-	Not shown
THY-1	0.767	-	Not shown

Table 6.2. Data with a trend in altered expression levels are shaded blue ($p<0.1$), data with statistically significant altered expression levels ($p<0.05$) are shaded green. Arrows indicate direction of altered expression, (↑, increase; ↓, decrease), '-' indicates no significant change. *$p<0.05$, **$p<0.01$, ***$p<0.001$. Abbreviations: APP, amyloid precursor protein; Aβ, β-amyloid; AT8, hyperphosphorylated tau; GSK-3β, glycogen synthase kinase-3β; HSF, heat shock factor; HSP, heat shock protein; P-HSP, phosphorylated heat shock protein; P-tau, phosphorylated tau; TARP, transmembrane AMPA regulatory protein; NS, not significant.

6.3.1.2 Immunohistochemistry

Immunohistochemical analysis showed no qualitative differences between IR1072-treated 7 month TASTPM female mice, compared to sham-treated controls (n=3 for each condition).

Effect of Chronic IR1072 Preconditioning on protein expression in female TASTPM mice, compared to age matched sham-treated controls, n=3 individual mice for each condition		
Antibody/Protein	Result: increase (↑) or decrease (↓)	Figure
AT8	No detectable change	Not shown
GSK-3β	No detectable change	Not shown

Table 6.3. Summary table of immunohistochemical analysis of protein expression.

Abbreviations: AT8, hyperphosphorylated tau; GSK-3β, glycogen synthase kinase-3β.

6.3.2 Male TASTPM Mice

6.3.2.1 Immunoblotting

Data were analysed using a two-tailed student's T test. Data shown represent mean ± SEM, n= number of replicates. Data is summarised in table 6.4.

IR1072 preconditioned male TASTPM mice displayed a 45.48% reduction in APP expression, a 98.79% lower HSF1 level, a 76.36% decrease in HSP105 expression, a 95.88% reduction in HSP70 levels and a 69.34% lower αB crystallin expression compared to age-matched sham treated controls.

IR1072 preconditioned male TASTPM mice showed a 39.76% trend for reduced AT8 expression compared to age-matched sham treated controls.

IR1072 preconditioned male TASTPM mice demonstrated a 92.54% higher HSP27 expression and a 92.11% increase in P-HSP27 levels compared to age-matched sham treated controls.

A)

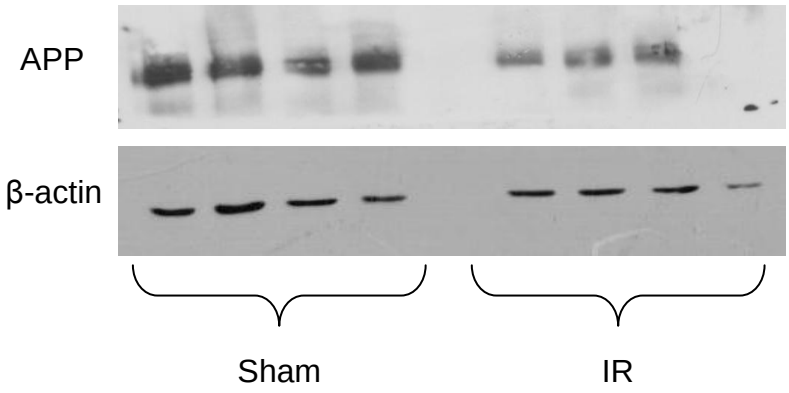

B)

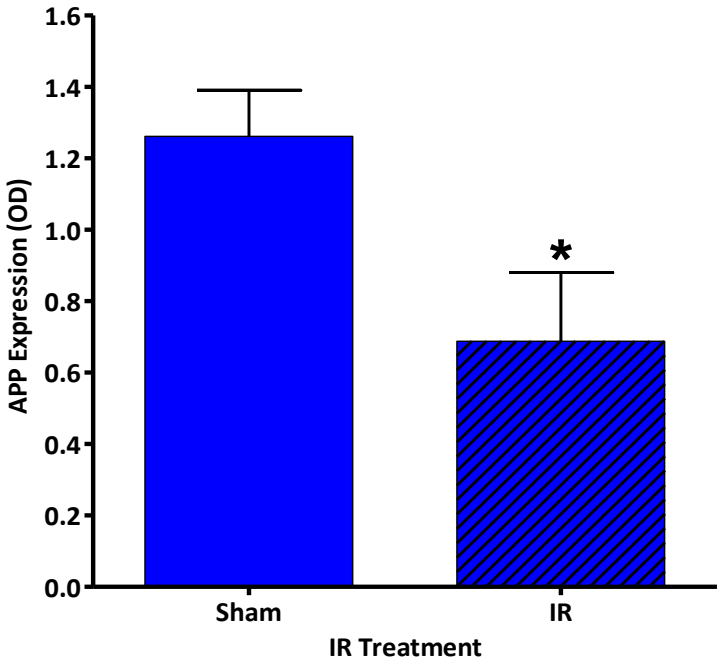

Figure 6.14. APP expression in chronic IR1072 preconditioned (*in vivo*) 7 month TASTPM male mice and Sham age matched controls. Each lane in A) demonstrates an individual mouse (n=4 for each condition) and B) represents quantitative analysis of APP expression, indicating that IR1072 treatment significantly decreases APP expression in preconditioned animals (*p<0.05), Mean values ± SEM. Abbreviations: APP, Amyloid precursor protein; OD, optical density.

A)

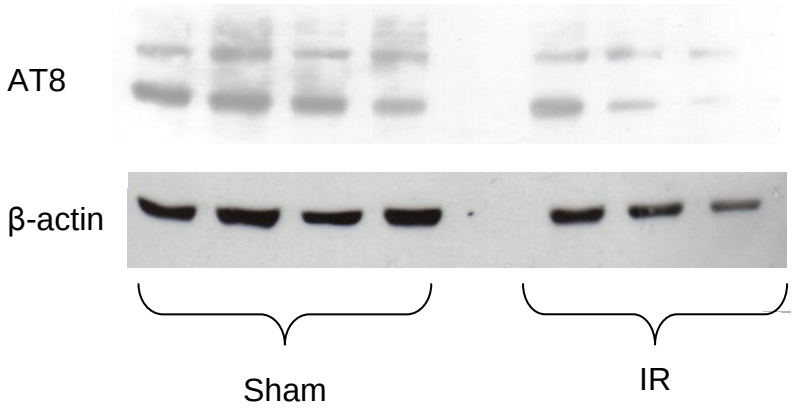

B)

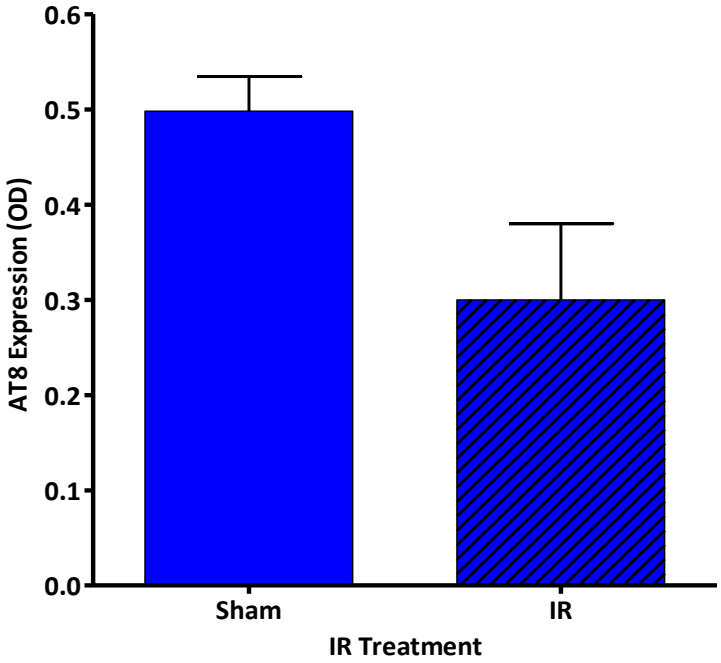

Figure 6.15. AT8 (hyperphosphorylated tau) expression in chronic IR1072 preconditioned (*in vivo*) 7 month TASTPM male mice and Sham age matched controls. Each lane in A) demonstrated in individual mouse (Sham, n=4, IR, n=3 for each condition) and B) represents quantitative analysis of AT8 expression. A trend for reduced expression of AT8 is observed in chronic IR treated animals, in comparison to Sham treated animals ($p<0.01$). Mean ± SEM. Abbreviations: AT8, hyperphosphorylated tau; OD, optical density.

A)

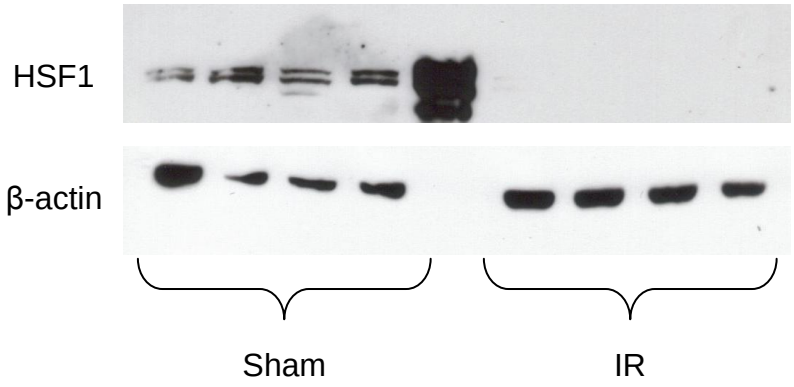

B)

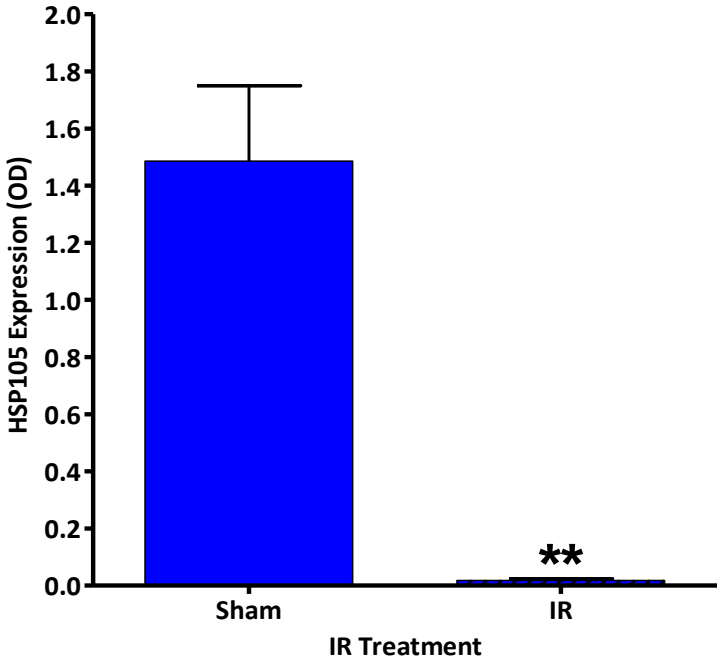

Figure 6.16. HSF1 expression in chronic IR1072 preconditioned (*in vivo*) 7 month TASTPM male mice and Sham age matched controls. Each lane in A) demonstrates an individual mouse (n=4 for each condition) and B) represents quantitative analysis of HSF1 expression, indicating that IR1072 treatment significantly decreases HSF1 expression in preconditioned animals (**p<0.01). Mean ± SEM. Abbreviations: HSF1, Heat Shock Factor 1; OD, optical density.

A)

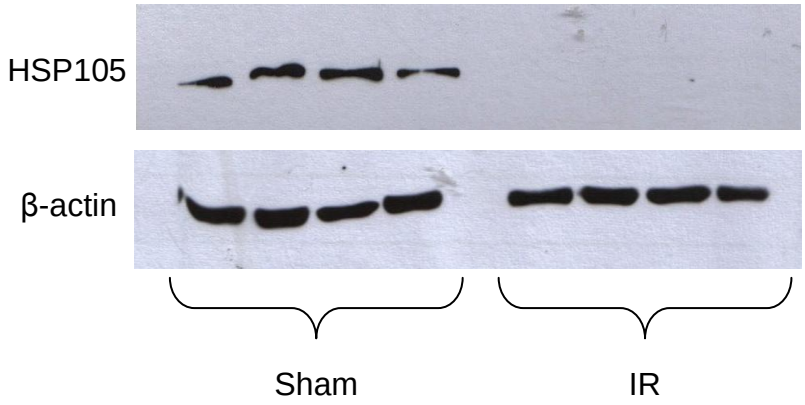

B)

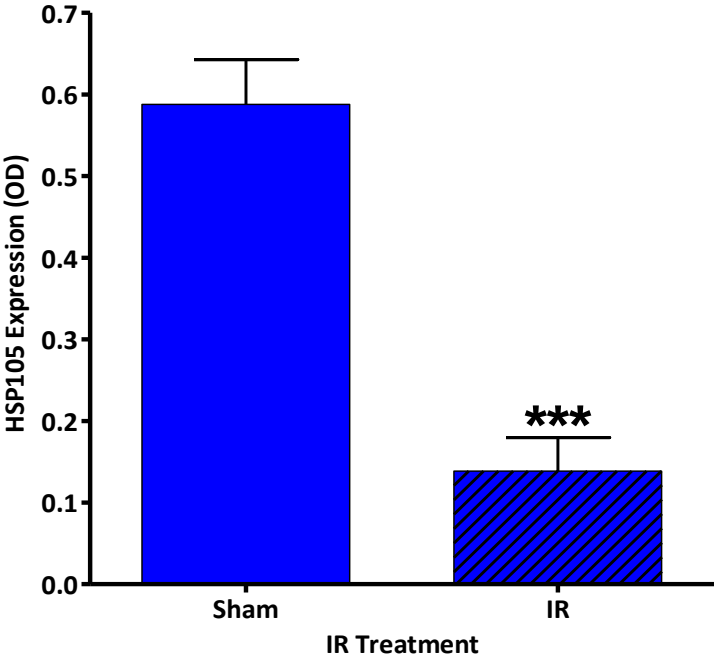

Figure 6.17. HSP105 expression in chronic IR1072 preconditioned (*in vivo*) 7 month TASTPM male mice and Sham age matched controls. Each lane in A) demonstrates an individual mouse (n=4 for each condition) and B) represents quantitative analysis of HSP105 expression, indicating that IR1072 treatment significantly increases HSP105 expression in preconditioned animals (***p<0.001). Mean ± SEM. Abbreviations: HSP105, Heat shock protein 105; OD, optical density.

A)

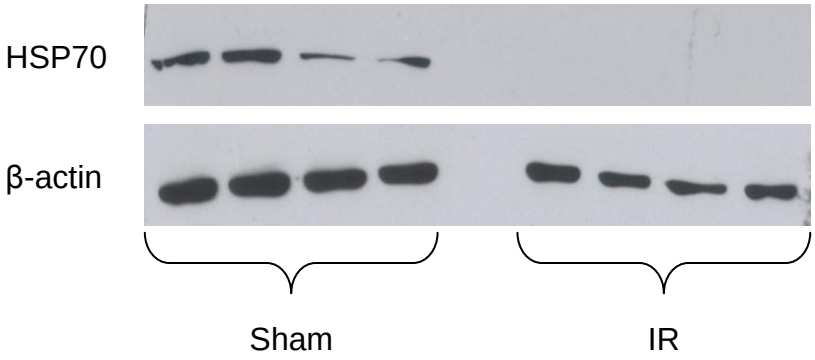

B)

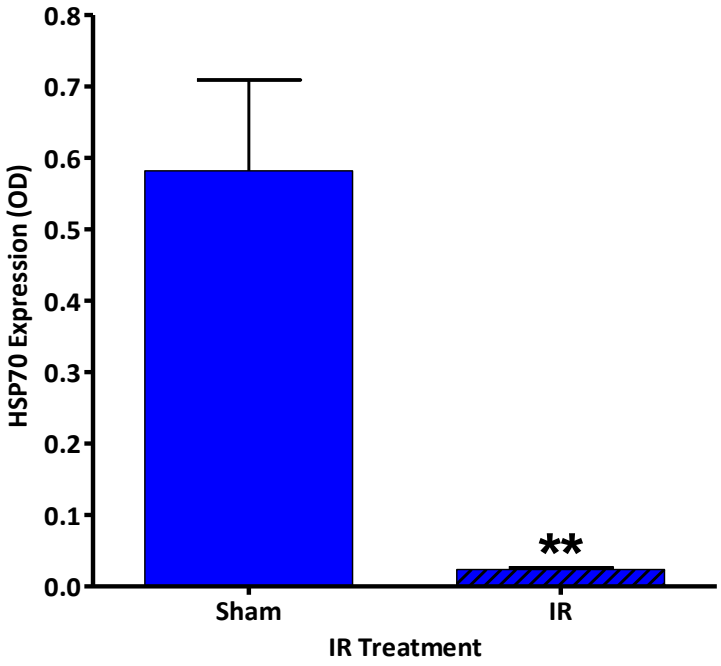

Figure 6.18. HSP70 expression in chronic IR1072 preconditioned (*in vivo*) 7 month TASTPM male mice and Sham age matched controls. Each lane in A) demonstrates an individual mouse (n=4 for each condition) and B) represents quantitative analysis of HSP70 expression, indicating that IR1072 treatment significantly increases HSP70 expression in preconditioned animals (**p<0.01). Mean ± SEM. Abbreviations: HSP70, Heat shock protein 70; OD, optical density.

A)

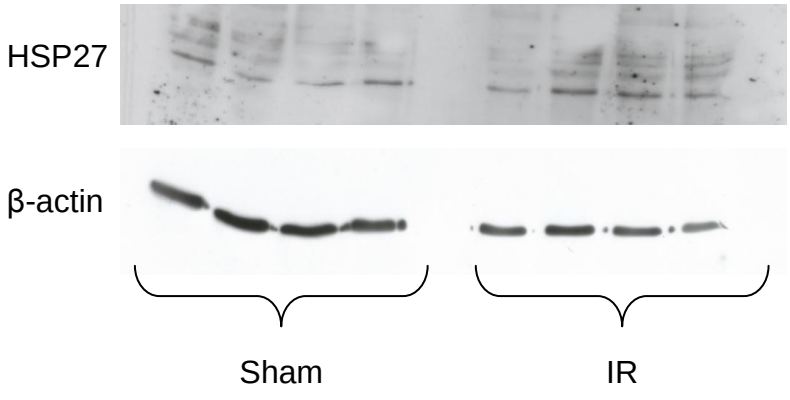

B)

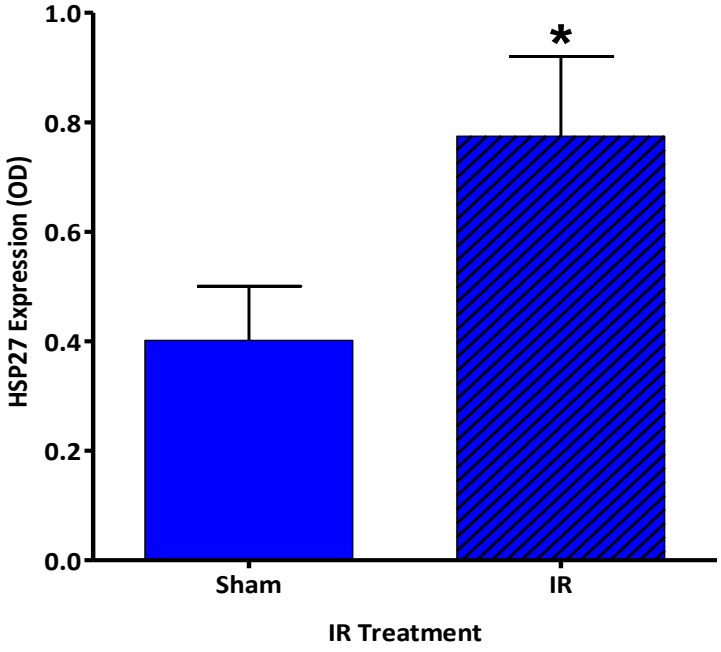

Figure 6.19. HSP27 expression in chronic IR1072 preconditioned (*in vivo*) 7 month TASTPM male mice and Sham age matched controls. Each lane in A) demonstrates an individual mouse (n=4 for each condition) and B) represents quantitative analysis of HSP27 expression, indicating that IR1072 treatment significantly increases HSP27 expression in preconditioned animals (*p<0.05). Mean ± SEM. Abbreviations: HSP27, heat shock protein 27; OD, optical density.

A)

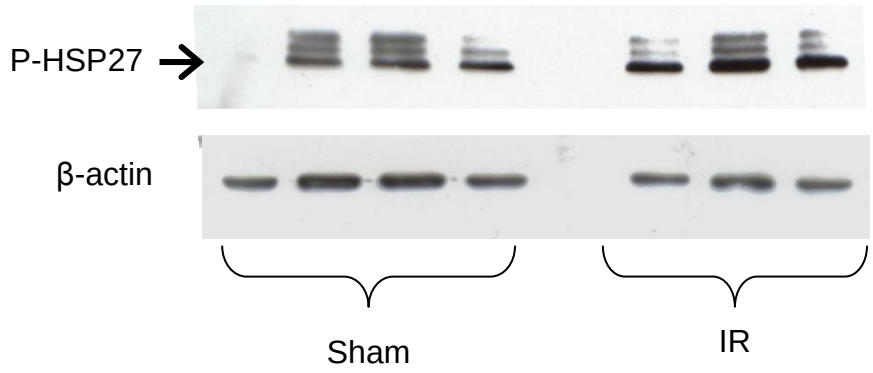

B)

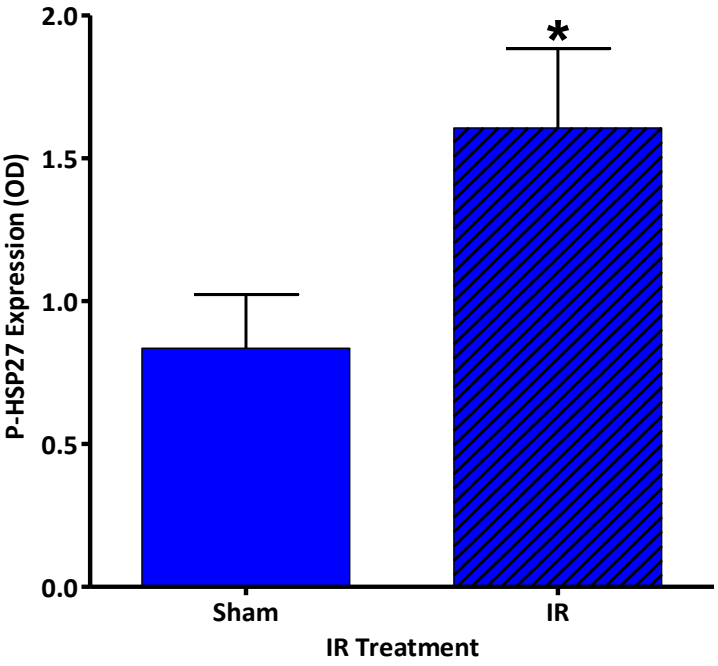

Figure 6.20. P-HSP27 expression in chronic IR1072 preconditioned (*in vivo*) 7 month TASTPM male mice and Sham age matched controls. Each lane in A) demonstrates an individual mouse (Sham, n=4, IR, n=3 for each condition) and B) represents quantitative analysis of P-HSP27 expression. Animals chronically treated with IR1072 showed a significantly increased expression of P-HSP27 compared to sham treated controls (*p<0.05). Mean ± SEM. Abbreviations: P-HSP27, phosphorylated heat shock protein 27; OD, optical density.

A)

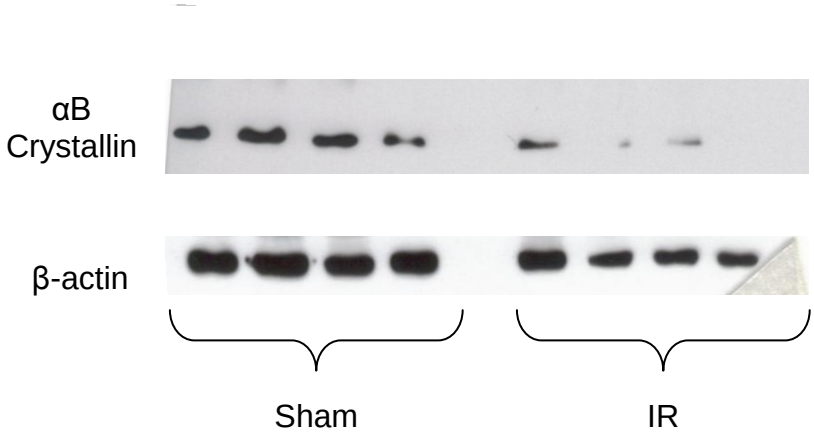

B)

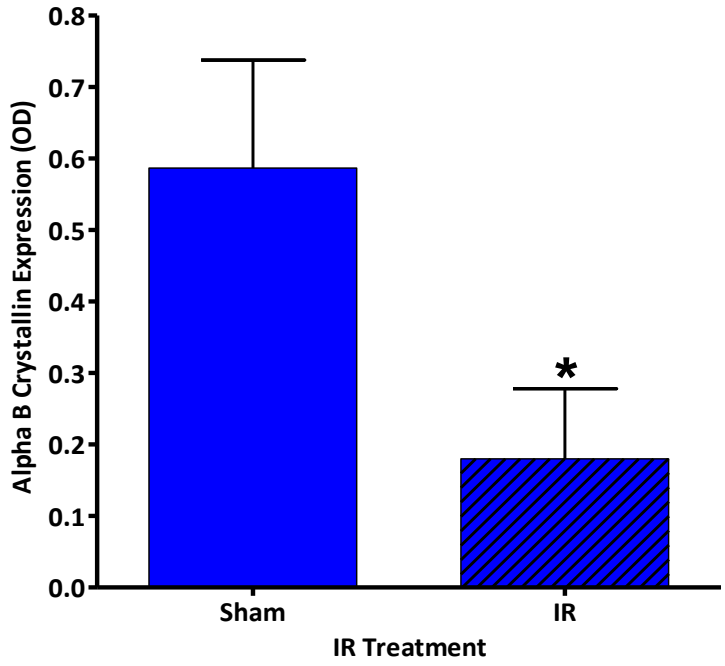

Figure 6.21. αB Crystallin expression in chronic IR1072 preconditioned (*in vivo*) 7 month TASTPM male mice and Sham age matched controls. Each lane in A) demonstrates an individual mouse (n=4 for each condition) and B) represents quantitative analysis of αB crystallin expression. Animals chronically treated with IR1072 showed a significantly decreased expression of αB Crystallin compared to sham treated controls (*p<0.05). Mean ± SEM. Abbreviations: OD, optical density.

Effect of Chronic IR1072 Preconditioning on protein expression in male TASTPM mice, compared to age matched sham-treated controls, n=3/4 for each condition			
Antibody/Protein	P Value	Result: increase or decrease	Figure
APP	*0.048	↓	Figure 6.14
$A\beta_{(1-40)}$	0.183	-	Not shown
$A\beta_{(1-42)}$	0.934	-	Not shown
Presenilin 1	0.390	-	Not shown
AT8	0.055	↓	Figure 6.15
P-Tau (S519)	0.998	-	Not shown
GSK-3β	0.686	-	Not shown
HSF1	**0.001	↓	Figure 6.16
HSP105	***<0.001	↓	Figure 6.17
HSP70	**0.005	↓	Figure 6.18
HSP27	*0.050	↑	Figure 6.19
P-HSP27	*0.034	↑	Figure 6.20
αB crystallin	*0.041	↓	Figure 6.21
TARP γ2	0.497	-	Not shown
TARP γ8	0.968	-	Not shown
THY-1	0.203	-	Not shown

Table 6.4. Data with a trend in altered expression levels are shaded blue ($p<0.1$), data with statistically significant altered expression levels ($p<0.05$) are shaded green. Arrows indicate direction of altered expression, (↑, increase; ↓, decrease), '-' indicates no significant change. *$p<0.05$, **$p<0.01$, ***$p<0.001$. Abbreviations: APP, amyloid precursor protein; Aβ, β-amyloid; AT8, hyperphosphorylated tau; GSK-3β, glycogen synthase kinase-3β; HSF, heat shock factor; HSP, heat shock protein; P-HSP, phosphorylated heat shock protein; P-tau, phosphorylated tau; TARP, transmembrane AMPA regulatory protein; NS, not significant.

6.3.2.2 Immunohistochemistry

Immunohistochemical analysis showed qualitative differences between IR1072-treated 7 month TASTPM male mice, compared to sham-treated controls (n=3 for each condition). Data shown in figure 6.22 is representative of all repeats.

Effect of Chronic IR1072 Preconditioning on protein expression in male TASTPM mice, compared to age matched sham-treated controls, n=3 for each condition		
Antibody/Protein	Result: increase (↑) or decrease (↓)	Figure
AT8	↓ CA1 and CA2/3	Figure 6.22
GSK-3β	No detectable change	Not shown

Table 6.5. Summary table of immunohistochemical analysis of protein expression.

Abbreviations: AT8, hyperphosphorylated tau; CA, cornu ammonis; GSK-3β, glycogen synthase kinase-3β.

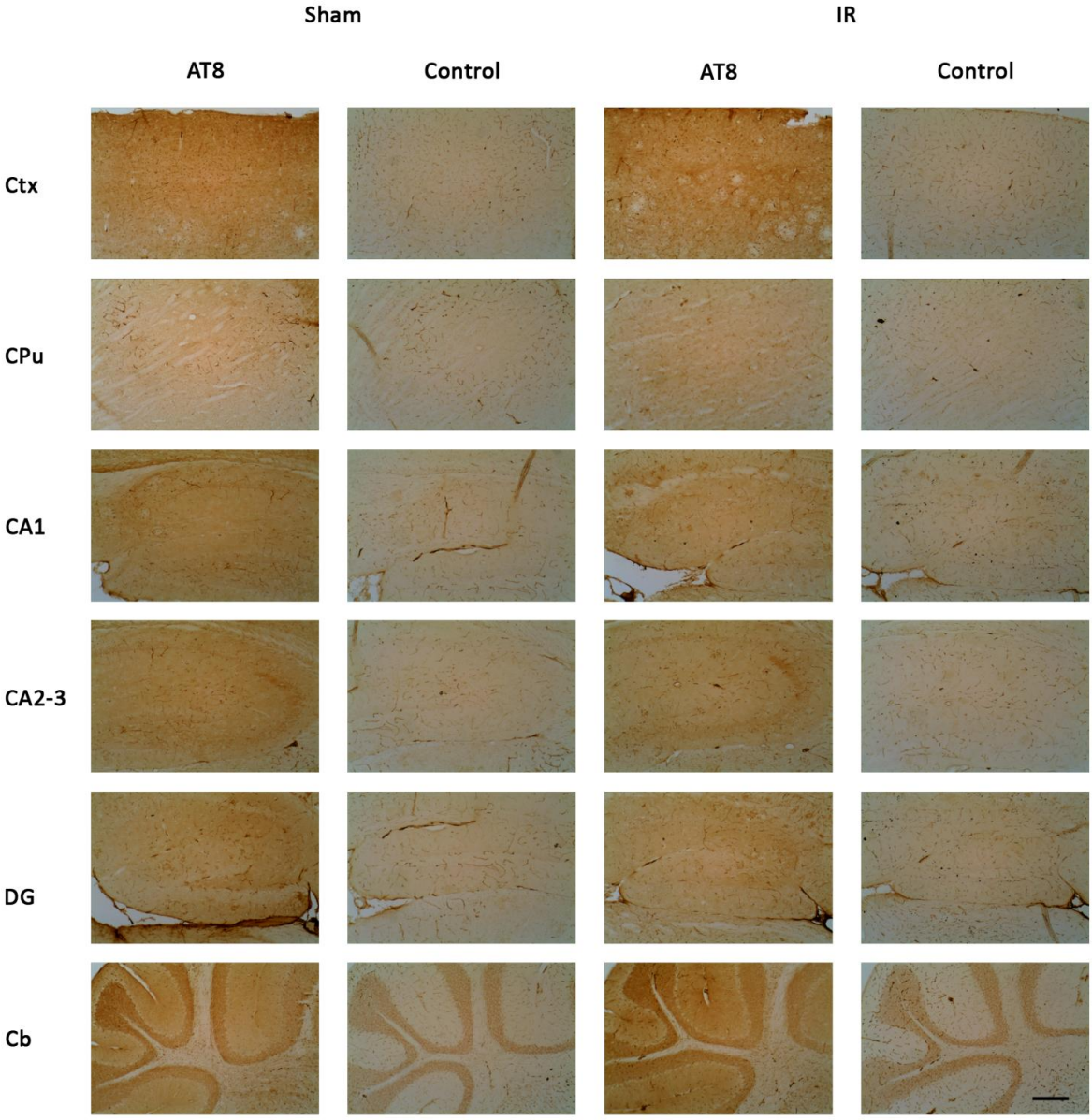

Figure 6.22. AT8 (hyperphosphorylated tau Ser202/Thr205) expression in chronically IR1072 treated and sham-treated (*in vivo*) 7 month old male TASTPM mice, each image is representative of staining, n=3 for each condition. Abbreviations: Ctx, cerebral cortex; CPu, caudate putamen; CA (1/2/3), Cornu ammonis; DG, Dentate Gyrus; Cb, Cerebellum; IR, Infrared at 1072 nm wavelength. Scale bar represents 200 μm.

6.4 TASTPM Mice: Mitochondrial respiratory studies

Mitochondria that were assayed in this part of the investigation were neither sham nor IR1072 exposed. The purpose of these assays was to determine whether endogenous levels of Complex I and II activity differ between male and female TASTPM mice of the same age, which was on average 6 months.

6.4.1 TASTPM Male and Female Mice: Liver

6.4.1.1 Complex I – Glutamate plus Malate

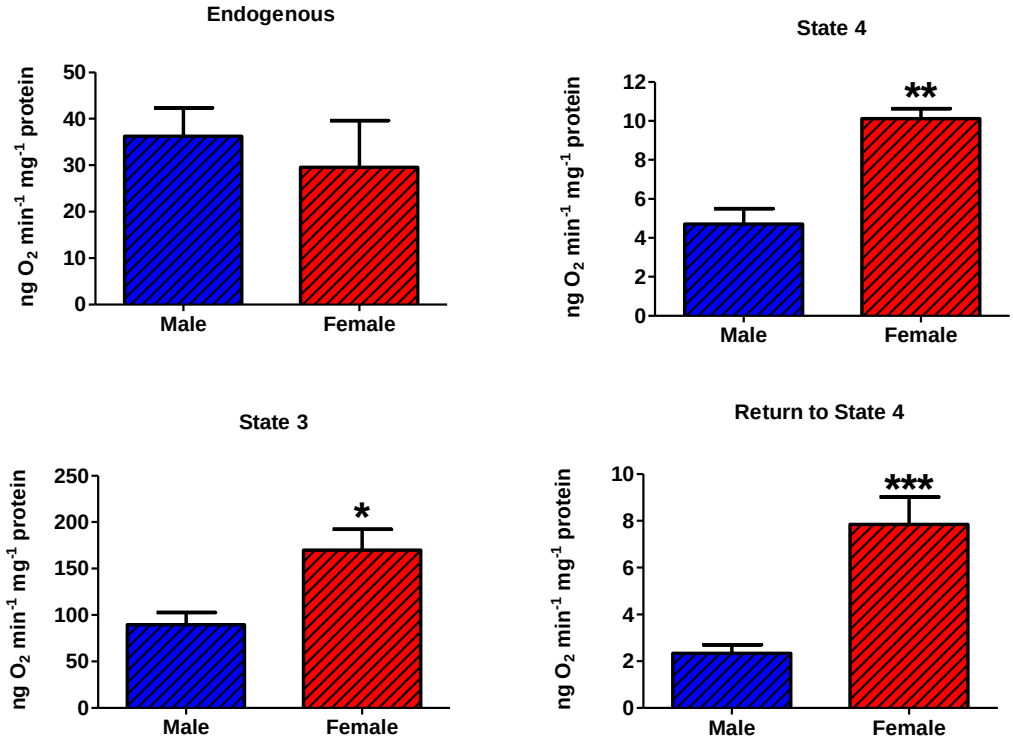

Figure 6.23. Differences between glutamate plus malate respiratory rates in age-matched male (n=6) and female (n=3) TASTPM mouse liver mitochondria (*in vivo*). Mean values ± SEM, *p<0.05, **p<0.01, ***p<0.001.

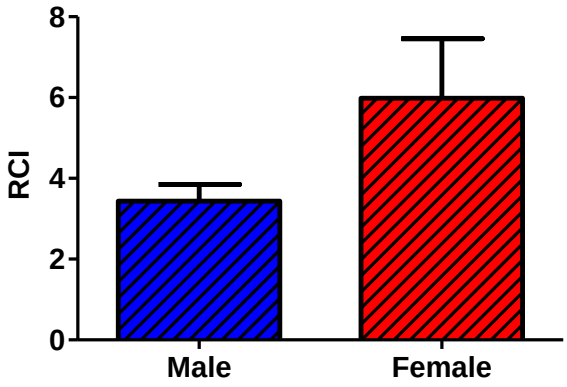

Figure 6.24. Difference between glutamate plus malate RCI in age-matched male (n=6) and female (n=3) TASTPM mouse liver mitochondria (*in vivo*). Mean values ± SEM.

Differences between electron transport chain Complex I activities, when comparing mitochondria isolated from liver tissue of female (n=3) to male (n=6) TASTPM mice of 6 months of age				
Respiratory rate (ng O_2 min^{-1} mg $protein^{-1}$)	P Value	Result: ↑/↓	Percentage change (%)	Figure
Endogenous	0.569	-	-	6.23
State 4	**0.003	↑	114.51	6.23
State 3	*0.013	↑	89.64	6.23
Return to State 4	***<0.001	↑	235.94	6.23
RCI	0.060	↑	72.01	6.24

Table 6.6. Data with a trend in altered activity are shaded blue (p<0.1), data with statistically significant altered activity levels (p<0.05) are shaded green. Arrows indicate direction of altered expression, (↑, increase; ↓, decrease), '-' indicates no significant change. *p<0.05; **p<0.01, ***p<0.001. Abbreviations: RCI, respiratory control index.

6.4.1.2 Complex II - Succinate

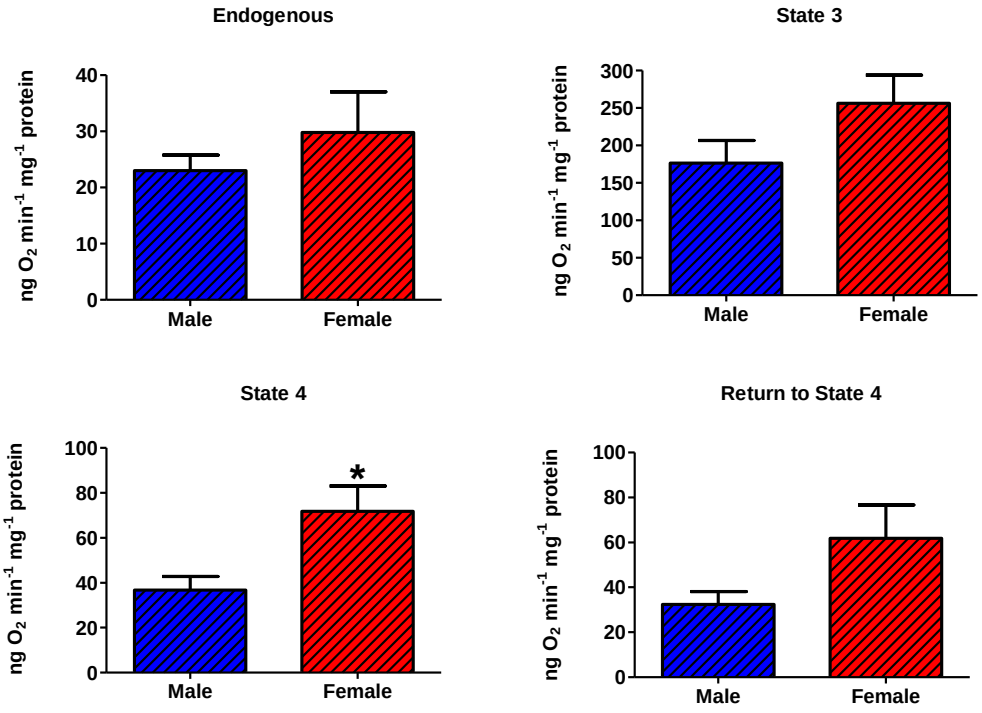

Figure 6.25. Differences between succinate respiratory rates in age-matched male (n=6) and female (n=3) TASTPM mouse liver mitochondria (*in vivo*). Mean values ± SEM, *p<0.05.

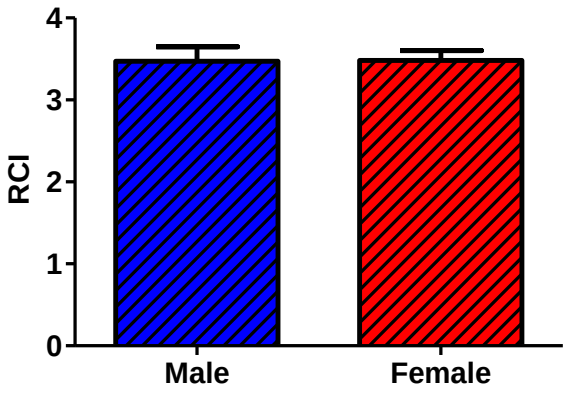

Figure 6.26. Difference between succinate RCI in age-matched male (n=6) and female (n=3) TASTPM mouse liver mitochondria (*in vivo*). Mean values ± SEM.

Differences between electron transport chain Complex II activities, when comparing mitochondria isolated from liver tissue of female (n=3) to male (n=6) TASTPM mice of 6 months of age				
Respiratory rate (ng O_2 min^{-1} mg $protein^{-1}$)	P Value	Result: ↑/↓	Percentage change (%)	Figure
Endogenous	0.310	-	-	6.25
State 4	*0.028	↑	95.51	6.25
State 3	0.158	-	-	6.25
Return to State 4	0.059	↑	90.05	6.25
RCI	0.978	-	-	6.26

Table 6.7. Data with a trend in altered activity are shaded blue ($p<0.1$), data with statistically significant altered activity levels ($p<0.05$) are shaded green. Arrows indicate direction of altered expression, (↑, increase; ↓, decrease), '-' indicates no significant change. *$p<0.05$; **$p<0.01$, ***$p<0.001$. Abbreviations: RCI, respiratory control index.

6.4.2 TASTPM Male and Female Mice: Brain

6.4.2.1 Complex I – Glutamate plus Malate

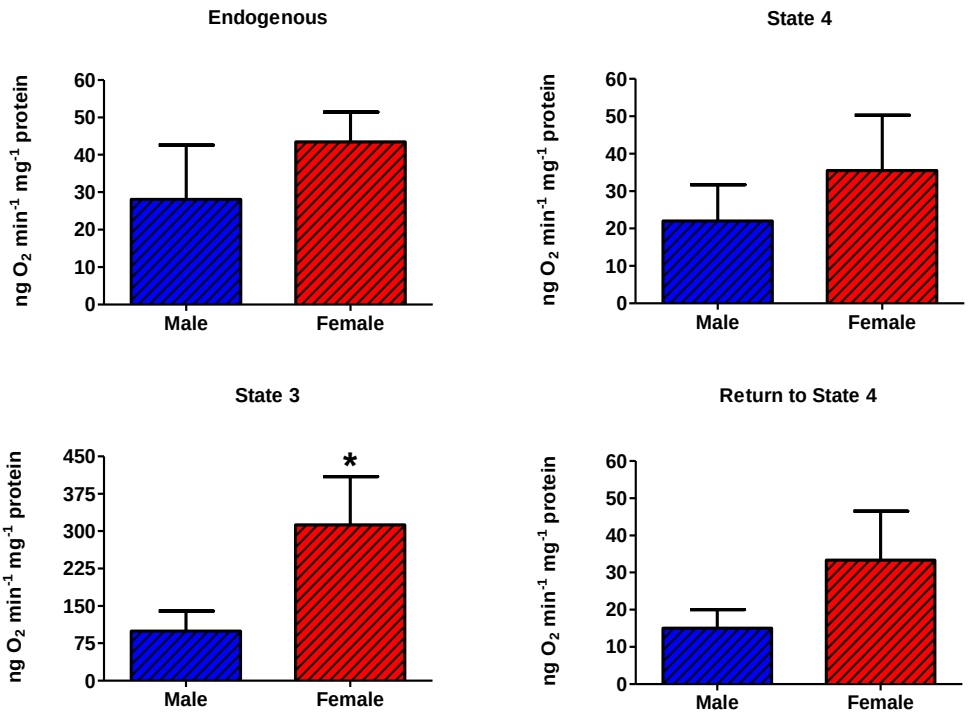

Figure 6.27. Differences between glutamate plus malate respiratory rates in age-matched male (n=6) and female (n=3) TASTPM mouse brain mitochondria (*in vivo*). Mean values ± SEM, *p<0.05.

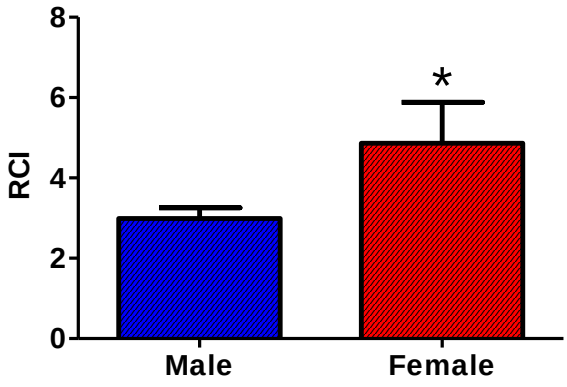

Figure 6.28. Difference between glutamate plus malate RCI in age-matched male (n=6) and female (n=3) TASTPM mouse brain mitochondria (*in vivo*). Mean values ± SEM, *p<0.05.

Differences between electron transport chain Complex I activities, when comparing mitochondria isolated from brain tissue of female (n=3) to male (n=6) TASTPM mice of 6 months of age				
Respiratory rate (ng O_2 min^{-1} mg $protein^{-1}$)	P Value	Result: ↑/↓	Percentage change (%)	Figure
Endogenous	0.507	-	-	6.27
State 4	0.459	-	-	6.27
State 3	*0.044	↑	215.47	6.27
Return to State 4	0.150	-	-	6.27
RCI	*0.047	↑	62.47	6.28

Table 6.8. Data with statistically significant altered activity levels are shaded green. Arrows indicate direction of altered expression, (↑, increase; ↓, decrease), '-' indicates no significant change. *p<0.05. Abbreviations: RCI, respiratory control index.

6.4.2.2 Complex II - Succinate

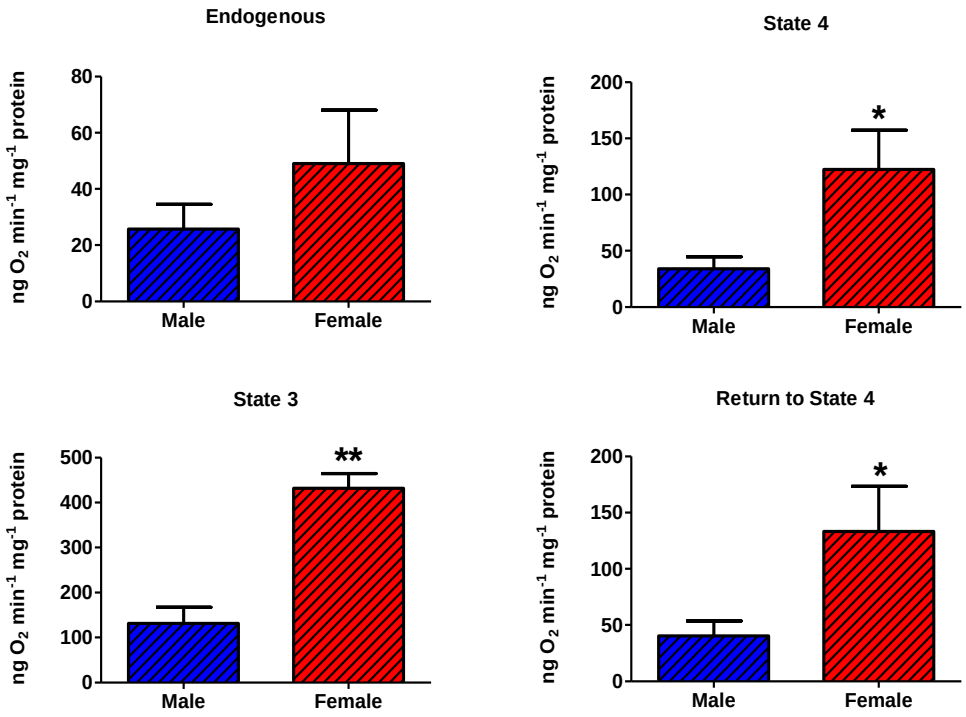

Figure 6.29. Differences between succinate respiratory rates in age-matched male (n=6) and female (n=3) TASTPM mouse brain mitochondria (*in vivo*). Mean values ± SEM, *p<0.05, **p<0.01.

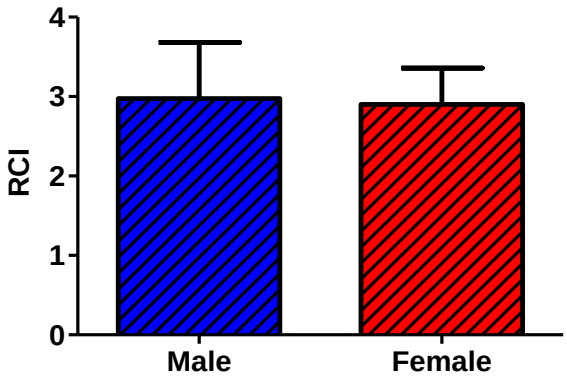

Figure 6.30. Difference between succinate RCI in age-matched male (n=6) and female (n=3) TASTPM mouse brain mitochondria (*in vivo*). Mean values ± SEM.

Differences between electron transport chain Complex II activities, when comparing mitochondria isolated from brain tissue of female (n=3) to male (n=6) TASTPM mice of 6 months of age				
Respiratory rate (ng O_2 min^{-1} mg $protein^{-1}$)	P Value	Result: ↑/↓	Percentage change (%)	Figure
Endogenous	0.236	-	-	6.29
State 4	*0.016	↑	249.93	6.29
State 3	**0.001	↑	229.02	6.29
Return to State 4	*0.026	↑	231.51	6.29
RCI	0.946	-	-	6.30

Table 6.9. Data with statistically significant altered activity levels are shaded green. Arrows indicate direction of altered expression, (↑, increase; ↓, decrease), '-' indicates no significant change. *p<0.05; **p<0.01. Abbreviations: RCI, respiratory control index.

6.5 Discussion

The aim of this chapter was to further establish protein changes that occur during ageing of the TASTPM mouse and to determine whether these proteins altered following chronic IR1072 exposure in age-matched male or female mice.

Pathway	Protein	TASTPM Timeline (Age in months)			Effect of chronic IR1072 exposure	
		3 vs. 7	3 vs. 12	7 vs. 12	♀	♂
Amyloid/tau	APP	-	-	-	↓**	↓*
	β-amyloid$_{(1-40)}$	-	-	-	-	-
	β-amyloid$_{(1-42)}$	Not determined			↓*	-
	PS-1	Not determined			↓*	-
	AT8	-	-	-	-	↓ (NS)
	P-Tau (S519)	-	-	-	↓ (NS)	-
	GSK-3β	-	-	-	-	-
Chaperones	HSF1	-	-	-	N/D	↓**
	HSP105	↓*	↓**	↓ (NS)	↑*	↓***
	HSP70	-	-	-	↑*	↓**
	HSP27	-	-	-	↑*	↑*
	P-HSP27	-	-	-	↑*	↑*
	αB Crystallin	↑**	↑**	↑ (NS)	↓***	↓*
TARPs	TARP γ2	-	↓ (NS)	-	↑***	-
	TARP γ8	-	-	-	-	-
	THY-1	Not determined			-	-

Table 6.10. Summary of effects of ageing in TASTPM mice and chronically IR treated mice, determined by western blotting. Abbreviations: APP, amyloid precursor protein; AT8, hyperphosphorylated tau; P-Tau (S519), phosphorylated tau at serine 519; GSK-3β, glycogen synthase kinase-3 beta; PS-1, Presenilin-1; HSF, heat shock factor; HSP, heat shock protein; P-HSP, phosphorylated heat shock protein; NS, non significant trend; N/D, not determined; TARP, transmembrane AMPA regulatory protein. *p<0.05; **p<0.01, ***p<0.001, '-' indicates no significant change.

The TASTPM transgenic line expresses the mutant APP and PS1 genes under the THY-1 promoter, considered a neuron specific promoter with a degree of region specific expression. Highest levels of THY-1 expression have been found in the striatum, hippocampus, cortex, cerebellum, with low level expression in the spinal cord and retina (Graham, 2011, Seki *et al.*, 2002). The areas associated with higher degrees of THY-1 expression are amongst the first areas that become progressively damaged in AD, and vice versa, with areas showing less expression reported to be affected later in disease progression or affected to a lesser extent. The expression of this promoter should not alter with age in the mouse, supported by the finding of no change in APP or $A\beta_{(1-40)}$ levels with increasing age via immunoblotting, with $A\beta_{(1-40)}$ data supported by previous immunohistochemical labelling data (Burroughs, 2010), however it was not possible to directly examine THY-1 levels in the TASTPM ageing timeline. It was not possible to investigate levels of $A\beta_{(1-42)}$, PS1 or THY-1 during ageing due to sample degradation; however it would be of significant interest to investigate these in ageing TASTPM mice. In future it would also be beneficial to directly investigate THY-1 expression, which could be examined using a luciferease promoter for the THY-1 gene for example, to determine whether it alters during ageing; as a neuron specific promoter some change in expression may be expected as a degree of neuronal death is a factor in disease progression in TASTPM mice, however only at a low level is neuronal loss observed.

The lack of change observed in Aβ levels with age of the TASTPM mouse investigated here, is perhaps not surprising as established plaques have been reported by three months of age and deposits of Aβ in the cortex by 2 months of

age (Howlett and Richardson, 2009). Therefore, the age of the mice investigated here, may be too old for any significant changes in Aβ levels to be observed. It is also important to note that Aβ investigated by immunoblotting is a measure of both soluble and insoluble protein. The quantity of plaque-type structures has been found to be increased with age (Burroughs, 2010, Howlett and Richardson, 2009, Hussain *et al.*, 2006) which may mean that the soluble proportion of Aβ is decreasing with age, however this cannot easily be determined via immunoblotting but could be further investigated with ELISA (enzyme-linked immunosorbant assay) based methodology (Wang *et al.*, 1999). Investigation of this nature of the Aβ protein would be interesting to determine following IR1072 exposure to establish whether the disease state may be modified by LLLT, Burroughs, 2010 has already established chronic IR1072 exposure reduces small Aβ plaques in the cortex and dentate gyrus (Burroughs, 2010, Howlett and Richardson, 2009, Hussain *et al.*, 2006).

Microtubule associated protein (MAP) tau is abnormally hyperphosphorylated in AD and aggregates as PHFs in neurofibrillary tangles (NFTs). The pattern of tau phosphorylation correlates with the loss of neuronal integrity (Augustinack *et al.*, 2002). Tau phosphorylated at Ser202/Thr205 (AT8 Antibody) is associated with both intracellular and extracellular NFTs (Goedert *et al.*, 1995), whereas tau phosphorylated at Ser199/Ser202 (P-tau S519 antibody; Hanger *et al.*, 2009) is associated with filamentous tau as it forms pre-NFT structures (Augustinack *et al.*, 2002). There was an increase in the level of tau phosphorylated at Ser202/Thr205 (Goedert *et al.*, 1995) with age of the TASTPM mice, however this was borderline non significant. These data provide support for immunolabelling with the AT8 antibody, which has previously been shown to

increase with age in the TASTPM mouse, significantly but not profoundly (Howlett *et al.*, 2008). However, the lack of significant change in levels of tau phosphorylated at Ser199/Ser202 and Ser202/Thr205 is perhaps not surprising as limited involvement of phosphorylated tau in the TASTPM disease progression has been reported. Phosphorylated tau has been shown to co-localise with dystrophic neurites adjacent to Aβ plaques but to be absent intracellularly in the TASTPM mouse (Howlett *et al.*, 2008). Concomitantly, no change was observed in GSK-3β levels (kinase responsible for phosphorylation of tau at these residues) in this investigation, whereas it has been reported to increase abnormally in the Alzheimer's disease brain, supporting minimal tau involvement in the disease state. Increased GSK-3β can repress HSF1, and therefore the chaperone response to protein aggregation/misfolding (Bhat *et al.*, 2004, Calderwood *et al.*, 2009). No change in levels of GSK-3β during increasing age of the TASTPM mouse may be due to an established disease state being present at an early age; therefore no notable increase is observed. However, it may also be due to the limited neuronal loss and limited tau involvement in the disease state mentioned previously, as high GSK-3β activity levels have been shown to lead to increased neuronal death and neurite retraction which are not observed in TASTPM mice (Bhat *et al.*, 2004). Phosphorylation of the Ser199/202 has been particularly implicated in neurofibrillary pathology of AD (Maurage *et al.*, 2003), something not significantly observed in this model (Howlett *et al.*, 2008, Kurt *et al.*, 2003) and something which was not found to alter with age of the TASTPM mouse in this investigation.

A significant age-dependent decrease in HSP105 levels was found in the TASTPM mice, along with a significant increase in levels of αB crystallin. No changes were observed in the levels of other heat shock proteins investigated in this study including HSP70, HSP27 and P-HSP27. It is also worth noting that there was no change in levels of HSF1 during the ageing process of TASTPM mice, supported by previously reported data that show no change in HSF1 levels during ageing but it is instead the activation of HSF1 that becomes compromised which ultimately results in the accumulation of aggregates (Calderwood *et al.*, 2009, Soti and Csermely, 2000).

If ageing cells become stressed due to high aggregate load there are fewer HSPs present to protect against damage, particularly those that are able to act at low concentrations of ATP which is the main function of HSP105. Reduced levels of HSP105 could suggest that the repression of HSC70 chaperone activity, by HSP105α via increased ATP hydrolysis (Yamagishi *et al.*, 2003) is somewhat reversed; potentially increasing the refolding capabilities of HSP70. However, despite no change in HSP70 levels, reduced levels of the co-chaperone HSP40 have previously been reported during ageing of TASTPM mice (Burroughs, 2010), a co-chaperone important for protein refolding. Therefore, despite reduced HSP105 inhibition of HSP70 chaperone activity, the concomitant lack of HSP40 suggests a persistent dampened ability for HSP70 to renature damaged proteins during ageing (Sahara *et al.*, 2007). Another factor to consider is the anti-apoptotic role of HSP105. HSP105 is able to inhibit the activation of JNK and therefore activation of a number of caspases (detailed in 1.3.2; Hatayama *et al.*, 2001); ergo lower HSP105 levels may result in

increased activity of pro-apoptotic proteins and thus cells become more susceptible to stress and are more likely to undergo apoptosis.

Increased levels of αB crystallin detected with increasing age of the TASTPM mice suggest that HSF1 is still able to be activated; indeed increased αB crystallin levels have been previously reported in patients with Alzheimer's disease, particularly in regions associated with senile plaques and neurofibrillary tangles (Bjorkdahl *et al.*, 2008, Mao *et al.*, 2001, Renkawek *et al.*, 1994). The highly significant profound down-regulation of αB crystallin following chronic IR1072 exposure in TASTPM mice is particularly interesting as it is one of the effects that occur in both the male and female mice. αB crystallin also appears to interact with $A\beta_{(1-40)}$ and $A\beta_{(1-42),}$ preventing fibril maturation and elongation (Narayanan *et al.*, 2006, Shammas *et al.*, 2011, Stege *et al.*, 1999, Yoo *et al.*, 2001). However, this interaction appears to occur via encouragement of oligomeric Aβ structure formation (Narayanan *et al.*, 2006) which is now widely believed to be the more toxic Aβ structure (Benilova *et al.*, 2012, Fandrich *et al.*, 2011, Haass and Selkoe, 2007), therefore increased αB crystallin during ageing could be causing increased Aβ toxicity. Conversely, αB crystallin has been shown to increase tau degradation as well as preventing phosphorylation and encouraging dephosphorylation of tau in N2a neuroblastoma cells (Bjorkdahl *et al.*, 2008), but there was no reduction in levels of phosphorylated tau investigated in this study despite the concomitant increase in αB crystallin. As well as this, increased αB crystallin levels could be working with HSP70 to incapacitate and re-fold aggregates as they have been reported to work synergistically (Ecroyd and Carver, 2009, Haslbeck *et al.*, 2005). Further work with αB crystallin, to identify the type of structures that the

small chaperone is associating with, tau and Aβ, would be crucial in order to understand the role of αB crystallin in the latter stages of disease progression.

There were a considerable number of differences in the effect of chronic IR1072 exposure, when compared to sham-treated animals, between male and female TASTPM mice. A critical factor to consider initially was whether chronic IR1072 had any effect on the expression of the THY-1 promoter itself. No change was observed in levels of THY-1 in female or male TASTPM mice that were chronically IR1072 treated, suggesting that any of the observed secondary changes in protein levels; particularly alterations in APP, APP-derived proteins and PS1, are not due to IR1072 affecting the transgene promoter.

A highly profound reduction in APP was found in the female and male mice chronically exposed to IR1072. It has previously been reported that female TASTPM mice have a higher amyloid-load than their male counterparts, with cerebral concentrations higher at all age point investigated, suggesting gonadal hormones may play a role in the processing of APP (Howlett *et al.*, 2004). Oestrogen loss at menopause had been associated with increased risk of Alzheimer's disease (Paganini-Hill and Henderson, 1994, Simpkins *et al.*, 1997), however the increased amyloid-load in the female TASTPM mouse is unlikely to be due to reproductive senescence as amyloid deposits can be observed from three months of age; indeed IR exposure was started at two months of age.

The unexpected finding of a significant reduction in APP in IR1072 exposed female and male mice may explain the concomitant significant reduction in levels of $A\beta_{(1-42)}$ in the female mice, however this is not present in male mice.

The absence of a reduction in Aβ, despite a reduction in APP, in male TASTPM mice may be due to a reduced production of the peptides in the first place. This may explain why there is no observable change in $A\beta_{(1-42)}$ levels in male TASTPM mice that have undergone chronic IR1072 exposure despite reduced APP, as it may be that the levels of non-toxic APP products are reduced but this was not investigated in this study. Androgens, strongly expressed in males, including testosterone and 5α-dihydrotestosterone, have been shown to reduce the secretion of Aβ peptides and enhance the secretion of non-amyloidogenic APP products, thus protecting against disease progression (Gouras *et al.*, 2000, Ramsden *et al.*, 2003). The APP gene contains a heat shock element, and it has been shown to become upregulated via a variety of stresses (ethanol, heat stress). Therefore the reduction in HSF1, which binds to the HSE to trigger transcription, may be a causal factor in the reduced levels of APP observed in male and female TASTPM mice (Dewji and Do, 1996, Dewji *et al.*, 1995). These data may explain why the effects of IR1072 on Aβ products are more significant in female TASTPM mice compared to males, as male androgens are able to prevent some of the toxic effects from APP-derived products; therefore the cell may be considered less stressed and a lower protective response is initiated via by IR1072 exposure. It is notable that despite reduction in the $A\beta_{(1-42)}$ peptide, no change in the $A\beta_{(1-40)}$ peptide in female mice was observed following chronic IR exposure. Why there appears to be discrimination between which Aβ peptide is removed in chronically IR1072 exposed female mice is unknown, but perhaps this suggests that the cell can discriminate which of the peptides is more toxic and prioritise the removal of the more toxic structure.

There were trends for decreased phosphorylated tau in both sexes following chronic IR exposure; however the male mice saw a reduction in levels of tau phosphorylated at the Ser202/Thr205, whereas female mice saw a trend for decreased levels of tau phosphorylated at the Ser199/Ser202 site. These data were supported with immunohistochemical analysis, a reduction in AT8 labelling was observed in the CA1/2/3 regions of the hippocampus, whereas females saw no reduction in AT8 staining across the brain. This is particularly interesting as the hippocampus is one of the first areas to become severely affected in Alzheimer's disease (Benilova *et al.*, 2012).

Treatment with IR1072 led to a reduced filamentous tau (Ser199/Ser202) expression indicating potential dual beneficial effects for IR1072 exposure upon amyloid and tau pathology, the former being more profound. However, the mechanism for this reduction in P-tau needs further investigation as levels of GSK-3β did not change, this is not to say that the activity of GSK-3β is not altered by IR1072 exposure. GSK-3β is known to phosphorylate tau on at least 14 of the 19 sites associated with PHF formation, including Ser199, Ser202, (which were both phosphorylated in the P-tau investigated in this study) Ser235, Ser396 and Ser404 (Hernandez *et al.*, 2009, Rankin *et al.*, 2007, Rankin *et al.*, 2008, Sun *et al.*, 2002, Voss and Gamblin, 2009). Immunohistochemical data supported these (immunoblotting) data, with no obvious change observed across the brain in GSK-3β levels in either sex following chronic IR1072 exposure. Further experiments are required to determine whether IR1072 irradiation may be reducing hyperphosphorylated tau levels via another kinase known to interact directly or indirectly with tau, such as cyclin-dependent

kinase-5 (cdk-5), cdc-2/cdk1 or MAP kinase and whether levels of tau which has been phosphorylated at other sites are also reduced (Sun *et al.*, 2002).

Despite no change in THY-1 expression, the level of PS1 was found to decrease in female TASTPM mice following chronic IR exposure, but this change was not observed in age-matched males. Mutations in PS1 are particularly associated with familial AD, and lead to increased deposition of Aβ. The mechanism of PS1 in Alzheimer's disease progression is not fully understood; PS1 comprises the major component of the γ-secretase which is responsible for the cleavage of APP C-terminal to produce $A\beta_{(1-40)}$ and $A\beta_{(1-42)}$. Mutations in PS1, have been shown to lead to favoured production of the 42 aa length Aβ peptide, which has been reported to be up to 10-fold more toxic than the 40 aa peptide (Matsuzaki, 2011). This increased production of $A\beta_{(1-42)}$ explains how mutations in PS1 lead to accelerated disease pathology and exacerbation of neuronal loss (Berezovska *et al.*, 2005, Hardy, 1997, Sudoh *et al.*, 1998). The TASTPM strain express the PS1 gene with M146V mutation, a mutation not known to cause any overt phenotype, although alterations in intracellular calcium signalling, increased excitotoxicity and reduced basal synaptic transmission have all been observed (Reviewed - Graham, 2011). The reduction in PS1 levels in chronically IR1072 exposed females TASTPM mice could also explain the reduced levels of $A\beta_{(1-42)}$ found, as less cleavage of APP by the mutated PS1 can occur. Female TASTPM mice, show greater Aβ deposition, as mentioned previously (Howlett *et al.*, 2004), and although they did not show a greater cognitive decline than their male counterparts, it may be that the disease state is more severe and subsequently the response to chronic

IR1072 exposure is greater with reduced $A\beta_{(1-42)}$ and PS1 leading to a reduced disease state.

There were also a considerable number of differences in the effects of chronic IR1072 exposure on the expression of a range of chaperone proteins between male and female TASTPM mice. On the whole, IR-treated male TASTPM mice generally displayed reduced expression of HSP and sHSP, compared to sham-treated controls. Significantly, this could be attributed to the notable reduction in HSF1 levels in male IR1072 exposed mice. HSF1, heat shock factor 1, is responsible for the induction of HSP expression, detailed in Chapter 1.3.1. The translocation of HSFs to the nucleus is required for chaperone expression; reduced HSF1 could mean that the cell is less able to initiate expression of proteins needed for refolding and in preventing initiation of apoptotic pathways needed for survival. Increased HSP27 levels may be responsible for reduced HSF1 levels by targeting HSF1 to sumoylation, a modification which blocks the transactivating capacity of HSF1, targeting it for removal. As well as this HSF1 is also able to be modified by CHIP (Calderwood *et al.*, 2009, Lanneau *et al.*, 2010). Of all of the chaperones investigated, HSP70, HSP105 and αB crystallin levels were significantly reduced, but expression of HSP27 and P-HSP27 were increased, HSP60 has also previously been reported to decrease following chronic IR exposure in male TASTPM mice (Burroughs, 2010). Unfortunately, immunoblotting data for HSF1 levels in female TASTPM mice was not obtained due to lack of material.

It is particularly interesting that levels of HSP27 and P-HSP27 were significantly increased in both male and female TASTPM mice exposed to chronic IR1072; as HSP27 in large oligomeric forms is a capable chaperone, whilst able to also

stabilise the actin cytoskeleton and more importantly act as a potent anti-apoptotic molecule via inhibiting a number of pathways including FAS-mediated cell death, see figure 1.12 (Samali *et al.*, 2001). Due to its small sized tetramers phosphorylated HSP27 is able to shuttle between the nucleus and the cytoplasm, targeting cellular aggregates toward the ubiquitin removal system, aiding cellular defence against aggregate accumulation (Lanneau *et al.*, 2010). HSP27 has also been shown to interact with hyperphosphorylated tau and target it for dephosphorylation by phosphatases (Koren *et al.*, 2009, Shimura *et al.*, 2004), a potential mechanism for the observed trend towards reduced phosphorylated tau in both male and female mice chronically exposed to IR1072. Interestingly, increased HSP27 expression has previously been reported in human fibroblasts following LLLT (400-2000 nm). This increase was accompanied by increased release of the anti-apoptotic proteins Bcl-2 and BCL-X_L (Frank *et al.*, 2004). These data support a neuroprotective role for increased HSP27 levels found in TASTPM mice chronically exposed to IR1072.

Chronic IR treatment of female TASTPM mice also resulted in the increase in levels of HSP70 and HSP105, with a reduction in αB crystallin levels. Previous work utilising LLLT at both 623.8 and 815 nm has also been shown to induce increased HSP70 expression. Investigations by Novoselova, (2006) found that even brief LLLT at 632.8 nm resulted in a pronounced increase in HSP70 expression in macrophages and lymphocytes, modulating immune system function (Novoselova *et al.*, 2006). Work by Souil, (2001) demonstrated that NIR at 815 nm significantly increased the expression of HSP70 in rat skin. In areas of wounding that were irradiated, increased HSP70 expression was found to persist for seven days following initial IR exposure, and the irradiated wounding

areas displayed improved tissue regeneration and healing (Souil *et al.*, 2001). These data suggest that following the initial LLLT, resulting in chaperone upregulation, may in turn trigger into action the cell's own mechanisms and alleviate stress in a long term manner.

Therefore, it is perhaps not surprisingly that chronic IR1072 exposure resulted in increased HSP70 expression in female mice. Increased HSP70 has also been shown to protect against neuronal injury (Yenari *et al.*, 1999, Yenari *et al.*, 2005). As well as the capacity to refold misfolded proteins, HSP70 has the ability to direct proteins toward the ubiquitin system via CHIP and BAG-1 that cannot be refolded, such as Aβ (Lanneau *et al.*, 2010). Indeed, extracellular HSP70 has been reported to remove Aβ in senile plaques via microglial driven phagocytosis (Evans *et al.*, 2006, Kakimura *et al.*, 2002), as well as preventing the aggregation of Aβ in the cytosol (Koren *et al.*, 2009, Magrane *et al.*, 2004). Upregulation of HSP70 has previously been shown to reduce Aβ levels, deposition, and Aβ-induced neurotoxicity (Hoshino *et al.*, 2011). The beneficial effects of HSP70 are not limited to Aβ, it has also been shown to bind hyperphosphorylated tau, prevent its oligomerisation and direct it towards degradation (Patterson *et al.*, 2011, Voss *et al.*, 2012). These roles for HSP70 and its increased expression in female TASTPM mice chronically exposed to IR1072, provide another potential explanation for the simultaneous reduction in $A\beta_{(1-42)}$ and P-tau.

Increased HSP105 levels were also found in female TASTPM mice chronically exposed to IR1072 compared to sham-treated controls. HSP105, as detailed in chapter 1.3.5, has been shown to negatively regulate the chaperone refolding capabilities of HSC70/HSP70 through hydrolysing ATP, forcing HSC70/HSP70

to act as a 'holding' chaperone with a much higher substrate affinity. By increasing binding time, the chance of the protein refolding correctly the first time of binding is increased (Yamagishi *et al.*, 2004, Yamagishi *et al.*, 2003, Yamagishi *et al.*, 2000). HSP105 can also induce HSP70 expression via STAT3, independent of HSFs (Saito *et al.*, 2009). As well as indirectly inducing neuroprotective mechanisms via HSP70, HSP105 has also been shown to suppress aggregate formation itself, to maintain tau in an unphosphorylated state, with HSP105 downregulation reported to increase $A\beta_{(1-42)}$ production and deposition (Eroglu *et al.*, 2010, Yamagishi *et al.*, 2010).

During ageing of the TASTPM mice, levels of TARP γ2 were found to drop at 7 months of age and at 12 months of age, compared to mice at 3 months of age. This may explain a number of the behavioural and developmental problems described in the TASTPM model (Pugh *et al.*, 2007). It was also interesting to find that female TASTPM mice demonstrated a significant increase in levels of TARP γ2 following chronic IR1072 exposure, whereas male mice showed no significant change, again this data suggest influence of LLLT over LTP, as discussed in Chapter 5, a promising secondary effect of chronic irradiation. Increased levels of TARP γ2 may improve some of the behaviour alterations observed in the TASTPM strain. TARP γ2 has also been proposed to decrease the rate of AMPA receptor desensitisation and increase the recovery rate from desensitisation, as well as increase AMPA receptor trafficking to both the cell surface and importantly the synapse. This increase in TARP γ2 may act to compensate for neurodegeneration or reverse some of the downregulation of AMPA receptors found to occur in Alzheimer's disease which is thought to contribute to cognitive decline which characterises the disease progression (Liu

et al., 2010). As mentioned in chapter 5, investigation of GluA1 and GluA2 levels would be beneficial to comprehend the impact of IR1072 on LTP and LTD.

Another factor to consider is whether gender differences in hormone levels affect heat shock protein levels, it has previously been established that basal levels of HSP expression differ between male and female rodents. Female rats have been shown to have decreased HSP27 and HSP90 levels in both muscle and heart tissue whilst increased levels of HSP60 and HSP70 in the kidney and heart respectively, compared to male rats (Voss *et al.*, 2003). Despite little investigation of gender differences in protein expression in the brain, these data suggest that basal expression differences are possible, leading to differing effects on expression levels following IR1072 exposure. It is important to consider that hormones may have an important impact on the biological effects of NIR at IR1072 and this is an important factor to investigate in the future.

Data shown in figures 6.23 - 6.30 are respiratory studies of mitochondria (Complex I and II) isolated from age-matched female and male TASTPM mice which have not been exposed to IR. It was somewhat surprising to find that female mice displayed consistently increased Complex I and Complex II activity in both liver and brain mitochondria, compared to male counterparts. The respiratory control index (RCI) for Complex I was significantly higher in both liver and brain mitochondria, although values for males were high enough for the mitochondria to be considered sufficiently coupled (see table 4.9; Campello *et al.*, 1964). These data suggest that certain ETC components are more tightly coupled to the mitochondrial membrane in female mice and that their mitochondrial activity is significantly higher than males and potentially more

efficient. More tightly coupled membranes are less likely to produce a greater number of damaging free radicals, due to increased activity levels. As discussed previously, electron transport chain components are considered to be the primary site for absorption of NIR (Gao and Xing, 2009, Karu, 1999, Karu *et al.*, 2004, Karu *et al.*, 2005), therefore investigating the level of mitochondrial respiratory activity in TASTPM mice may provide an understanding as to the secondary effects of NIR absorption. Significantly higher respiratory rates in female over male TASTPM mice may mean that female mice are able to absorb a greater quantity of IR1072 and are more susceptible to the biological effects of NIR absorption. The redox state of cells has previously been shown to be important in magnitude of biological effects following NIR, more reduced cells are more susceptible to the effects of NIR (Gao and Xing, 2009, Karu, 1999, Karu, 2008). With a greater number of electrons available, Complex I and II are able to be more active. It can therefore be hypothesised that as female mitochondria have more active Complex I and II respiratory rates than males, their cells are in a more reduced state and therefore more susceptible to LLLT which is why the magnitude of effects, on the proteins investigated here, following chronic IR1072 irradiation in female TASTPM mice appear to be significantly greater than in chronically irradiated male TASTPM mice.

These data suggest a plethora of mechanisms and proteins that could be involved in the reduction of APP, $A\beta_{(1-42)}$ and P-tau observed in this mouse model of Alzheimer's disease following chronic IR1072 exposure, and endogenous mitochondrial ETC complex activity may play a key role in determining the magnitude of these effects.

The next chapter investigates the effects of IR1072 exposure on *Caenorhabditis elegans*, a well-characterised animal model of ageing. This chapter is designed to determine whether IR1072 exposure has an effect on *C. elegans* lifespan longevity, and whether these effects can be magnified with alternate IR1072 exposure protocols. Most importantly, *C. elegans* is used to aid in the determination of proteins/pathways that underpin the observed beneficial biological effects reported in the mouse model systems previously investigated in this thesis.

Chapter 7: Using *Caenorhabditis elegans* to understand IR1072

7.1 Introduction

Work with the nematode *Caenorhabditis elegans* was adopted in order to aid in the elucidation of the molecular mechanism through which IR1072 elicits its biological effects and to determine signalling/molecular pathways that are critical for these effects. The nematode was also used in order to establish whether IR1072 could also modulate a further biological system than those previously investigated.

7.1.1 Anatomy and Life cycle

The nematode *Caenorhabditis elegans* was the first model system to show that a single gene mutation was able to extend lifespan. From the identification of this age-1 gene mutation in the 1980's (Friedman and Johnson, 1988a), *C. elegans* has become a well used and thus well characterised, model for the study of ageing. The nematodes are comprised of only 959 somatic cells, enclosed by a sturdy but flexible external structure called the cuticle. Nematodes are able to move through striated muscle fibres attached to the cuticle, food is taken in through the mouth, compressed and pumped by the pharynx into the intestine, which runs the entirety of the nematode. *C. elegans* are typically grown on agar plates with a lawn of bacteria to act as a food source, but they can be grown axenically, in liquid culture media or on agar plates (Hobert, 2005, White *et al.*, 1986).

Adult nematodes are either male of self-fertilising hermaphrodites, however hermaphrodites are unable to cross-fertilise with other hermaphrodites. Males typically comprise a very small fraction (~0.1%) of the offspring from hermaphrodites, and are different in appearance to hermaphrodite nematodes, see figure 7.1 (Johnson, 2003).

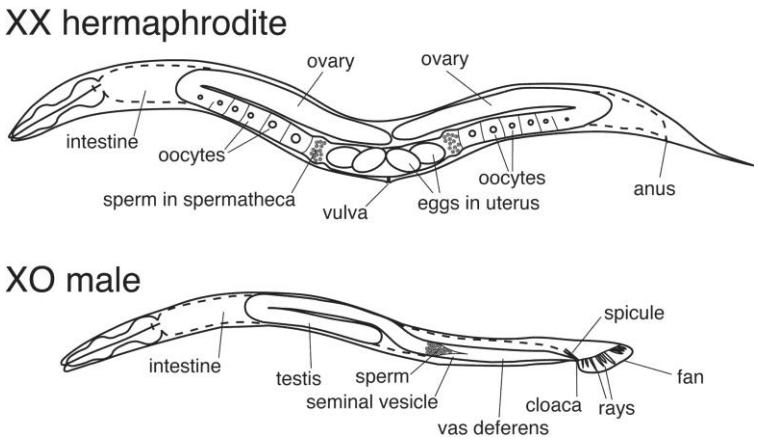

Figure 7.1. Differences between hermaphrodite and male *C. elegans* (Zarkower, 2006)

C. elegans have a very short life span, with a life cycle consisting of four larval stages, termed L1-L4 (see figure 7.2), on average, a nematode lifespan is 18-20 days when grown at 20°C, reaching 25-30 days when grown at lower temperatures, such as 10-14°C on agar plates. At 25°C the average lifespan of nematodes drops to between 7-11 days (Johnson, 2003, Klass, 1977). Development occurs relatively quickly with eggs able to develop into reproductive adults after three days at 25°C. Reproduction is largely finished by the fifth day of adulthood, but is completely ceased by day 10 of adulthood; on

average each hermaphrodite can lay 300 eggs during their reproductive period (Johnson, 2003, Klass, 1977, Olsen *et al.*, 2006b).

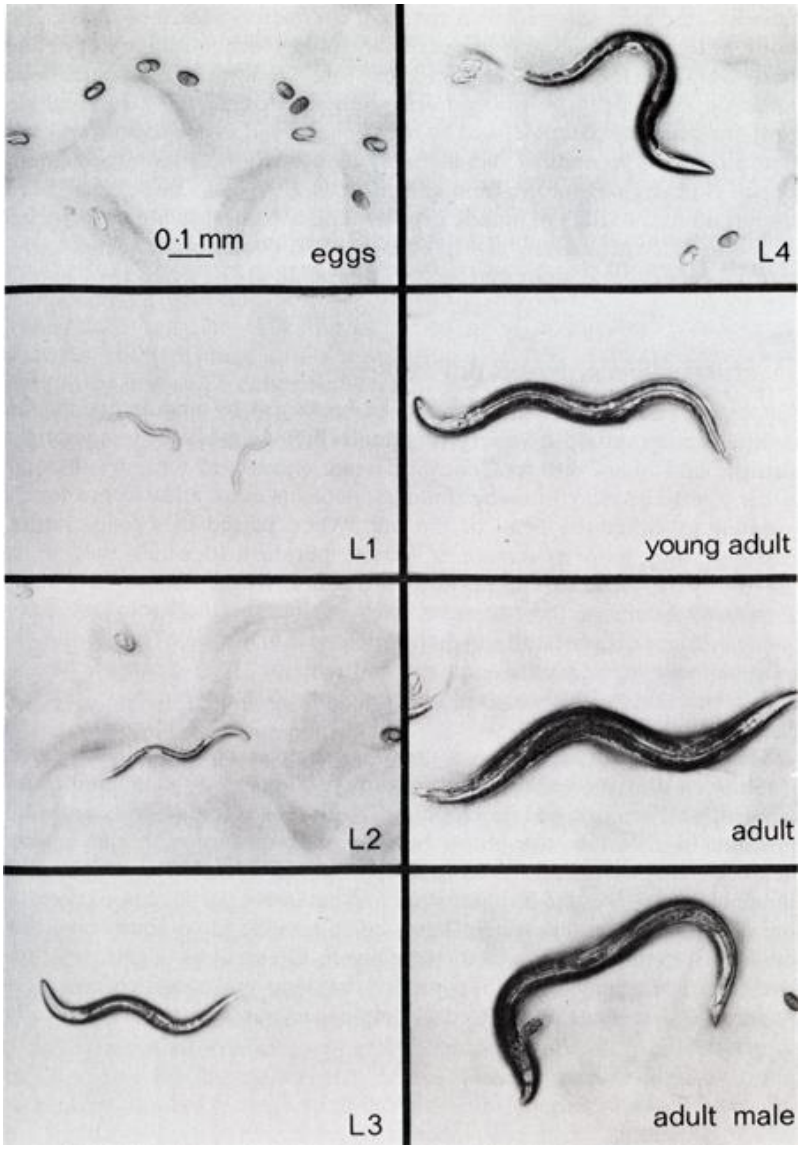

Figure 7.2. Stages of *C. elegans* development (Wood, 1988).

C. elegans are a particularly distinguished model in which to study ageing. Their lifespan is able to be easily modulated through the use of genetic manipulation; a significant number of mutations have already been identified in *C. elegans*

which alter the rate of ageing, some mutations have been shown to extend lifespan by three or four times that of wild-type nematodes. Lifespan can also be significantly extended via environmental influences such as temperature, diet, reproduction and oxygen levels (Riddle, 1997). The aims of using a relatively simple model, such as *C. elegans*, are to help understand human ageing and how this process increases risk of certain diseases such as neurodegenerative disorders.

7.1.2 Advantages and Disadvantages in Investigating Neurodegenerative Disorders

The nervous system of *C. elegans* has been extensively studied. It consists of 302 neurons and 56 glial cells. There are 118 classes of neurons in the adult hermaphrodite, the position of which is reproducible from nematode to nematode (Hobert, 2005, White *et al.*, 1986). This lack of variation has enabled the positions and connectivity of approximately 6000 synapses, 700 gap junctions and 2000 neuromuscular junctions to be established, with approximately 57,000 interconnections mapped in total (Chalfie and Jorgensen, 1998, Schafer, 2005, White *et al.*, 1986).

In comparison to vertebrate system which contains billions of neurons, the nematode *C. elegans* possesses a relatively small, well characterised nervous system in which to study molecular and cellular processes. *C. elegans* have enabled the identification of a number of proteins involved in the development of nervous system function, pharmacological mechanisms of action of

psychotropic drugs and a significant amount of data about genes involved in ageing and longevity (Kenyon, 2010, Riddle, 1997, Schafer, 2005).

The *C. elegans* nervous system shares a number of similarities with that of vertebrates including the neurotransmitters that are present. Glutamate acts in the nervous system, monoamines act as modulatory neurotransmitters, with acetylcholine acting as the major excitatory neurotransmitter at neuromuscular junctions and GABA as the major inhibitory neurotransmitter. However, there are a number of differences between the vertebrate and nematode nervous systems; neurons are more simple, with each usually only having one process and they lack postsynaptic specialisations seen in vertebrates. It also appears that the majority of cellular connections occur via gap junctions (Chalfie and Jorgensen, 1998). It is important to note that *C. elegans* lack genes encoding voltage-gated sodium channels, and therefore action potentials are thought to rely on voltage-gated calcium channels and graded potentials in order to initiate neuronal signalling, unlike the vertebrate system. However, *C. elegans* do express motor neurones, sensory neurones and interneurons (Chalfie and Jorgensen, 1998, Sawin *et al.*, 2000) and 42% of human disease related genes have a nematode orthologue (Culetto and Sattelle, 2000).

Synaptic connectivity is very different in *C. elegans* to the human brain, an example being behavioural alterations following the loss of dopamine neurons. In the nematode, the loss of dopaminergic neurons increase the motor activity so much that the nematodes are unable to slow down to eat, the opposite of which occurs in Parkinson's disease (Jorgensen, 2004, Wolozin *et al.*, 2011). Considerable understanding of neuronal connectivity has been gained through extensive mapping of connections in the nematode system. However, the

electron microscopy data does not give functionality, i.e. synaptic neurotransmitter specificity and whether these are excitatory or inhibitory. Work is underway to provide further detail to this extensive mapping; regarding behavioural, neurochemical and activity mapping. Therefore despite defining *C. elegans* as a 'well characterised model of ageing' a significant amount remains unknown (Riddle, 1997, Schafer, 2005).

There are many advantages and disadvantages to using *C. elegans* in ageing research. The nematodes are essentially cheap and easy to propagate, they display no apparent ill-effects of inbreeding, their genome has been completely sequenced and the development of each individual worm is almost identical. Strains are also able to cryogenically stored for long periods of time, with no observable detrimental effects. Nematodes are short lived, making them an ideal model to investigate processes/genes involved in ageing. Their lifespan has been shown to be dramatically modified following the mutation of genes implicated in the ageing process such as *daf-2* and *daf-16* (nematode equivalents to the insulin receptor and FOXO (Forkhead Family Box O) transcription factor, respectively), both part of the first metabolic process discovered to regulate ageing. Signalling from the DAF-2 receptor to the DAF-16 transcription factor has been shown to control longevity and metabolism, with mutations in *daf-2* extending lifespan (Dorman *et al.*, 1995, Lee *et al.*, 2003). The primary role of *daf-2* is to negatively regulate DAF-16, which is important during normal development of the nematode but in the adult; reducing/removing *daf-2* activity enables DAF-16 to increase longevity to up to three fold that of a wild-type nematode (Kenyon, 2011, Kenyon, 2010, Ogg *et al.*, 1997). DAF-16 is the primary downstream effector of *daf-2* signalling, with

DAF-16 able to enter the nucleus and effect the expression of a number of genes, including *hsf-1.* It has also been identified that HSF1 is required for *daf-2* mutations to extend lifespan, suggesting that DAF-16 and HSF1 act together to activate genes, including those for heat shock proteins, to result in this effect (Hsu *et al.*, 2003).

There are however, disadvantages in using *C. elegans* as a model system, particularly when using the nematode as an investigative tool to further understand human ageing. Major differences stem from the large evolutionary separation of nematodes from mammals. Nematodes are invertebrates; possess no circulatory system, nor immune system. However they do display declining physiological processes with age including reproductive senescence, reduced movement, defection frequency, pharyngeal pumping, sperm number and loss of tissue integrity (reviewed - Huang *et al.*, 2004). Nematodes have four defined stages of ageing, Stage I – progeny production, from L4 stage to the end of the self-fertilisation period; Stage II – post-reproductive period, vigorous movement; Stage III – reduced motor activity; Stage IV – minimal motor activity, cessation of pharyngeal pumping until the end of lifespan (Huang *et al.*, 2004). These features, along with lifespan analysis, enable comprehension of phenotype generation through manipulation of particular genes/proteins in the ageing process (Johnson, 2003, 2008, Klass, 1977).

Gene expression can be readily modified in *C. elegans*, through generation of knock down strains, RNAi (RNA interference) or gene deletion. The use of RNAi in *C. elegans* is a powerful method to study the genome of the organism. RNAi functions to inactivate specific genes through propagating the nematode on *E. coli* lawns which express double stranded RNA, analogous to genes under

investigation, which are then able to post-transcriptionally silence expression of the target gene, it has however not been shown to be successful for every gene. Through this method, interaction of nematode chaperones with certain substrates has been investigated, including in several mutant nematode strains that express the β-amyloid peptide (Fonte *et al.*, 2002, Kapulkin *et al.*, 2005, Olsen *et al.*, 2006b).

Many studies have found that mutations attributed to human disease display similar types of dysfunction when induced in *C. elegans*. Despite approximately one third of genes in mammals having no homologues in nematodes, cross-species translation of function is thought to derive from high levels of homology in functional domains which are often hidden through apparent low-level total protein homology (Johnson, 2003, Olsen *et al.*, 2006b, Wolozin *et al.*, 2011). Another difficulty is biochemical analysis of individual nematodes; due to their small size (adults are approximately 1 mm in length), individually they do not provide a great deal of material to assay and thus large quantities are required. The thick cuticle can also prove difficult to penetrate and bacterial colonisation of the gut can result in sample contamination. These factors make biochemical analysis of individual nematodes particularly difficult. But the transparent nature of the nematodes enables *in vivo* study of fluorescently tagged proteins in great depth. As well as this, *C. elegans* can be used in electrophysiological and pharmacological investigation. Patch-clamping is particularly difficult; again due to the tough nature of the cuticle, but via the use of embryonic *C. elegans* cells in culture, many obstacles faced with adult nematodes can be overcome (Bianchi and Driscoll, 2006, Johnson, 2003).

Nematodes represent a superb platform for preliminary screening of putative therapeutic medications before moving into transgenic mammals. *C. elegans* are a particularly useful model in identification of genes and molecular mechanisms involved in ageing, providing they are conserved. The simplicity of the nematode and the ability to genetically manipulate the organism makes it a valuable stepping stone, bridging the gap between the simplicity of *in vitro* studies and the complexity of the human brain (Wolozin *et al.*, 2011).

Providing IR1072 has an effect in *C. elegans*, the nematodes also provide a suitable system to aid in investigating the essential pathways for biological effects responsible for the absorbance of IR1072. Providing IR1072 had beneficial effects, another aim of this investigation was to begin to look at absorbance profiles of protein fractions from *C. elegans* to help identify where the primary photoacceptor may lie and to verify whether profiles obtained with nematodes had commonalities with mammalian absorbance profiles.

7.1.3 *C. elegans* and Heat Shock Proteins

Expression of specific proteins in *C. elegans* in response to heat stress was first reported by Snutch & Baillie in 1984. It was found that *C. elegans* express a range of heat shock proteins, spanning in molecular weights from 16-81 kDa, which have been defined to include HSP19, HSP25, HSP29, HSP38, HSP41, HSP81 and members of the HSP16, HSP60 and HSP70 families (Heschl and Baillie, 1989, Snutch and Baillie, 1984).

C. elegans have a highly conserved HSP70 family. This family is made up of constitutively expressed, inducible and pseudogenes with a minimum of nine proteins transcribed across at least three subfamilies (Heschl and Baillie, 1989). The molecular structure of HSP70 in *C. elegans* has high homology with the Dnak equivalent in *E. coli*, both molecules have a C-terminal substrate binding domains and a highly conserved ATP binding domain at the N-terminus, much the same as mammalian HSP70, and are expressed in the mitochondrion, endoplasmic reticulum lumen and cytoplasm (Heschl and Baillie, 1989, Yenari *et al.*, 1999).

Another extensively studied HSP family is the non constitutively expressed HSP16. The proteins within this family are related to the mammalian α-crystallin small heat shock protein family, so far four different genes which encode HSP16 family members have been identified, HSP16 expression is thought to be dependent upon exposure to heat stress (Dawe *et al.*, 2006, Stringham *et al.*, 1992). It is also interesting that accumulation of HSP16 has been observed with age of the nematode, and at particularly high concentrations in long-lived *age-1* mutant strains. Mutations in *age-1* render nematodes resistant to heat shock and have reported to cause up to a 65% increase in mean lifespan. The *age-1* gene acts downstream of *daf-2* in the insulin-like signalling pathway and encodes the nematode equivalent of mammalian catalytic subunit of PI3K (Friedman and Johnson, 1988a, b, Morris *et al.*, 1996), emphasising the possibility for molecular chaperones to act as promoters of longevity (Walker and Lithgow, 2003).

C. elegans provide a useful model to investigate function of chaperone inscribed genes, as knockout mouse models of chaperone genes have been

shown to produce models with minimal phenotypes considering the broad role of chaperones in cellular processes and maintenance. This leads to the idea that the mammalian system has compensatory mechanisms in place to cope with a degree of chaperone deficiency, although these are yet to be defined.

Heat shock proteins have been shown to be important in longevity in *C. elegans* as well as mammals. Over expression of chaperones, including HSP70 and HSP16 family members, result in increased lifespan. Indeed early stress to induce higher endogenous levels of HSPs, results in the improved ability of the nematode to withstand stress in later life and therefore increase survival rates (Leitz *et al.*, 2002, Lithgow *et al.*, 1995, Olsen *et al.*, 2006a, Wu *et al.*, 2009). Silencing of *hsf-1* expression, which is required to bind to the HSE in order to induce HSP production (see figure 1.11), results in decreased longevity (Garigan *et al.*, 2002, Morley and Morimoto, 2004, Olsen *et al.*, 2006a, b). Lifespan extension by HSF1 over-expression has also been reported to function together with the transcription factor DAF-16 to activate a subset of genes, including those that express for sHSPs, which are ultimately responsible for longevity (Hsu *et al.*, 2003).

These data show *C. elegans* to be an appropriate translational model to investigate disease and could provide important insights into chaperone function in ageing with the ability to use such technologies as RNAi to deftly target specific genes and thus potential compensatory mechanisms.

7.2 Results

7.2.1 Initial Exposure Protocol

All strains used in this investigation and their associated mutations are defined in table 2.2.

Prior to the use of *C. elegans* to investigate the molecular mechanism of IR1072 action, it needed to be established whether IR1072 has a clear effect on the nematode. Lifespan analysis was used as a measure of animal wellbeing. All lifespans were analysed as described in 2.9.5., utilising the Kaplan-Meier survival model, with statistical significance determined using Log-Rank and Wilcoxon analysis.

Initial experiments were conducted using SS104, *glp-4 (bn2)I*, strain. Nematodes were shifted from 15°C to 25°C, to induce sterility, when nematodes reached L3/L4 stage (see figure 7.2) and lifespan experiments were started 24 hours after this shift, when nematodes were young adults. Equipment was as described in figure 2.4, and 2.9.1, with the treatment protocol as described in 2.9.2.

Preliminary experiments using 35 mm plates are shown in figure 7.3 and 7.4. Figure 7.3 identified non-significant change in lifespan for SS104, *glp-4 (bn2)I*, when exposed to IR1072 for three minutes or six minutes, compared to sham treated controls. However, 12 minute exposure protocol resulted in an 11% increase in lifespan, significantly extending lifespan of the nematodes exposed to IR1072 compared to sham treated controls, detailed in figure 7.4 and table 7.1.

The experimental protocol 2.9.3, was conducted using 60 mm agar plates (to avoid drying) and to identify whether the effect would be maintained using an alternate treatment protocol, still utilising the SS104, *glp-4 (bn2)I*, strain. These data showed a significant increase in mean lifespan, 16%, for the nematodes exposed to IR1072 for 12 minutes, compared to sham treated controls. Figure 7.5 combines data from two individual experimental repeats, see table 7.12 for individual repeat data.

Protocol 2.9.3 was conducted using the N2, *C. elegans* wild isolate. These data show a significant increase in mean lifespan, 13%, for the nematodes exposed to IR1072 for 12 minutes, compared to sham treated controls. Figure 7.6 combines data from two individual experimental repeats, see table 7.12 for individual repeat data.

Following the discovery of a consistent increase in lifespan in SS104, *glp-4 (bn2)I,* nematodes exposed to IR1072, it was important to determine whether this longevity was due to a direct effect of IR1072 on the nematode or longevity was indirectly induced through affecting the bacterial lawn. It has previously been determined that proliferating bacteria accumulate in the gut and pharynx of nematodes as they age, having an adverse effect on lifespan. Exposure of nematodes to aminoglycosides, such as kanamycin, which limit bacterial proliferation, have previously been shown to extend nematode lifespan (Garigan *et al.*, 2002). However the role of bacterial proliferation in the limitation of nematode lifespan is debated. Other researchers demonstrate increased lifespan of *C. elegans* via manipulation of *E. coli* independently of proliferation (Virk *et al.*, 2012). Therefore it was important to determine whether IR1072 was reducing bacterial proliferation and thus increasing lifespan. In order to

investigate whether the lifespan extension was maintained in the presence of kanamycin, as described by Garigan *et al* (2002), protocol 2.9.3 was repeated using SS104, *glp-4 (bn2)I*, with kanamycin treated-OP50, as described in 2.9.6. 12 minute IR1072 exposure of nematodes in the presence of a kanamycin-treated OP50 food source resulted in a 10% extension of the mean lifespan, compared to sham treated controls, which were also exposed to kanamycin treated-OP50. Data shown in Figure 7.7, combines two lifespans analyses, for individual lifespan data, see table 7.12 (Garigan *et al.*, 2002).

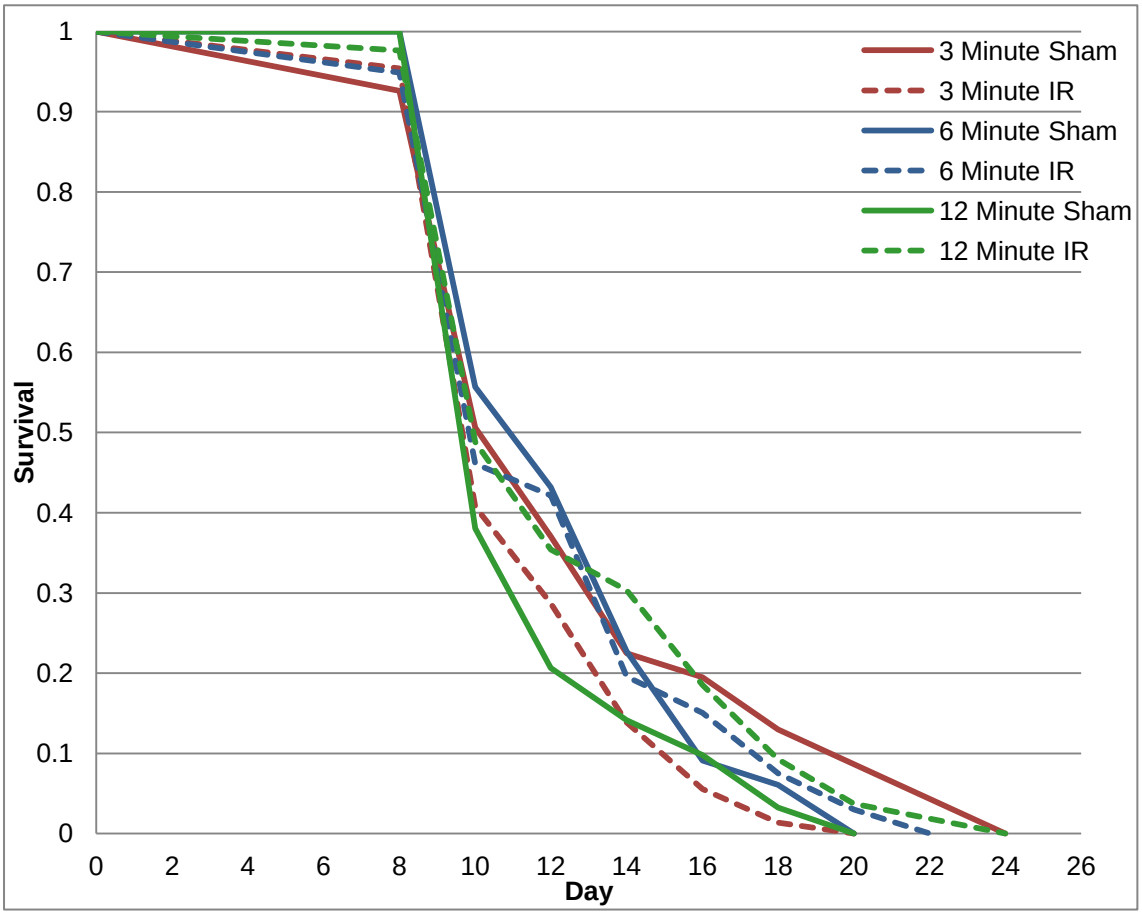

Figure 7.3. Lifespans of SS104, *glp-4 (bn2)I*, nematodes exposed to 12 minute, 6 minute or 3 minute IR1072 exposures and sham-treated controls.

	IR1072 Treatment Condition					
	3 Minute		6 Minute		12 Minute	
	Sham	IR	Sham	IR	Sham	IR
Total number of worms	81	109	90	78	93	85
Total died	66	102	86	72	92	73
Total censored	15	7	4	6	1	12
Mean	13.224	11.714	12.735	12.567	11.717	12.949
Standard Error	0.620	0.262	0.326	0.418	0.293	0.458
Log-rank	*0.035		0.989		*0.026	
Wilcoxon	0.194		0.340		0.088	

Table 7.1. All data refers to figure 7.3, all lifespans were carried out at 25°C.

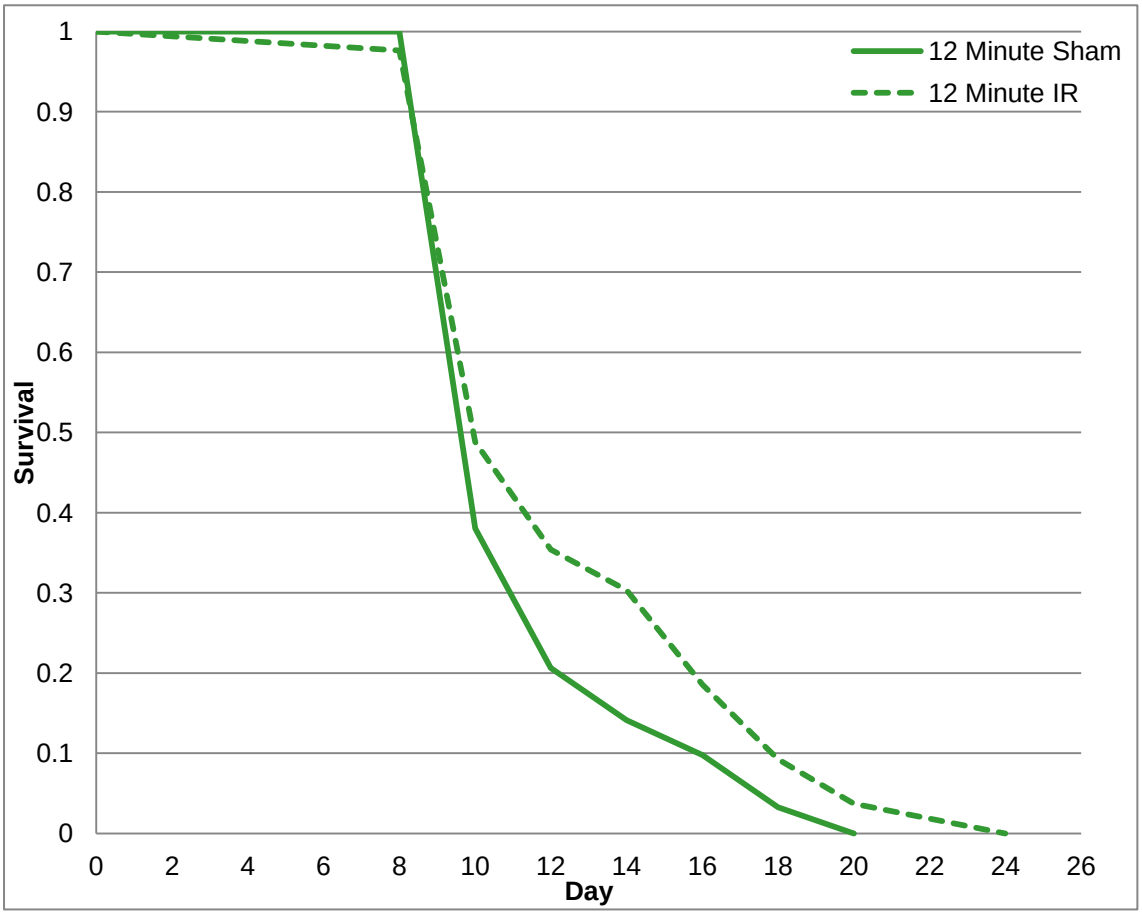

Figure 7.4. Lifespans of SS104, *glp-4 (bn2)I*, nematodes exposed to IR1072 for 12 minutes and sham-treated controls, from figure 7.3.

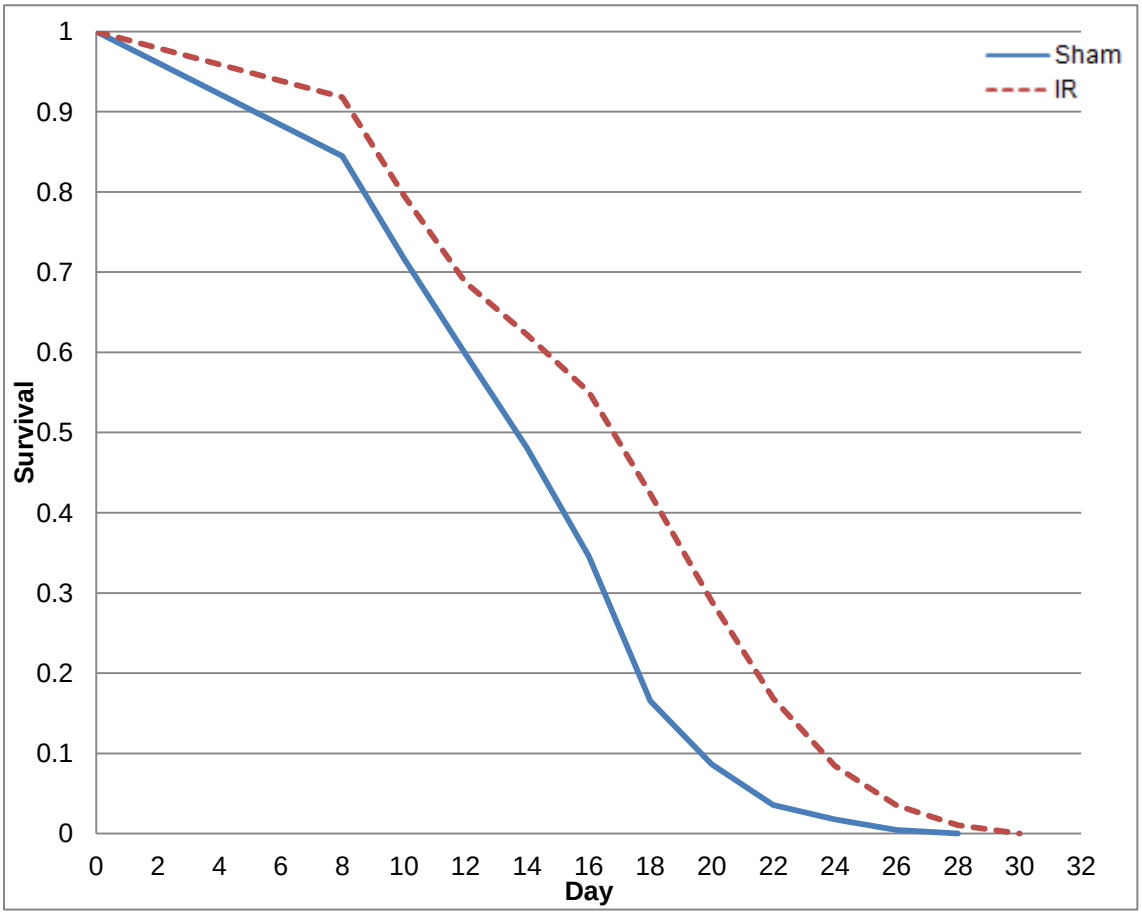

Figure 7.5. Lifespans of SS104, *glp-4 (bn2)I*, nematodes exposed to IR1072 as described in 2.9.3, and sham treated controls, n=2 repeat lifespans.

	IR1072 Treatment Condition	
	Sham	IR Exposed
Total number of worms	405	342
Total died	394	316
Total censored	11	26
Mean	14.789	17.165
Standard Error	0.234	0.311
Log-rank	*<0.001	
Wilcoxon	*<0.001	

Table 7.2. All data refers to figure 7.5, all lifespans were carried out at 25°C.

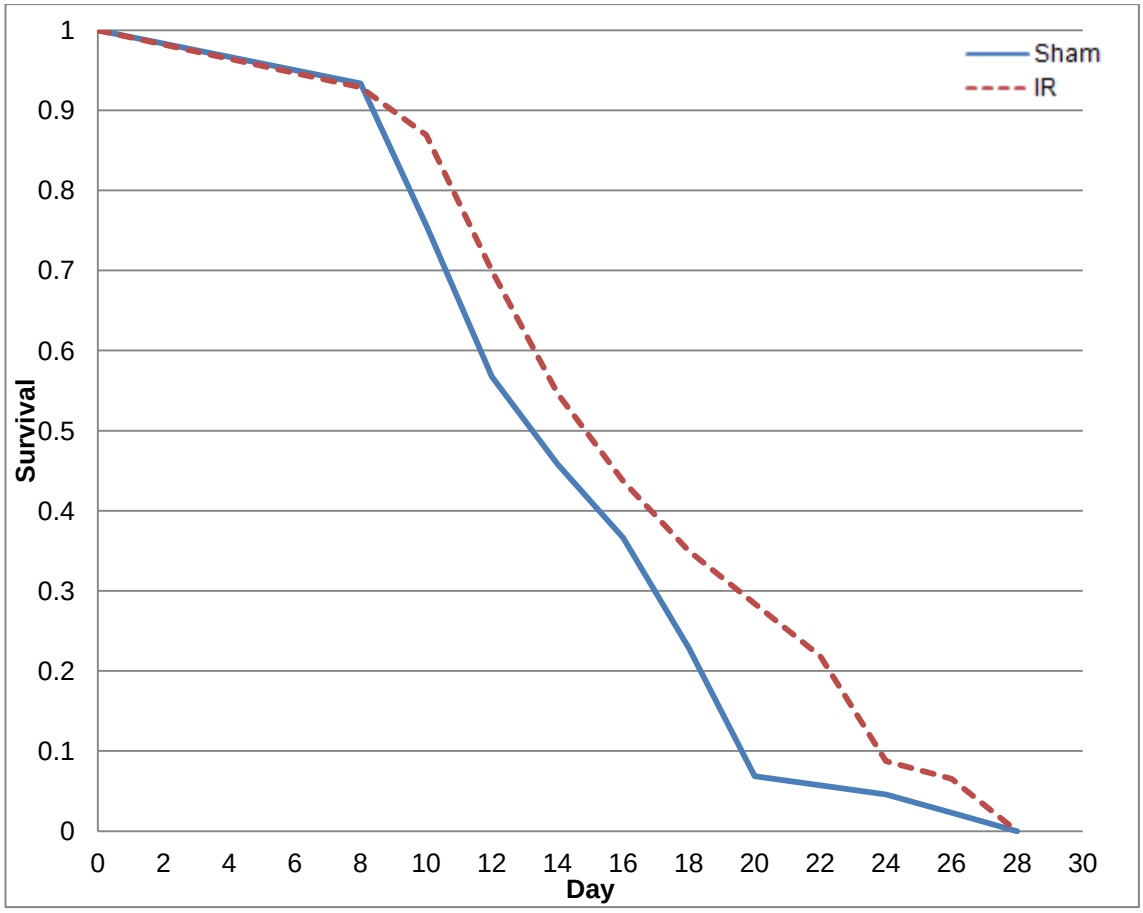

Figure 7.6. Lifespans of N2, *C. elegans* wild isolate nematodes exposed to IR1072 as described in 2.9.3, and sham treated controls.

	IR1072 Treatment Condition	
	Sham	IR Exposed
Total number of worms	90	70
Total died	51	48
Total censored	39	22
Mean	15.034	16.975
Standard Error	0.665	0.820
Log-rank	0.071	
Wilcoxon	0.176	

Table 7.3. All data refers to figure 7.6, all lifespans were carried out at 25°C.

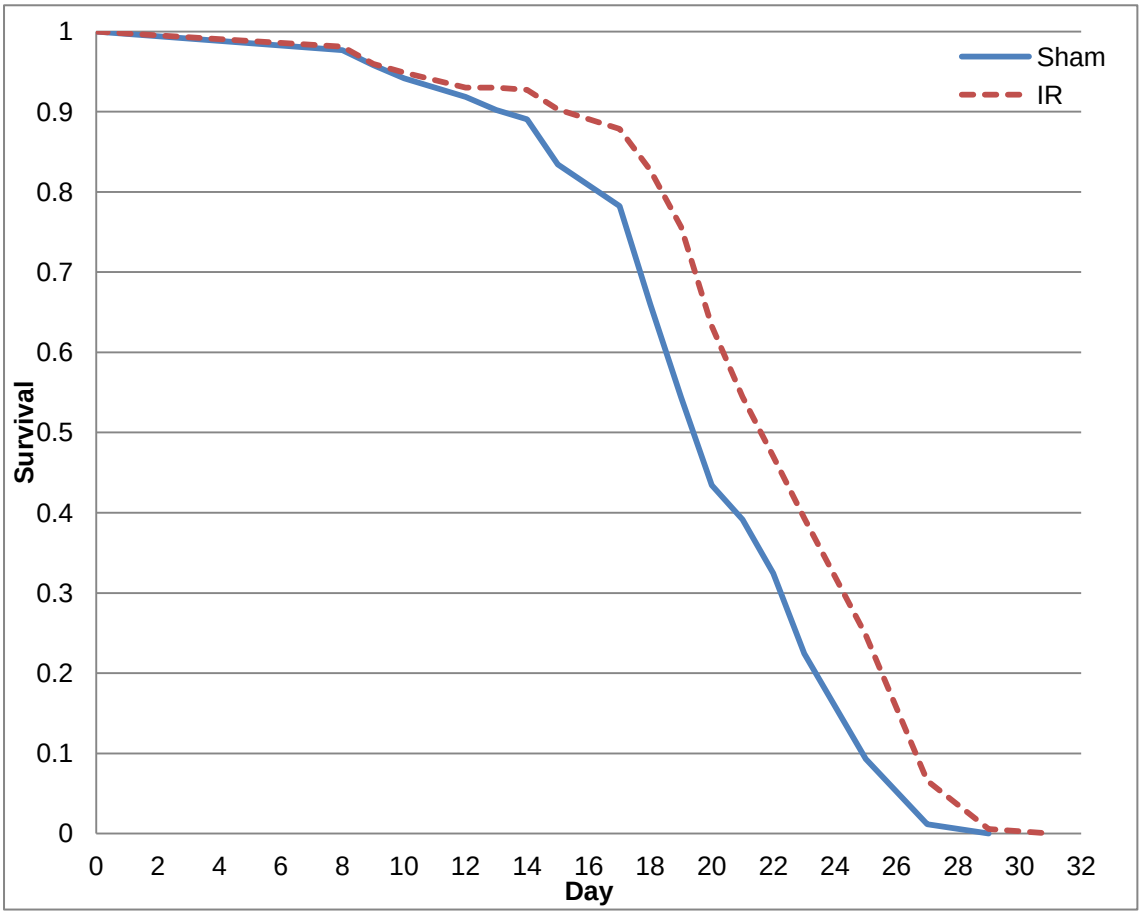

Figure 7.7. Lifespans of SS104, *glp-4 (bn2)I*, nematodes exposed to IR1072 as described in 2.9.3, and sham treated controls, conducted on kanamycin-treated OP50, n=2 repeat lifespans.

	IR1072 Treatment Condition	
	Sham	IR Exposed
Total number of worms	431	373
Total died	407	365
Total censored	24	8
Mean	19.981	21.964
Standard Error	0.228	0.256
Log-rank	*<0.001	
Wilcoxon	*<0.001	

Table 7.4. All data refers to figure 7.7, all lifespans were carried out at 25°C.

7.2.2 Bacterial Viability

Bacterial proliferation in the intestine of *C. elegans* has been suggested to be a cause of death in the nematode although this is debated, as detailed previously (Garigan *et al.*, 2002, Virk *et al.*, 2012). Therefore, in order to determine whether IR1072 was effecting bacterial proliferation and resulting in increased longevity, the viability of OP50 was determined following IR1072 exposure, with kanamycin acting as a positive control. The method followed was described as in 2.9.1 and 2.9.2.

Control plates showed no significant difference in quantity of colony forming units (CFUs) ($x10^8$) (n=12, 19.730 ± 0.775) compared to IR-treated plates (n=12, 19.650 ± 0.425). However, kanamycin-treated plates showed a significant reduction in the quantity of CFUs (n=12, 15.330 ± 0.609, ***p<0.001) compared to both control and IR treated plates.

CFUs were analysed using a one-way ANOVA with a Bonferroni's multiple comparison post test. Data shown represents mean ± SEM.

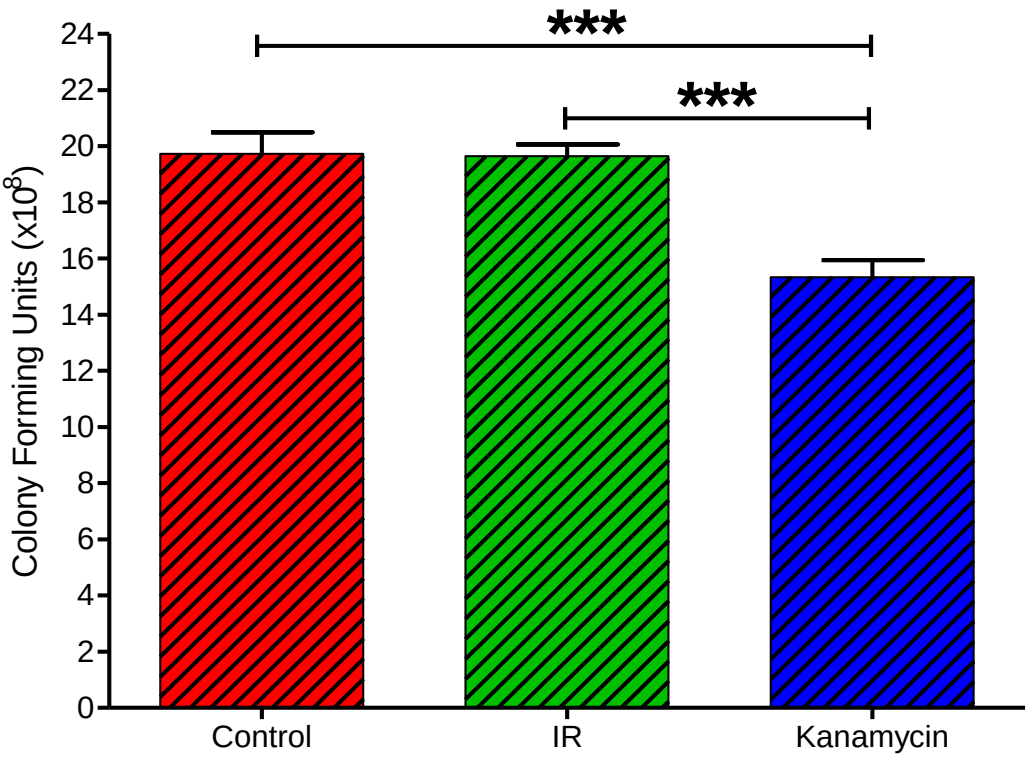

Figure 7.8. A column graph to show IR1072 exposure has no significant effect on bacterial viability. Mean values ± SEM. A significant reduction in viability was found for kanamycin – treated bacteria (***p<0.001) compared to control and IR1072 treated bacteria. All other comparisons were non-significant.

7.2.3 Alternate Exposure Protocol

An important potential theory for lifespan extension for *C. elegans,* which warranted further investigation, was the concept that repeated mild heat treatments may be the cause of increased longevity. Despite lifespans being conducted in temperature controlled incubators, it was possible that the heating of the LED array during 12 minute exposures would cause mild heating of the nematodes. Repeated mild heat stress in has been reported to result in a significant extension of lifespan in *C. elegans* (Leitz *et al.*, 2002, Lithgow *et al.*, 1995, Wu *et al.*, 2009), with particular extension when exposed at L4 stage (Olsen *et al.*, 2006a). Work by Olsen, 2006, identified that temperature shifting nematodes for several hours on consecutive days significantly increased their lifespan, utilising two strains with GFP-tagged promoters of heat shock proteins heat stress was shown to increase the activity of these promoters (Olsen *et al.*, 2006a). Small temperature rises, as little as 2.5 °C, using microwaves, have also been reported to induce expression of heat shock proteins. Rises from 25 to 27.5°C have been shown to directly result in induction of HSP16 expression, although the mechanism of this action has been shown to be complex (Dawe *et al.*, 2006) and the power ratings the nematodes were exposed to are up to fifty times greater (Leitz *et al.*, 2002) than the beneficial range established for infrared light (Hamblin and Demidova, 2006).

In order to investigate this theory, a thermocouple (copper/copper-nickel, type T. Detailed within appendix II) was used to measure temperature change in agar plates before, during and after the 12 minute exposure period. It was found that a 3°C change in temperature occurred during this time, as shown in figure 7.9. The standard fitted cooling fans were sufficient to maintain temperature for

approximately six minutes, but after this time the temperature of the equipment was not able to be sufficiently counteracted by the fans. Therefore a third treatment protocol was started.

It was decided that in order to remove any potential for the increased lifespan to be due to temperature, the exposure timings required changing. Via the use of the thermocouple, several short treatment times were investigated which would reduce the time the equipment was on, eliminating heating. In order to perform this change in protocol, more sophisticated methods of altering the timings of the LED array were required. Previous work had utilised timer plugs, however at this point a computer programme was written using LabVIEW™ (National Instruments, Texas, USA) which enabled control of on/off cycle of the array using a USB-controlled relay interface (Phidgets, Inc. USA) in conjunction with the set-up of a permanent thermocouple within the temperature controlled incubator. The LabVIEW™ programme was also configured to measure the electrical current across the thermocouple every second. This enabled the internal temperature of the agar plates to be continually monitored. Utilising this technology, multiple short cycle timings could be easily investigated and manipulated. Many timing ratios were investigated to identify timings which did not result in a measurable change in temperature during the ‘on’ period of the LED array, a number of these timings are shown in figures 7.9 – 7.13. However as is evident in the figures, many of these resulted in considerable rises in temperature. Shorter timing periods were investigated that did not cause a recordable rise in temperature. However, when a number of these were carried forward to lifespan protocol; the longevity effect was not always maintained, an example shown in figure 7.12, with the lifespan data from this protocol shown in

figure 7.14 and summarised in table 7.5. Ultimately, the protocol outlined in 2.9.4 was established, the thermocouple recording from which is shown in figure 7.13.

The treatment protocol was followed as described in 2.9.4 and conducted at 25°C.

All lifespans were analysed as described in 2.9.5. Utilising the Kaplan-Meier survival model, with statistical significance determined using Log-Rank and Wilcoxon analysis.

Chronic IR1072 exposure on SS104, *glp-4 (bn2)I*, resulted in a 12% increase in lifespan, compared to sham-treated controls, n=3 individual lifespan experiments, figure 7.15 shows pooled data. Statistical analysis is shown in table 7.6, data is summarised in table 7.12. Therefore it was established that the new exposure protocol maintained the increased longevity previously observed, however in a moderately weaker form.

In order to understand the pathways through which the lifespan effect was occurring several mutants were investigated. As previously mentioned, mutations in the insulin/insulin-like growth factor pathway extend lifespan but functional DAF-16 is required for that effect (Lee *et al.*, 2003). Therefore to determine whether the IR1072-induce longevity occurred via a DAF-16 dependent pathway, lifespans were conducted with a *daf-16* mutant nematode. Chronic IR1072 exposure on GR1307, *daf-16 (mgDf50) I*, had no significant effect on lifespan compared to sham-treated controls, n=2 individual lifespan experiments, figure 7.16 shows pooled data. Statistical analysis is shown in table 7.7., data is summarised in table 7.12.

As the lifespan effect appeared to be dependent on functional DAF-16, it was decided to investigate one of the major downstream effectors of DAF-16, HSF1. This enabled investigation of more specific proteins required for the IR1072-induced increase in longevity. Lifespan studies were conducted using a strain with mutated *hsf-1*. Chronic IR1072 exposure on PS3551, *hsf-1(sy441) I*, had no significant effect on lifespan compared to sham-treated controls, data shown in figure 7.17. Statistical analysis is shown in table 7.8 and table 7.12.

Despite the *C. elegans* expressing a number of homologues to mammalian chaperones, it is not possible to investigate the specific roles of a number of these proteins as knockout of the genes proves lethal. The nematode equivalent to mammalian HSP70, HSP3, however was able to be investigated and is a protein of interest considering its significant role in a number of important homeostasis processes and the identification of it's consistent upregulation following IR1072 exposure in murine studies. Chronic IR1072 exposure on RB1104, *hsp-3 (ok1083) X*, had no significant effect on lifespan compared to sham-treated controls, n=3 individual lifespan experiments, figure 7.18 shows pooled data. Statistical analysis is shown in table 7.9., data is summarised in table 7.12.

Chronic IR1072 exposure on N2, *C. elegans* wild isolate, resulted in a 10% increase in lifespan compared to sham-treated controls, n=2 individual lifespan experiments, figure 7.19 shows pooled data. Statistical analysis is shown in table 7.10., data is summarised in table 7.12.

Previously it has been discussed that the primary photoacceptor for infrared light lies within the mitochondria. Therefore it was decided to investigate

whether IR1072 exposure was damaging to the nematode mitochondria. A mutant strain was investigated which expressed HSP6 under a GFP promoter. HSP6 is a mitochondrial specific heat shock protein expressed at the onset damaging mitochondrial stress (Benedetti *et al.*, 2006). Chronic IR1072 exposure on SJ4100 [*zcIs13 hsp-6::gfp]*, resulted in an 8% increase in lifespan compared to sham-treated controls, but no change in GFP expression (data not shown). Lifespan shown in figure 7.20 shows, statistical analysis is shown in table 7.11., data is summarised in table 7.12.

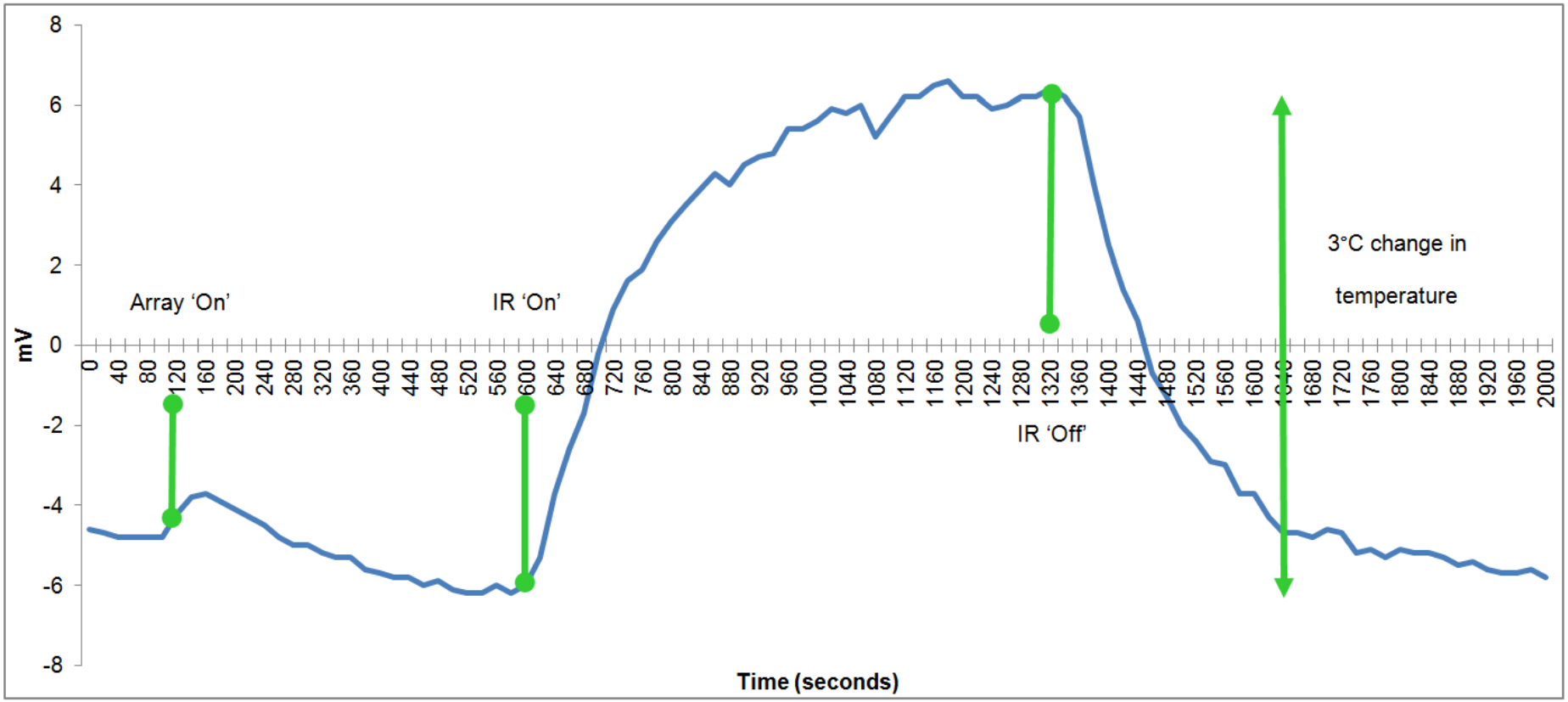

Figure 7.9. Data shown represent change in voltage during 12 minute IR1072 exposure. Change in voltage was measured by placing a type T thermocouple (copper vs. copper-nickel) on the surface of an agar plate. Temperature change was calculated using reference table shown in appendix II. This reference table was used for all calculations relating to determination of temperature change during IR exposure.

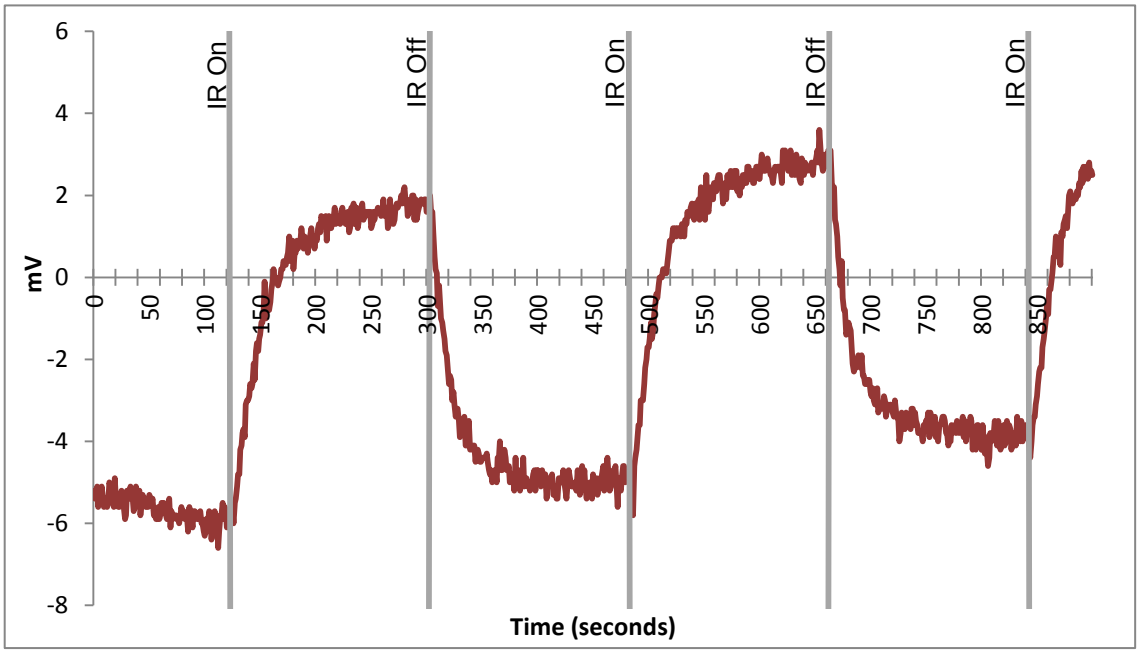

Figure 7.10. Data shown to represent the temperature change found when investigating a novel IR1072 protocol. Data shown is three minutes on, followed by three minutes off. This resulted in a 2°C change in temperature.

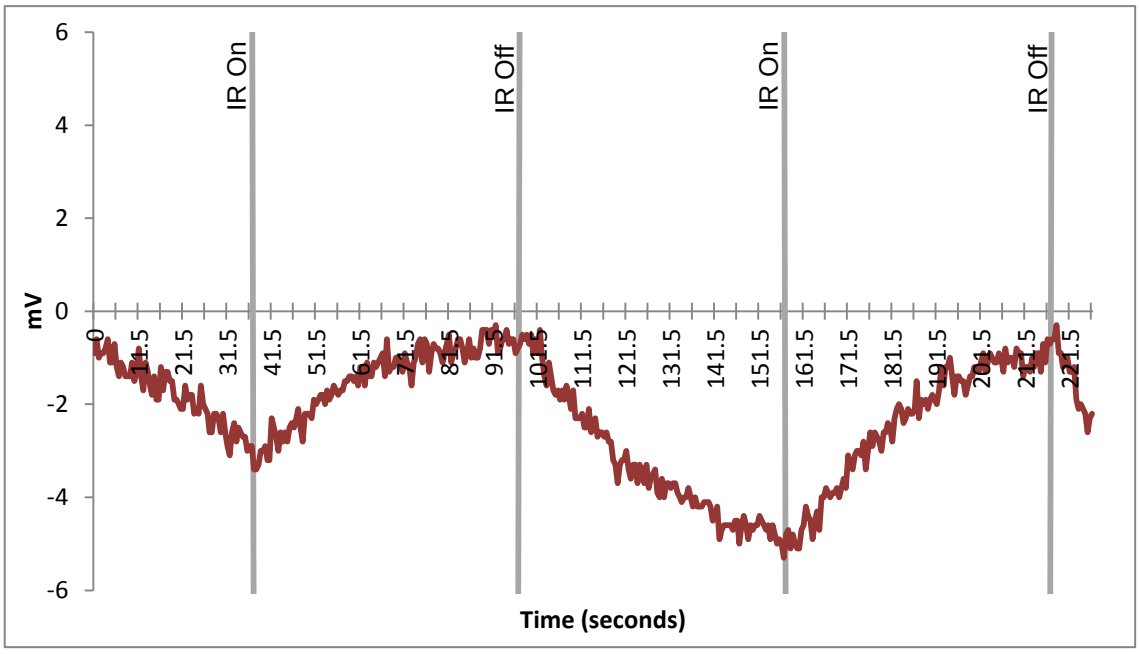

Figure 7.11. Data shown to represent the temperature change found when investigating a novel IR1072 protocol. Data shown is one minute on, followed by one minute off. This resulted in a change in temperature of approximately 0.5°C.

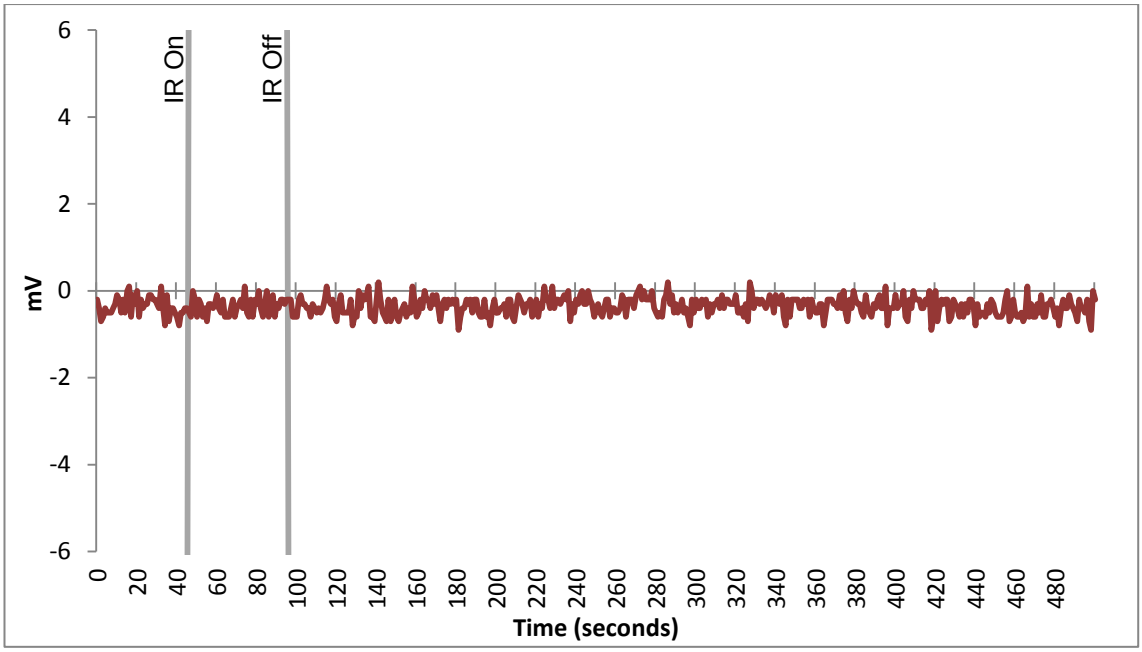

Figure 7.12. Data shown is fifty seconds on, followed by 750 seconds off. This resulted in no change in temperature and the lifespan extension effect previously observed was eliminated, as shown in figure 7.14 and table 7.5.

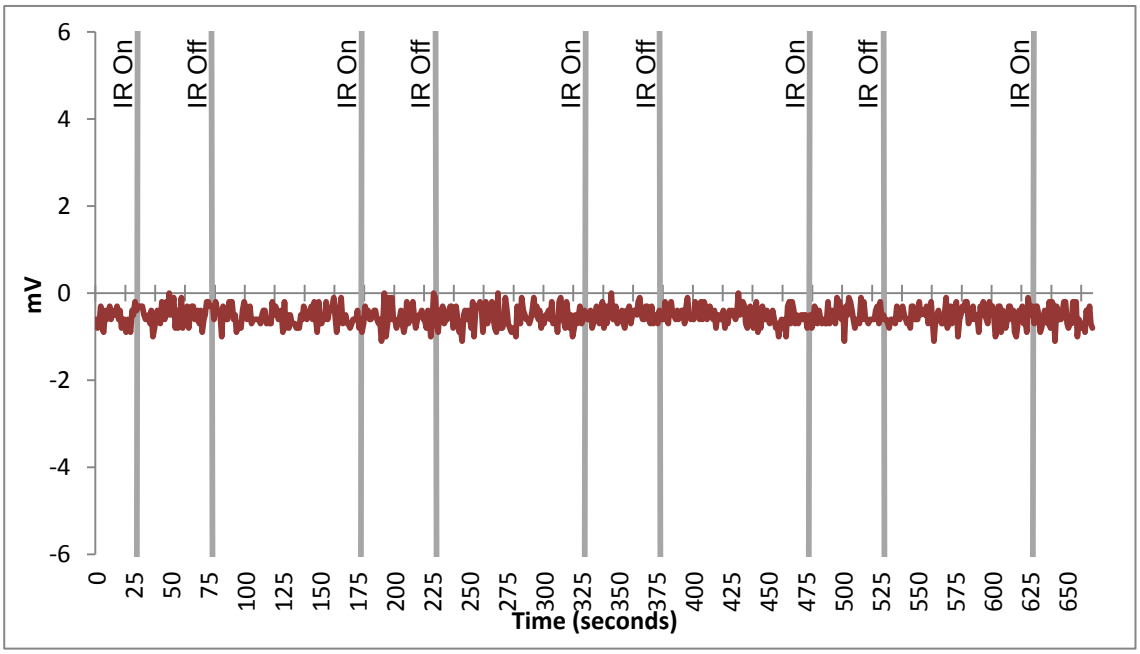

Figure 7.13. Data shown represents measurements taken during a protocol whereby infrared 1072 nm was on for 50 seconds and off for 100 seconds. This was carried through to become treatment protocol 2.9.4.

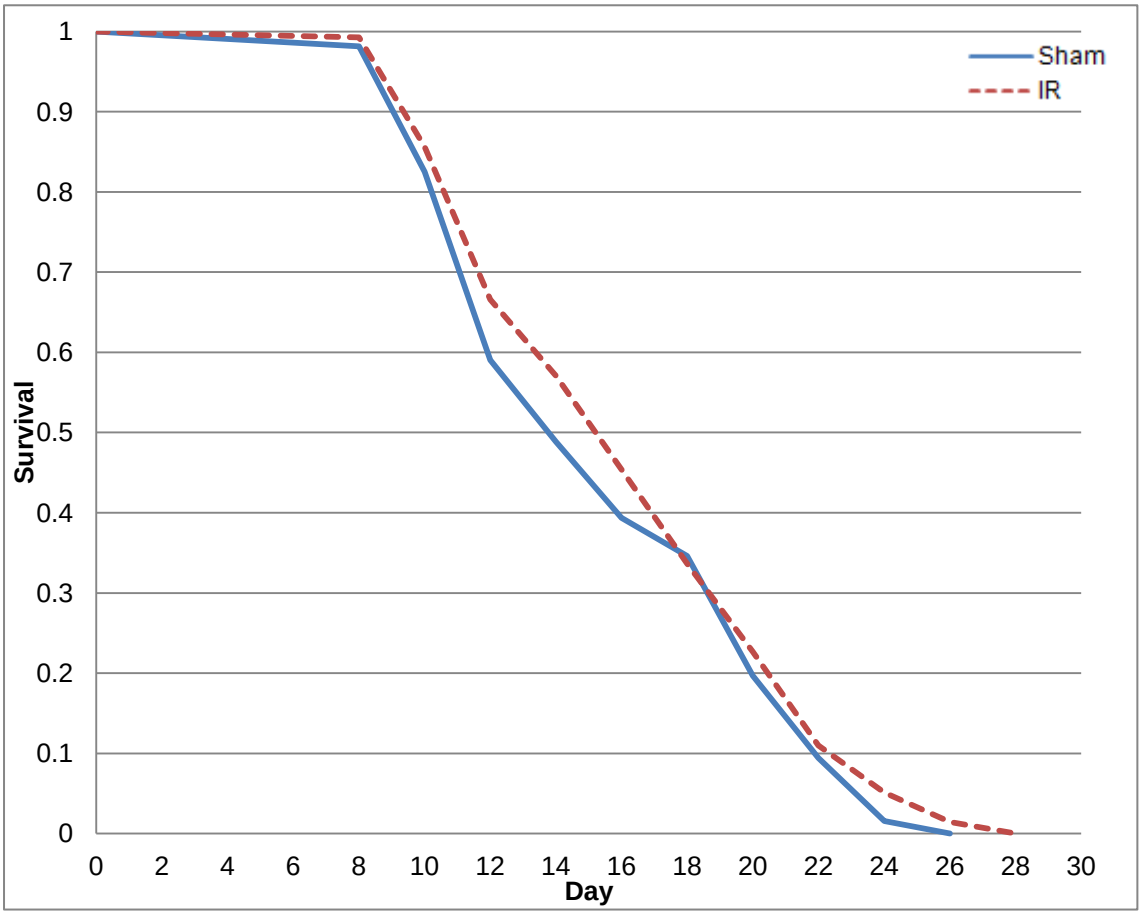

Figure 7.14. Lifespan conducted using SS104, *glp-4 (bn2)I* nematodes. Treatment protocol used: 50 seconds IR1072 on, followed by 750 seconds off. This was repeated over 24 hours, every three days.

	IR1072 Treatment Condition	
	Sham	IR Exposed
Total number of worms	162	141
Total died	146	137
Total censored	16	4
Mean	15.865	16.557
Standard Error	0.393	0.423
Log-rank	0.239	
Wilcoxon	0.237	

Table 7.5. All Data refers to figure 7.14, all lifespans were carried out at 25°C.

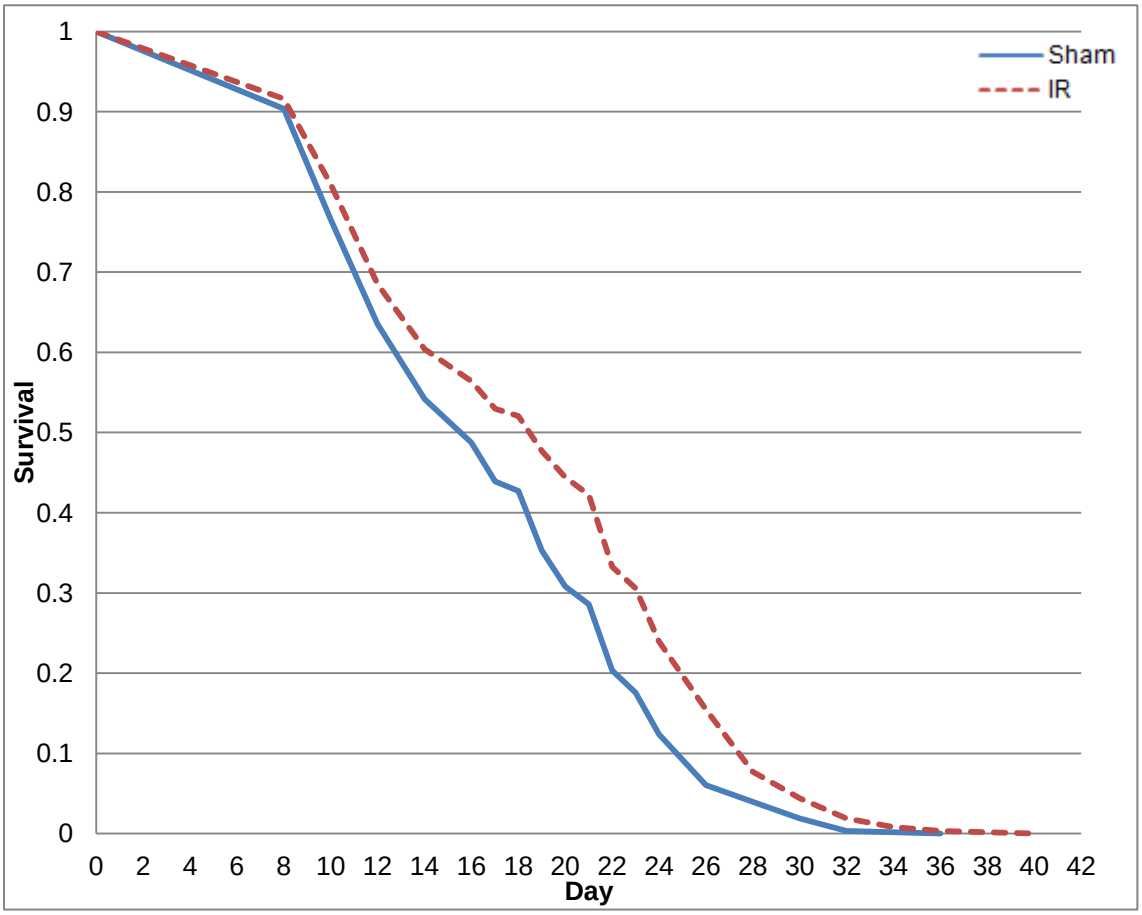

Figure 7.15. A graph to show the effect of treatment protocol 2.9.4 on SS104, *glp-4 (bn2)I*, nematode lifespan compared to sham-treated controls, n=3 repeat lifespans.

	IR1072 Treatment Condition	
	Sham	IR Exposed
Total number of worms	710	730
Total died	645	665
Total censored	65	64
Mean	16.818	18.752
Standard Error	0.248	0.282
Log-rank	*<0.001	
Wilcoxon	*<0.001	

Table 7.6. All data refers to figure 7.15, all lifespans were carried out at 25°C.

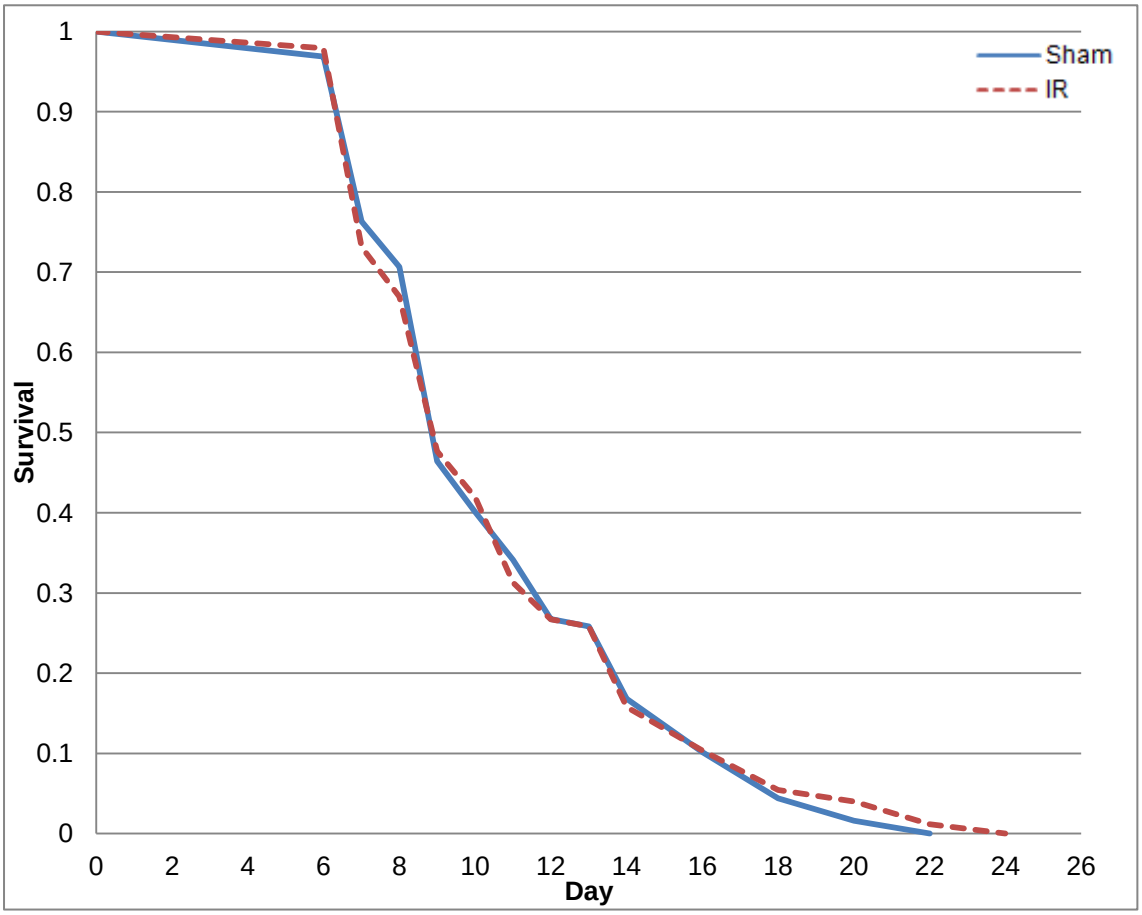

Figure 7.16. A graph to show the effect of treatment protocol 2.9.4 on GR1307, *daf-16 (mgDf50) I*, nematode lifespan compared to sham-treated controls, n=2 repeat lifespans.

	IR1072 Treatment Condition	
	Sham	IR Exposed
Total number of worms	510	431
Total died	447	365
Total censored	63	66
Mean	10.829	10.848
Standard Error	0.183	0.215
Log-rank	0.833	
Wilcoxon	0.644	

Table 7.7. All data refers to figure 7.16, all lifespans were carried out at 25°C.

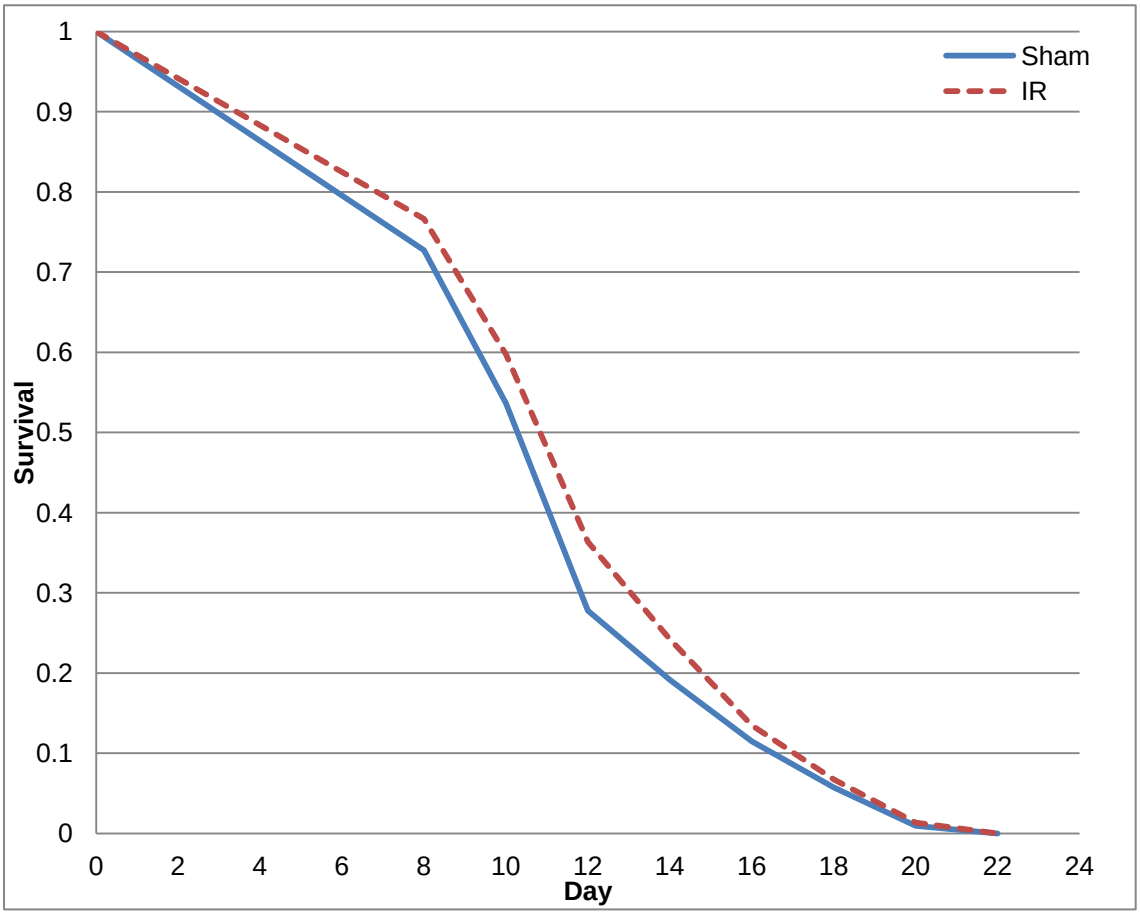

Figure 7.17. A graph to show the effect of treatment protocol 2.9.4 on PS3551, *hsf-1(sy441) I*, nematode lifespan compared to sham-treated controls.

	IR1072 Treatment Condition	
	Sham	IR Exposed
Total number of worms	110	77
Total died	107	76
Total censored	3	1
Mean	11.830	12.370
Standard Error	0.350	0.430
Log-rank	0.366	
Wilcoxon	0.304	

Table 7.8. All data refers to figure 7.17, all lifespans were carried out at 25°C.

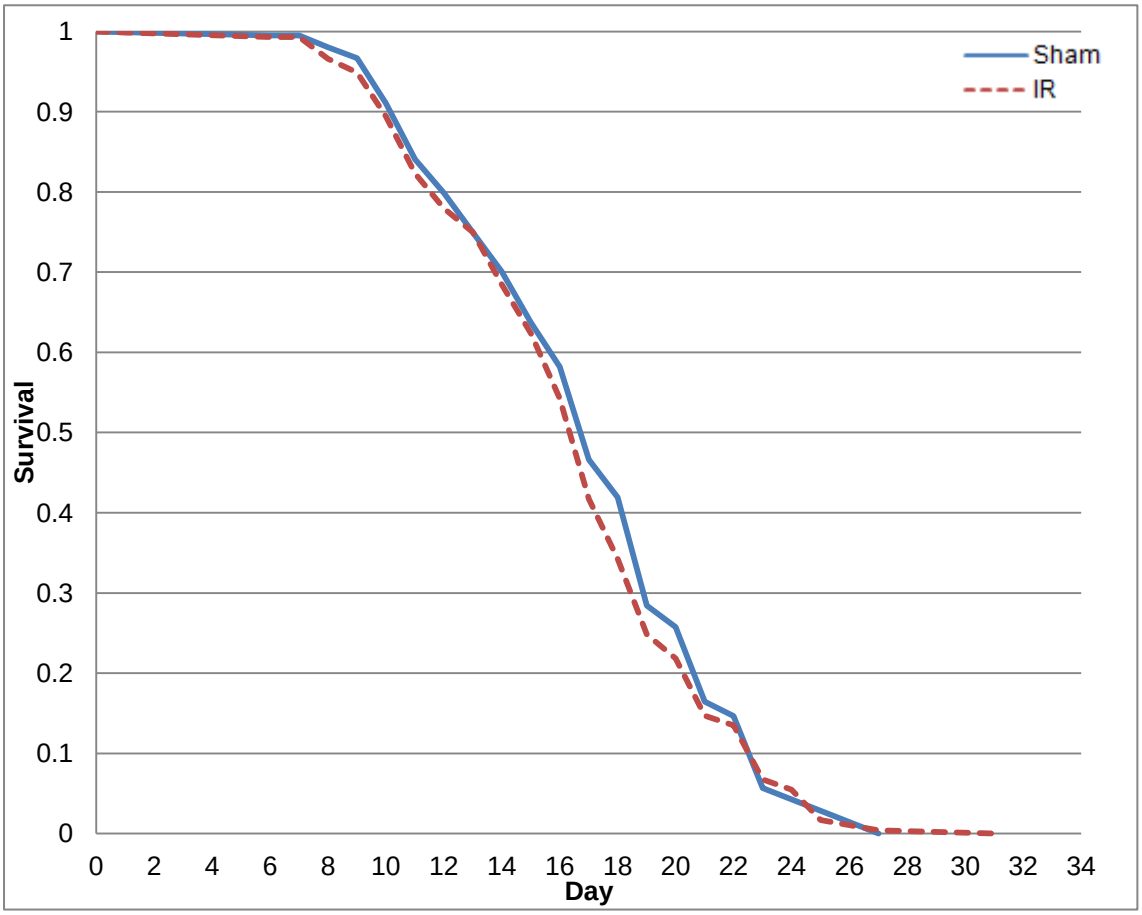

Figure 7.18. A graph to show the effect of treatment protocol 2.9.4 on RB1104, *hsp-3 (ok1083) X*, nematode lifespan compared to sham-treated controls, n=3 repeat lifespans.

	IR1072 Treatment Condition	
	Sham	IR Exposed
Total number of worms	599	441
Total died	364	279
Total censored	235	162
Mean	17.066	16.681
Standard Error	0.229	0.267
Log-rank	0.242	
Wilcoxon	0.206	

Table 7.9. All data refers to figure 7.18, all lifespans were carried out at 25°C.

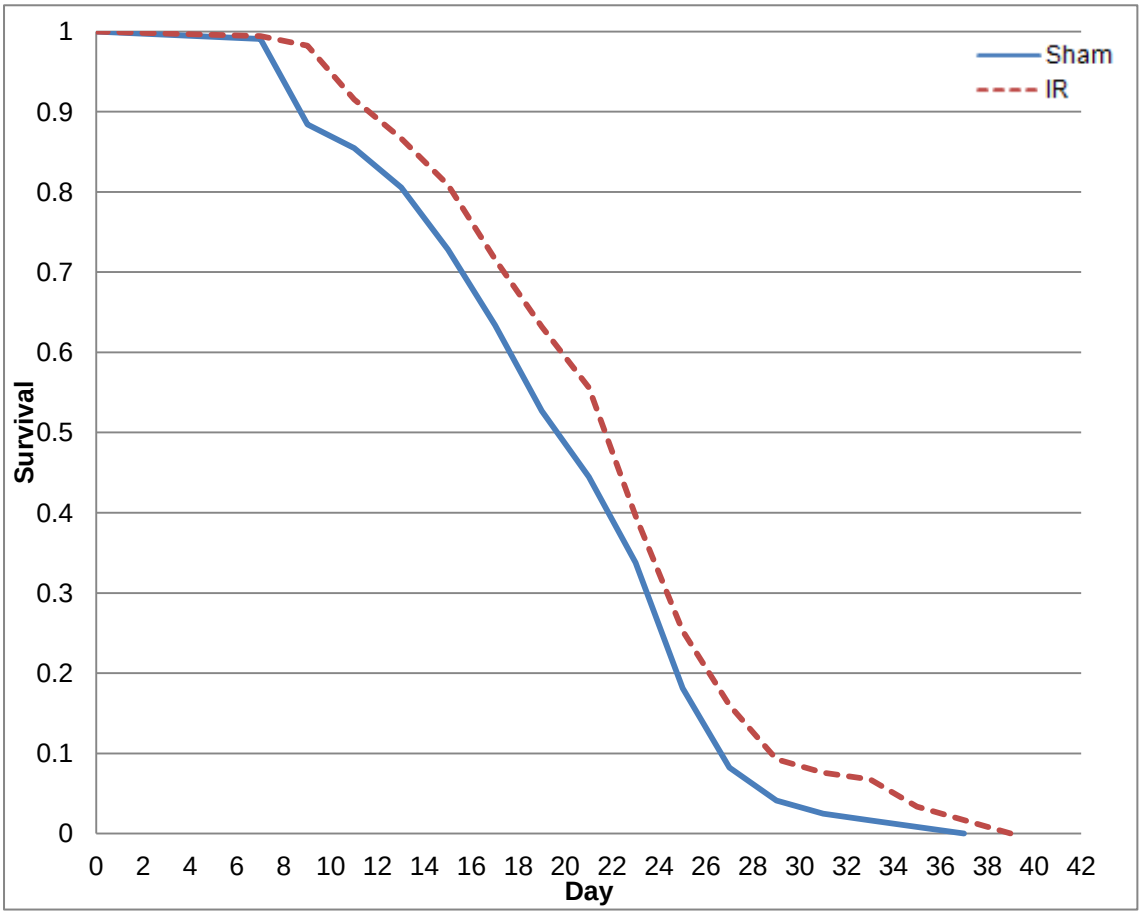

Figure 7.19. A graph to show the effect of treatment protocol 2.9.4 on N2, *C. elegans* wild isolate nematode, lifespan compared to sham-treated controls, n=2 repeat lifespans.

	IR1072 Treatment Condition	
	Sham	IR Exposed
Total number of worms	462	382
Total died	335	271
Total censored	137	111
Mean	20.136	22.167
Standard Error	0.541	0.610
Log-rank	*0.012	
Wilcoxon	*0.010	

Table 7.10. All data refers to figure 7.19, all lifespans were carried out at 25°C.

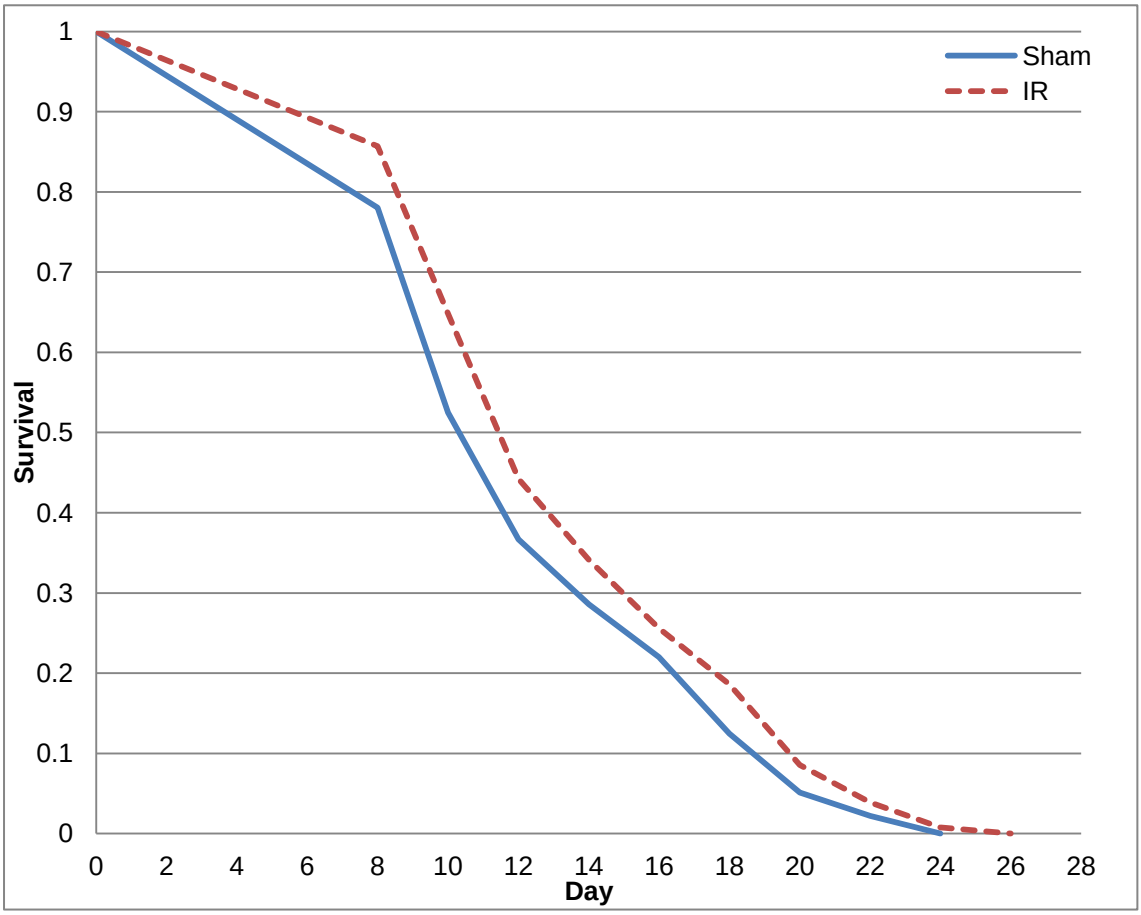

Figure 7.20. A graph to show the effect of treatment protocol 2.9.3 on SJ4100, [*zcIs13 hsp-6::gfp]*, nematode lifespan compared to sham-treated controls.

	IR1072 Treatment Condition	
	Sham	IR Exposed
Total number of worms	164	161
Total died	145	136
Total censored	19	25
Mean	12.753	13.727
Standard Error	0.365	0.395
Log-rank	0.056	
Wilcoxon	*0.033	

Table 7.11. All data refers to figure 7.20, all lifespans were carried out at 25°C.

Table 7.12. A summary table of individual nematode lifespans with are combined in the figures included in Chapter 7: Using *Caenorhabditis elegans* to Understand IR1072. Abbreviations: KAN, kanamycin.

Strain	IR1072 Protocol	IR1072 or Sham	Mean Lifespan (days)	Total (n=)	Dead (n=)	Censor (n=)	% Lifespan Increase	Statistical Analysis		Figure
								Log-Rank	Wilcoxon	
SS104, *glp-4 (bn2)I*	3 mins	Sham	13.224	81	66	15	-	*0.035	0.194	7.4
		IR	11.714	109	102	7				
	6 mins	Sham	12.735	90	86	4	-	0.989	0.340	7.3
		IR	12.567	78	72	6				
	12 mins	Sham	11.717	93	92	1	11	*0.026	0.088	
		IR	12.949	85	73	12				
	2.9.3 (12 mins)	Sham	14.319	211	206	5	11	*<0.001	*0.002	7.5
		IR	15.865	190	188	2				
		Sham	15.297	194	188	6	24	*<0.001	*<0.001	
		IR	18.888	152	128	24				
	2.9.3 + KAN	Sham	19.346	205	195	10	11	*<0.001	*<0.001	7.7
		IR	21.386	161	155	6				
		Sham	20.558	226	209	17	9	*<0.001	*<0.001	
		IR	22.395	212	210	2				
N2, wild type isolate	2.9.3	Sham	15.034	90	51	39	13	0.072	0.176	7.6
		IR	16.975	70	48	32				

SS104, *glp-4 (bn2)I*	2.9.4 (50 seconds on, 100 off)	Sham	16.464	155	147	8	13	*<0.001	*0.003	7.15
		IR	18.671	200	162	38				
		Sham	17.937	318	277	41	8	*0.008	*0.020	
		IR	19.446	281	270	11				
		Sham	16.119	237	233	4	12	*<0.001	*0.004	
		IR	18.081	252	217	35				
GR1307, *daf-16 (mgDf50)*	2.9.4	Sham	8.559	262	237	25	-	0.323	0.692	7.16
		IR	8.705	257	214	43				
		Sham	13.322	248	210	38	-	0.247	0.654	
		IR	13.658	174	151	23				
PS3551, *hsf-1(sy441) I*	2.9.4	Sham	11.830	110	107	3	-	0.366	0.304	7.17
		IR	12.370	77	76	1				
RB1104, *hsp-3 (ok1083) X*	2.9.4	Sham	14.667	157	119	38	-	0.531	0.812	7.18
		IR	14.931	156	116	40				
		Sham	17.057	238	141	97	-	0.776	0.937	
		IR	17.056	173	106	67				
		Sham	19.342	204	104	100	-	0.884	0.272	
		IR	19.029	112	57	55				
N2, wild type isolate	2.9.4	Sham	20.136	213	133	80	10	*0.012	*0.010	7.19
		IR	22.167	178	121	57				
		Sham	19.684	259	202	57	10	*0.012	*0.010	
		IR	21.588	204	150	54				
SJ4100, [*zcIs 13 hsp-6::gfp]*,	2.9.4	Sham	12.753	164	145	19	8	0.056	*0.033	7.20
		IR	13.727	161	136	25				

7.2.4 Absorption Spectra of Nematode Protein Extracts

Nematode extracts were prepared as described in 2.11, and a Lowry assay performed (see 2.3.1). Each sample was then diluted to 1 mg/ml. The absorbance spectrum of both soluble protein (supernatant) and insoluble protein (pellet) was measured using a Shimadzu spectrophotometer from 1500 nm to 600 nm.

Each sample was measured three times and the average absorbance (after correction for baseline values) is plotted in figure 7.21. The shaded area in the figure refers to the wavelength of light emitted by the 1072 nm LEDs, which have a bandwidth of 25 nm.

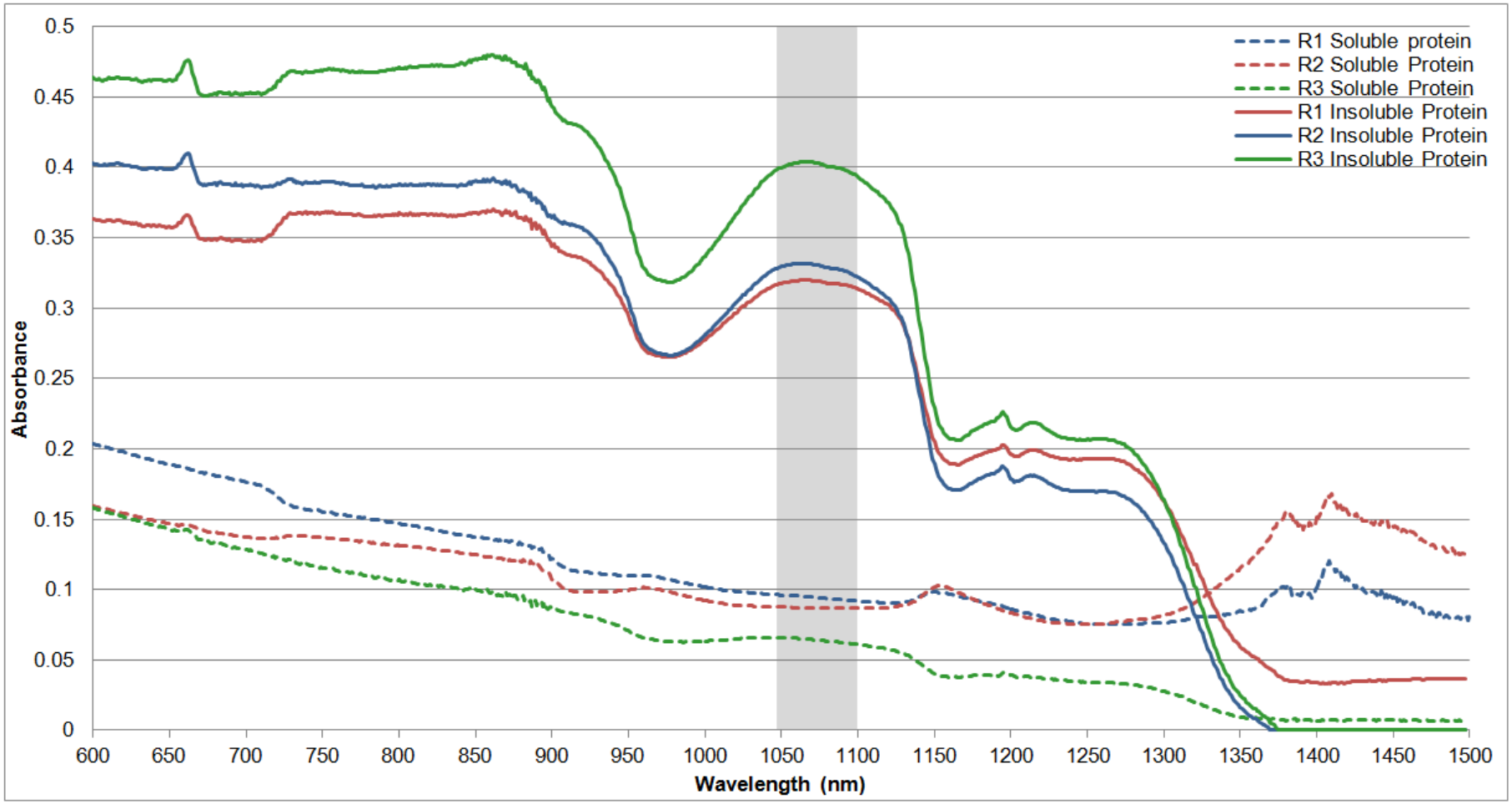

Figure 7.21. Absorption spectra of soluble (dashed lines) and insoluble (solid lines) protein extract from SS104, *glp-4 (bn2)I,* nematodes. The shaded area represents the bandwidth of LEDs used for IR1072 exposure, R refers to repeat number.

7.3 Discussion

The aim of this chapter was to determine whether IR1072 has an effect on the lifespan on *C. elegans* and if this occurred, to utilise this model system to identify proteins/pathways involved in any lifespan effect.

These experiments have established that IR1072 exposure of *C. elegans* is able to extend lifespan significantly utilising a range of exposure times. Initial experiments, where nematodes were treated every day for 12 minutes over the duration of their adult lifespan, was altered to exposure every four hours for 24 hours, repeated every three days for their adult lifespan; in order to determine whether the observed increase in lifespan could be augmented by more frequent exposures, which was found to be the case with mean lifespan increasing from 11% to 16%. Due to limited equipment availability, repeating exposures every three days also allowed for additional lifespans to be conducted alongside each other.

It is important to note that lifespan analyses utilising the Kaplan-Meier survival model employ two statistical tests; Log-rank and Wilcoxon. These tests bias differences that occur during the survival curve in different manners. The Log-rank analysis weights differences that occur at the start and end of the survival curve equally. However, the Wilcoxon analysis, concentrates on the number of nematodes at risk and weights changes that occur at the start of the survival curve higher than those that occur later on in the survival curve (Allison, 2010). Therefore upon analysis of survival data, it is interesting to note that the degree of significance for some lifespans alters when the Log-rank and Wilcoxon statistics are compared. The lifespans, initial 12 minute and three minute IR

exposures, figure 7.3 and 7.4, are both significant ($p<0.05$) for Log-rank analysis but show trends toward or no significant difference between sham and IR exposed groups when subject to Wilcoxon analysis. Therefore, this suggests that the initial few exposures of IR1072 are not sufficient to significantly reduce the number of individuals which die at the start of the lifespan but when accounting for the entire lifespan, the number of individuals surviving throughout is significantly greater in the IR exposed condition. In the lifespans that were conducted following these initial exposures, the Log-rank and Wilcoxon analyses were both significant, this suggest that the repeated nature of protocol 2.9.4 (50 seconds on, 100 seconds off over 24 hours, repeated every three days) is now sufficient to start increasing the lifespan of the nematodes at risk after the first sets of exposures.

It would of interest to investigate whether a single 24 hour exposure set had any impact on total lifespan and whether this single set is sufficient to induce a steady shift toward increased longevity in *C. elegans*. The fact that the majority of lifespan data displayed highly significant increases in longevity in the IR1072 exposed condition, when examining both the Log-rank and Wilcoxon statistics, repeated, frequent exposures are more effective at increasing lifespan.

Investigations using kanamycin-treated OP50 bacteria in conjunction with exposure to IR1072 have shown that the lifespan extension effect of IR1072 is maintained in the presence of kanamycin and IR1072 exposure had no effect on bacterial proliferation, shown in figure 7.7 and 7.8 respectively. It was therefore determined that the mechanism of action is most likely to occur directly via NIR interaction with the nematode directly, rather than extend the nematode lifespan via its food source. Verification of this could be achieved

through recording pharyngeal pumping rates of sham and IR exposed animals as stresses have been shown to reduce pumping rates, causing dietary restriction and then increased longevity (Jones and Candido, 1999).

As detailed in figure 7.9, 12 minute exposure to IR1072 resulted in a 3°C rise in temperature in the incubator during this period. As mentioned previously, repeated mild heat stress has been reported to extend the lifespan of the nematode *C. elegans* (Leitz *et al.*, 2002, Olsen *et al.*, 2006a). Therefore to investigate whether this rise in temperature was sufficient to induce expression of chaperone proteins, namely HSP16.2 (αB crystallin homologue), a mutant nematode strain with this protein GFP-tagged was used. HSP16 family members have been reported to be expressed following temperatures rises of 2.5°C from 25°C (Dawe *et al.*, 2006) and as HSPs have been shown to be manipulated by IR1072 in murine model systems that have been irradiated in this investigation, it was of interest to examine whether heating may be responsible for the induced lifespan extension effect.

Strains utilised in the Olsen, 2006, study, CL2070, *dvIs70 [hsp-16.2::gfp; rol-6(su1006)],* which expresses HSP16.2 via a GFP-tagged promoter, and SJ4005, *zcIs4 (hsp-4::GFP),* which expresses HSP4, also via a GFP-tagged promoter, were exposed to IR1072 using the same protocol as describe in 2.9.4 for 12 days and GFP-levels regularly monitored by eye, utilising a Leica Model MZ9.5 with the appropriate filter, no increase in GFP expression was observed in either strain following IR1072 (data not shown). This strain was chosen because HSP4 is a homologue to GRP78; a member of the HSP70 family which is localised to the endoplasmic reticulum, its expression would be expected following the onset of the unfolded protein response. The lack of GFP-HSP4

expression following IR1072 exposure suggests that exposure is not stress inducing. The SJ4100, [*zcIs13 hsp-6::gfp*], strain were used in lifespan experiments, HSP6 is expressed specially following mitochondrial stress and governs the mitochondrial-specific unfolded protein response. The lack of observable GFP-HSP6 expression in this strain suggests that IR1072 is not causing stress to the mitochondria and a lifespan extension effect is still observed.

However, it was also determined that strains expressing proteins under GFP-tagged promoters are not particularly sensitive to mild heat stress, as the strains required exposure to 30°C for over one hour and 37°C for a minimum of 36 minutes to observe any increase in GFP levels. Significant chemical intervention was required to achieve an observable increase in GFP levels, using tunicamycin (1-5 µg/ml, HSP4; Calfon *et al.*, 2002, Yoneda *et al.*, 2004) and ethidium bromide (25-125 µg/ml, HSP6; Yoneda *et al.*, 2004), or significant heat exposure (one hour at 37°C, HSP16.2 this study; four hours at 27.5°C, HSP16.2; Dawe *et al.*, 2006), data not shown. These suggest that GFP based biomarkers may not be sensitive markers of moderate stress (Dawe *et al.*, 2006).

The development of protocol 2.9.4 resulted in significant extension of SS104, *glp-4 (bn2)I,* lifespan, without the possibility of the effect being due to heating. Further work with a range of strains of *C. elegans* was performed in order to further elucidate a potential mechanism of action. Through using the GR1307, *daf-16 (mgDf50) I*, strain the lifespan effect was eliminated. This strain is a homozygous knock out for DAF-16, a FOXO-family transcription factor. DAF-16 is a forkhead transcription factor which is able to regulate a range of genes

involved in development, metabolism, stress responses and longevity via insulin/insulin-like growth factor signalling including Akt kinases and the DAF-12 nuclear hormone receptor (Lee *et al.*, 2003, Murphy *et al.*, 2003, Singh and Aballay, 2006). The removal of any lifespan effect suggests that a DAF-16 pathway is required for IR1072-induced longevity. Knockdown of *hsf-1* expression in the PS3551, *hsf-1(sy441) I*, strain also resulted in the eradication of the lifespan effect found with SS104, *glp-4 (bn2)I*, strain. This gives further evidence to support that the longevity induced by IR1072 is a product of a DAF-16 derived pathway as HSF1 regulated proteins, such as chaperones, are one of the main downstream effectors of this pathway, see figure 7.22 (Singh and Aballay, 2006), DAF16 and HSF1 are both required to activate HSP expression. Loss of HSF1 function has been previously reported to result in decreased longevity (Garigan *et al.*, 2002) and increased copies result in increased lifespan (Hsu *et al.*, 2003, Morley and Morimoto, 2004), as outlined in the Introduction 7.1.3.

Further lifespan studies utilising the RB1104 strain, a nematode with a deletion affecting HSP3, found that the loss of this chaperone also resulted in the loss of the longevity effect. This was particularly interesting as it provided an insight into particular heat shock proteins that are required for longevity effect observed following chronic IR1072 exposure. HSP3, a homologue to GRP78, an ER based member of the HSP70 family, has previously been shown to interact with Aβ, suggesting a protective action to direct Aβ toward refolding or degradation rather than secretion (Fonte *et al.*, 2002). These lifespans were conducted alongside SS104 and N2 lifespans to act as positive controls.

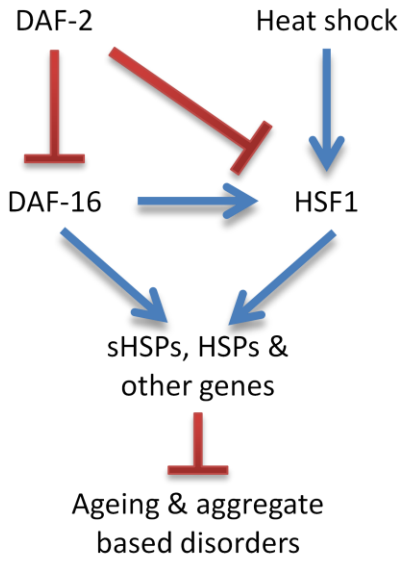

Figure 7.22. HSF1 activated by Heat shock (HS) and the DAF-2/DAF-16 pathway enhances protection against protein aggregation based disease. Abbreviations: HSF1, Heat Shock Factor 1; HSP, Heat Shock Protein; sHSP, small Heat Shock Protein.

It is also interesting to note that previous work investigating whether compensatory mechanisms of chaperones in nematodes occur, as in mammalian systems, RNAi knock down of HSP3 resulted in HSP4 (a second GRP78 homologue in nematodes) upregulation (which is also upregulated when other ER based chaperones are compromised). This is a very clear example of a chaperone compensatory mechanism, as both HSP3 and HSP4 encode members of the HSP70 family and presumably have similar function. This compensatory mechanism was also significant enough to prevent an increase in toxicity following the onset of Aβ expression (Kapulkin *et al.*, 2005). However, it appears that the detrimental effect of HSP3 knock down in the strain used in the lifespans within this investigation was not able to be compensated for by HSP4 upregulation. Assuming HSP3 would be able to be act in a similar protective manner as HSP4 in lifespan extension, as is suggested in the literature, no compensatory lifespan extension effect was observed in the RB1104 strain

when exposed to IR1072 (see table 7.12 and figure 7.18). This suggests that significant stresses, such as aggregates, are required to be present in order for sufficient compensation mechanisms to be initiated and these are not found during 'normal' nematode ageing, or that HSP4 does not function in the same manner as HSP3 in the ageing of *C. elegans*. Downregulation of individual chaperones has been shown to reduce longevity, but not as significantly as reduction in HSF1 itself, suggests that networks of chaperones function together in longevity (Morley and Morimoto, 2004).

It would be of significant interest to conduct lifespan studies with further strains of *C. elegans* with other heat shock proteins knocked out/removed to identify whether any other chaperones are essential in the longevity response seen with chronic IR1072 treatment. However, it is not possible to generate knock out strains for the majority of the chaperones identified in *C. elegans* as they are detailed as lethal (see wormbase.org), thus limiting the investigation of roles of other chaperone proteins found to be altered in the mouse models which have been investigated in this research, and their role in NIR lifespan extension. This limitation could be tackled by attempting RNAi of proteins of interest in adult nematodes.

The absorption spectra generated from both soluble and insoluble protein fractions of *C. elegans* homogenates provides some interesting data. These were preliminary experiments and only investigated *C. elegans* which had not been IR1072 exposed as a great quantity of nematodes were required in order to isolate sufficient quantities of protein in order to read the spectrum. In future it would be of interest to also investigate the absorption spectra of nematodes exposed to IR1072 in order to identify whether the peaks in absorption alter.

There do not appear to be any significant peaks in absorbance in the soluble fraction of protein at the range of wavelengths emitted by the LED IR1072 array. However, there is a broad peak in absorbance in the insoluble fraction, containing membrane bound/associated proteins, ranging from 1150 – 1000 nm, which appears to peak in the shaded section that identifies the range of wavelength emitted by the LEDs. These data also provide information that identifies that there is a peak in absorbance at the wavelength of IR of interest, suggesting that there is indeed a primary photoacceptor present in the nematode. These data also give a valuable insight into where (protein fraction) to search for the photoacceptor which is responsible for the absorption of IR1072 in the nematode. There remains a great deal of research to be done with this data however, as the structure responsible for the absorption of IR1072 remains unknown. Preliminary work with absorption spectra for bacterial cultures has not identified a peak in absorbance in the infrared region of interest. Work using mass spectroscopy would begin to unravel what biological material is responsible for the broad absorption peak seen from 1150 - 1000 nm in figure 7.21.

7.4 Future work

To further explore the role of HSP3 in the longevity effect observed following chronic IR1072, it would be beneficial to utilise RNAi against *hsp3* to verify that this is not a strain specific loss of effect – RNAi could be used to knock out expression in the N2 or SS104 strain, strains where lifespan increases has been repeatedly verified in this investigation. Concurrently a HSP3 transgene could be introduced back into the RB1104 strain. Through adding HSP3 back into the strain, it would be of great interest to investigate whether the lifespan effect could be reinstated and to establish that the loss of effect is not a product of the strain mutation process.

Investigation of other available chaperone knock out strains or via RNAi in adult nematodes, particularly those which have been shown to compensate for other chaperones, such as HSP4, and nematode orthologues to chaperone proteins which have been shown to be altered in mice that have been chronically exposed to IR1072, including HSP16.2 (nematode equivalent to mammalian αB crystallin), would be of great interest to investigate.

Microarray screens to identify genes whose expression is altered following IR1072 exposure is another possible set of experiments to conduct. However, even when genes are identified that are altered, further lifespans with the genes of interest removed or RNAi-targeted may not provide definitive answers as to the role of these genes in the biological effects of IR1072 because the phenotype of IR1072 exposure is not particularly strong. If the lifespan extension was of greater magnitude, it would be easier to identify genes of

interest in the biological effect of LLLT at this wavelength in *C. elegans*. However, initial microarray work would be significantly informative.

Future work with *C. elegans* and IR1072 would be to investigate the effects on models of disease, particularly focussing on models of Alzheimer's disease; there are several models of Alzheimer's disease which express the toxic β-amyloid$_{(1-42)}$ peptide. Nematodes that express the peptide in their muscle wall display progressive paralysis, but nematodes that express the β-amyloid peptide pan-neuronally display no apparent phenotype despite having neuronal deposits of Aβ (Link, 2006, Link *et al.*, 2003, Wolozin *et al.*, 2011). This raises questions of the validity of such models, as expression driven by different promoters and in different cell types has profound effects on the end phenotype. Another issue is that *C. elegans* do not express APP, or the β-secretase that cleaves APP prior to γ-secretase creating the Aβ$_{(1-42)}$ toxic fragment, so the processing of APP cannot be examined. Cellular response to neuronal damage appears to depend on the location of the cell damage, different responses depending on the closeness to the soma, an added complication when utilising this model to investigate a human disease (Link, 2006, Link *et al.*, 2003, Wolozin *et al.*, 2011), therefore choice of strain and the obtained results must be carefully considered.

Nematode models of AD do show oxidative stress, as in human cases and some strains have been shown to have tau-based toxicity, loss of GABA-ergic neurons, motor dysfunction and premature death. A lack of immune system also means the effects of microglial activation in AD cannot be investigated in the nematode models, as although nematodes have glia they function as sensory receptive sites, acting like neuronal sheaths not dissimilar to the role of

Schwann cells to muscle fibres. Nevertheless, nematode models have proved useful for examining the oxidation processes that occur immediately prior to Aβ deposition and for identifying genes that are activated when Aβ is expressed, as some models only begin to express Aβ upon temperature shift of the nematodes (Dimitriadi and Hart, 2010, Leung *et al.*, 2008, Link, 2006, Link *et al.*, 2003, Wolozin *et al.*, 2011).

Investigations by Fonte, 2002, found that much like in the human system, a range of intracellular chaperone proteins interacted with β-amyloid, in a *C. elegans* strain expressing the human sequence of the peptide. Utilising co-immunoprecipitation, the investigators found that six chaperone proteins bound to Aβ; including two HSP70 family members, three HSP16 family members and another protein that is believed to regulate HSP70 function. These data suggest that even in *C. elegans* Aβ is aptly recognised as an abnormal protein and is targeted for removal, via chaperones much like as has been reported in AD (Fonte *et al.*, 2002). This mechanism is not specific to Aβ, protein aggregation increases with nematode age and it is believed that increased copies of *hsf-1* or specific heat shock protein genes counteract protein aggregation resulting in longevity, a mechanism by which may be utilised by IR1072 (Fonte *et al.*, 2002, Walker and Lithgow, 2003, Wolozin *et al.*, 2011). Lifespan experiments with IR1072 and this model would be of significant interest to conduct.

In the future, it would be of significant interest to explore the effects of alternate IR1072 exposure protocols; and to conduct lifespan studies with *daf-2* mutant strains to identify whether IR1072 can further extend nematodes with long lifespans. It would also be important to assess metabolic ageing of IR1072

exposed nematode. This could be conducted through examining mobility, pharyngeal pumping, lucigenin and ADP/ATP levels (Huang *et al.*, 2004).

Caenorhabditis elegans are a very valuable model system to begin research into the mechanism through which IR1072 elicits its biological effects, but as a system it has a number of limitations many of which restrict the translation of results to the understanding of human disease. However, in this investigation the nematode has provided a significant insight into the proteins/processes responsible for the biological effects of IR1072 observed in a number of murine models, aiding in the direction of further research and comprehension of the purported NIR mechanism of action.

Chapter 8: Overall Discussion and Future Work

The aim of this project was to elucidate the photobiological effects of LLLT at IR1072 through the use of *in vivo* and *in vitro* systems, encompassing the use of two mouse strains, CD-1 and TASTPM; murine neuronal culture cell line CAD, and the well-characterised model of ageing, *Caenorhabditis elegans*.

Previous investigations using IR1072 have established a number of significant effects of LLLT on several biological systems. Work by Bradford, 2005, established a cytoprotective effect of IR1072 against UVA toxicity on human lymphocytes and Burroughs, 2010, found IR1072 exposure provided a concentration-dependent protection of rat primary cultures against glutamate-induced excitotoxicity (Bradford *et al.*, 2005, Burroughs, 2010).

Therefore, an aim for this investigation was to determine whether IR1072 could protect against other insults; Aβ, a causal factor in AD, and hydrogen peroxide, a by-product of cellular damage commonly detected alongside the degeneration of AD. This investigation has shown the beneficial effects of IR1072 exposure in a clonal CAD neuronal cell line, where IR1072 exposure is able to protect against both hydrogen peroxide insults and Aβ insults to a significant degree. As with excitotoxic insults utilising glutamate (Burroughs, 2010), IR1072 exposure provided an insult-severity-dependent level of protection against cell death. Interestingly, a significant level of protection was consistently observed following Aβ insults despite the use of high concentrations which may only be on the limits of realistic *in vivo* concentrations (Benilova *et al.*, 2012, Hu *et al.*, 2009).

However, a significant number of studies, utilising a range of NIR wavelengths have consistently demonstrated that LLLT can cause proliferation in a number of cell types; fibroblasts (Hawkins and Abrahamse, 2006, Taniguchi *et al.*, 2009, Vinck *et al.*, 2003), osteoblasts (Kreisler *et al.*, 2003, Pires Oliveira *et al.*, 2008, Ueda and Shimizu, 2003), muscle cells and epithelial cells (Sommer *et al.*, 2001, Whelan *et al.*, 2001). Therefore, absence of increased proliferation in this investigation suggests that this wavelength is indeed protecting against cell death rather than causing proliferation of the cells, to mask the level of cell death that occurs as a result of toxic insults.

The mechanism of this neuroprotection requires further investigation. The use of the CAD system provides a suitable model system in which to determine protein changes underlying neuroprotection. The levels of a number of proteins, particularly chaperones, are increased following IR1072 exposure *in vivo*. A number of chaperones have been reported to interact with Aβ *in vivo* and *in vitro*, therefore further characterisation of the CAD cell line is required to determine if these proteins are involved in the neuroprotective response mounted against the toxicity of Aβ. Work in our laboratory has already established that CAD cells do not express αB crystallin, a sHSP reported to exacerbate Aβ toxicity (Mao *et al.*, 2001, Narayanan *et al.*, 2006, Shammas *et al.*, 2011, Stege *et al.*, 1999, Yoo *et al.*, 2001) and consistently shown to be modulated by IR1072 in murine tissue in this investigation.

As discussed in introduction 1.1.3, the primary site of the absorption of NIR is believed to occur through photoacceptors located in the mitochondria, particularly cytochrome *c* oxidase. Previous work with IR1072 found acute exposure increased ETC activity, via complex II in the brain 7 month old CD-1

mice (Burroughs, 2010). The finding that female TASTPM mice have higher levels of Complex I and Complex II activity than their male counterparts, in control conditions is particularly interesting. This finding may provide an explanation for the considerable differences in the effects of chronic IR1072 exposure on protein levels in female TASTPM mice compared to males. This higher endogenous ETC activity in female mice may be a result of a naturally reduced mitochondrial state, with more electrons available to increase the activity of the ETC, as cells with a more reduced oxidation state are reported to be more susceptible to the biological effects of NIR (Gao and Xing, 2009, Hamblin and Demidova, 2006, Karu, 1999, Karu, 2008, Karu *et al.*, 2005). It is also interesting to note that following acute IR1072 exposure, 3 month old CD-1 mice saw reduced Complex I and II activity in liver mitochondria, but increased Complex II activity in brain mitochondria, whereas there was no change in Complex I activity. Altered liver complex activity is perhaps not surprising, as liver chromophores are reported to accept up to 50% of NIR (Beauvoit *et al.*, 1995, Beauvoit *et al.*, 1994). Thus the Complex I activity may appear reduced because there are not sufficient electrons available to generate an adequate proton gradient as the cells are overloaded with ATP. The cell's pool of ADP/ATP is finite to the availability of P_i, limiting the production of further ATP if there is little ADP available**.**

Altered Complex I and Complex II activity in CD-1 mitochondria following acute IR1072 exposure, supports data previously obtained demonstrating effects on LLLT, at a range of wavelengths, on both Complex I (Liang *et al.*, 2008, Rojas *et al.*, 2008, Ying *et al.*, 2008, Zhang *et al.*, 2009) and Complex II (Burroughs, 2010, Silveira *et al.*, 2009, Silveira *et al.*, 2007) activity levels. This range of

data suggests that ETC components, which were previously purported to be strict absorbers of light in the blue spectral region, such as Complex I, cannot be categorised as simply, as modulation of their activity levels have been reported in a number of systems, at a number of wavelengths within the NIR range and following a number of different exposure protocols.

A commonly reported secondary effect of LLLT is increased calcium levels, potentially as a result of increased ATP receptor binding due to increased ATP turnover following increased ETC activity. Calcium is a universal signalling molecule with the ability to modulate a significant number of mechanisms, including synaptic plasticity (see Introduction 1.8). Modulation of synaptic plasticity by LLLT could provide an explanation for the improved working memory observed in CD-1 mice following acute IR1072 exposure in a 3D maze (Michalikova *et al.*, 2008). However, calcium signalling was not investigated in this study, but it is of significant interest to research in the future.

It is interesting to note that following acute IR1072 exposure, there was no significant change in ATP levels reported in CAD neuroblastoma cells. However, ATP levels were only measured immediately following IR exposure and at four hours following IR exposure. It may be the case therefore that there is no change in ATP levels following IR exposure or that the change was transient and occurred at a time point between the times investigated. It may be that four hours after exposure, the excess ATP generated has been utilised for the initiation of other signalling processes and cannot therefore be detected. To further investigate the effect of IR1072 on ATP levels it would be useful to look at levels of both ATP and ADP and to determine whether the ATP:ADP ratio alters following IR1072 at a greater number of time points following exposure

and at a greater range of IR1072 exposure periods. It would also be of significant interest to investigate ATP levels in mouse tissue that had been irradiated, however this would require a significant number of additional methodological considerations to achieve a required level of sensitivity in detection (Khan, 2003).

Several reactions are reported to occur following absorption of NIR, including alteration of the redox state and increased electron transfer (Karu *et al.*, 1995). As previously mentioned, the oxidation state of the system being irradiated can determine the magnitude of the secondary effects elicited through LLLT (Karu, 1999, Karu, 2008, Karu *et al.*, 2005)**.** As well as this, a reaction called 'thermal relaxation' is postulated to occur. This process occurs from a small amount of local transient heating of photoacceptors during the absorption of NIR (not heating the entire cell), resulting in alterations in biochemical activity (Karu *et al.*, 1995, Karu *et al.*, 1994). This mechanism may explain the robust nature in which alterations in heat shock protein expression are observed in all tissue investigated in this study, without any apparent negative results reported relating to local heating.

The effects of IR1072 on the proteins investigated here were not all the same when comparing between CD-1 and TASTPM mice, although several similarities were present, particularly between male TASTPM and CD-1 young mice. However, there were a number of variations, this is most likely to be due to strain differences as both lines have different genetic backgrounds and the levels of cellular stress are believed to be considerably different between the two strains, as by 7 months of age TASTPM mice have a significant amyloid load and display some neuronal loss (Howlett *et al.*, 2008), whereas

amyloidosis in CD-1 mice only becomes detectable at 8 months and 12 months of age for female and male mice respectively, and occurs in a systemic manner, rather than specific deposition in the brain (Engelhardt *et al.*, 1993). This may also account for the differences observed when identifying proteins that alter with age in both the TASTPM and CD-1 strains. Another important factor to take into account when considering the results in this investigation is that the majority of samples analysed are taken from male mice, CD-1 and TASTPM timelines and all CD-1 Young and Old homogenates are from males only. A considerable number of proteins that were investigated following chronic IR1072 exposure were found to be differentially affected when comparing male to female in the TASTPM strain. This raises the question of whether gender differences, such as hormonal levels, are responsible for the differing magnitudes of secondary effects of IR1072 observed between male and female TASTPM mice.

A limitation of this study is the volume of data obtained through western blotting. Western blotting is a particularly useful technique to determine the presence (or absence) of a particular protein within a tissue sample, it has a significant degree of sensitivity, it can detect nanogram quantities of protein and it has a high degree of specificity, due to its ability to separate proteins by molecular weight, charge and conformation. The major advantage of western blotting is the availability of specific antibodies against proteins and the ease of visualisation of protein bands via fluorescence. However analysis of western blotting is only semi-quantitative, comparisons of bands is relative to band density across the membrane used and advanced techniques, such as mass spectrometry, would be required to verify proteins following western blotting.

Mass spectrometry of a sample can be used to not only determine the quantity of the protein of interest that is present but it can also give information regarding modification of the protein, modification which can only be estimated by protein size from western blotting. In conjunction with the obtained western blotting data, ELISAs could be performed on samples. The ELISA methodology would enable greater detail to be obtained regarding the nature of the proteins in question, such as Aβ. An ELISA would enable the quantity of soluble and insoluble Aβ present; however western blotting would only detect the quantity of total Aβ. As mentioned previously, now that proteins of interest have been determined it would also be of significant interest to conduct microarrays to identify activity of genes of interest. However, western blotting provides a superb, replicable, semi-quantitative technique to begin investigating proteins of interest (Bolt and Mahoney, 1997, Chery *et al.*, 2006, Cox and Mann, 2007, Mann, 2008, Wang *et al.*, 1999).

Work with *C. elegans* has provided important insights into mechanisms of LLLT as well as secondary effects of absorbance. This investigation has found that IR1072 has beneficial effects on more systems than previously established. Through a variety of protocols, this investigation has established that IR1072 can extend lifespan of a number of *C. elegans* strains. More significantly than this, the use of *C. elegans* has provided important insight into mechanisms of increased longevity and has determined that the longevity effect depends on the insulin/insulin-like growth factor pathway in the nematode. The nematode orthologue of HSP70 (HSP3) was found to be essential for the longevity effect induced via IR1072 exposure. This result emphasises the importance of heat shock proteins in the beneficial effects of IR1072, as HSP70 is one heat shock

protein which has been consistently altered in both TASTPM and CD-1 mice following IR1072 exposure. The use of *C. elegans* as a model system has enabled important investigation into signalling processes involved in beneficial secondary effects of LLLT. As mentioned in chapter 7, there are several further experiments to conduct in order to verify the role of HSP3 in the observed increase in nematode longevity following IR1072 exposure. Despite important insights gained through the use of *C. elegans*, they are not an entirely suitable model to investigate many of the other heat shock proteins which have been found to be significantly altered in mammalian tissue reported in this thesis, as knock-out strains of many HSPs have been found to be lethal. The CAD neuroblastoma cell line could act to provide more information in this respect, as the cell line is further characterised by our laboratory, a range of important chaperones could be transfected into the cell line, if they are not already present, or overexpressed to determine whether the already beneficial and neuroprotective effects of IR1072 can be augmented through upregulation of the cell lines own protective mechanisms.

8.1 Further work

Investigations into IR1072 treatment protocols - Very few permutations of the IR exposure protocol have been investigated in mammalian experiments, largely due to time constraints and costs. Work with *C. elegans* enabled investigation of a number of exposure protocols, some of which showed no beneficial effects whilst others improved on already extended longevity. However, the repetitive nature of a number of the protocols conducted with

nematodes are not suitable for work with mammals, therefore careful consideration of appropriate procedures is required. This demonstrates that different protocols may have differing degrees of magnitude in achievable biological effects. Future work with alternate exposure protocols in mammalian tissues would be interesting to conduct to determine if the proteins altered in this investigation are able to be further modified.

Investigations into ageing in female mice - The timeline samples investigated in this research used only male samples of both CD-1 and TASTPM mice. Work to investigate whether the same proteins found to be altered in age in male mice are modified in female mice, and whether they are varied to the same degree would be important to undertake. These data would also aid in the understanding of differential effects observed between male and female TASTPM mice exposed to chronic IR1072.

Investigations into the effects of chronic IR1072 exposure on female CD-1 mice - This investigation focussed on 'young' and 'old' male CD-1 mice that were chronically irradiated. As observed with TASTPM mice, effects of chronic IR1072 exposure differ significantly between sexes. Studies paralleled in female CD-1 mice would aid in determining whether differences found between male and female TASTPM mice are limited to one strain or are consistent across strains.

Investigations into the effects of chronic IR1072 exposure on further age points of TASTPM mice - Following the observation that the effects of chronic IR1072 differ between CD-1 mice treated from 2 months of age to those treated from 7 months of age, similar investigations with TASTPM mice chronically

irradiated from later age points would be of significant interest. This may pose difficulties due to the high degree of early mortality that has been found in the TASTPM mice maintained at the University of Durham LSSU facility. It would also be of interest to investigate mice exposed from birth due to the fact that amyloid deposition is apparent from two months of age in the TASTPM strain.

Investigations into calcium, ATP and other signalling molecules - Recording levels of these molecules, which are frequently reported to be altered following LLLT, would be worthwhile to establish in mammalian systems before and after IR1072 exposure. Electrophysiology and the CAD cell line could be used to investigate some of these components *in vitro*. Investigation of such signalling molecules would be important in understanding how large scale protein changes are initiated.

Investigations into other proteins of interest in IR1072 exposed mice - As previously stated, to aid in understanding of HSPs and reduced Aβ levels, it would be advantageous to investigate CHIP, Akt, phosphorylated-αB crystallin and GluA1 and to build on GluA2 data obtained. It would also be of interest to investigate levels of APP immunohistochemically and levels of non-amyloidogenic APP products. Significant reduction in male and female TASTPM mice of APP was found through immunoblotting, the area/s of the brain have reduced levels.

Investigations with the CAD cells line - Characterisation of the CAD cell line is required and following this, the cell line could be manipulated to examine certain protein roles, including overexpression of HSPs, pharmacological induction of HSPs, in the absence and presence of Aβ. Work with the CAD cell

line could also aid in the determination of how IR1072 alters ΔΨm potential, ROS levels and mitochondrial motility. The work with cell lines could be continued to examine the effect of IR1072 on variants with excess or reduced numbers of mitochondria, and in conjunction with Aβ.

Investigations to determine mechanism of action - Insights from *C. elegans*, determined HSP3, nematode HSP70 equivalent, appeared to be crucial for IR-induced longevity. Therefore utilising RNAi of HSP3 in wild-type strains would help determine whether the knockout of IR1072 induced longevity in HSP3 deficient nematodes is merely due to an unwanted effect of generating the mutant strain. As well as RNAi, outcrossing of the HSP3 knockout strain would be important to undertake to identify that the lack of IR1072 induced longevity in this strain is dependent on HSP3 alone and not due to an unknown confounding factor affecting the mutant strain.

Investigations into primary photoacceptors of IR1072 - The bulk of data published regarding photoacceptors for the infra-red region focuses on wavelengths from 600-800 nm. There has been very little research into establishing photoacceptors that are responsible for the biological effects observed with wavelengths longer than 800 nm. Determination of the photoacceptor for 1072 nm would significantly enhance the understanding of mechanism of action. Work in this investigation has looked at absorbance profile for a selection of isolated cellular components, including mammalian mitochondria and soluble and insoluble protein fractions from nematodes. These data have shown peaks in absorbance which encompass 1072 nm, however further work needs to be carried out to determine precisely which proteins are responsible for this absorbance band. Mass spectrometry could aid

in this investigation. Determination of the primary photoacceptor would also aid in the acceptance of IR1072 as a beneficial treatment for neurodegenerative disorders.

8.2 Future Applications

Based on this research, a double blind, placebo controlled Phase II pilot clinical trial was recently completed in the USA to assess the effect of IR1072 exposure on the behavioural and cognitive symptoms associated with the early and mid stages of dementia in Alzheimer's disease patients. The outcome of which is currently under analysis. (www.clinicaltrials.gov)

Appendix I - Source of Materials

1.0 Sigma Aldrich, Dorset, UK

‘Luminol’ 5-Amino-1,4-pthalazinedione free acid
10X PBS
ADP (Adenosine 5’-diphosphate sodium salt)
Agar
Anti-β actin (ascites fluid)
Bovine Serum Albumin, essentially fatty acid free
Calcium Chloride
Cholesterol
Copper (II) Sulfate, min 99%
Developing cassettes
D-Mannitol
DPX Mountant
Ethidium bromide
Ethyleneglycotetraacetic Acid (EGTA)
Ethylenediaminetetraacetic Acid (EDTA)
Folin-Ciolcalteau phenol reagent
Kodak D-19 Developer
Kodak Fixative
L(-) Glutamic acid (non-animal salt)
L(-) Malic acid disodium salt
Magnesium sulphate
p-coumaric Acid
Peptone N-Z Soy BL7, Enzymatic hydrolysate
Percoll® (pH 8.5-9.5 at 25°C)
Potassium Phosphate
Potassium phosphate monobasic (KH_2PO_4)
Pre-Stained Standard Molecular Weight Markers
Sodium Azide
Sodium Dodecyl Sulphate (SDS)
Sodium succinate dibasic hexahydrate, min 99%
Triton-X100
Poly-d Lysine

1.1 VWR/BDH Laboratory Supplies, Leicestershire, UK

Acrylogel 3 Solution 40% (v/v)

Ammonium persulphate

Bromophenol Blue

Dimethyl sulphoxide (DMSO)

Disodium Phosphate (Na_2PO_4)

Glycerol

Isopropanol

N,N,N',N'-teranethylethylenediamine (TEMED)

Potassium chloride

Potassium phosphate

Sodium Carbonate

Sodium Chloride

Sodium Dihydrogen Phosphate (NaH_2PO_4)

Sodium hydrogen carbonate

Sodium hydroxide

Sodium potassium tartrate

Sucrose

Wheaton Glass dounce homogeniser

1.2 Durham University

Ethanol

Marvel

1.3 Fisher Scientific, Leicestershire, UK

Cling film

Dithiothreitol (DTT)

DMEM/F12 plus glutamax

Glycerol

Glycine

Hamilton Microliter 700 Series Syringe Model 705

Horseradish peroxidase linked anti-mouse antibody

Horseradish peroxidase linked anti-rabbit antibody

Hydrochloric acid 1M

Hyperfilm™

Methanol
Nitrocellulose Pore size 0.45 µm
Paraformaldehyde
Sodium Chloride
Tris-base

1.4 Invitrogen

Alexa fluor 488
ATP Determination Assay
DAPI (4',6-diamidino-2-phenylindole)

1.5 Cambrex Bio Science, Verviers, Belgium

Foetal Calf Serum

1.6 Promega Limited, Southampton, UK

CytoTox96® Non-radioactive Cytotoxicity Assay

1.7 Vector Laboratories, Peterborough, UK

Biotinylated antibodies, rabbit and mouse
M.O.M.™ Immunodetection Kit
Vectastain® ABC Kit

1.8 Calbiochem, Nottingham, UK

Protease inhibitor cocktail set III
Mowiol

1.9 Ascent scientific - Now part of AbCam Biochemicals, Cambridge, UK

β-amyloid$_{(1-42)}$ human peptide
Tunicamycin

1.10 Pierce

Pierce SuperSignal West Pico Chemiluminescent Substrate
Horseradish peroxidise linked anti-goat antibody

Appendix II – Thermocouple Reference Table

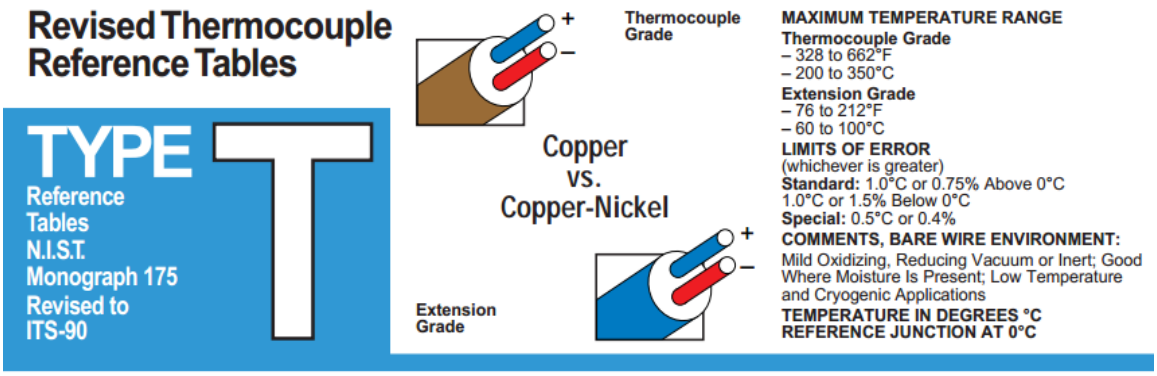

Thermoelectric Voltage in Millivolts

°C	-10	-9	-8	-7	-6	-5	-4	-3	-2	-1	0	°C
-260	-6.258	-6.256	-6.255	-6.253	-6.251	-6.248	-6.245	-6.242	-6.239	-6.236	-6.232	-260
-250	-6.232	-6.228	-6.223	-6.219	-6.214	-6.209	-6.204	-6.198	-6.193	-6.187	-6.180	-250
-240	-6.180	-6.174	-6.167	-6.160	-6.153	-6.146	-6.138	-6.130	-6.122	-6.114	-6.105	-240
-230	-6.105	-6.096	-6.087	-6.078	-6.068	-6.059	-6.049	-6.038	-6.028	-6.017	-6.007	-230
-220	-6.007	-5.996	-5.985	-5.973	-5.962	-5.950	-5.938	-5.926	-5.914	-5.901	-5.888	-220
-210	-5.888	-5.876	-5.863	-5.850	-5.836	-5.823	-5.809	-5.795	-5.782	-5.767	-5.753	-210
-200	-5.753	-5.739	-5.724	-5.710	-5.695	-5.680	-5.665	-5.650	-5.634	-5.619	-5.603	-200
-190	-5.603	-5.587	-5.571	-5.555	-5.539	-5.523	-5.506	-5.489	-5.473	-5.456	-5.439	-190
-180	-5.439	-5.421	-5.404	-5.387	-5.369	-5.351	-5.334	-5.316	-5.297	-5.279	-5.261	-180
-170	-5.261	-5.242	-5.224	-5.205	-5.186	-5.167	-5.148	-5.128	-5.109	-5.089	-5.070	-170
-160	-5.070	-5.050	-5.030	-5.010	-4.989	-4.969	-4.949	-4.928	-4.907	-4.886	-4.865	-160
-150	-4.865	-4.844	-4.823	-4.802	-4.780	-4.759	-4.737	-4.715	-4.693	-4.671	-4.648	-150
-140	-4.648	-4.626	-4.604	-4.581	-4.558	-4.535	-4.512	-4.489	-4.466	-4.443	-4.419	-140
-130	-4.419	-4.395	-4.372	-4.348	-4.324	-4.300	-4.275	-4.251	-4.226	-4.202	-4.177	-130
-120	-4.177	-4.152	-4.127	-4.102	-4.077	-4.052	-4.026	-4.000	-3.975	-3.949	-3.923	-120
-110	-3.923	-3.897	-3.871	-3.844	-3.818	-3.791	-3.765	-3.738	-3.711	-3.684	-3.657	-110
-100	-3.657	-3.629	-3.602	-3.574	-3.547	-3.519	-3.491	-3.463	-3.435	-3.407	-3.379	-100
-90	-3.379	-3.350	-3.322	-3.293	-3.264	-3.235	-3.206	-3.177	-3.148	-3.118	-3.089	-90
-80	-3.089	-3.059	-3.030	-3.000	-2.970	-2.940	-2.910	-2.879	-2.849	-2.818	-2.788	-80
-70	-2.788	-2.757	-2.726	-2.695	-2.664	-2.633	-2.602	-2.571	-2.539	-2.507	-2.476	-70
-60	-2.476	-2.444	-2.412	-2.380	-2.348	-2.316	-2.283	-2.251	-2.218	-2.186	-2.153	-60
-50	-2.153	-2.120	-2.087	-2.054	-2.021	-1.987	-1.954	-1.920	-1.887	-1.853	-1.819	-50
-40	-1.819	-1.785	-1.751	-1.717	-1.683	-1.648	-1.614	-1.579	-1.545	-1.510	-1.475	-40
-30	-1.475	-1.440	-1.405	-1.370	-1.335	-1.299	-1.264	-1.228	-1.192	-1.157	-1.121	-30
-20	-1.121	-1.085	-1.049	-1.013	-0.976	-0.940	-0.904	-0.867	-0.830	-0.794	-0.757	-20
-10	-0.757	-0.720	-0.683	-0.646	-0.608	-0.571	-0.534	-0.496	-0.459	-0.421	-0.383	-10
0	-0.383	-0.345	-0.307	-0.269	-0.231	-0.193	-0.154	-0.116	-0.077	-0.039	0.000	0
0	0.000	0.039	0.078	0.117	0.156	0.195	0.234	0.273	0.312	0.352	0.391	0
10	0.391	0.431	0.470	0.510	0.549	0.589	0.629	0.669	0.709	0.749	0.790	10
20	0.790	0.830	0.870	0.911	0.951	0.992	1.033	1.074	1.114	1.155	1.196	20
30	1.196	1.238	1.279	1.320	1.362	1.403	1.445	1.486	1.528	1.570	1.612	30
40	1.612	1.654	1.696	1.738	1.780	1.823	1.865	1.908	1.950	1.993	2.036	40
°C	0	1	2	3	4	5	6	7	8	9	10	°C

°C	0	1	2	3	4	5	6	7	8	9	10	°C
50	2.036	2.079	2.122	2.165	2.208	2.251	2.294	2.338	2.381	2.425	2.468	50
60	2.468	2.512	2.556	2.600	2.643	2.687	2.732	2.776	2.820	2.864	2.909	60
70	2.909	2.953	2.998	3.043	3.087	3.132	3.177	3.222	3.267	3.312	3.358	70
80	3.358	3.403	3.448	3.494	3.539	3.585	3.631	3.677	3.722	3.768	3.814	80
90	3.814	3.860	3.907	3.953	3.999	4.046	4.092	4.138	4.185	4.232	4.279	90
100	4.279	4.325	4.372	4.419	4.466	4.513	4.561	4.608	4.655	4.702	4.750	100
110	4.750	4.798	4.845	4.893	4.941	4.988	5.036	5.084	5.132	5.180	5.228	110
120	5.228	5.277	5.325	5.373	5.422	5.470	5.519	5.567	5.616	5.665	5.714	120
130	5.714	5.763	5.812	5.861	5.910	5.959	6.008	6.057	6.107	6.156	6.206	130
140	6.206	6.255	6.305	6.355	6.404	6.454	6.504	6.554	6.604	6.654	6.704	140
150	6.704	6.754	6.805	6.855	6.905	6.956	7.006	7.057	7.107	7.158	7.209	150
160	7.209	7.260	7.310	7.361	7.412	7.463	7.515	7.566	7.617	7.668	7.720	160
170	7.720	7.771	7.823	7.874	7.926	7.977	8.029	8.081	8.133	8.185	8.237	170
180	8.237	8.289	8.341	8.393	8.445	8.497	8.550	8.602	8.654	8.707	8.759	180
190	8.759	8.812	8.865	8.917	8.970	9.023	9.076	9.129	9.182	9.235	9.288	190
200	9.288	9.341	9.395	9.448	9.501	9.555	9.608	9.662	9.715	9.769	9.822	200
210	9.822	9.876	9.930	9.984	10.038	10.092	10.146	10.200	10.254	10.308	10.362	210
220	10.362	10.417	10.471	10.525	10.580	10.634	10.689	10.743	10.798	10.853	10.907	220
230	10.907	10.962	11.017	11.072	11.127	11.182	11.237	11.292	11.347	11.403	11.458	230
240	11.458	11.513	11.569	11.624	11.680	11.735	11.791	11.846	11.902	11.958	12.013	240
250	12.013	12.069	12.125	12.181	12.237	12.293	12.349	12.405	12.461	12.518	12.574	250
260	12.574	12.630	12.687	12.743	12.799	12.856	12.912	12.969	13.026	13.082	13.139	260
270	13.139	13.196	13.253	13.310	13.366	13.423	13.480	13.537	13.595	13.652	13.709	270
280	13.709	13.766	13.823	13.881	13.938	13.995	14.053	14.110	14.168	14.226	14.283	280
290	14.283	14.341	14.399	14.456	14.514	14.572	14.630	14.688	14.746	14.804	14.862	290
300	14.862	14.920	14.978	15.036	15.095	15.153	15.211	15.270	15.328	15.386	15.445	300
310	15.445	15.503	15.562	15.621	15.679	15.738	15.797	15.856	15.914	15.973	16.032	310
320	16.032	16.091	16.150	16.209	16.268	16.327	16.387	16.446	16.505	16.564	16.624	320
330	16.624	16.683	16.742	16.802	16.861	16.921	16.980	17.040	17.100	17.159	17.219	330
340	17.219	17.279	17.339	17.399	17.458	17.518	17.578	17.638	17.698	17.759	17.819	340
350	17.819	17.879	17.939	17.999	18.060	18.120	18.180	18.241	18.301	18.362	18.422	350
360	18.422	18.483	18.543	18.604	18.665	18.725	18.786	18.847	18.908	18.969	19.030	360
370	19.030	19.091	19.152	19.213	19.274	19.335	19.396	19.457	19.518	19.579	19.641	370
380	19.641	19.702	19.763	19.825	19.886	19.947	20.009	20.070	20.132	20.193	20.255	380
390	20.255	20.317	20.378	20.440	20.502	20.563	20.625	20.687	20.748	20.810	20.872	390
°C	0	1	2	3	4	5	6	7	8	9	10	°C

Figure II.1. Thermocouple reference table

Obtained from http://www.omega.com/thermocouples.html

References

ABISAMBRA, J. F., BLAIR, L. J., HILL, S. E., JONES, J. R., KRAFT, C., ROGERS, J., KOREN, J., 3RD, JINWAL, U. K., LAWSON, L., JOHNSON, A. G., WILCOCK, D., O'LEARY, J. C., JANSEN-WEST, K., MUSCHOL, M., GOLDE, T. E., WEEBER, E. J., BANKO, J. & DICKEY, C. A. 2010. Phosphorylation dynamics regulate Hsp27-mediated rescue of neuronal plasticity deficits in tau transgenic mice. *J Neurosci,* 30**,** 15374-82.

ABRAMOV, E., DOLEV, I., FOGEL, H., CICCOTOSTO, G. D., RUFF, E. & SLUTSKY, I. 2009. Amyloid-beta as a positive endogenous regulator of release probability at hippocampal synapses. *Nat Neurosci,* 12**,** 1567-76.

ADAMS, B., FITCH, T., CHANEY, S. & GERLAI, R. 2002. Altered performance characteristics in cognitive tasks: comparison of the albino ICR and CD1 mouse strains. *Behav Brain Res,* 133**,** 351-61.

ALLISON, P. D. 2010. *Survival Analysis Using SAS: A Practical Guide, Second Edition*, SAS Institute.

ANCKAR, J. & SISTONEN, L. 2011. Regulation of HSF1 function in the heat stress response: implications in aging and disease. *Annu Rev Biochem,* 80**,** 1089-115.

ARRIGO, A. P., SIMON, S., GIBERT, B., KRETZ-REMY, C., NIVON, M., CZEKALLA, A., GUILLET, D., MOULIN, M., DIAZ-LATOUD, C. & VICART, P. 2007. Hsp27 (HspB1) and alphaB-crystallin (HspB5) as therapeutic targets. *FEBS Lett,* 581**,** 3665-74.

AUGUSTINACK, J. C., SCHNEIDER, A., MANDELKOW, E. M. & HYMAN, B. T. 2002. Specific tau phosphorylation sites correlate with severity of neuronal cytopathology in Alzheimer's disease. *Acta Neuropathol,* 103**,** 26-35.

AVRAMOPOULOS, D. 2009. Genetics of Alzheimer's disease: recent advances. *Genome Med,* 1**,** 34.

BALDUCCI, C. & FORLONI, G. 2011. APP transgenic mice: their use and limitations. *Neuromolecular Med,* 13**,** 117-37.

BATS, C., GROC, L. & CHOQUET, D. 2007. The interaction between Stargazin and PSD-95 regulates AMPA receptor surface trafficking. *Neuron,* 53**,** 719-34.

BEAUVOIT, B., EVANS, S. M., JENKINS, T. W., MILLER, E. E. & CHANCE, B. 1995. Correlation between the light scattering and the mitochondrial content of normal tissues and transplantable rodent tumors. *Anal Biochem,* 226**,** 167-74.

BEAUVOIT, B., KITAI, T. & CHANCE, B. 1994. Contribution of the mitochondrial compartment to the optical properties of the rat liver: a theoretical and practical approach. *Biophys J,* 67**,** 2501-10.

BEERE, H. M. 2004. "The stress of dying": the role of heat shock proteins in the regulation of apoptosis. *J Cell Sci,* 117**,** 2641-51.

BEERE, H. M. 2005. Death versus survival: functional interaction between the apoptotic and stress-inducible heat shock protein pathways. *J Clin Invest,* 115**,** 2633-9.

BENEDETTI, C., HAYNES, C. M., YANG, Y., HARDING, H. P. & RON, D. 2006. Ubiquitin-like protein 5 positively regulates chaperone gene expression in the mitochondrial unfolded protein response. *Genetics,* 174**,** 229-39.

BENILOVA, I., KARRAN, E. & DE STROOPER, B. 2012. The toxic Abeta oligomer and Alzheimer's disease: an emperor in need of clothes. *Nat Neurosci,* 15**,** 349-57.

BENN, S. C. & WOOLF, C. J. 2004. Adult neuron survival strategies--slamming on the brakes. *Nat Rev Neurosci,* 5**,** 686-700.

BEREZOVSKA, O., LLEO, A., HERL, L. D., FROSCH, M. P., STERN, E. A., BACSKAI, B. J. & HYMAN, B. T. 2005. Familial Alzheimer's disease presenilin 1 mutations cause alterations in the conformation of presenilin and interactions with amyloid precursor protein. *J Neurosci,* 25**,** 3009-17.

BERGMANS, B. A. & DE STROOPER, B. 2010. gamma-secretases: from cell biology to therapeutic strategies. *Lancet Neurol,* 9**,** 215-26.

BHAT, R. V., BUDD HAEBERLEIN, S. L. & AVILA, J. 2004. Glycogen synthase kinase 3: a drug target for CNS therapies. *J Neurochem,* 89**,** 1313-7.

BIANCHI, L. & DRISCOLL, M. 2006. Culture of embryonic C. elegans cells for electrophysiological and pharmacological analyses. *WormBook***,** 1-15.

BJORKDAHL, C., SJOGREN, M. J., ZHOU, X., CONCHA, H., AVILA, J., WINBLAD, B. & PEI, J. J. 2008. Small heat shock proteins Hsp27 or alphaB-crystallin and the protein components of neurofibrillary tangles: tau and neurofilaments. *J Neurosci Res,* 86**,** 1343-52.

BOLT, M. W. & MAHONEY, P. A. 1997. High-efficiency blotting of proteins of diverse sizes following sodium dodecyl sulfate-polyacrylamide gel electrophoresis. *Anal Biochem,* 247**,** 185-92.

BRAAK, H. & BRAAK, E. 1991. Neuropathological stageing of Alzheimer-related changes. *Acta Neuropathol,* 82**,** 239-59.

BRAAK, H. & BRAAK, E. 1995. Staging of Alzheimer's disease-related neurofibrillary changes. *Neurobiol Aging,* 16**,** 271-8; discussion 278-84.

BRAAK, H. & BRAAK, E. 1997. Frequency of stages of Alzheimer-related lesions in different age categories. *Neurobiol Aging,* 18**,** 351-7.

BRADFORD, A., BARLOW, A. & CHAZOT, P. L. 2005. Probing the differential effects of infrared light sources IR1072 and IR880 on human lymphocytes: evidence of selective cytoprotection by IR1072. *J Photochem Photobiol B,* 81**,** 9-14.

BROOKES, P. S., LEVONEN, A. L., SHIVA, S., SARTI, P. & DARLEY-USMAR, V. M. 2002. Mitochondria: regulators of signal transduction by reactive oxygen and nitrogen species. *Free Radic Biol Med,* 33**,** 755-64.

BURROUGHS, S. L. 2010. *Photobiomodulation with IR1072nm in the murine CNS:in vitro and in vivo studies.* Ph.D Philosophy, University of Durham.

BUTOW, R. A. & AVADHANI, N. G. 2004. Mitochondrial signaling: the retrograde response. *Mol Cell,* 14**,** 1-15.

CALABRESE, V., SCAPAGNINI, G., RAVAGNA, A., GIUFFRIDA STELLA, A. M. & BUTTERFIELD, D. A. 2002. Molecular chaperones and their roles in neural cell differentiation. *Dev Neurosci,* 24**,** 1-13.

CALDERWOOD, S. K., MAMBULA, S. S., GRAY, P. J., JR. & THERIAULT, J. R. 2007. Extracellular heat shock proteins in cell signaling. *FEBS Lett,* 581**,** 3689-94.

CALDERWOOD, S. K., MURSHID, A. & PRINCE, T. 2009. The shock of aging: molecular chaperones and the heat shock response in longevity and aging--a mini-review. *Gerontology,* 55**,** 550-8.

CALFON, M., ZENG, H., URANO, F., TILL, J. H., HUBBARD, S. R., HARDING, H. P., CLARK, S. G. & RON, D. 2002. IRE1 couples endoplasmic reticulum load to secretory capacity by processing the XBP-1 mRNA. *Nature,* 415**,** 92-6.

CAMPELLO, A. P., VOSS, D. O., FREIRE, S. A. & BACILA, M. 1964. The Role of Citrate on the Respiratory Control of Isolated Rat Heart Sarcosomes. *J Biol Chem,* 239**,** 3842-6.

CHALFIE, M. & JORGENSEN, E. M. 1998. C. elegans neuroscience: genetics to genome. *Trends Genet,* 14**,** 506-12.

CHANCE, B. & WILLIAMS, G. R. 1956a. The respiratory chain and oxidative phosphorylation. *Adv Enzymol Relat Subj Biochem,* 17**,** 65-134.

CHANCE, B. & WILLIAMS, G. R. 1956b. Respiratory enzymes in oxidative phosphorylation. VI. The effects of adenosine diphosphate on azide-treated mitochondria. *J Biol Chem,* 221**,** 477-89.

CHEN, S. & BROWN, I. R. 2007. Neuronal expression of constitutive heat shock proteins: implications for neurodegenerative diseases. *Cell Stress Chaperones,* 12**,** 51-8.

CHEN, X. J., KOVACEVIC, N., LOBAUGH, N. J., SLED, J. G., HENKELMAN, R. M. & HENDERSON, J. T. 2006. Neuroanatomical differences between mouse strains as shown by high-resolution 3D MRI. *Neuroimage,* 29**,** 99-105.

CHERY, C., MOENS, L., CORNELIS, R. & VANCHAECKE, F. 2006. Capabilities and limitations of gel electrophoresis for elemental speciation: A laboratory experience. *Pure Appl. Chem.,* 78**,** 91-103.

CHINNERY, P. F. & SCHON, E. A. 2003. Mitochondria. *J Neurol Neurosurg Psychiatry,* 74**,** 1188-99.

CONNELL, P., BALLINGER, C. A., JIANG, J., WU, Y., THOMPSON, L. J., HOHFELD, J. & PATTERSON, C. 2001. The co-chaperone CHIP regulates protein triage decisions mediated by heat-shock proteins. *Nat Cell Biol,* 3**,** 93-6.

COX, J. & MANN, M. 2007. Is proteomics the new genomics? *Cell,* 130**,** 395-8.

CULETTO, E. & SATTELLE, D. B. 2000. A role for Caenorhabditis elegans in understanding the function and interactions of human disease genes. *Hum Mol Genet,* 9**,** 869-77.

DAWE, A. S., SMITH, B., THOMAS, D. W., GREEDY, S., VASIC, N., GREGORY, A., LOADER, B. & DE POMERAI, D. I. 2006. A small temperature rise may contribute towards the apparent induction by microwaves of heat-shock gene expression in the nematode Caenorhabditis Elegans. *Bioelectromagnetics,* 27**,** 88-97.

DE VOS, K. J., GRIERSON, A. J., ACKERLEY, S. & MILLER, C. C. 2008. Role of axonal transport in neurodegenerative diseases. *Annu Rev Neurosci,* 31**,** 151-73.

DEHLE, F. C., ECROYD, H., MUSGRAVE, I. F. & CARVER, J. A. 2010. alphaB-Crystallin inhibits the cell toxicity associated with amyloid fibril formation by kappa-casein and the amyloid-beta peptide. *Cell Stress Chaperones,* 15**,** 1013-26.

DESMET, K. D., PAZ, D. A., CORRY, J. J., EELLS, J. T., WONG-RILEY, M. T., HENRY, M. M., BUCHMANN, E. V., CONNELLY, M. P., DOVI, J. V., LIANG, H. L., HENSHEL, D. S., YEAGER, R. L., MILLSAP, D. S., LIM, J., GOULD, L. J., DAS, R., JETT, M., HODGSON, B. D., MARGOLIS, D. & WHELAN, H. T. 2006. Clinical and experimental applications of NIR-LED photobiomodulation. *Photomed Laser Surg,* 24**,** 121-8.

DEWJI, N. N. & DO, C. 1996. Heat shock factor-1 mediates the transcriptional activation of Alzheimer's beta-amyloid precursor protein gene in response to stress. *Brain Res Mol Brain Res,* 35**,** 325-8.

DEWJI, N. N., DO, C. & BAYNEY, R. M. 1995. Transcriptional activation of Alzheimer's beta-amyloid precursor protein gene by stress. *Brain Res Mol Brain Res,* 33**,** 245-53.

DIMITRIADI, M. & HART, A. C. 2010. Neurodegenerative disorders: insights from the nematode Caenorhabditis elegans. *Neurobiol Dis,* 40**,** 4-11.

DONOGHUE, P. 2009. *Molecular Pharmacology of AMPA Receptor Trafficking Proteins - TARPs - Evidence for an Association with 5HT2c Receptors.* Ph.D Philosophy, University of Durham.

DORMAN, J. B., ALBINDER, B., SHROYER, T. & KENYON, C. 1995. The age-1 and daf-2 genes function in a common pathway to control the lifespan of Caenorhabditis elegans. *Genetics,* 141**,** 1399-406.

DOU, F., NETZER, W. J., TANEMURA, K., LI, F., HARTL, F. U., TAKASHIMA, A., GOURAS, G. K., GREENGARD, P. & XU, H. 2003. Chaperones increase association of tau protein with microtubules. *Proc Natl Acad Sci U S A,* 100**,** 721-6.

DOUGAL, G. & KELLY, P. 2001. A pilot study of treatment of herpes labialis with 1072 nm narrow waveband light. *Clin Exp Dermatol,* 26**,** 149-54.

DUCHEN, M. R. 2004. Roles of mitochondria in health and disease. *Diabetes,* 53 Suppl 1**,** S96-102.

ECKERT, A., SCHMITT, K. & GOTZ, J. 2011. Mitochondrial dysfunction - the beginning of the end in Alzheimer's disease? Separate and synergistic modes of tau and amyloid-beta toxicity. *Alzheimers Res Ther,* 3**,** 15.

ECROYD, H. & CARVER, J. A. 2009. Crystallin proteins and amyloid fibrils. *Cell Mol Life Sci,* 66**,** 62-81.

EELLS, J. T., HENRY, M. M., SUMMERFELT, P., WONG-RILEY, M. T., BUCHMANN, E. V., KANE, M., WHELAN, N. T. & WHELAN, H. T. 2003. Therapeutic photobiomodulation for methanol-induced retinal toxicity. *Proc Natl Acad Sci U S A,* 100**,** 3439-44.

EELLS, J. T., WONG-RILEY, M. T., VERHOEVE, J., HENRY, M., BUCHMAN, E. V., KANE, M. P., GOULD, L. J., DAS, R., JETT, M., HODGSON, B. D., MARGOLIS, D. & WHELAN, H. T. 2004. Mitochondrial signal transduction in accelerated wound and retinal healing by near-infrared light therapy. *Mitochondrion,* 4**,** 559-67.

EL-AGNAF, O. M., NAGALA, S., PATEL, B. P. & AUSTEN, B. M. 2001. Non-fibrillar oligomeric species of the amyloid ABri peptide, implicated in familial British dementia, are more potent at inducing apoptotic cell death than protofibrils or mature fibrils. *J Mol Biol,* 310**,** 157-68.

ELLIS, R. J. & VAN DER VIES, S. M. 1991. Molecular chaperones. *Annu Rev Biochem,* 60**,** 321-47.

ENGELHARDT, J. A., GRIES, C. L. & LONG, G. G. 1993. Incidence of spontaneous neoplastic and nonneoplastic lesions in Charles River CD-1 mice varies with breeding origin. *Toxicol Pathol,* 21**,** 538-41.

ENNACEUR, A., MICHALIKOVA, S., VAN RENSBURG, R. & CHAZOT, P. L. 2006. Models of anxiety: responses of mice to novelty and open spaces in a 3D maze. *Behav Brain Res,* 174**,** 9-38.

ENNACEUR, A., MICHALIKOVA, S., VAN RENSBURG, R. & CHAZOT, P. L. 2008. Detailed analysis of the behavior and memory performance of middle-aged male and female CD-1 mice in a 3D maze. *Behav Brain Res,* 187**,** 312-26.

ENWEMEKA, C. S. 2004. Therapeutic Light. *Rehab Management,* 17**,** 20-5, 56-7.

ERNSTER, L. 1993. P/O ratios--the first fifty years. *Faseb J,* 7**,** 1520-4.

EROGLU, B., MOSKOPHIDIS, D. & MIVECHI, N. F. 2010. Loss of Hsp110 leads to age-dependent tau hyperphosphorylation and early accumulation of insoluble amyloid beta. *Mol Cell Biol,* 30**,** 4626-43.

EVANS, C. G., WISEN, S. & GESTWICKI, J. E. 2006. Heat shock proteins 70 and 90 inhibit early stages of amyloid beta-(1-42) aggregation in vitro. *J Biol Chem,* 281**,** 33182-91.

EYLES, S. J. & GIERASCH, L. M. 2010. Nature's molecular sponges: small heat shock proteins grow into their chaperone roles. *Proc Natl Acad Sci U S A,* 107**,** 2727-8.

FANDRICH, M., SCHMIDT, M. & GRIGORIEFF, N. 2011. Recent progress in understanding Alzheimer's beta-amyloid structures. *Trends Biochem Sci,* 36**,** 338-45.

FONTE, V., KAPULKIN, V., TAFT, A., FLUET, A., FRIEDMAN, D. & LINK, C. D. 2002. Interaction of intracellular beta amyloid peptide with chaperone proteins. *Proc Natl Acad Sci U S A,* 99**,** 9439-44.

FORSTL, H. & KURZ, A. 1999. Clinical features of Alzheimer's disease. *Eur Arch Psychiatry Clin Neurosci,* 249**,** 288-90.

FRANK, S., OLIVER, L., LEBRETON-DE COSTER, C., MOREAU, C., LECABELLEC, M. T., MICHEL, L., VALLETTE, F. M., DUBERTRET, L. & COULOMB, B. 2004. Infrared radiation affects the mitochondrial pathway of apoptosis in human fibroblasts. *J Invest Dermatol,* 123**,** 823-31.

FRIEDMAN, D. B. & JOHNSON, T. E. 1988a. A mutation in the age-1 gene in Caenorhabditis elegans lengthens life and reduces hermaphrodite fertility. *Genetics,* 118**,** 75-86.

FRIEDMAN, D. B. & JOHNSON, T. E. 1988b. Three mutants that extend both mean and maximum life span of the nematode, Caenorhabditis elegans, define the age-1 gene. *J Gerontol,* 43**,** B102-9.

FRITH, C. H. & CHANDRA, M. 1991. Incidence, distribution, and morphology of amyloidosis in Charles Rivers CD-1 mice. *Toxicol Pathol,* 19**,** 123-7.

GANDY, S. 2005. The role of cerebral amyloid beta accumulation in common forms of Alzheimer disease. *J Clin Invest,* 115**,** 1121-9.

GAO, X. & XING, D. 2009. Molecular mechanisms of cell proliferation induced by low power laser irradiation. *J Biomed Sci,* 16**,** 4.

GARIGAN, D., HSU, A. L., FRASER, A. G., KAMATH, R. S., AHRINGER, J. & KENYON, C. 2002. Genetic analysis of tissue aging in Caenorhabditis elegans: a role for heat-shock factor and bacterial proliferation. *Genetics,* 161**,** 1101-12.

GARRIDO, C. 2002. Size matters: of the small HSP27 and its large oligomers. *Cell Death Differ,* 9**,** 483-5.
GARRIDO, C., PAUL, C., SEIGNEURIC, R. & KAMPINGA, H. H. 2012. The small heat shock proteins family: The long forgotten chaperones. *Int J Biochem Cell Biol*.
GIULIANI, A., LORENZINI, L., GALLAMINI, M., MASSELLA, A., GIARDINO, L. & CALZA, L. 2009. Low infra red laser light irradiation on cultured neural cells: effects on mitochondria and cell viability after oxidative stress. *BMC Complement Altern Med,* 9**,** 8.
GLENNER, G. G. & WONG, C. W. 1984. Alzheimer's disease: initial report of the purification and characterization of a novel cerebrovascular amyloid protein. *Biochem Biophys Res Commun,* 120**,** 885-90.
GOEDERT, M., JAKES, R. & VANMECHELEN, E. 1995. Monoclonal antibody AT8 recognises tau protein phosphorylated at both serine 202 and threonine 205. *Neurosci Lett,* 189**,** 167-9.
GORDON, S. A. & SURREY, K. 1960. Red and far-red action on oxidative phosphorylation. *Radiat Res,* 12**,** 325-39.
GOURAS, G. K., XU, H., GROSS, R. S., GREENFIELD, J. P., HAI, B., WANG, R. & GREENGARD, P. 2000. Testosterone reduces neuronal secretion of Alzheimer's beta-amyloid peptides. *Proc Natl Acad Sci U S A,* 97**,** 1202-5.
GRAHAM, L. 2011. *Characterisation of transgenic mouse models of Alzheimer's disease.* University of Dundee.
GRILLO, S. L., DUGGETT, N. A., ENNACEUR, A. & CHAZOT, P. L. 2013. Non-invasive infra-red therapy (1072 nm) reduces β-amyloid protein levels in the brain of an Alzheimer's Disease mouse model, TASTPM. *Journal of Photochemistry and Photobiology B: Biology***,** http://dx.doi.org/10.1016/j.jphotobiol.2013.02.015.
GUO, J. L. & LEE, V. M. 2011. Seeding of normal Tau by pathological Tau conformers drives pathogenesis of Alzheimer-like tangles. *J Biol Chem,* 286**,** 15317-31.
GUZHOVA, I., KISLYAKOVA, K., MOSKALIOVA, O., FRIDLANSKAYA, I., TYTELL, M., CHEETHAM, M. & MARGULIS, B. 2001. In vitro studies show that Hsp70 can be released by glia and that exogenous Hsp70 can enhance neuronal stress tolerance. *Brain Res,* 914**,** 66-73.
HAASS, C. & SELKOE, D. J. 2007. Soluble protein oligomers in neurodegeneration: lessons from the Alzheimer's amyloid beta-peptide. *Nat Rev Mol Cell Biol,* 8**,** 101-12.
HAMBLIN, M. R. & DEMIDOVA, T. N. 2006. Mechanisms of low level light therapy. *Proc. of SPIE,* 6140**,** 614001-12.
HANGER, D. P., ANDERTON, B. H. & NOBLE, W. 2009. Tau phosphorylation: the therapeutic challenge for neurodegenerative disease. *Trends Mol Med,* 15**,** 112-9.
HARDY, J. 1997. Amyloid, the presenilins and Alzheimer's disease. *Trends Neurosci,* 20**,** 154-9.
HARDY, J. & ALLSOP, D. 1991. Amyloid deposition as the central event in the aetiology of Alzheimer's disease. *Trends Pharmacol Sci,* 12**,** 383-8.
HARTLEY, D. M., WALSH, D. M., YE, C. P., DIEHL, T., VASQUEZ, S., VASSILEV, P. M., TEPLOW, D. B. & SELKOE, D. J. 1999. Protofibrillar intermediates of amyloid beta-protein induce acute electrophysiological

changes and progressive neurotoxicity in cortical neurons. *J Neurosci,* 19**,** 8876-84.

HARTUNG, T., BALLS, M., BARDOUILLE, C., BLANCK, O., COECKE, S., GSTRAUNTHALER, G. & LEWIS, D. 2002. Good Cell Culture Practice. ECVAM Good Cell Culture Practice Task Force Report 1. *Altern Lab Anim,* 30**,** 407-14.

HASLBECK, M., FRANZMANN, T., WEINFURTNER, D. & BUCHNER, J. 2005. Some like it hot: the structure and function of small heat-shock proteins. *Nat Struct Mol Biol,* 12**,** 842-6.

HATAYAMA, T., HONDA, K. & YUKIOKA, M. 1986. HeLa cells synthesize a specific heat shock protein upon exposure to heat shock at 42 degrees C but not at 45 degrees C. *Biochem Biophys Res Commun,* 137**,** 957-63.

HATAYAMA, T., YAMAGISHI, N., MINOBE, E. & SAKAI, K. 2001. Role of hsp105 in protection against stress-induced apoptosis in neuronal PC12 cells. *Biochem Biophys Res Commun,* 288**,** 528-34.

HATAYAMA, T. & YASUDA, K. 1998. Association of HSP105 with HSC70 in high molecular mass complexes in mouse FM3A cells. *Biochem Biophys Res Commun,* 248**,** 395-401.

HAWKINS, D. H. & ABRAHAMSE, H. 2006. The role of laser fluence in cell viability, proliferation, and membrane integrity of wounded human skin fibroblasts following helium-neon laser irradiation. *Lasers Surg Med,* 38**,** 74-83.

HENDRICK, J. P. & HARTL, F. U. 1993. Molecular chaperone functions of heat-shock proteins. *Annu Rev Biochem,* 62**,** 349-84.

HENSHEL, D., LIM, J., SANDERS, R., ALI, Z., PATEL, A., GOPALAKRISHNAN, S., LARK, D., SNYDER, A. C., EELLS, J. T. & WATKINS, J. 2009. 57. Photobiomodulation reduces cellular oxidative stress in an animal model of diabetes. *Mitochondrion,* 9**,** 1-1.

HERNANDEZ, F., DE BARREDA, E. G., FUSTER-MATANZO, A., GONI-OLIVER, P., LUCAS, J. J. & AVILA, J. 2009. The role of GSK3 in Alzheimer disease. *Brain Res Bull,* 80**,** 248-50.

HESCHL, M. F. & BAILLIE, D. L. 1989. Characterization of the hsp70 multigene family of Caenorhabditis elegans. *DNA,* 8**,** 233-43.

HOBERT, O. 2005. Specification of the nervous system. *WormBook***,** 1-19.

HOMBURGER, F., RUSSFIELD, A. B., WEISBURGER, J. H., LIM, S., CHAK, S. P. & WEISBURGER, E. K. 1975. Aging changes in CD-1 HaM/ICR mice reared under standard laboratory conditions. *J Natl Cancer Inst,* 55**,** 37-45.

HOSHINO, T., MURAO, N., NAMBA, T., TAKEHARA, M., ADACHI, H., KATSUNO, M., SOBUE, G., MATSUSHIMA, T., SUZUKI, T. & MIZUSHIMA, T. 2011. Suppression of Alzheimer's disease-related phenotypes by expression of heat shock protein 70 in mice. *J Neurosci,* 31**,** 5225-34.

HOWLETT, D. R. 2006. P1-034: Quantification of cortical neurodegeneration in APP X PS1 transgenic mice. *Alzheimer's & dementia : the journal of the Alzheimer's Association,* 2**,** S104.

HOWLETT, D. R., BOWLER, K., SODEN, P. E., RIDDELL, D., DAVIS, J. B., RICHARDSON, J. C., BURBIDGE, S. A., GONZALEZ, M. I., IRVING, E. A., LAWMAN, A., MIGLIO, G., DAWSON, E. L., HOWLETT, E. R. & HUSSAIN, I. 2008. Abeta deposition and related pathology in an APP x

PS1 transgenic mouse model of Alzheimer's disease. *Histol Histopathol,* 23**,** 67-76.

HOWLETT, D. R. & RICHARDSON, J. C. 2009. The pathology of APP transgenic mice: a model of Alzheimer's disease or simply overexpression of APP? *Histol Histopathol,* 24**,** 83-100.

HOWLETT, D. R., RICHARDSON, J. C., AUSTIN, A., PARSONS, A. A., BATE, S. T., DAVIES, D. C. & GONZALEZ, M. I. 2004. Cognitive correlates of Abeta deposition in male and female mice bearing amyloid precursor protein and presenilin-1 mutant transgenes. *Brain Res,* 1017**,** 130-6.

HSU, A. L., MURPHY, C. T. & KENYON, C. 2003. Regulation of aging and age-related disease by DAF-16 and heat-shock factor. *Science,* 300**,** 1142-5.

HU, X., CRICK, S. L., BU, G., FRIEDEN, C., PAPPU, R. V. & LEE, J. M. 2009. Amyloid seeds formed by cellular uptake, concentration, and aggregation of the amyloid-beta peptide. *Proc Natl Acad Sci U S A,* 106**,** 20324-9.

HUANG, C., XIONG, C. & KORNFELD, K. 2004. Measurements of age-related changes of physiological processes that predict lifespan of Caenorhabditis elegans. *Proc Natl Acad Sci U S A,* 101**,** 8084-9.

HUANG, Y. & MUCKE, L. 2012. Alzheimer mechanisms and therapeutic strategies. *Cell,* 148**,** 1204-22.

HUANG, Y. Y., CHEN, A. C., CARROLL, J. D. & HAMBLIN, M. R. 2009. Biphasic dose response in low level light therapy. *Dose Response,* 7**,** 358-83.

HURTADO, O., DE CRISTOBAL, J., SANCHEZ, V., LIZASOAIN, I., CARDENAS, A., PEREIRA, M. P., COLADO, M. I., LEZA, J. C., LORENZO, P. & MORO, M. A. 2003. Inhibition of glutamate release by delaying ATP fall accounts for neuroprotective effects of antioxidants in experimental stroke. *Faseb J,* 17**,** 2082-4.

HUSSAIN, I., HAWKINS, J., HARRISON, D., COLLIER, S., VINSON, M., BURBIDGE, S. A. & DAVIS, J. B. 2006. P1-033: The identification of distinct pools of Aβ in the brains of TASTPM mice. *Alzheimer's & dementia : the journal of the Alzheimer's Association,* 2**,** S104.

HYLANDER, B. L., CHEN, X., GRAF, P. C. & SUBJECK, J. R. 2000. The distribution and localization of hsp110 in brain. *Brain Res,* 869**,** 49-55.

ISHIHARA, K., YASUDA, K. & HATAYAMA, T. 1999. Molecular cloning, expression and localization of human 105 kDa heat shock protein, hsp105. *Biochim Biophys Acta,* 1444**,** 138-42.

ISOBE, I., YANAGISAWA, K. & MICHIKAWA, M. 2000. A possible model of senile plaques using synthetic amyloid beta-protein and rat glial culture. *Exp Neurol,* 162**,** 51-60.

ITTNER, L. M. & GOTZ, J. 2011. Amyloid-beta and tau--a toxic pas de deux in Alzheimer's disease. *Nat Rev Neurosci,* 12**,** 65-72.

JAYA, N., GARCIA, V. & VIERLING, E. 2009. Substrate binding site flexibility of the small heat shock protein molecular chaperones. *Proc Natl Acad Sci U S A,* 106**,** 15604-9.

JOHNSON, L. V., WALSH, M. L., BOCKUS, B. J. & CHEN, L. B. 1981. Monitoring of relative mitochondrial membrane potential in living cells by fluorescence microscopy. *J Cell Biol,* 88**,** 526-35.

JOHNSON, T. E. 2003. Advantages and disadvantages of Caenorhabditis elegans for aging research. *Exp Gerontol,* 38**,** 1329-32.

JOHNSON, T. E. 2008. Caenorhabditis elegans 2007: the premier model for the study of aging. *Exp Gerontol,* 43**,** 1-4.

JONES, D. & CANDIDO, E. P. 1999. Feeding is inhibited by sublethal concentrations of toxicants and by heat stress in the nematode Caenorhabditis elegans: relationship to the cellular stress response. *J Exp Zool,* 284**,** 147-57.

JORGENSEN, E. M. 2004. Dopamine: should I stay or should I go now? *Nat Neurosci,* 7**,** 1019-21.

KAKIMURA, J., KITAMURA, Y., TAKATA, K., UMEKI, M., SUZUKI, S., SHIBAGAKI, K., TANIGUCHI, T., NOMURA, Y., GEBICKE-HAERTER, P. J., SMITH, M. A., PERRY, G. & SHIMOHAMA, S. 2002. Microglial activation and amyloid-beta clearance induced by exogenous heat-shock proteins. *Faseb J,* 16**,** 601-3.

KAMENETZ, F., TOMITA, T., HSIEH, H., SEABROOK, G., BORCHELT, D., IWATSUBO, T., SISODIA, S. & MALINOW, R. 2003. APP processing and synaptic function. *Neuron,* 37**,** 925-37.

KANG, J., LEMAIRE, H. G., UNTERBECK, A., SALBAUM, J. M., MASTERS, C. L., GRZESCHIK, K. H., MULTHAUP, G., BEYREUTHER, K. & MULLER-HILL, B. 1987. The precursor of Alzheimer's disease amyloid A4 protein resembles a cell-surface receptor. *Nature,* 325**,** 733-6.

KANSKI, J., VARADARAJAN, S., AKSENOVA, M. & BUTTERFIELD, D. A. 2002. Role of glycine-33 and methionine-35 in Alzheimer's amyloid beta-peptide 1-42-associated oxidative stress and neurotoxicity. *Biochim Biophys Acta,* 1586**,** 190-8.

KAPULKIN, W. J., HIESTER, B. G. & LINK, C. D. 2005. Compensatory regulation among ER chaperones in C. elegans. *FEBS Lett,* 579**,** 3063-8.

KARU, T. 1999. Primary and secondary mechanisms of action of visible to near-IR radiation on cells. *J Photochem Photobiol B,* 49**,** 1-17.

KARU, T. 2010a. Mitochondrial mechanisms of photobiomodulation in context of new data about multiple roles of ATP. *Photomed Laser Surg,* 28**,** 159-60.

KARU, T., PYATIBRAT, L. & KALENDO, G. 1995. Irradiation with He-Ne laser increases ATP level in cells cultivated in vitro. *J Photochem Photobiol B,* 27**,** 219-23.

KARU, T., TIPHLOVA, O., ESENALIEV, R. & LETOKHOV, V. 1994. Two different mechanisms of low-intensity laser photobiological effects on Escherichia coli. *J Photochem Photobiol B,* 24**,** 155-61.

KARU, T. I. 1988. Molecular Mechanism of the Therapeutic Effect of Low-Intensity Laser Radiation. *Lasers in the Life Sciences,* 2**,** 53-74.

KARU, T. I. 2008. Mitochondrial signaling in mammalian cells activated by red and near-IR radiation. *Photochem Photobiol,* 84**,** 1091-9.

KARU, T. I. 2010b. Multiple roles of cytochrome c oxidase in mammalian cells under action of red and IR-A radiation. *IUBMB Life,* 62**,** 607-10.

KARU, T. I. & KOLYAKOV, S. F. 2005. Exact action spectra for cellular responses relevant to phototherapy. *Photomed Laser Surg,* 23**,** 355-61.

KARU, T. I., PYATIBRAT, L. V. & AFANASYEVA, N. I. 2004. A novel mitochondrial signaling pathway activated by visible-to-near infrared radiation. *Photochem Photobiol,* 80**,** 366-72.

KARU, T. I., PYATIBRAT, L. V., KOLYAKOV, S. F. & AFANASYEVA, N. I. 2005. Absorption measurements of a cell monolayer relevant to

phototherapy: reduction of cytochrome c oxidase under near IR radiation. *J Photochem Photobiol B,* 81**,** 98-106.
KAYED, R., HEAD, E., THOMPSON, J. L., MCINTIRE, T. M., MILTON, S. C., COTMAN, C. W. & GLABE, C. G. 2003. Common structure of soluble amyloid oligomers implies common mechanism of pathogenesis. *Science,* 300**,** 486-9.
KENYON, C. 2011. The first long-lived mutants: discovery of the insulin/IGF-1 pathway for ageing. *Philos Trans R Soc Lond B Biol Sci,* 366**,** 9-16.
KENYON, C. J. 2010. The genetics of ageing. *Nature,* 464**,** 504-12.
KHAKH, B. S. & BURNSTOCK, G. 2009. The double life of ATP. *Sci Am,* 301**,** 84-90, 92.
KHAN, H. A. 2003. Bioluminometric assay of ATP in mouse brain: Determinant factors for enhanced test sensitivity. *J Biosci,* 28**,** 379-82.
KING, M., NAFAR, F., CLARKE, J. & MEAROW, K. 2009. The small heat shock protein Hsp27 protects cortical neurons against the toxic effects of beta-amyloid peptide. *J Neurosci Res,* 87**,** 3161-75.
KLASS, M. R. 1977. Aging in the nematode Caenorhabditis elegans: major biological and environmental factors influencing life span. *Mech Ageing Dev,* 6**,** 413-29.
KOREN, J., 3RD, JINWAL, U. K., LEE, D. C., JONES, J. R., SHULTS, C. L., JOHNSON, A. G., ANDERSON, L. J. & DICKEY, C. A. 2009. Chaperone signalling complexes in Alzheimer's disease. *J Cell Mol Med,* 13**,** 619-30.
KRANENBURG, O., BOUMA, B., GENT, Y. Y., AARSMAN, C. J., KAYED, R., POSTHUMA, G., SCHIKS, B., VOEST, E. E. & GEBBINK, M. F. 2005. Beta-amyloid (Abeta) causes detachment of N1E-115 neuroblastoma cells by acting as a scaffold for cell-associated plasminogen activation. *Mol Cell Neurosci,* 28**,** 496-508.
KREISLER, M., CHRISTOFFERS, A. B., WILLERSHAUSEN, B. & D'HOEDT, B. 2003. Effect of low-level GaAlAs laser irradiation on the proliferation rate of human periodontal ligament fibroblasts: an in vitro study. *J Clin Periodontol,* 30**,** 353-8.
KUDVA, Y. C., HIDDINGA, H. J., BUTLER, P. C., MUESKE, C. S. & EBERHARDT, N. L. 1997. Small heat shock proteins inhibit in vitro A beta(1-42) amyloidogenesis. *FEBS Lett,* 416**,** 117-21.
KURT, M. A., DAVIES, D. C., KIDD, M., DUFF, K. & HOWLETT, D. R. 2003. Hyperphosphorylated tau and paired helical filament-like structures in the brains of mice carrying mutant amyloid precursor protein and mutant presenilin-1 transgenes. *Neurobiol Dis,* 14**,** 89-97.
KURT, M. A., DAVIES, D. C., KIDD, M., DUFF, K., ROLPH, S. C., JENNINGS, K. H. & HOWLETT, D. R. 2001. Neurodegenerative changes associated with beta-amyloid deposition in the brains of mice carrying mutant amyloid precursor protein and mutant presenilin-1 transgenes. *Exp Neurol,* 171**,** 59-71.
LAFERLA, F. M. 2010. Pathways linking Abeta and tau pathologies. *Biochem Soc Trans,* 38**,** 993-5.
LANNEAU, D., WETTSTEIN, G., BONNIAUD, P. & GARRIDO, C. 2010. Heat shock proteins: cell protection through protein triage. *ScientificWorldJournal,* 10**,** 1543-52.

LEE, S. S., KENNEDY, S., TOLONEN, A. C. & RUVKUN, G. 2003. DAF-16 target genes that control C. elegans life-span and metabolism. *Science,* 300**,** 644-7.

LEITZ, G., FALLMAN, E., TUCK, S. & AXNER, O. 2002. Stress response in Caenorhabditis elegans caused by optical tweezers: wavelength, power, and time dependence. *Biophys J,* 82**,** 2224-31.

LEMIRE, B. D., BEHRENDT, M., DECORBY, A. & GASKOVA, D. 2009. C. elegans longevity pathways converge to decrease mitochondrial membrane potential. *Mech Ageing Dev,* 130**,** 461-5.

LEUNG, M. C., WILLIAMS, P. L., BENEDETTO, A., AU, C., HELMCKE, K. J., ASCHNER, M. & MEYER, J. N. 2008. Caenorhabditis elegans: an emerging model in biomedical and environmental toxicology. *Toxicol Sci,* 106**,** 5-28.

LIANG, H. L., WHELAN, H. T., EELLS, J. T., MENG, H., BUCHMANN, E., LERCH-GAGGL, A. & WONG-RILEY, M. 2006. Photobiomodulation partially rescues visual cortical neurons from cyanide-induced apoptosis. *Neuroscience,* 139**,** 639-49.

LIANG, H. L., WHELAN, H. T., EELLS, J. T. & WONG-RILEY, M. T. 2008. Near-infrared light via light-emitting diode treatment is therapeutic against rotenone- and 1-methyl-4-phenylpyridinium ion-induced neurotoxicity. *Neuroscience,* 153**,** 963-74.

LIANG, J. J. 2000. Interaction between beta-amyloid and lens alphaB-crystallin. *FEBS Lett,* 484**,** 98-101.

LINK, C. D. 2006. C. elegans models of age-associated neurodegenerative diseases: lessons from transgenic worm models of Alzheimer's disease. *Exp Gerontol,* 41**,** 1007-13.

LINK, C. D., TAFT, A., KAPULKIN, V., DUKE, K., KIM, S., FEI, Q., WOOD, D. E. & SAHAGAN, B. G. 2003. Gene expression analysis in a transgenic Caenorhabditis elegans Alzheimer's disease model. *Neurobiol Aging,* 24**,** 397-413.

LITHGOW, G. J., WHITE, T. M., MELOV, S. & JOHNSON, T. E. 1995. Thermotolerance and extended life-span conferred by single-gene mutations and induced by thermal stress. *Proc Natl Acad Sci U S A,* 92**,** 7540-4.

LIU, S. J., GASPERINI, R., FOA, L. & SMALL, D. H. 2010. Amyloid-beta decreases cell-surface AMPA receptors by increasing intracellular calcium and phosphorylation of GluR2. *J Alzheimers Dis,* 21**,** 655-66.

LORENZO, A. & YANKNER, B. A. 1994. Beta-amyloid neurotoxicity requires fibril formation and is inhibited by congo red. *Proc Natl Acad Sci U S A,* 91**,** 12243-7.

LOWRY, O. H., ROSEBROUGH, N. J., FARR, A. L. & RANDALL, R. J. 1951. Protein measurement with the Folin phenol reagent. *J Biol Chem,* 193**,** 265-75.

MACARIO, A. J. & CONWAY DE MACARIO, E. 2005. Sick chaperones, cellular stress, and disease. *N Engl J Med,* 353**,** 1489-501.

MACARIO, A. J. & CONWAY DE MACARIO, E. 2007. Chaperonopathies by defect, excess, or mistake. *Ann N Y Acad Sci,* 1113**,** 178-91.

MAGRANE, J., SMITH, R. C., WALSH, K. & QUERFURTH, H. W. 2004. Heat shock protein 70 participates in the neuroprotective response to

intracellularly expressed beta-amyloid in neurons. *J Neurosci,* 24**,** 1700-6.
MAN, H. Y. 2011. GluA2-lacking, calcium-permeable AMPA receptors--inducers of plasticity? *Curr Opin Neurobiol,* 21**,** 291-8.
MANN, M. 2008. Can proteomics retire the western blot? *J Proteome Res,* 7**,** 3065.
MAO, J. J., KATAYAMA, S., WATANABE, C., HARADA, Y., NODA, K., YAMAMURA, Y. & NAKAMURA, S. 2001. The relationship between alphaB-crystallin and neurofibrillary tangles in Alzheimer's disease. *Neuropathol Appl Neurobiol,* 27**,** 180-8.
MARKHAM, A., CAMERON, I., FRANKLIN, P. & SPEDDING, M. 2004. BDNF increases rat brain mitochondrial respiratory coupling at complex I, but not complex II. *Eur J Neurosci,* 20**,** 1189-96.
MATHUR, A., HONG, Y., KEMP, B. K., BARRIENTOS, A. A. & ERUSALIMSKY, J. D. 2000. Evaluation of fluorescent dyes for the detection of mitochondrial membrane potential changes in cultured cardiomyocytes. *Cardiovasc Res,* 46**,** 126-38.
MATSUZAKI, K. 2011. Formation of Toxic Amyloid Fibrils by Amyloid beta-Protein on Ganglioside Clusters. *Int J Alzheimers Dis,* 2011**,** 956104.
MATTSON, M. P. & LIU, D. 2003. Mitochondrial potassium channels and uncoupling proteins in synaptic plasticity and neuronal cell death. *Biochem Biophys Res Commun,* 304**,** 539-49.
MAURAGE, C. A., SERGEANT, N., RUCHOUX, M. M., HAUW, J. J. & DELACOURTE, A. 2003. Phosphorylated serine 199 of microtubule-associated protein tau is a neuronal epitope abundantly expressed in youth and an early marker of tau pathology. *Acta Neuropathol,* 105**,** 89-97.
MAYER, M. P. & BUKAU, B. 2005. Hsp70 chaperones: cellular functions and molecular mechanism. *Cell Mol Life Sci,* 62**,** 670-84.
MEARES, G. P., ZMIJEWSKA, A. A. & JOPE, R. S. 2008. HSP105 interacts with GRP78 and GSK3 and promotes ER stress-induced caspase-3 activation. *Cell Signal,* 20**,** 347-58.
MEDRADO, A. P., SOARES, A. P., SANTOS, E. T., REIS, S. R. & ANDRADE, Z. A. 2008. Influence of laser photobiomodulation upon connective tissue remodeling during wound healing. *J Photochem Photobiol B,* 92**,** 144-52.
MICHALIKOVA, S., ENNACEUR, A., VAN RENSBURG, R. & CHAZOT, P. L. 2008. Emotional responses and memory performance of middle-aged CD1 mice in a 3D maze: effects of low infrared light. *Neurobiol Learn Mem,* 89**,** 480-8.
MICHALIKOVA, S., VAN RENSBURG, R., CHAZOT, P. L. & ENNACEUR, A. 2010. Anxiety responses in Balb/c, c57 and CD-1 mice exposed to a novel open space test. *Behav Brain Res,* 207**,** 402-17.
MIRONOV, S. L. 2007. ADP regulates movements of mitochondria in neurons. *Biophys J,* 92**,** 2944-52.
MIZUMORI, S. J., ROSENZWEIG, M. R. & KERMISCH, M. G. 1982. Failure of mice to demonstrate spatial memory in the radial maze. *Behav Neural Biol,* 35**,** 33-45.
MOCHIZUKI-ODA, N., KATAOKA, Y., CUI, Y., YAMADA, H., HEYA, M. & AWAZU, K. 2002. Effects of near-infra-red laser irradiation on adenosine

triphosphate and adenosine diphosphate contents of rat brain tissue. *Neurosci Lett,* 323**,** 207-10.

MORLEY, J. F. & MORIMOTO, R. I. 2004. Regulation of longevity in Caenorhabditis elegans by heat shock factor and molecular chaperones. *Mol Biol Cell,* 15**,** 657-64.

MORRIS, J. Z., TISSENBAUM, H. A. & RUVKUN, G. 1996. A phosphatidylinositol-3-OH kinase family member regulating longevity and diapause in Caenorhabditis elegans. *Nature,* 382**,** 536-9.

MOSSER, D. D., CARON, A. W., BOURGET, L., DENIS-LAROSE, C. & MASSIE, B. 1997. Role of the human heat shock protein hsp70 in protection against stress-induced apoptosis. *Mol Cell Biol,* 17**,** 5317-27.

MOSSER, D. D., CARON, A. W., BOURGET, L., MERIIN, A. B., SHERMAN, M. Y., MORIMOTO, R. I. & MASSIE, B. 2000. The chaperone function of hsp70 is required for protection against stress-induced apoptosis. *Mol Cell Biol,* 20**,** 7146-59.

MUCHOWSKI, P. J. & WACKER, J. L. 2005. Modulation of neurodegeneration by molecular chaperones. *Nat Rev Neurosci,* 6**,** 11-22.

MURPHY, C. T., MCCARROLL, S. A., BARGMANN, C. I., FRASER, A., KAMATH, R. S., AHRINGER, J., LI, H. & KENYON, C. 2003. Genes that act downstream of DAF-16 to influence the lifespan of Caenorhabditis elegans. *Nature,* 424**,** 277-83.

NARAYANAN, S., KAMPS, B., BOELENS, W. C. & REIF, B. 2006. alphaB-crystallin competes with Alzheimer's disease beta-amyloid peptide for peptide-peptide interactions and induces oxidation of Abeta-Met35. *FEBS Lett,* 580**,** 5941-6.

NICHOLL, I. D. & QUINLAN, R. A. 1994. Chaperone activity of alpha-crystallins modulates intermediate filament assembly. *EMBO J,* 13**,** 945-53.

NICHOLLS, D. G. & BUDD, S. L. 2000. Mitochondria and neuronal survival. *Physiol Rev,* 80**,** 315-60.

NOVOSELOVA, E. G., GLUSHKOVA, O. V., CHERENKOV, D. A., CHUDNOVSKY, V. M. & FESENKO, E. E. 2006. Effects of low-power laser radiation on mice immunity. *Photodermatol Photoimmunol Photomed,* 22**,** 33-8.

O'BRIEN, R. J. & WONG, P. C. 2011. Amyloid precursor protein processing and Alzheimer's disease. *Annu Rev Neurosci,* 34**,** 185-204.

OGG, S., PARADIS, S., GOTTLIEB, S., PATTERSON, G. I., LEE, L., TISSENBAUM, H. A. & RUVKUN, G. 1997. The Fork head transcription factor DAF-16 transduces insulin-like metabolic and longevity signals in C. elegans. *Nature,* 389**,** 994-9.

OH, H. J., EASTON, D., MURAWSKI, M., KANEKO, Y. & SUBJECK, J. R. 1999. The chaperoning activity of hsp110. Identification of functional domains by use of targeted deletions. *J Biol Chem,* 274**,** 15712-8.

OHTSUKA, K. & SUZUKI, T. 2000. Roles of molecular chaperones in the nervous system. *Brain Res Bull,* 53**,** 141-6.

OJHA, J., KARMEGAM, R. V., MASILAMONI, J. G., TERRY, A. V. & CASHIKAR, A. G. 2011. Behavioral defects in chaperone-deficient Alzheimer's disease model mice. *PLoS One,* 6**,** e16550.

OKADA, E., FIRBANK, M., SCHWEIGER, M., ARRIDGE, S. R., COPE, M. & DELPY, D. T. 1997. Theoretical and experimental investigation of near-

infrared light propagation in a model of the adult head. *Appl Opt,* 36**,** 21-31.

OLSEN, A., VANTIPALLI, M. C. & LITHGOW, G. J. 2006a. Lifespan extension of Caenorhabditis elegans following repeated mild hormetic heat treatments. *Biogerontology,* 7**,** 221-30.

OLSEN, A., VANTIPALLI, M. C. & LITHGOW, G. J. 2006b. Using Caenorhabditis elegans as a model for aging and age-related diseases. *Ann N Y Acad Sci,* 1067**,** 120-8.

OLSSON, T., HANSSON, O., NYLANDSTED, J., JAATTELA, M., SMITH, M. L. & WIELOCH, T. 2004. Lack of neuroprotection by heat shock protein 70 overexpression in a mouse model of global cerebral ischemia. *Exp Brain Res,* 154**,** 442-9.

OW, Y. P., GREEN, D. R., HAO, Z. & MAK, T. W. 2008. Cytochrome c: functions beyond respiration. *Nat Rev Mol Cell Biol,* 9**,** 532-42.

OWEN-REECE, H., ELWELL, C. E., HARKNESS, W., GOLDSTONE, J., DELPY, D. T., WYATT, J. S. & SMITH, M. 1996. Use of near infrared spectroscopy to estimate cerebral blood flow in conscious and anaesthetized adult subjects. *Br J Anaesth,* 76**,** 43-8.

PAGANINI-HILL, A. & HENDERSON, V. W. 1994. Estrogen deficiency and risk of Alzheimer's disease in women. *Am J Epidemiol,* 140**,** 256-61.

PARCELLIER, A., SCHMITT, E., BRUNET, M., HAMMANN, A., SOLARY, E. & GARRIDO, C. 2005. Small heat shock proteins HSP27 and alphaB-crystallin: cytoprotective and oncogenic functions. *Antioxid Redox Signal,* 7**,** 404-13.

PASSARELLA, S., CASAMASSIMA, E., MOLINARI, S., PASTORE, D., QUAGLIARIELLO, E., CATALANO, I. M. & CINGOLANI, A. 1984. Increase of proton electrochemical potential and ATP synthesis in rat liver mitochondria irradiated in vitro by helium-neon laser. *FEBS Lett,* 175**,** 95-9.

PATIL, S. S., SUNYER, B., HOGER, H. & LUBEC, G. 2009. Evaluation of spatial memory of C57BL/6J and CD1 mice in the Barnes maze, the Multiple T-maze and in the Morris water maze. *Behav Brain Res,* 198**,** 58-68.

PATTERSON, K. R., WARD, S. M., COMBS, B., VOSS, K., KANAAN, N. M., MORFINI, G., BRADY, S. T., GAMBLIN, T. C. & BINDER, L. I. 2011. Heat shock protein 70 prevents both tau aggregation and the inhibitory effects of preexisting tau aggregates on fast axonal transport. *Biochemistry,* 50**,** 10300-10.

PEARSON, R. C. & POWELL, T. P. 1989. The neuroanatomy of Alzheimer's disease. *Rev Neurosci,* 2**,** 101-22.

PEREZ, N., SUGAR, J., CHARYA, S., JOHNSON, G., MERRIL, C., BIERER, L., PERL, D., HAROUTUNIAN, V. & WALLACE, W. 1991. Increased synthesis and accumulation of heat shock 70 proteins in Alzheimer's disease. *Brain Res Mol Brain Res,* 11**,** 249-54.

PIRES OLIVEIRA, D. A., DE OLIVEIRA, R. F., ZANGARO, R. A. & SOARES, C. P. 2008. Evaluation of low-level laser therapy of osteoblastic cells. *Photomed Laser Surg,* 26**,** 401-4.

PREVILLE, X., SALVEMINI, F., GIRAUD, S., CHAUFOUR, S., PAUL, C., STEPIEN, G., URSINI, M. V. & ARRIGO, A. P. 1999. Mammalian small stress proteins protect against oxidative stress through their ability to

increase glucose-6-phosphate dehydrogenase activity and by maintaining optimal cellular detoxifying machinery. *Exp Cell Res,* 247**,** 61-78.

PUGH, P. L., RICHARDSON, J. C., BATE, S. T., UPTON, N. & SUNTER, D. 2007. Non-cognitive behaviours in an APP/PS1 transgenic model of Alzheimer's disease. *Behav Brain Res,* 178**,** 18-28.

QI, Y., WANG, J. K., MCMILLIAN, M. & CHIKARAISHI, D. M. 1997. Characterization of a CNS cell line, CAD, in which morphological differentiation is initiated by serum deprivation. *J Neurosci,* 17**,** 1217-25.

RAMSDEN, M., NYBORG, A. C., MURPHY, M. P., CHANG, L., STANCZYK, F. Z., GOLDE, T. E. & PIKE, C. J. 2003. Androgens modulate beta-amyloid levels in male rat brain. *J Neurochem,* 87**,** 1052-5.

RANKIN, C. A., SUN, Q. & GAMBLIN, T. C. 2007. Tau phosphorylation by GSK-3beta promotes tangle-like filament morphology. *Mol Neurodegener,* 2**,** 12.

RANKIN, C. A., SUN, Q. & GAMBLIN, T. C. 2008. Pre-assembled tau filaments phosphorylated by GSK-3b form large tangle-like structures. *Neurobiol Dis,* 31**,** 368-377.

READ, D. E. & GORMAN, A. M. 2009. Heat shock protein 27 in neuronal survival and neurite outgrowth. *Biochem Biophys Res Commun,* 382**,** 6-8.

REDDY, P. H. 2011. Abnormal tau, mitochondrial dysfunction, impaired axonal transport of mitochondria, and synaptic deprivation in Alzheimer's disease. *Brain Res,* 1415**,** 136-48.

RENKAWEK, K., VOORTER, C. E., BOSMAN, G. J., VAN WORKUM, F. P. & DE JONG, W. W. 1994. Expression of alpha B-crystallin in Alzheimer's disease. *Acta Neuropathol,* 87**,** 155-60.

RICHARDSON, J. C., KENDAL, C. E., ANDERSON, R., PRIEST, F., GOWER, E., SODEN, P., GRAY, R., TOPPS, S., HOWLETT, D. R., LAVENDER, D., CLARKE, N. J., BARNES, J. C., HAWORTH, R., STEWART, M. G. & RUPNIAK, H. T. 2003. Ultrastructural and behavioural changes precede amyloid deposition in a transgenic model of Alzheimer's disease. *Neuroscience,* 122**,** 213-28.

RIDDLE, D. L. 1997. *C. elegans II,* Plainview, N.Y., Cold Spring Harbor Laboratory Press.

ROGALLA, T., EHRNSPERGER, M., PREVILLE, X., KOTLYAROV, A., LUTSCH, G., DUCASSE, C., PAUL, C., WIESKE, M., ARRIGO, A. P., BUCHNER, J. & GAESTEL, M. 1999. Regulation of Hsp27 oligomerization, chaperone function, and protective activity against oxidative stress/tumor necrosis factor alpha by phosphorylation. *J Biol Chem,* 274**,** 18947-56.

ROJAS, J. C., LEE, J., JOHN, J. M. & GONZALEZ-LIMA, F. 2008. Neuroprotective effects of near-infrared light in an in vivo model of mitochondrial optic neuropathy. *J Neurosci,* 28**,** 13511-21.

SAHARA, N., MAEDA, S., YOSHIIKE, Y., MIZOROKI, T., YAMASHITA, S., MURAYAMA, M., PARK, J. M., SAITO, Y., MURAYAMA, S. & TAKASHIMA, A. 2007. Molecular chaperone-mediated tau protein metabolism counteracts the formation of granular tau oligomers in human brain. *J Neurosci Res,* 85**,** 3098-108.

SAITO, Y., YAMAGISHI, N. & HATAYAMA, T. 2007. Different localization of Hsp105 family proteins in mammalian cells. *Exp Cell Res,* 313**,** 3707-17.

SAITO, Y., YAMAGISHI, N. & HATAYAMA, T. 2009. Nuclear localization mechanism of Hsp105beta and its possible function in mammalian cells. *J Biochem,* 145**,** 185-91.

SAMALI, A., HOLMBERG, C. I., SISTONEN, L. & ORRENIUS, S. 1999. Thermotolerance and cell death are distinct cellular responses to stress: dependence on heat shock proteins. *FEBS Lett,* 461**,** 306-10.

SAMALI, A., ROBERTSON, J. D., PETERSON, E., MANERO, F., VAN ZEIJL, L., PAUL, C., COTGREAVE, I. A., ARRIGO, A. P. & ORRENIUS, S. 2001. Hsp27 protects mitochondria of thermotolerant cells against apoptotic stimuli. *Cell Stress Chaperones,* 6**,** 49-58.

SAWIN, E. R., RANGANATHAN, R. & HORVITZ, H. R. 2000. C. elegans locomotory rate is modulated by the environment through a dopaminergic pathway and by experience through a serotonergic pathway. *Neuron,* 26**,** 619-31.

SCHAFER, W. R. 2005. Deciphering the neural and molecular mechanisms of C. elegans behavior. *Curr Biol,* 15**,** R723-9.

SCHEFFLER, I. E. 2001. A century of mitochondrial research: achievements and perspectives. *Mitochondrion,* 1**,** 3-31.

SCHMITT, K., GRIMM, A., KAZMIERCZAK, A., STROSZNAJDER, J. B., GOTZ, J. & ECKERT, A. 2012. Insights into Mitochondrial Dysfunction: Aging, Amyloid-beta, and Tau-A Deleterious Trio. *Antioxid Redox Signal,* 16**,** 1456-66.

SCHOLZEN, T. & GERDES, J. 2000. The Ki-67 protein: from the known and the unknown. *J Cell Physiol,* 182**,** 311-22.

SEKI, M., NAWA, H., MORIOKA, T., FUKUCHI, T., OITE, T., ABE, H. & TAKEI, N. 2002. Establishment of a novel enzyme-linked immunosorbent assay for Thy-1; quantitative assessment of neuronal degeneration. *Neurosci Lett,* 329**,** 185-8.

SHAMMAS, S. L., WAUDBY, C. A., WANG, S., BUELL, A. K., KNOWLES, T. P., ECROYD, H., WELLAND, M. E., CARVER, J. A., DOBSON, C. M. & MEEHAN, S. 2011. Binding of the molecular chaperone alphaB-crystallin to Abeta amyloid fibrils inhibits fibril elongation. *Biophys J,* 101**,** 1681-9.

SHANKAR, G. M., LI, S., MEHTA, T. H., GARCIA-MUNOZ, A., SHEPARDSON, N. E., SMITH, I., BRETT, F. M., FARRELL, M. A., ROWAN, M. J., LEMERE, C. A., REGAN, C. M., WALSH, D. M., SABATINI, B. L. & SELKOE, D. J. 2008. Amyloid-beta protein dimers isolated directly from Alzheimer's brains impair synaptic plasticity and memory. *Nat Med,* 14**,** 837-42.

SHARP, F. R., MASSA, S. M. & SWANSON, R. A. 1999. Heat-shock protein protection. *Trends Neurosci,* 22**,** 97-9.

SHERMAN, M. Y. & GOLDBERG, A. L. 2001. Cellular defenses against unfolded proteins: a cell biologist thinks about neurodegenerative diseases. *Neuron,* 29**,** 15-32.

SHIMURA, H., MIURA-SHIMURA, Y. & KOSIK, K. S. 2004. Binding of tau to heat shock protein 27 leads to decreased concentration of hyperphosphorylated tau and enhanced cell survival. *J Biol Chem,* 279**,** 17957-62.

SHINOHARA, H., INAGUMA, Y., GOTO, S., INAGAKI, T. & KATO, K. 1993. Alpha B crystallin and HSP28 are enhanced in the cerebral cortex of patients with Alzheimer's disease. *J Neurol Sci,* 119**,** 203-8.

SILVEIRA, P. C., SILVA, L. A., FRAGA, D. B., FREITAS, T. P., STRECK, E. L. & PINHO, R. 2009. Evaluation of mitochondrial respiratory chain activity in muscle healing by low-level laser therapy. *J Photochem Photobiol B,* 95**,** 89-92.

SILVEIRA, P. C., STRECK, E. L. & PINHO, R. A. 2007. Evaluation of mitochondrial respiratory chain activity in wound healing by low-level laser therapy. *J Photochem Photobiol B,* 86**,** 279-82.

SIMPKINS, J. W., GREEN, P. S., GRIDLEY, K. E., SINGH, M., DE FIEBRE, N. C. & RAJAKUMAR, G. 1997. Role of estrogen replacement therapy in memory enhancement and the prevention of neuronal loss associated with Alzheimer's disease. *Am J Med,* 103**,** 19S-25S.

SINGH, V. & ABALLAY, A. 2006. Heat-shock transcription factor (HSF)-1 pathway required for Caenorhabditis elegans immunity. *Proc Natl Acad Sci U S A,* 103**,** 13092-7.

SNUTCH, T. P. & BAILLIE, D. L. 1984. A high degree of DNA strain polymorphism associated with the major heat shock gene in Caenorhabditis elegans. *Mol Gen Genet,* 195**,** 329-35.

SOMMER, A. P., BIESCHKE, J., FRIEDRICH, R. P., ZHU, D., WANKER, E. E., FECHT, H. J., MERELES, D. & HUNSTEIN, W. 2012. 670 nm laser light and EGCG complementarily reduce amyloid-beta aggregates in human neuroblastoma cells: basis for treatment of Alzheimer's disease? *Photomed Laser Surg,* 30**,** 54-60.

SOMMER, A. P., PINHEIRO, A. L., MESTER, A. R., FRANKE, R. P. & WHELAN, H. T. 2001. Biostimulatory windows in low-intensity laser activation: lasers, scanners, and NASA's light-emitting diode array system. *J Clin Laser Med Surg,* 19**,** 29-33.

SOO, E. T., NG, Y. K., BAY, B. H. & YIP, G. W. 2008. Heat shock proteins and neurodegenerative disorders. *ScientificWorldJournal,* 8**,** 270-4.

SOTI, C. & CSERMELY, P. 2000. Molecular chaperones and the aging process. *Biogerontology,* 1**,** 225-33.

SOTI, C. & CSERMELY, P. 2003. Aging and molecular chaperones. *Exp Gerontol,* 38**,** 1037-40.

SOUIL, E., CAPON, A., MORDON, S., DINH-XUAN, A. T., POLLA, B. S. & BACHELET, M. 2001. Treatment with 815-nm diode laser induces long-lasting expression of 72-kDa heat shock protein in normal rat skin. *Br J Dermatol,* 144**,** 260-6.

STEGE, G. J., RENKAWEK, K., OVERKAMP, P. S., VERSCHUURE, P., VAN RIJK, A. F., REIJNEN-AALBERS, A., BOELENS, W. C., BOSMAN, G. J. & DE JONG, W. W. 1999. The molecular chaperone alphaB-crystallin enhances amyloid beta neurotoxicity. *Biochem Biophys Res Commun,* 262**,** 152-6.

STETLER, R. A., GAO, Y., SIGNORE, A. P., CAO, G. & CHEN, J. 2009. HSP27: mechanisms of cellular protection against neuronal injury. *Curr Mol Med,* 9**,** 863-72.

STRINGHAM, E. G., DIXON, D. K., JONES, D. & CANDIDO, E. P. 1992. Temporal and spatial expression patterns of the small heat shock

(hsp16) genes in transgenic Caenorhabditis elegans. *Mol Biol Cell,* 3**,** 221-33.
SUDOH, S., KAWAMURA, Y., SATO, S., WANG, R., SAIDO, T. C., OYAMA, F., SAKAKI, Y., KOMANO, H. & YANAGISAWA, K. 1998. Presenilin 1 mutations linked to familial Alzheimer's disease increase the intracellular levels of amyloid beta-protein 1-42 and its N-terminally truncated variant(s) which are generated at distinct sites. *J Neurochem,* 71**,** 1535-43.
SUN, W., QURESHI, H. Y., CAFFERTY, P. W., SOBUE, K., AGARWAL-MAWAL, A., NEUFIELD, K. D. & PAUDEL, H. K. 2002. Glycogen synthase kinase-3beta is complexed with tau protein in brain microtubules. *J Biol Chem,* 277**,** 11933-40.
SUN, Y. & MACRAE, T. H. 2005. The small heat shock proteins and their role in human disease. *Febs J,* 272**,** 2613-27.
SWEETMAN, A. J. & WEETMAN, D. F. 1969. Polarographic assay of monoamine oxidase. *Br J Pharmacol,* 37**,** 550P.
TABNER, B. J., EL-AGNAF, O. M., TURNBULL, S., GERMAN, M. J., PALEOLOGOU, K. E., HAYASHI, Y., COOPER, L. J., FULLWOOD, N. J. & ALLSOP, D. 2005. Hydrogen peroxide is generated during the very early stages of aggregation of the amyloid peptides implicated in Alzheimer disease and familial British dementia. *J Biol Chem,* 280**,** 35789-92.
TANIGUCHI, D., DAI, P., HOJO, T., YAMAOKA, Y., KUBO, T. & TAKAMATSU, T. 2009. Low-energy laser irradiation promotes synovial fibroblast proliferation by modulating p15 subcellular localization. *Lasers Surg Med,* 41**,** 232-9.
THORNBERRY, N. A. 1998. Caspases: key mediators of apoptosis. *Chem Biol,* 5**,** R97-103.
TRIMMER, P. A., SCHWARTZ, K. M., BORLAND, M. K., DE TABOADA, L., STREETER, J. & ORON, U. 2009. Reduced axonal transport in Parkinson's disease cybrid neurites is restored by light therapy. *Mol Neurodegener,* 4**,** 26.
TSAI, C. L., CHEN, J. C. & WANG, W. J. 2001. Near-Infrared Absorption Property of Biological Soft Tissue Constituents. *Journal of Medical and Biological Engineering,* 21**,** 7-14.
TURTURICI, G., SCONZO, G. & GERACI, F. 2011. Hsp70 and its molecular role in nervous system diseases. *Biochem Res Int,* 2011**,** 618127.
UEDA, Y. & SHIMIZU, N. 2003. Effects of pulse frequency of low-level laser therapy (LLLT) on bone nodule formation in rat calvarial cells. *J Clin Laser Med Surg,* 21**,** 271-7.
VANDENBERGHE, W., NICOLL, R. A. & BREDT, D. S. 2005. Stargazin is an AMPA receptor auxiliary subunit. *Proc Natl Acad Sci U S A,* 102**,** 485-90.
VINCK, E. M., CAGNIE, B. J., CORNELISSEN, M. J., DECLERCQ, H. A. & CAMBIER, D. C. 2003. Increased fibroblast proliferation induced by light emitting diode and low power laser irradiation. *Lasers Med Sci,* 18**,** 95-9.
VIRK, B., CORREIA, G., DIXON, D. P., FEYST, I., JIA, J., OBERLEITNER, N., BRIGGS, Z., HODGE, E., EDWARDS, R., WARD, J., GEMS, D. & WEINKOVE, D. 2012. Excessive folate synthesis limits lifespan in the C. elegans: E. coli aging model. *BMC Biol,* 10**,** 67.

VOISINE, C., PEDERSEN, J. S. & MORIMOTO, R. I. 2010. Chaperone networks: tipping the balance in protein folding diseases. *Neurobiol Dis,* 40**,** 12-20.

VOSS, K., COMBS, B., PATTERSON, K. R., BINDER, L. I. & GAMBLIN, T. C. 2012. Hsp70 alters tau function and aggregation in an isoform specific manner. *Biochemistry,* 51**,** 888-98.

VOSS, K. & GAMBLIN, T. C. 2009. GSK-3beta phosphorylation of functionally distinct tau isoforms has differential, but mild effects. *Mol Neurodegener,* 4**,** 18.

VOSS, M. R., STALLONE, J. N., LI, M., CORNELUSSEN, R. N., KNUEFERMANN, P. & KNOWLTON, A. A. 2003. Gender differences in the expression of heat shock proteins: the effect of estrogen. *Am J Physiol Heart Circ Physiol,* 285**,** H687-92.

WALKER, G. A. & LITHGOW, G. J. 2003. Lifespan extension in C. elegans by a molecular chaperone dependent upon insulin-like signals. *Aging Cell,* 2**,** 131-9.

WAN, B., LANOUE, K. F., CHEUNG, J. Y. & SCADUTO, R. C., JR. 1989. Regulation of citric acid cycle by calcium. *J Biol Chem,* 264**,** 13430-9.

WANG, J., DICKSON, D. W., TROJANOWSKI, J. Q. & LEE, V. M. 1999. The levels of soluble versus insoluble brain Abeta distinguish Alzheimer's disease from normal and pathologic aging. *Exp Neurol,* 158**,** 328-37.

WELCH, W. J. 1992. Mammalian stress response: cell physiology, structure/function of stress proteins, and implications for medicine and disease. *Physiol Rev,* 72**,** 1063-81.

WHELAN, H. T., SMITS, R. L., JR., BUCHMAN, E. V., WHELAN, N. T., TURNER, S. G., MARGOLIS, D. A., CEVENINI, V., STINSON, H., IGNATIUS, R., MARTIN, T., CWIKLINSKI, J., PHILIPPI, A. F., GRAF, W. R., HODGSON, B., GOULD, L., KANE, M., CHEN, G. & CAVINESS, J. 2001. Effect of NASA light-emitting diode irradiation on wound healing. *J Clin Laser Med Surg,* 19**,** 305-14.

WHITE, J. G., SOUTHGATE, E., THOMSON, J. N. & BRENNER, S. 1986. The structure of the nervous system of the nematode Caenorhabditis elegans. *Philos Trans R Soc Lond B Biol Sci,* 314**,** 1-340.

WILHELMUS, M. M., BOELENS, W. C., OTTE-HOLLER, I., KAMPS, B., DE WAAL, R. M. & VERBEEK, M. M. 2006a. Small heat shock proteins inhibit amyloid-beta protein aggregation and cerebrovascular amyloid-beta protein toxicity. *Brain Res,* 1089**,** 67-78.

WILHELMUS, M. M., DE WAAL, R. M. & VERBEEK, M. M. 2007. Heat shock proteins and amateur chaperones in amyloid-Beta accumulation and clearance in Alzheimer's disease. *Mol Neurobiol,* 35**,** 203-16.

WILHELMUS, M. M., OTTE-HOLLER, I., WESSELING, P., DE WAAL, R. M., BOELENS, W. C. & VERBEEK, M. M. 2006b. Specific association of small heat shock proteins with the pathological hallmarks of Alzheimer's disease brains. *Neuropathol Appl Neurobiol,* 32**,** 119-30.

WINKLHOFER, K. F., TATZELT, J. & HAASS, C. 2008. The two faces of protein misfolding: gain- and loss-of-function in neurodegenerative diseases. *EMBO J,* 27**,** 336-49.

WOGULIS, M., WRIGHT, S., CUNNINGHAM, D., CHILCOTE, T., POWELL, K. & RYDEL, R. E. 2005. Nucleation-dependent polymerization is an

essential component of amyloid-mediated neuronal cell death. *J Neurosci,* 25**,** 1071-80.

WOLOZIN, B., GABEL, C., FERREE, A., GUILLILY, M. & EBATA, A. 2011. Watching worms whither: modeling neurodegeneration in C. elegans. *Prog Mol Biol Transl Sci,* 100**,** 499-514.

WONG-RILEY, M. T., LIANG, H. L., EELLS, J. T., CHANCE, B., HENRY, M. M., BUCHMANN, E., KANE, M. & WHELAN, H. T. 2005. Photobiomodulation directly benefits primary neurons functionally inactivated by toxins: role of cytochrome c oxidase. *J Biol Chem,* 280**,** 4761-71.

WOOD, W. B. 1988. *The Nematode Caenorhabditis Elegans*, Cold Spring Harbor Laboratory.

WU, D., CYPSER, J. R., YASHIN, A. I. & JOHNSON, T. E. 2009. Multiple mild heat-shocks decrease the Gompertz component of mortality in Caenorhabditis elegans. *Exp Gerontol,* 44**,** 607-12.

YAMAGISHI, N., FUJII, H., SAITO, Y. & HATAYAMA, T. 2009. Hsp105beta upregulates hsp70 gene expression through signal transducer and activator of transcription-3. *Febs J,* 276**,** 5870-80.

YAMAGISHI, N., GOTO, K., NAKAGAWA, S., SAITO, Y. & HATAYAMA, T. 2010. Hsp105 reduces the protein aggregation and cytotoxicity by expanded-polyglutamine proteins through the induction of Hsp70. *Exp Cell Res,* 316**,** 2424-33.

YAMAGISHI, N., ISHIHARA, K. & HATAYAMA, T. 2004. Hsp105alpha suppresses Hsc70 chaperone activity by inhibiting Hsc70 ATPase activity. *J Biol Chem,* 279**,** 41727-33.

YAMAGISHI, N., ISHIHARA, K., SAITO, Y. & HATAYAMA, T. 2003. Hsp105 but not Hsp70 family proteins suppress the aggregation of heat-denatured protein in the presence of ADP. *FEBS Lett,* 555**,** 390-6.

YAMAGISHI, N., NISHIHORI, H., ISHIHARA, K., OHTSUKA, K. & HATAYAMA, T. 2000. Modulation of the chaperone activities of Hsc70/Hsp40 by Hsp105alpha and Hsp105beta. *Biochem Biophys Res Commun,* 272**,** 850-5.

YAMAGISHI, N., YOKOTA, M., YASUDA, K., SAITO, Y., NAGATA, K. & HATAYAMA, T. 2011. Characterization of stress sensitivity and chaperone activity of Hsp105 in mammalian cells. *Biochem Biophys Res Commun,* 409**,** 90-5.

YASUDA, K., NAKAI, A., HATAYAMA, T. & NAGATA, K. 1995. Cloning and expression of murine high molecular mass heat shock proteins, HSP105. *J Biol Chem,* 270**,** 29718-23.

YENARI, M. A., GIFFARD, R. G., SAPOLSKY, R. M. & STEINBERG, G. K. 1999. The neuroprotective potential of heat shock protein 70 (HSP70). *Mol Med Today,* 5**,** 525-31.

YENARI, M. A., LIU, J., ZHENG, Z., VEXLER, Z. S., LEE, J. E. & GIFFARD, R. G. 2005. Antiapoptotic and anti-inflammatory mechanisms of heat-shock protein protection. *Ann N Y Acad Sci,* 1053**,** 74-83.

YING, R., LIANG, H. L., WHELAN, H. T., EELLS, J. T. & WONG-RILEY, M. T. 2008. Pretreatment with near-infrared light via light-emitting diode provides added benefit against rotenone- and MPP+-induced neurotoxicity. *Brain Res,* 1243**,** 167-73.

YONEDA, T., BENEDETTI, C., URANO, F., CLARK, S. G., HARDING, H. P. & RON, D. 2004. Compartment-specific perturbation of protein handling

activates genes encoding mitochondrial chaperones. *J Cell Sci,* 117**,** 4055-66.

YOO, B. C., KIM, S. H., CAIRNS, N., FOUNTOULAKIS, M. & LUBEC, G. 2001. Deranged expression of molecular chaperones in brains of patients with Alzheimer's disease. *Biochem Biophys Res Commun,* 280**,** 249-58.

YOUNG, A. E., GERMON, T. J., BARNETT, N. J., MANARA, A. R. & NELSON, R. J. 2000. Behaviour of near-infrared light in the adult human head: implications for clinical near-infrared spectroscopy. *Br J Anaesth,* 84**,** 38-42.

ZARKOWER, D. 2006. WormBook. *In:* MEYER, B. J. (ed.) *Somatic Sex Determination.* The *C.elegans* Research Community.

ZHANG, R., MIO, Y., PRATT, P. F., LOHR, N., WARLTIER, D. C., WHELAN, H. T., ZHU, D., JACOBS, E. R., MEDHORA, M. & BIENENGRAEBER, M. 2009. Near infrared light protects cardiomyocytes from hypoxia and reoxygenation injury by a nitric oxide dependent mechanism. *J Mol Cell Cardiol,* 46**,** 4-14.

ZHENG, H., JIANG, M., TRUMBAUER, M. E., SIRINATHSINGHJI, D. J., HOPKINS, R., SMITH, D. W., HEAVENS, R. P., DAWSON, G. R., BOYCE, S., CONNER, M. W., STEVENS, K. A., SLUNT, H. H., SISODA, S. S., CHEN, H. Y. & VAN DER PLOEG, L. H. 1995. beta-Amyloid precursor protein-deficient mice show reactive gliosis and decreased locomotor activity. *Cell,* 81**,** 525-31.